INFORMATION TO USERS

This manuscript has been reproduced from the microfilm master. UMI films the text directly from the original or copy submitted. Thus, some thesis and dissertation copies are in typewriter face, while others may be from any type of computer printer.

The quality of this reproduction is dependent upon the quality of the copy submitted. Broken or indistinct print, colored or poor quality illustrations and photographs, print bleedthrough, substandard margins, and improper alignment can adversely affect reproduction.

In the unlikely event that the author did not send UMI a complete manuscript and there are missing pages, these will be noted. Also, if unauthorized copyright material had to be removed, a note will indicate the deletion.

Oversize materials (e.g., maps, drawings, charts) are reproduced by sectioning the original, beginning at the upper left-hand corner and continuing from left to right in equal sections with small overlaps. Each original is also photographed in one exposure and is included in reduced form at the back of the book.

Photographs included in the original manuscript have been reproduced xerographically in this copy. Higher quality 6" x 9" black and white photographic prints are available for any photographs or illustrations appearing in this copy for an additional charge. Contact UMI directly to order.

UMI

A Bell & Howell Information Company
300 North Zeeb Road, Ann Arbor MI 48106-1346 USA
313/761-4700 800/521-0600

QUANTUM FLUCTUATIONS IN CONDENSED MATTER SYSTEMS: SQUEEZED STATES IN PHONONS AND JOSEPHSON JUNCTIONS

by

Xuedong Hu

A dissertation submitted in partial fulfillment
of the requirements for the degree of
Doctor of Philosophy
(Physics)
in The University of Michigan
1996

Doctoral Committee:

Associate Professor Franco Nori, Chairman
Assistant Professor Stuart Field
Professor Robert Lewis
Assistant Professor Alberto Rojo
Professor Alejandro Uribe-Ahumada

To my wife, Qingyang

and my parents, Fengzhen and Xiaoxuan

Acknowledgments

I would like to first thank my advisor, Professor Franco Nori, for his insight that led me to this thesis. His contagious enthusiasm kept me motivated through the most trying times during my tenure as a graduate student, and his guidance helped me greatly in my research.

I wish to thank all the colleagues with whom I have discussed the material in this thesis, for these discussions have helped me to refine many of the sections. In particular, I would like to thank Hailin Wang; he showed me the way when I began learning about squeezed states. I would also like to thank Saad Hebboul, Roberto Merlin, Nicolás Bonadeo, Jayson Cohen, Jeff Siegel, Dan Kilper, and especially Shin-Ichiro Tamura for providing many constructive suggestions which have made Chapter 3 more complete and readable. I also thank Dian Song for the numerous and often enlightening discussions which helped me to clarify many ideas involved in Chapter 5.

During my six years at the University of Michigan, I have had the good fortune to study and work together with some great friends. In particular, I would like to thank very enjoyable conversations with Ji Li, Radu Manuca, Chi-ming Chen, Charles Reichhardt, Cindy Olson and Jared Groth. Yeong-Lieh Lin deserves special thanks for his friendship and spiritual encouragement.

Table of Contents

List of Figures

List of Tables

List of Appendices

Chapter 1

Introduction

1.1 Motivation

The term "noise" is typically associated with unpleasant audible signals. Noise can be found everywhere, often in the form of unwanted electrical and audio disturbances. Technically, noise is any fluctuation that is not part of the signal. In physics, it means "spontaneous fluctuations". The quantities which fluctuate spontaneously with time are typically the number of active particles and their momenta, or distribution in energy states. In most, but not all cases, a signature of the noise process is that the elementary events, which contribute to the noise, occur at random. For classical systems, like most electronic devices, the origin of the noise is *thermal*. This noise is a result of spontaneous fluctuations in the number and energy of the active particles in the electronic device. This thermal noise can be understood in terms of statistical thermodynamics. For devices which operate at low temperatures, however, thermal noise can be quite small and *quantum* fluctuations become important. In this thesis we study quantum fluctuations, or quantum noise, in two systems: superconducting tunnel junctions and quantized sound waves.

In the history of modern physics, physicists have fought a never-ending battle to reduce measurement noise in their experiments. Indeed, there are many examples where the reduction of measurement noise has produced significant advances in physics. Better measurements lead to new theories, and the discoveries of new physical phenomena lead to new experiments of higher precision.[1] Three examples of this are: the theory and experiment on the photo-electric effect, atomic spectroscopy and quantum mechanics, as well as the

[1] For example, the first measurement of the speed of light, done in 1676 by the Danish astronomer Roemer, was off by about 30% [1]. Three hundred years later, in the early 1970s, the speed of light was measured with an error of only 1 part in 10^9 [1]. Indeed, this measurement is so accurate that in 1983 an international agreement was reached to use the speed of light for the definition of length, replacing the old meter block [2].

Lamb shift measurement and the theory of quantum electrodynamics [3, 4]. At the end of many struggles to reduce experimental noise, however, there is a fundamental limit below which the noise level cannot be lowered. This limit is given by the Heisenberg uncertainty principle.

1.2 Quantum Noise

According to the Heisenberg uncertainty principle, the product of the variances, $\langle(\Delta A)^2\rangle$ and $\langle(\Delta B)^2\rangle$, of two Hermitian operators A and B satisfies the following inequality [5]:

$$\langle(\Delta A)^2\rangle \, \langle(\Delta B)^2\rangle \geq \frac{1}{4} \, |\langle[A, \, B]\rangle|^2 \, , \tag{1.1}$$

where $\langle(\Delta A)^2\rangle = \langle A^2\rangle - \langle A\rangle^2$, $\langle(\Delta B)^2\rangle = \langle B^2\rangle - \langle B\rangle^2$, and $[A, \, B] = AB - BA$ is the commutator between A and B. Therefore, if A and B commute, these two operators can be simultaneously measured to an arbitrarily high degree of precision. That is, their quantum fluctuations[2] $\sqrt{\langle(\Delta A)^2\rangle}$ and $\sqrt{\langle(\Delta B)^2\rangle}$ can be simultaneously zero. On the other hand, if $[A, \, B] \neq 0$, the ultimate precision[3] of measuring A will be limited by how much one wants to know B. Furthermore, these measurements also depend on the quantum-mechanical state $|\psi\rangle$ of the system, as illustrated by the definition of variance: $\langle(\Delta A)^2\rangle = \langle\psi|A^2|\psi\rangle - \langle\psi|A|\psi\rangle^2$. If the equal sign in the above inequality (1.1) holds for a particular state $|\phi\rangle$, that state is called a minimum uncertainty state.

Let us consider an optical example. In classical physics, the wave representing darkness has no undulations. Since it is flat, it would not even be considered to be a wave. On the other hand, according to quantum mechanics, even when no light is present, there must still be some fluctuations in complete "darkness". Quantum mechanically, the wave is flat to within some small degree of uncertainty. Therefore, even in a vacuum, with no external light sources, there must still be small quantum fluctuations in the electromagnetic field.

A similar example can be found in solid crystals. In classical physics, the ground state of the crystal, which might be called the ultimate "quiet" state, is when all the atoms sit exactly at the equilibrium position and do not move at all. In this case, no waves (e.g., sound) propagate along the atomic chains. On the other hand, in quantum mechanics,

[2]The term "fluctuations" refers to the standard deviation $\sqrt{\langle(\Delta A)^2\rangle}$, which is the simplest measure of uncertainty or fluctuations. However, the variance $\langle(\Delta A)^2\rangle$ is often also referred to as fluctuations. Thus, we will use the term "fluctuations" to denote both of them.

[3]For a particle, a precise measurement at time t of its position $x(t)$, with $\Delta x(t) = 0$, results in a diverging $\Delta p(t)$. This, in turn, produces an infinite $\Delta x(t+\delta t)$. In other words, the infinite uncertainty in $p(t)$ produces an infinite uncertainty in the future location. Therefore, a precise measurement of $x(t)$ makes further precise measurements of x impossible. It is thus preferable to measure $x(t)$ and $p(t)$ with comparable uncertainties.

the atoms cannot sit still, because the vanishing of fluctuations Δx in the displacement of an atom along the x direction would mean the divergence of the fluctuations in its corresponding momentum: $\Delta p_x \geq \hbar/\Delta x$. This occurs because the position and momentum operators do not commute. In other words, the atoms cannot simultaneously have both a fixed position and a zero velocity. Therefore, even in complete "quietness"—when no classical atomic vibrations occur (i.e., when no classical sound propagates), there must still be small quantum fluctuations in the positions and momenta of the atoms.

1.3 Squeezed States of Light

Is there a way around the quantum noise limit set by the uncertainty principle? The answer is "yes". Notice that in the inequality (1.1) the limit is set on the *product* of the fluctuations. If we are only interested in one of the operators, there are states in which the noise in the quantity of interest is suppressed while the other quantity has large fluctuations. Such states have been realized in quantum optics. They are called squeezed states of light.

To proceed further, let us recall that the electromagnetic radiation in each standing-wave mode in a cavity resonator is analogous to an harmonic oscillator [6]. The displacement x and the momentum p of the oscillator correspond to the electric and magnetic field of the radiation mode, respectively. The electric and magnetic fields of the radiation mode at each point in space are 90° out of phase in time, as the position and velocity of an oscillator. The energy of the standing-wave field flows back and forth between electric and magnetic, as the energy of the oscillator flows back and forth between potential and kinetic. The quantization of the total energy of the oscillator implies having only an integral number of photons in the radiation mode.

The analogy to an harmonic oscillator also extends to traveling electromagnetic waves. The electric field for a monochromatic plane wave may be decomposed into two quadrature components with time dependence $\cos\omega t$ and $\sin\omega t$ respectively. Instead of electric and magnetic fields, it is the in-phase and out-of-phase quadratures that are analogous to the displacement of momentum of an oscillator.

A coherent state is the closest quantum counterpart to a classical field. It is also the ideal state for the photons produced by a laser. In such a coherent state, the fluctuations in the two quadratures are equal and minimize the uncertainty product given by the Heisenberg uncertainty relation: $\langle(\Delta A)^2\rangle\ \langle(\Delta B)^2\rangle = \frac{1}{4}|\langle[A,\ B]\rangle|^2$. The quantum fluctuations in a coherent state are randomly distributed in phase and are equal to the zero-point fluctuations.

The standard quantum limit to the reduction of noise in a signal is given by these zero-point fluctuations.

The experimental advances during the early days of lasers led to extensive theoretical research, and eventually to the first systematic description of photon coherent states in the early sixties [7]. Years later, and after much research on the quantum fluctuation properties of coherent states, squeezed states of photons were theoretically proposed [8, 9]. Their experimental realization occurred about ten years later [10] and it has attracted widespread attention [11]. In a squeezed state, one quantum dynamical variable becomes quieter while its conjugate variable noisier than their corresponding vacuum or coherent state values. Indeed, the essence of squeezed states is to redistribute the noise in a light beam, so that parts of the light (one quadrature) wave are less noisy than before, although other parts (the other quadrature) of the wave become noisier. Such a redistribution generally also occurs within one quadrature, so that at some times the quadrature is quieter, while at the other times it becomes noisier. Some examples are schematically illustrated in Figs. 1.1 and 1.2.

To envision squeezed states from the perspective of classical harmonic oscillators, let us imagine the following situation. Consider an ensemble of identical oscillators vibrating with the same frequency and all having nearly the same displacement x_0 from equilibrium at $t = 0$, but with a very wide distribution of momenta. A quarter cycle later, this ensemble would have a very wide distribution of displacements due to the wide range of initial momenta. However, after one-half cycle, the uncertainty in the displacement has undergone an oscillation because the oscillators would again gather together, but on the other side of the equilibrium position, near $-x_0$. On the other hand, in quantum mechanics, if all the oscillators started with nearly the same initial displacement, then the Heisenberg principle would automatically force their initial momenta to be spread over a wide range.

The ability of squeezed states to reduce or "squeeze" quantum noise gives them a promising future in different applications ranging from gravitational wave detection to optical communications [11]. In addition, squeezed states form a novel and exciting group of states and can provide new insight into quantum mechanical fluctuations. They also allow unique opportunities for the study of Quantum Electrodynamics (e.g., by enhancing the lifetime of atomic excited states) [12].

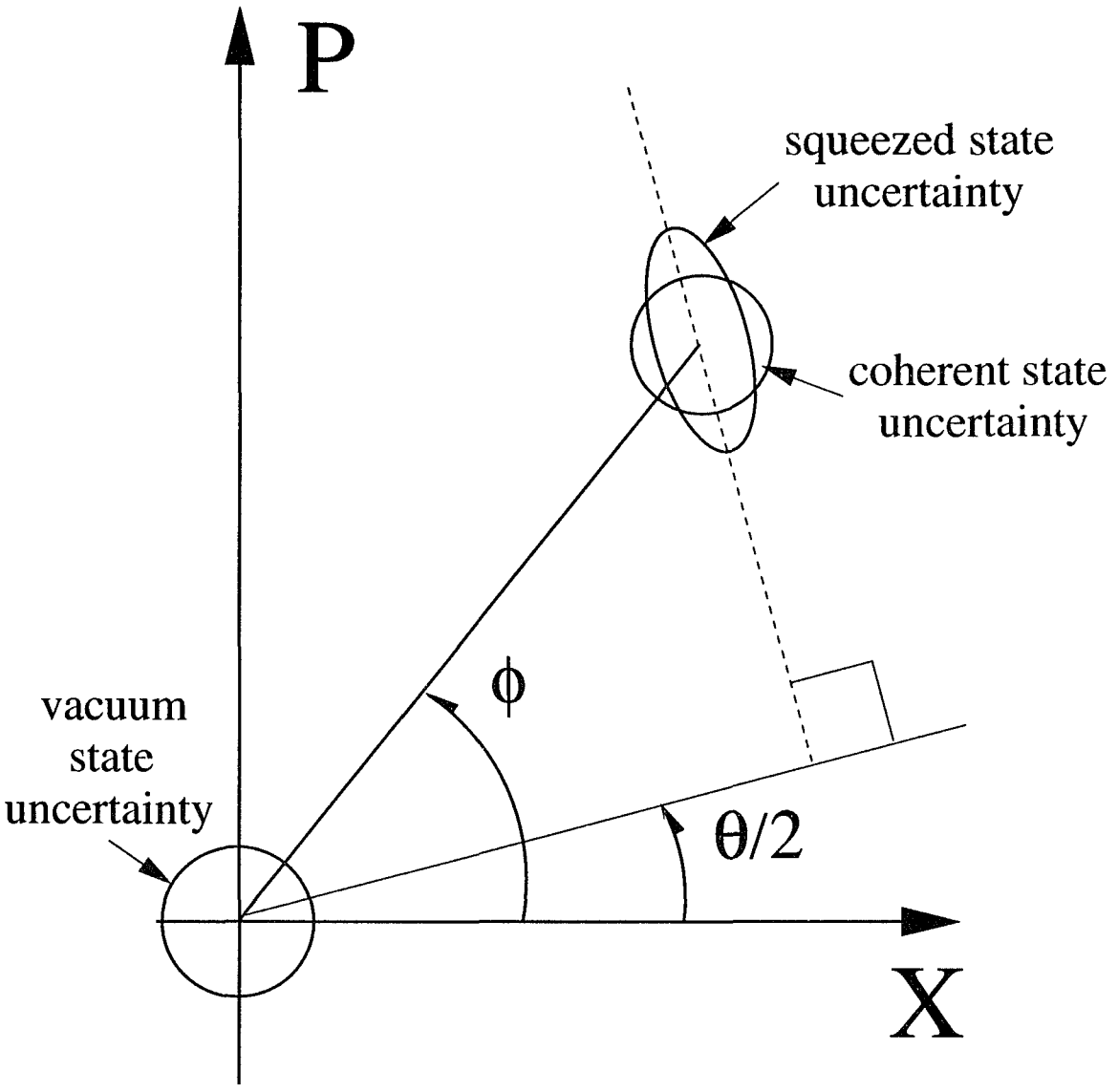

Figure 1.1: Schematic diagram of the uncertainty areas in the generalized coordinate and momentum (X, P) phase space of a photon squeezed state (ellipse) and a photon coherent state (circle). Here X and P are the two quadratures of the electric field. Notice that the photon coherent state has the same uncertainty area as the vacuum state (circle at the origin), and that its area is circular, while the squeezed state has an elliptical uncertainty area. Therefore, in the direction parallel to the $\theta/2$ line, the squeezed state has a smaller noise than the coherent state.

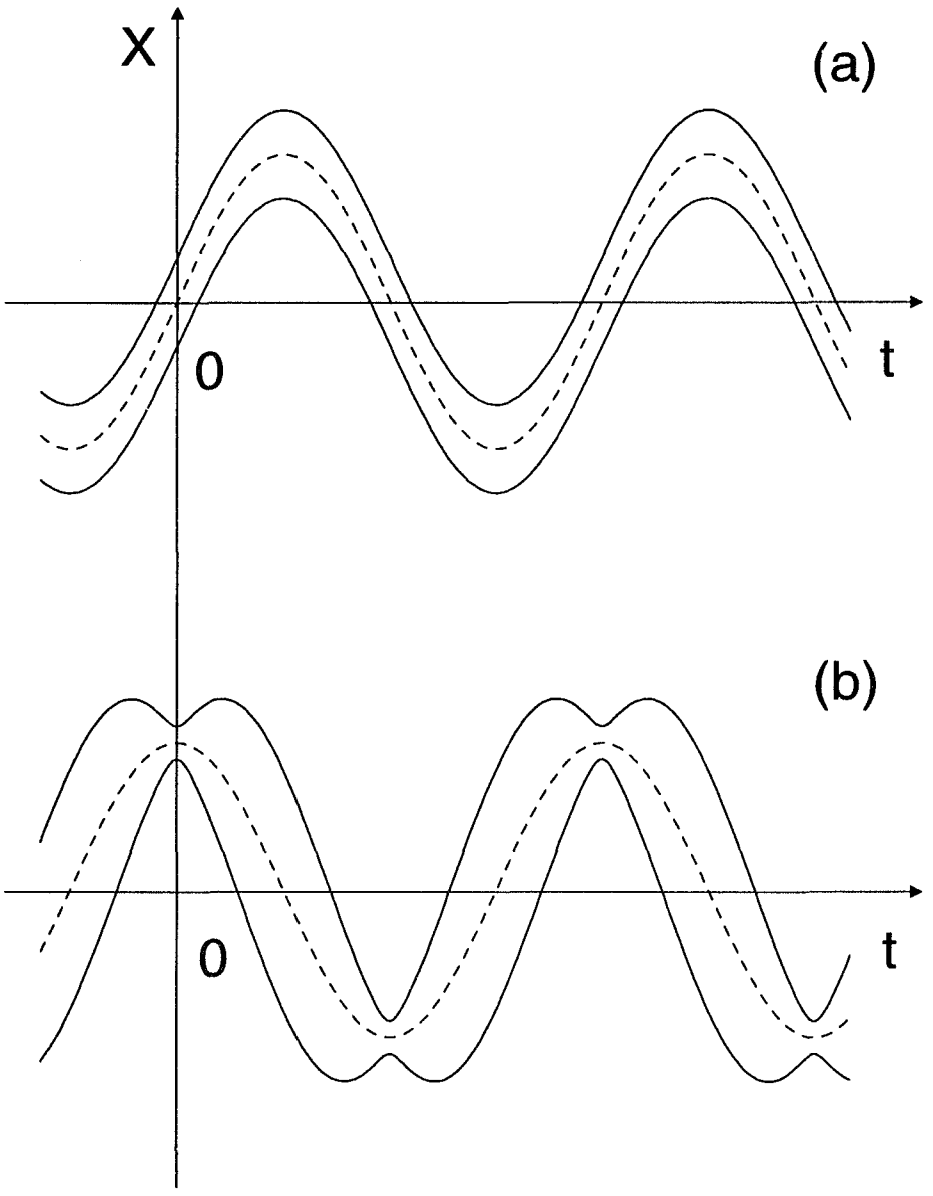

Figure 1.2: Schematic diagram of the time evolution of the expectation value $\langle X \rangle$ and the fluctuation $\sqrt{\langle (\Delta X)^2 \rangle}$ of the dimensionless quadrature X of an electric field in a photon coherent state (a) and a squeezed state (b). Here dashed lines represent $\langle X \rangle$, while solid lines represent the envelopes $\langle X \rangle \pm \sqrt{\langle (\Delta X)^2 \rangle}$, which are the upper and lower bounds of the fluctuating quantity X. (a) A single-mode photon coherent state $|\alpha\rangle$, where $\langle X \rangle = 2Re(\alpha e^{-i\omega t}) = 2|\alpha| \sin \omega t$, which means that α is purely imaginary; and $\langle (\Delta X)^2 \rangle = 2$. (b) A single-mode photon squeezed state $|\alpha e^{-i\omega t}, \xi(t)\rangle$, where the squeezing factor $\xi(t)$ satisfies $\xi(t) = re^{-2i\omega t}$. Here, $\langle X \rangle = 2|\alpha| \cos \omega t$, which means that α is real, and its fluctuation is $\langle (\Delta X)^2 \rangle = 2(e^{-2r} \cos^2 \omega t + e^{2r} \sin^2 \omega t)$. Notice that the squeezing effect appears at the times when $\langle X \rangle$ reaches its maxima.

1.4 Controlling Quantum Noise in Condensed Matter Systems

In most situations, a classical description is adequate to describe macroscopic physical phenomena in condensed matter, where *thermal* noise is much larger than any *quantum* noise so that the later can be neglected. However, at low temperatures coherent effects (e.g., Bose-Einstein condensation of Cooper pairs [14]) and quantum noise can play a crucial role. For instance, Josephson junctions provide an example of macroscopic quantum coherent phenomenon, where quantum fluctuations can be important. Moreover, a recent study [15] shows that quantum noise in the atomic positions can indeed influence observable quantities (e.g., the Raman line-shape) even when temperatures are not very low.

Non-quantum-optics analogs of squeezed states are now being vigorously pursued. For example, "classical" squeezed states are currently being studied by several groups [16, 17]. Their goal is to use mechanical parametric amplifiers to reduce or de-amplify thermal mechanical noise in ultra-small magnetic cantilevers [16] and trapped ions [17].

This thesis addresses the following question: Is it possible to control quantum fluctuations in condensed matter systems, in analogy to the the case for optical ones? We explore this issue in two condensed matter examples: phonons and Josephson junctions [18, 19, 20, 21, 22].

The modulation of the quantum fluctuations in the photon field is significant because of the very high precision achieved by optical measurements. Although most condensed matter experiments do not produce such high-accuracy results, two exceptions to this rule are the quantum Hall effect and the Josephson effect. For instance, the most precise measurement of energy levels has been achieved not in the traditional context of atomic-optical physics, but with superconducting tunneling Josephson junctions [23], to an astounding accuracy of three parts in 10^{19}. Aside from suppressing quantum fluctuations, squeezed states can also lead to changes in the physical properties in the system, thus are also interesting from a fundamental viewpoint.

Phonons, the quanta of lattice vibrations, are the first condensed matter system we chose to study.[4] One important reason to choose phonons is that these elementary excitations are bosons, as are photons. Indeed, there are many similarities between phonons and photons, although significant differences also exist (see Section 3.2 for a detailed comparison). Since

[4] Our results on phonon squeezing, published in Phys. Rev. Lett. **76**, 2294 (1996) and in Phys. Rev. B **53**, 2419 (1996), have also been featured in Physics News Update, Number 261, March 6, 1996, published by the American Institute of Physics.

a phonon traveling through a solid is equivalent to the propagation of a slight disturbance in the local arrangement of atoms in the solid, the creation of squeezed phonon states would lead to the possibility of reducing the quantum fluctuations of atomic displacements to below the zero-point noise level.

We have studied the dynamics and quantum fluctuation properties of coherent and squeezed phonon states. In particular, we have calculated the experimentally-observable time-evolution and fluctuations of the lattice amplitude operator $u(\pm\mathbf{q}) = b_{\mathbf{q}}+b^{\dagger}_{-\mathbf{q}}+b^{\dagger}_{\mathbf{q}}+b_{-\mathbf{q}}$ in various phonon states. We show that the averages $\langle u(\pm\mathbf{q})\rangle$ are sinusoidal functions of time in both coherent and squeezed states. However, for squeezed states the fluctuation $\langle(\Delta u(\pm\mathbf{q}))^2\rangle$ is periodically smaller than its coherent state value 2, which is also the vacuum state noise level. Therefore, phonon squeezed states are periodically quieter than the vacuum state. We then propose several different possible generating mechanisms, emphasizing phonon parametric down-conversion processes and an alternative approach based on phonon-photon interactions. We also propose a detection scheme based on reflectivity measurements.

It is difficult to generate squeezed states because they have noise levels which are even lower than the one for the vacuum state. Indeed, the experimental and theoretical development of photon coherent and squeezed states took decades. Likewise, the experimental realization of phonon squeezed states might require years of further theoretical and experimental work. Nevertheless, we believe that theoretical results in quantum phonon optics can help the development of the corresponding experiments. We hope that our effort, which is only a glimpse into a very rich and new field, will lead to more theoretical and experimental developments in the still unexplored area of quantum phonon optics and the "manipulation" of phonon quantum fluctuations.

In the second part of this thesis (Chapters 4 and 5), we study the quantum fluctuation properties of Josephson junctions, and propose a possible way of manipulating the precision limitations imposed by quantum noise. In light of the recent advances in micro-fabrication and the general interest in the possible manipulation and minimization of quantum noise, we ask the following question: how do quantum fluctuations affect Cooper pair tunneling in a Josephson junction? To answer this, we need to first compute its quantum fluctuations and understand how they behave in different physical situations involving Josephson junctions. We develop a theory of the quantum mechanical squeezed states in Josephson junctions, and identify and list their properties. In particular, we diagonalize several Hamiltonians

corresponding to different configurations containing Josephson junctions, find their eigenstates, and calculate the corresponding fluctuations. We also construct the time-evolution operators for the various cases considered here. From them, and with different initial states, we calculate the time evolution of the variances of the conjugate variables of the system. These provide a measure of the quantum fluctuations of the charge and the phase difference of the Josephson junction.

1.5 Overview of the Thesis

The topic presented in this thesis cuts through somewhat different sub-areas of physics: quantum optics and condensed matter physics. This poses special problems in the presentation of the material—problems not found in more specialized works. For instance, no standard book devoted to phonons discusses the notion of modulating the quantum fluctuations of atomic displacements. Furthermore, discussions on squeezed states in the quantum optics literature use a formalism and language quite different from the one used in condensed matter physics. In several Appendices, we briefly summarize the essential results on squeezed states needed in our work. A clear presentation of these concepts is needed because our work is intended for a wide readership of researchers working in different areas of condensed matter physics.

The first part of this thesis (Chapters 2 and 3) focus on phonon squeezed states, while the second part (Chapters 4 and 5) focus on the quantum fluctuation properties of Josephson junctions.

Chapter 1 presents a pedagogical and nontechnical introduction to quantum noise and squeezed states. It also contains an overview of the thesis. Chapter 2 summarizes our results on phonon squeezing, which are then presented in more detail in Chapter 3. There we focus on a few simple models in which analytical results can be obtained for coherent and squeezed phonon states [18, 19, 20]. We give a fully quantum mechanical description of coherent phonons, and calculate the averages and fluctuations of the atomic displacements and lattice amplitude operators (see Section 3.3 for definitions), among other quantities. The previously available theories on the generating mechanisms of coherent phonons [41, 44, 49] all use *classical* equations of motion to describe phonon dynamics, while here we focus on a *quantum* description of phonon coherent states. Afterwards, we investigate the quantum squeezed states of phonons, calculate their fluctuations, and compare them to the values obtained for coherent states. We discuss four different approaches to generate phonon squeezed

states. These approaches are based on a variety of physical processes, including three-phonon interactions, second-order Raman scattering, photon-phonon interactions that lead to polaritons, and short-time number-conserving single-mode phonon-phonon interactions. Detailed calculations are presented on the parametric down-conversion process based on three-phonon interactions. We also propose a detection scheme for squeezed phonon states. The core of this approach is the phonon-photon interaction, through which the information on phonons can be transfered to the reflected light from a crystal. A phase-sensitive optical detection method can then be used to decipher the phonon information.

Chapter 4 summarizes our results on the intrinsic quantum fluctuations of the charge and phase of a Josephson junction in various circumstances. These are discussed in detail in Chapter 5. In particular, we consider a Josephson junction in a variety of situations, i.e., coupled to one or several of the following circuit elements: a capacitor, an inductor (in a superconducting ring), and an applied current-source. Needless to say, this list is not exhaustive, since other interactions with the environment can be devised. We use the small-phase approximation (described in Chapter 5) because we work in the strong coupling limit and treat the metastable states as nearly localized. We then proceed to solve for the ground and excited states near the potential minima of the various configurations. The ground states are squeezed vacuum or coherent states, while the excited states are a class of squeezed number states. In each case we calculate the quantum fluctuations of phase ϕ and Cooper pair number n over the junction. We also construct the approximate time evolution operators for the configurations considered. Another approach we employ uses the rotating wave approximation, which is basically also a first-order approximation in energy. The solution of the full problem, without approximations, is quite difficult and would require a much more numerical approach which is beyond the scope of this thesis. The limitations, and possible extensions, of our approach are discussed in detail at the end of this chapter.

1.6 Open Problems and Future Applications

In this section we discuss some open problems in the field of modulating quantum fluctuations.

In both the phonon and Josephson junction cases, our analytical results cannot be obtained without several simplifications of the most complete models. In particular, we study single-mode and two-mode phonon states throughout Chapter 3, while in a generic crystal lattice, phonon modes are crowded together. In Chapter 5, we use a small-phase

approximation to expand the Josephson coupling potential, and a short-time approximation to further simplify the algebra. Therefore, our work in this thesis provides a first stepping stone to a more complete approach.

For phonons, we consider the case where an optical phonon, excited by an incoming laser, decays into one pair of acoustic phonons. This is, of course, not the general case. Phonons generally decay into a continuum of (acoustic phonon) modes. How to include into our calculation this "decay into a continuum of modes" is certainly the most immediate challenge.

Another problem is associated with detection schemes. Currently available phonon detection schemes are generally wide-band, while the scheme we propose is influenced by sources such as optical noise, imperfect surfaces, and the very small relative change of the crystal reflectivity due to phonons.

Within our model, there is also room for further research. For example, to better describe the modes involved, approaches using Langevin and master equations can be employed. In these approaches, noise is a more integral part of the description. Furthermore, it is easier to include the effect of temperature and inter-mode interactions.

We have not studied the possible change in the physical properties of a crystal that has squeezed phonons. For example, electrons are constantly scattered off phonons. If the fluctuations in phonons are suppressed, what will be the effect on the electrons? Will they have a longer coherence length? Will the mean free path increase? What is the effect on the overall electrical conductance of the crystal? Further research needs to be done to answer these questions.

Another problem related to phonon squeezed states is the possibility of producing phonon cavities, especially for high-energy acoustic phonons. Squeezing can be achieved for a short period of time, using an incoming laser pulse, or can be maintained continuously by employing a continuous-wave (CW) laser. In our study, we focus on a light-pulse-generated phonon squeezed state whose lifetime is short. To achieve squeezing in a continuous manner, it is important to have a cavity or a mode-selector for the particular mode (or modes) so that stimulated emission is possible. Furthermore, phonon cavities are not only interesting because of their importance to continuous squeezing, they are also a crucial ingredient for a "phonon maser", which is the phonon analogue of the conventional photon maser.

In the case of Josephson junctions (JJ), there are also many opportunities for further research. First of all, we have studied the coupling of Josephson junctions to simple and

discrete circuit elements only, such as inductors and capacitors. In the more practical situations, the circuits involved generally have distributed inductance and capacitance. How to include these kind of "continuous elements" into our model is not clear at present. Furthermore, we have studied mostly isolated Josephson junction circuits. In other words, the configurations are not affected by any external disturbance. The JJ squeezed states are eigenstates of the various system configurations. The squeezing effect is the intrinsic property of the Josephson junctions, primarily due to the nonlinearity of the Josephson coupling. To change or extract this effect, a coupling to an external pump or detector is indispensable. Indeed, it would be interesting to study a coupling between an external single mode of electromagnetic radiation and a Josephson junction circuit. A particular way of coupling has been suggested [95], but many questions still remain unanswered.

Another interesting problem is the inclusion of quasiparticle tunneling into the Josephson junction circuit model. At any finite temperature, quasiparticles are excited. There is a finite probability for them to tunnel through the Josephson junction. Is there any coherence in this tunneling? If there is, how can it be described? In most of the current literature, the Caldeira-Leggett formalism [94] has been used to describe the effect of quasiparticles on the Cooper pairs. Is there any other way to describe it? It is also important to better understand the effect of quasiparticles for the following reason. SQUIDs (Superconducting Quantum Interference Devices) are widely used for high-precision measurements of small magnetic fields; they work at high biasing current when quasiparticle tunneling is an integral part of the current. Furthermore, it is the quasiparticle tunneling that leads to variations in the voltage across the junction, which is the output signal. Therefore, to study quasiparticle tunneling and its interaction with the Cooper pairs has very practical applications.

In our study of quantum noise in Josephson junctions, we focus on the limit of $E_J \gg E_C$. It would certainly be of interest to also study the opposite limit. Indeed, when $E_J \ll E_C$, the junction is in the Bloch-oscillation regime [89], with a strong Coulomb blockade effect. As pointed out in Ref. [89], this effect leads to coherent tunneling and a very accurate measure for current. How will quantum fluctuations perturb such a coherent tunneling effect? To what degree? Furthermore, many of the currently available single-electron electrometers [89] work in the regime where charging and Josephson coupling energies are comparable: $E_J \approx E_C$. Therefore, it would certainly be useful to also study the quantum fluctuation properties in that regime.

Aside from phonon and Josephson junction systems, there are other bosonic systems in

condensed matter physics. Magnons, ^{4}He, excitons, and the composite bosonic excitations in quantum Hall systems are a few examples. What are the quantum fluctuation properties of these systems? Are there analogies with squeezed photon or phonon states? How to generate and detect novel non-classical states in these systems? Indeed, the field of "quantum noise control" in condensed matter systems is still wide open, and we hope that our results motivate further work in this new area.

Chapter 2

Squeezed Phonon States

This chapter is a summary of our ideas and results on squeezed phonon states [18, 19, 20]; these are presented in detail in Chapter 3. We study squeezed quantum states of phonons, which allow the possibility of modulating the quantum fluctuations of atomic displacements below the zero-point quantum noise level of coherent phonon states. We calculate the corresponding expectation values and fluctuations of both the atomic displacement and the lattice amplitude operators, and also investigate the possibility of generating squeezed phonon states using a three-phonon parametric down-conversion process based on phonon-phonon interactions. We also study an alternative approach of squeezing quantum noise in the atomic displacement using a polariton-based approach. Furthermore, we propose a detection scheme based on reflectivity measurements.

2.1 Introduction

Photon squeezed states have attracted much attention during the past decade [11]. These states are important because they can achieve lower quantum noise than the zero-point fluctuations of the vacuum or coherent states. Thus they provide a way of manipulating quantum fluctuations and have a promising future in different applications ranging from optical communications to gravitational wave detection [11]. Indeed, squeezed states are currently being explored in a variety of non-quantum-optics systems, including classical squeezed states [16, 17]. Here we study the properties of *phonon* squeezed states and explore the possibility of generating these states through phonon-phonon interactions. After briefly presenting the quantum mechanical description of various kinds of phonon states, we study a simple model for generating phonon squeezed states, in which analytical results can be obtained [18, 19, 20]. We also propose a scheme for detecting this squeezing effect.

In most macroscopic situations, a classical description is adequate. However, the quan-

tum fluctuations of a phonon system can be dominant at low enough temperatures. Indeed, a recent study shows that quantum fluctuations in the atomic positions can influence observable quantities (e.g., the Raman line-shape) [15] even when temperatures are not very low.

An experimentally observable quantity for a phonon system is the real part of the Fourier transform of the atomic displacement:[1]

$$Re\,(u_\alpha(\mathbf{q})) = \sum_\lambda \sqrt{\hbar/8m\omega_{\mathbf{q}\lambda}}\left\{U^\lambda_{\mathbf{q}\alpha}(b_{\mathbf{q}\lambda} + b^\dagger_{-\mathbf{q}\lambda}) + U^{\lambda\,*}_{\mathbf{q}\alpha}(b_{-\mathbf{q}\lambda} + b^\dagger_{\mathbf{q}\lambda})\right\} . \tag{2.1}$$

For simplicity, hereafter we will drop the branch subscript λ, assume that $U_{\mathbf{q}\alpha}$ is real, and define a $\mathbf{q}$-mode dimensionless lattice amplitude operator:

$$u(\pm\mathbf{q}) = b_{\mathbf{q}} + b^\dagger_{-\mathbf{q}} + b_{-\mathbf{q}} + b^\dagger_{\mathbf{q}} . \tag{2.2}$$

This operator contains essential information on the lattice dynamics, including quantum fluctuations. It is the phonon analog of the electric field in the photon case.

2.2 Phonon Quantum States

2.2.1 Phonon Vacuum and Number States

When no phonon is excited, the crystal is in the phonon vacuum state $|0\rangle$. The eigenstates of the harmonic phonon Hamiltonian are number states which satisfy

$$b_{\mathbf{q}}|n_{\mathbf{q}}\rangle = \sqrt{n_{\mathbf{q}}}|n_{\mathbf{q}} - 1\rangle . \tag{2.3}$$

The phonon number and the phase of atomic vibrations are conjugate variables. Thus, due to the uncertainty principle, the phase is arbitrary when the phonon number is certain, as it is the case with any number state $|n_{\mathbf{q}}\rangle$. Therefore, the expectation values of the atomic displacement $\langle n_{\mathbf{q}}|u_{i\alpha}|n_{\mathbf{q}}\rangle$ and $\mathbf{q}$-mode lattice amplitude $\langle n_{\mathbf{q}}|u(\pm\mathbf{q})|n_{\mathbf{q}}\rangle$ vanish due to the randomness in the phase of the atomic displacements.

2.2.2 Phonon Coherent States

A single-mode ($\mathbf{q}$) phonon coherent state[2] is an eigenstate of a phonon annihilation operator:

$$b_{\mathbf{q}}|\beta_{\mathbf{q}}\rangle = \beta_{\mathbf{q}}|\beta_{\mathbf{q}}\rangle . \tag{2.4}$$

[1] A phonon with quasi-momentum $\mathbf{p} = \hbar\mathbf{q}$ and branch subscript λ has energy $\epsilon_{\mathbf{q}\lambda} = \hbar\omega_{\mathbf{q}\lambda}$; the corresponding creation and annihilation operators satisfy the boson commutation relations: $[b_{\mathbf{q}'\lambda'},\ b^\dagger_{\mathbf{q}\lambda}] = \delta_{\mathbf{q}\mathbf{q}'}\delta_{\lambda\lambda'}$, $[b_{\mathbf{q}\lambda},\ b_{\mathbf{q}'\lambda'}] = 0$. The atomic displacements $u_{i\alpha}$ of a crystal lattice are given by $u_{i\alpha} = (1/\sqrt{Nm})\sum^N_{\mathbf{q}\lambda} U^\lambda_{\mathbf{q}\alpha}Q^\lambda_{\mathbf{q}}e^{i\mathbf{q}\cdot\mathbf{R}_i}$. Here $\mathbf{R}_i$ refer to the equilibrium lattice positions, α to a particular direction, and $Q^\lambda_{\mathbf{q}} = \sqrt{\hbar/2\omega_{\mathbf{q}\lambda}}(b_{\mathbf{q}\lambda} + b^\dagger_{-\mathbf{q}\lambda})$ is the normal-mode amplitude operator.

[2] A single-mode phonon coherent state can be generated by the Hamiltonian $H = \hbar\omega_{\mathbf{q}}(b^\dagger_{\mathbf{q}}b_{\mathbf{q}} + 1/2) + \lambda^*_{\mathbf{q}}(t)\,b_{\mathbf{q}} + \lambda_{\mathbf{q}}(t)\,b^\dagger_{\mathbf{q}}$ and an appropriate initial state. Here $\lambda_{\mathbf{q}}(t)$ represents the interaction strength between

It can also be generated by applying a phonon displacement operator $D_{\mathbf{q}}(\beta_{\mathbf{q}})$ to the phonon vacuum state

$$\begin{aligned} |\beta_{\mathbf{q}}\rangle &= D_{\mathbf{q}}(\beta_{\mathbf{q}})|0\rangle = \exp(\beta_{\mathbf{q}} b_{\mathbf{q}}^{\dagger} - \beta_{\mathbf{q}}^{*} b_{\mathbf{q}})|0\rangle \\ &= \exp(-|\beta_{\mathbf{q}}|^2/2) \sum_{n_{\mathbf{q}}=0}^{\infty} \frac{\beta_{\mathbf{q}}^{n_{\mathbf{q}}}}{\sqrt{n_{\mathbf{q}}!}} |n_{\mathbf{q}}\rangle \,. \end{aligned} \tag{2.5}$$

Thus it can be seen that a phonon coherent state is a phase coherent superposition of number states. Moreover, coherent states are a set of minimum-uncertainty states which are as noiseless as the vacuum state.[3] Coherent states are also the quantum states that best describe the classical harmonic oscillators [57].

2.2.3 Phonon Squeezed States

In order to reduce quantum noise to a level below the zero-point fluctuation level, we need to consider phonon squeezed states. Quadrature squeezed states are generalized coherent states [58]. Here "quadrature" refers to the dimensionless coordinate and momentum. Compared to coherent states, squeezed ones can achieve smaller variances for one of the quadratures during certain time intervals and are therefore helpful for decreasing quantum noise.[4]

A single-mode quadrature phonon squeezed state is generated from a vacuum state as

$$|\alpha_{\mathbf{q}}, \xi\rangle = D_{\mathbf{q}}(\alpha_{\mathbf{q}}) S_{\mathbf{q}}(\xi)|0\rangle \,, \tag{2.6}$$

$$S_{\mathbf{q}}(\xi) = \exp(\xi^{*} b_{\mathbf{q}}^{2}/2 - \xi b_{\mathbf{q}}^{\dagger 2}/2) \,. \tag{2.7}$$

---

phonons and the external source. More specifically, if the initial state is a vacuum state, $|\psi(0)\rangle = |0\rangle$, then the state vector $|\psi\rangle$ becomes a single-mode phonon coherent state thereafter $|\psi(t)\rangle = |\Lambda_{\mathbf{q}}(t)\, e^{-i\omega_{\mathbf{q}} t}\rangle$, where $\Lambda_{\mathbf{q}}(t) = -i/\hbar \int_{-\infty}^{t} \lambda_{\mathbf{q}}(\tau)\, e^{i\omega_{\mathbf{q}}\tau} d\tau$ is the coherent amplitude of mode $\mathbf{q}$. If the initial state is a single-mode coherent state $|\psi(0)\rangle = |\alpha_{\mathbf{q}}\rangle$, then the state vector at time t takes the form $|\psi(t)\rangle = |\,\{\Lambda_{\mathbf{q}}(t) + \alpha_{\mathbf{q}}\}\, e^{-i\omega_{\mathbf{q}} t}\rangle$, which is still coherent.

[3] In the phonon vacuum state, the fluctuations of the atomic displacement operator are identical for all atoms in the lattice $\langle(\Delta u_{\alpha})^2\rangle_{\rm vac} \equiv \langle(u_{\alpha})^2\rangle_{\rm vac} - \langle u_{\alpha}\rangle_{\rm vac}^2 = \sum_{\mathbf{q}}^{N} \hbar |U_{\mathbf{q}\alpha}|^2/(2Nm\omega_{\mathbf{q}\alpha})$ and $\langle(\Delta u(\pm\mathbf{q}))^2\rangle_{\rm vac} = 2$. The fluctuations in a phonon number state are larger than in the vacuum state: $\langle(\Delta u_{l\alpha})^2\rangle_{\rm num} = \hbar |U_{\mathbf{q}\alpha}|^2 n_{\mathbf{q}}/Nm\omega_{\mathbf{q}\alpha} + \sum_{\mathbf{q}'\neq\mathbf{q}}^{N} \hbar |U_{\mathbf{q}'\alpha}|^2/(2Nm\omega_{\mathbf{q}'\alpha})$ and $\langle(\Delta u(\pm\mathbf{q}))^2\rangle_{\rm num} = 2 + 2n_{\mathbf{q}}$. In a single-mode ($\mathbf{q}$) phonon coherent state $|\Lambda_{\mathbf{q}}(t)\, e^{-i\omega_{\mathbf{q}} t}\rangle$, the fluctuation in the atomic displacements is $\langle(\Delta u_{l\alpha})^2\rangle_{\rm coh} = \sum_{\mathbf{q}}^{N} \hbar |U_{\mathbf{q}\alpha}|^2/2Nm\omega_{\mathbf{q}\alpha}$. The unexcited modes are in the vacuum state and thus all contribute to the noise in the form of zero point fluctuations. Furthermore, $\langle(\Delta u(\pm\mathbf{q}))^2\rangle_{\rm coh} = 2$, which is exactly the same as in the phonon vacuum state.

[4] It is important to point out that the squeezing effect is quite general. In fact, any diagonalizable system can be "squeezed" in some manner by an appropriate choice of initial states. For example, consider a free oscillator $H = a^{\dagger}a$, and define $d = \mu a + \nu a^{\dagger}$, where μ and ν are complex scalars. In order for d to be a boson operator, μ and ν must satisfy the relation $|\mu|^2 - |\nu|^2 = 1$. Then the Hamiltonian becomes $H = (|\mu|^2 + |\nu|^2) d^{\dagger}d - (\mu\nu d^{\dagger\,2} + \mu^{*}\nu^{*} d^2) + |\nu|^2$. The generalized "displacement" $d + d^{\dagger}$ is a mixture of the original displacement $(a + a^{\dagger})/\sqrt{2}$ and momentum $-i(a - a^{\dagger})/\sqrt{2}$. If we are interested in a quantity such as $d + d^{\dagger}$, and it is observable, the squeezing effect can be obtained when the initial state is a coherent state of mode "d", i.e., $d|\delta\rangle = \delta|\delta\rangle$. On the other hand, such a hybrid quantity $d + d^{\dagger}$ might not be physically interesting and/or observable. In other words, the squeezing effect is only relevant when it is related to the observables.

A two-mode quadrature phonon squeezed state is generated as

$$|\alpha_{\mathbf{q}_1}, \alpha_{\mathbf{q}_2}, \xi\rangle = D_{\mathbf{q}_1}(\alpha_{\mathbf{q}_1}) D_{\mathbf{q}_2}(\alpha_{\mathbf{q}_2}) S_{\mathbf{q}_1,\mathbf{q}_2}(\xi)|0\rangle\,, \tag{2.8}$$

$$S_{\mathbf{q}_1,\mathbf{q}_2}(\xi) = \exp(\xi^* b_{\mathbf{q}_1} b_{\mathbf{q}_2} - \xi b^\dagger_{\mathbf{q}_1} b^\dagger_{\mathbf{q}_2})\,. \tag{2.9}$$

Here $D_{\mathbf{q}}(\alpha_{\mathbf{q}})$ is the coherent state displacement operator with $\alpha_{\mathbf{q}} = |\alpha_{\mathbf{q}}|e^{i\phi}$; $S_{\mathbf{q}}(\xi)$ and $S_{\mathbf{q}_1,\mathbf{q}_2}(\xi)$ are the single- and two-mode squeezing operator,[5] and $\xi = re^{i\theta}$ is the complex squeezing factor with $r \geq 0$ and $0 \leq \theta < 2\pi$. The two-mode phonon quadrature operators have the form

$$X(\mathbf{q}, -\mathbf{q}) = (b_{\mathbf{q}} + b^\dagger_{\mathbf{q}} + b_{-\mathbf{q}} + b^\dagger_{-\mathbf{q}})/2^{3/2} = 2^{-3/2} u(\pm\mathbf{q})\,, \tag{2.10}$$

$$P(\mathbf{q}, -\mathbf{q}) = (b_{\mathbf{q}} - b^\dagger_{\mathbf{q}} + b_{-\mathbf{q}} - b^\dagger_{-\mathbf{q}})/(2^{3/2} i)\,. \tag{2.11}$$

We have considered two cases where squeezed states were involved in modes $\pm\mathbf{q}$. In the first case, the system is in a two-mode ($\pm\mathbf{q}$) squeezed state $|\alpha_{\mathbf{q}}, \alpha_{-\mathbf{q}}, \xi\rangle$, ($\xi = re^{i\theta}$), with fluctuations

$$\langle(\Delta u(\pm\mathbf{q}))^2\rangle_{\rm sq} = 2(e^{-2r}\cos^2\frac{\theta}{2} + e^{2r}\sin^2\frac{\theta}{2})\,. \tag{2.12}$$

In the second case, the system is in a single-mode squeezed state $|\alpha_{\mathbf{q}}, \xi\rangle$, ($\alpha_{\mathbf{q}} = |\alpha_{\mathbf{q}}|e^{i\phi}$), in the first mode and an arbitrary coherent state $|\beta_{-\mathbf{q}}\rangle$ in the second mode. The fluctuation is now

$$\langle(\Delta u(\pm\mathbf{q}))^2\rangle_{\rm sq} = 1 + e^{-2r}\cos^2(\phi + \frac{\theta}{2}) + e^{2r}\sin^2(\phi + \frac{\theta}{2})\,. \tag{2.13}$$

In both of these cases, $\langle(\Delta u(\pm\mathbf{q}))^2\rangle_{\rm sq}$ can be smaller than in coherent states.

2.3 Phonon Parametric Down-conversion Process

Now we propose a scheme to generate phonon squeezed states.[6] This scheme is based on a "phonon" parametric down-conversion process (e.g., the decaying process: LO phonon $\rightarrow$ two LA phonons, where LO refers to Longitudinal Optical and LA to Longitudinal Acoustic), which in turn is based on three-phonon interactions. Typically, three-phonon interactions are the dominant anharmonic processes in a phonon system and the lowest order perturbation to the harmonic Hamiltonian. We will neglect all the higher order

[5]The squeezing operator $S_{\mathbf{q}_1,\mathbf{q}_2}(\xi)$ can be produced by the following Hamiltonian: $H_{\mathbf{q}_1,\mathbf{q}_2} = \hbar\omega_{\mathbf{q}_1} b^\dagger_{\mathbf{q}_1} b_{\mathbf{q}_1} + \hbar\omega_{\mathbf{q}_2} b^\dagger_{\mathbf{q}_2} b_{\mathbf{q}_2} + \zeta(t) b^\dagger_{\mathbf{q}_1} b^\dagger_{\mathbf{q}_2} + \zeta^*(t) b_{\mathbf{q}_1} b_{\mathbf{q}_2}$. The time-evolution operator has the form $U(t) = \exp(-iH_0 t/\hbar)$ $\exp[\xi^*(t) b_{\mathbf{q}_1} b_{\mathbf{q}_2} - \xi(t) b^\dagger_{\mathbf{q}_1} b^\dagger_{\mathbf{q}_2}]$, where $H_0 = \hbar\omega_{\mathbf{q}_1} b^\dagger_{\mathbf{q}_1} b_{\mathbf{q}_1} + \hbar\omega_{\mathbf{q}_2} b^\dagger_{\mathbf{q}_2} b_{\mathbf{q}_2}$ and $\xi(t) = \frac{i}{\hbar}\int_{-\infty}^{t} \zeta(\tau) e^{i(\omega_{\mathbf{q}_1} + \omega_{\mathbf{q}_2})\tau} d\tau$. Here $\xi(t)$ is the squeezing factor, and $\zeta(t)$ is the strength of the interaction between the phonon system and the external source; this interaction allows the generation and absorption of two phonons at a time.

[6]The following single-mode anharmonic Hamiltonian $H = \hbar\omega_{\mathbf{q}} b^\dagger_{\mathbf{q}} b_{\mathbf{q}} + \hbar\lambda_{\mathbf{q}} (b^\dagger_{\mathbf{q}} b_{\mathbf{q}})^2$ also produces squeezed phonons in mode $\mathbf{q}$ when the initial state is coherent.

interactions because they are generally much weaker than the third-order ones. For all parametric processes, the pump wave (of phonons in this case) must be very strong because the generic parametric processes are generally nonlinear and weak. This pumping process can be realized by using two pulse lasers to illuminate a crystal. With appropriate laser frequencies and directions, coherent LO phonons of the pump mode at the Brillouin-Zone-center can be generated through, for example, stimulated Raman scattering (provided that the pump mode is Raman active), as discussed, e.g., in Refs. [60, 35].

The Hamiltonian for the whole process initiated by the Raman scattering is (see Fig. 3.1)

$$\begin{aligned} H_{\rm param} &= H_0 + H_{\rm Raman} + H_{\rm anh} \qquad (2.14) \\ H_0 &= \hbar\omega_{\mathbf{k}_1} a^\dagger_{\mathbf{k}_1} a_{\mathbf{k}_1} + \hbar\omega_{\mathbf{k}_2} a^\dagger_{\mathbf{k}_2} a_{\mathbf{k}_2} + \sum_{\mathbf{q}} \hbar\omega_{\mathbf{q}} b^\dagger_{\mathbf{q}} b_{\mathbf{q}} \\ H_{\rm Raman} &= \eta a_{\mathbf{k}_1} a^\dagger_{\mathbf{k}_2} b^\dagger_{\mathbf{q}_p} + \eta^* a^\dagger_{\mathbf{k}_1} a_{\mathbf{k}_2} b_{\mathbf{q}_p} \\ H_{\rm anh} &= \lambda_{\mathbf{q}_s\mathbf{q}_i} b_{\mathbf{q}_p} b^\dagger_{\mathbf{q}_s} b^\dagger_{\mathbf{q}_i} + \lambda^*_{\mathbf{q}_s\mathbf{q}_i} b^\dagger_{\mathbf{q}_p} b_{\mathbf{q}_s} b_{\mathbf{q}_i} \\ &\quad + \sum_{\mathbf{q}'\mathbf{q}''} (\lambda_{\mathbf{q}'\mathbf{q}''} b_{\mathbf{q}_p} b^\dagger_{\mathbf{q}'} b^\dagger_{\mathbf{q}''} + \lambda^*_{\mathbf{q}'\mathbf{q}''} b^\dagger_{\mathbf{q}_p} b_{\mathbf{q}'} b_{\mathbf{q}''}) \,. \end{aligned}$$

Here a (b) refer to photon (phonon) operators. The higher- (lower-) energy incident photon mode is labeled by $\mathbf{k}_1$ ($\mathbf{k}_2$). Notice that the lower energy photon mode is generally called Stokes mode in the context of Raman scattering. The sums over $\mathbf{q}'$ and $\mathbf{q}''$ in $H_{\rm anh}$ represent decay channels other than the special one with acoustic signal and idler modes.

We now consider two mean field averages in order to simplify an otherwise analytically intractable problem. The first mean field is over the photons. The photons in the incident modes $\mathbf{k}_1$ and $\mathbf{k}_2$ (often denoted by "laser" and "Stokes" light) originate from two lasers. As long as these two incident laser modes are not strongly perturbed by the Raman scattering process, we can treat both of these incoming photon states as coherent states $|\alpha_{\mathbf{k}_1} e^{-i\omega_{\mathbf{k}_1} t}\rangle$ and $|\alpha_{\mathbf{k}_2} e^{-i\omega_{\mathbf{k}_2} t}\rangle$, and perform a mean field average over them. The second mean field average is over the LO pump mode phonons. Since phonons produced by coherent or stimulated Raman scattering are initially in coherent states, we denote this pump mode phonon coherent state as $|\beta_0(t)\rangle$, with $\langle\beta_0(t)|b_{\mathbf{q}_p}|\beta_0(t)\rangle = \beta_0(t)$. Since these LO phonons are in coherent states, the results from the average over the pump mode phonons are c-numbers with a well-behaved time-dependence. Now we drop all the c-number terms because they will not affect our results. In addition, we will also drop all the phonon modes involved in the decay channels other than the special one consisting of the signal modes, considering them only weakly coupled to the pump mode; i.e., we assume $\lambda_{\mathbf{q}'\mathbf{q}''} \ll \lambda_{\mathbf{q}_s\mathbf{q}_i}$.

The Hamiltonian now becomes

$$\begin{aligned} H'_{\rm param} &= \hbar\omega_{\mathbf{q}_s} b^\dagger_{\mathbf{q}_s} b_{\mathbf{q}_s} + \hbar\omega_{-\mathbf{q}_s} b^\dagger_{-\mathbf{q}_s} b_{-\mathbf{q}_s} \\ &+\lambda_{\mathbf{q}_s,-\mathbf{q}_s}\,\beta_0(t)\, b^\dagger_{\mathbf{q}_s} b^\dagger_{-\mathbf{q}_s} + \lambda^*_{\mathbf{q}_s,-\mathbf{q}_s}\,\beta^*_0(t)\, b_{\mathbf{q}_s} b_{-\mathbf{q}_s}, \end{aligned} \tag{2.15}$$

where $\beta_0(t)$ is the coherent amplitude of the pump mode phonons. We use $H_0 + H_{\rm Raman}$ to determine $\beta_0(t)$, and then substitute it back into $H_{\rm param}$ to obtain $H'_{\rm param}$. Here we have implicitly assumed that the Raman scattering process is stronger than the anharmonic scattering. According to our previous discussion, the two-mode LA phonon system will evolve into a two-mode squeezed state $|\alpha_{\mathbf{q}_s}, \alpha_{-\mathbf{q}_s}, \xi(t)\rangle$ from an initial coherent or vacuum state, with a squeezing factor of

$$\xi(t) = \frac{i}{\hbar}\int_0^t \lambda_{\mathbf{q}_s,-\mathbf{q}_s}\,\beta_0(\tau)\, e^{2i\omega_{\mathbf{q}_s}\tau} d\tau\,. \tag{2.16}$$

which is only valid in the very short time limit (i.e., small t).

In summary, we have just considered generating two-mode LA phonon squeezed states $|\alpha_{\mathbf{q}_s}, \alpha_{-\mathbf{q}_s}, \xi(t)\rangle$ by using the three-phonon anharmonic interaction.[7] The higher-energy LO phonon mode, which is called the "pump" mode, is driven into a coherent state through stimulated Raman scattering. This mode in turn is used as a pump in the parametric amplification process involving itself and the two lower-energy LA phonon modes ($\pm\mathbf{q}_s$), the signal and the idler. Both of these modes can here be called "signal" because the "idler" mode is not really "idle"; indeed, it is actively involved in the squeezing process. In conclusion, we have shown that the LA phonons in the two signal modes ($\pm\mathbf{q}_s$) are in a two-mode squeezed state if (i) the LO pump mode is in a coherent state and (ii) we can neglect the other decay channels.

2.4 Polariton Approach

So far we have studied phonon squeezing through phonon-phonon interactions. Here we focus on how to squeeze quantum noise in the atomic displacements using an alternative and quite different approach: through phonon-photon interactions. The essential idea is that the incident (coherent or squeezed) photons introduce a correlation between the $\pm\mathbf{k}$ phonon modes. This correlation can produce suppression of quantum noise in the atomic displacements of the lattice.

[7] We have also studied a second-order Raman scattering process. Similar to the phonon parametric process, if the two incident light beams are in coherent states, the acoustic phonons generated by the second-order Raman scattering are in a two-mode squeezed state. A mean field average over the photons is also required in this case.

When an ionic crystal is illuminated by light, there can be a strong coupling between photons and the local polarization of the crystal in the form of transverse optical (TO) phonons. Photons and TO phonons with the same wave vector can thus form polaritons [78]. Although now phonons and photons are not separable in a polariton, we can still study the quantum noise in the atomic displacements. Let us consider the simplest Hamiltonian [78] describing the above scenario: $H_{\rm polariton} = \sum_{\mathbf{k}} \left\{ E_{1\mathbf{k}}\, a_{\mathbf{k}}^{\dagger} a_{\mathbf{k}} + E_{2\mathbf{k}} b_{\mathbf{k}}^{\dagger}\, b_{\mathbf{k}} + E_{3\mathbf{k}} \left(a_{\mathbf{k}}^{\dagger} b_{\mathbf{k}} - a_{\mathbf{k}} b_{\mathbf{k}}^{\dagger} - a_{\mathbf{k}} b_{-\mathbf{k}} + a_{-\mathbf{k}}^{\dagger} b_{\mathbf{k}}^{\dagger} \right) \right\}$, where $E_{1\mathbf{k}} = \hbar ck$, $E_{2\mathbf{k}} = \hbar\omega_0\sqrt{1+\chi}$, and $E_{3\mathbf{k}} = i\left(\hbar^2 ck\omega_0\chi/4\sqrt{1+\chi}\right)^{1/2}$. Here $\mathbf{k}$ is the wave vector for both photons and phonons and ω_0 is the bare phonon frequency. χ is the dimensionless dielectric susceptibility of the crystal (the strength of the phonon-photon interaction) defined by $\chi\omega_0^2\varepsilon_0\mathbf{E} = \ddot{\mathbf{P}} + \omega_0^2\mathbf{P}$, where $\mathbf{E}$ is the electric field of the incoming light and $\mathbf{P}$ is the polarization generated by optical phonons in the crystal. In $H_{\rm polariton}$, the two free oscillator sums correspond to free photons and free phonons, while the mixing terms come from the interaction $\mathbf{E}\cdot\mathbf{P}$ between photons and phonons. The phonon energy $E_{2\mathbf{k}}$ has been corrected, as ω_0 is substituted by $\omega_0\sqrt{1+\chi}$, so that we have "dressed" phonons.

Our goal is to compute the fluctuations of the lattice amplitude operator $u(\pm\mathbf{k},t) = b_{\mathbf{k}}(t) + b_{-\mathbf{k}}^{\dagger}(t) + b_{-\mathbf{k}}(t) + b_{\mathbf{k}}^{\dagger}(t)$. In a two-mode ($\pm\mathbf{k}$) coherent state $|\alpha_{\mathbf{q}},\, \alpha_{-\mathbf{q}}\rangle$, its variance is $\langle[\Delta u(\pm\mathbf{q})]^2\rangle_{\rm coh} = 2$. Therefore, if at any given time we obtain a value less than 2, the lattice amplitude of the relevant mode is squeezed. In our calculation, we diagonalize the polariton Hamiltonian and find the time-dependence of $u(\pm\mathbf{q})$. The Appendix D presents in more detail the derivation of the time-evolution of $u(\pm\mathbf{q})$.

Our results show that the fluctuation property of $u(\pm\mathbf{q})$ sensitively depends on the $t = 0$ initial state $|\psi(0)\rangle$ of both TO phonons and photons. Our results are summarized in Table 3.2, and some numerical examples are shown in Fig. 3.7. These calculations focus on the case where ck is close to ω_0 (the bare phonon frequency, which is typically ~ 10 THz for optical phonons) and thus our typical time is ~ 0.1 ps. More specifically, squeezing effects in $u(\pm\mathbf{k})$ are relatively strong for either one of the following two sets of $t = 0$ initial states: (i) photon and phonon coherent states, or (ii) single-mode photon squeezed state and phonon vacuum state. For instance, the maximum squeezing exponent r is 0.015 when the incident photon state has a squeezing factor $\xi = 0.1e^{2ickt}$ (where ck is the photon frequency). On the other hand, with an initial two-mode photon ($\pm\mathbf{k}$) squeezed state and two-mode ($\pm\mathbf{k}$) phonon vacuum state, the squeezing effect in $u(\pm\mathbf{k})$ is weak. We have also used initial conditions with a single-mode photon squeezed state and thermal states in the two phonon

modes.

Figure 3.8 shows the temperature dependence of the squeezing effect for several values of the dielectric susceptibility χ of the crystal. Our numerical results show that squeezing effects are overshadowed by the thermal noise for small χ, while for larger χ (e.g., $\chi = 0.5$) the squeezing effect can exist up to $T \approx 250$ K, as illustrated in Fig. 3.8.

2.5 Detection Schemes

It is possible to directly detect a single-mode phonon squeezed state with phonon counters [24, 77] such as superconducting tunnel junction bolometers and vibronic detectors. The signature of a single-mode squeezed state is a sub-Poissonian phonon number distribution in that mode. However, these phonon counters are either wide-band, or have low efficiency. Therefore, direct detection might not be the best method to detect the squeezing effect.

Phase-sensitive schemes such as homodyne and heterodyne detectors are most often used to detect photon squeezed states because of their ability to lock phase with the electric field of the measured state [58]. There appears to be no available phase-sensitive detection method for phonons. A promising candidate might be measuring the intensity of a reflected probe light [35]. This method has already been used to detect phonon amplitudes, since the reflectivity is linearly related to the atomic displacements in a crystal. The value of the lattice amplitude operator can be extracted by making a Fourier analysis on the sample reflectivity. If squeezing should happen, its effect will be contained in the Fourier components of the intensity of the reflected light. In this manner the information on the squeezing effect in the phonons is also carried by the reflected light in the form of squeezing of the photon intensity. We can then use a standard optical detection method to determine whether the related light is squeezed or not. One shortcoming of this method is that it is not direct. In the measurement there can be noise added into the signal, such as the intensity fluctuation of the original probe light, the efficiency for the reflected light to pick up the signals in the phonons, etc. Needless to say, further research needs to be done on how to realize this phase-sensitive detection scheme, and we hope that our initial proposals stimulate further theoretical and experimental work on this problem.

2.6 Discussion

Phonon squeezing depends on the absolute value r and also on the phase θ of the squeezing factor $\xi(t) = re^{i\theta}$. More explicitly,

$$\langle(\Delta u(\pm\mathbf{q}))^2\rangle_{\rm sq} = 2\left(e^{-2r}\cos^2\frac{\theta}{2} + e^{2r}\sin^2\frac{\theta}{2}\right). \tag{2.17}$$

Only when θ is close to 0 is noise suppressed in the lattice amplitude operator. This means that in order to suppress the noise, the squeezing factor $\xi(t)$ has to have a dominant positive real part so that $\cos\theta > \tanh r$. The squeezing factor obtained from the three-phonon process is $\xi(t) = \frac{i}{\hbar}\int_0^t \lambda\,\alpha(\tau)\,e^{i(\omega_s+\omega_i)\tau}d\tau$, where the real number λ is the strength of the interaction and α is the amplitude of the phonon coherent state in the pump mode. From this expression for $\xi(t)$ we can see that the squeezing effect only appears during certain time intervals. If $\alpha(t)$ does not depend on time or has a periodic dependence on time, squeezing will be periodic in time, which makes phase-sensitive detection easier to achieve.

To make the above schemes work, some noise problems have to be overcome. First, any attempt to generate or detect squeezed states should be at low temperatures to avoid thermal noise in the crystal. For instance, the excitation energy of a 10THz optical phonon corresponds to a temperature of about 100K. Therefore, the experiment might have to be carried out at a temperature well below 100K, such as 10K or lower. Second, the fluctuations in the laser intensity and in the interaction between the laser and the crystal has to be very small, so that they will not suppress the noise reduction process in the squeezing effect. Indeed, one of the possible ways to reduce the noise coming from the laser beam is to use a beam of squeezed photons. Finally, the incoherence in the procedure itself has to be minimized. For example, the finite lifetime of pump mode phonons does not favor the generation of squeezed states because it gives rise to an additional noise in the intensity of the mode. Therefore, we need long lifetime LO phonons, which can be realized in, for instance, materials with weak anharmonic interactions and low concentration of isotopic defects (e.g., diamond). Furthermore, here we have studied a discrete-mode phonon parametric process. A continuous-mode model will be discussed elsewhere.

2.7 Conclusions

We have investigated the dynamics and quantum fluctuation properties of phonon squeezed states. In particular, we calculate the experimentally observable time evolution and fluctuation of the lattice amplitude operator $u(\pm\mathbf{q})$, and show that $\langle u(\pm\mathbf{q})\rangle_{\rm sq}$ is a sinusoidal

function of time, while $\langle(\Delta u(\pm\mathbf{q}))^2\rangle_{\rm sq}$ is periodically smaller than the vacuum and coherent state value 2. In other words, phonon squeezed states are periodically quieter than the vacuum state. Here we have summarized two approaches to generate phonon squeezed states.

The first approach is based on a three-phonon process where the higher energy optical phonon mode is coherently pumped. We show that the two lower-energy acoustic phonon modes, with the phonons produced by the decay of the higher energy optical coherent phonons, can be in a two-mode phonon quadrature squeezed state given appropriate initial conditions. We achieve this by dealing separately with (*i*) the optical excitation of the pump mode optical phonons and (*ii*) the anharmonic scattering of the pump mode phonons into the lower-energy acoustic phonons.

The second approach to generate phonon squeezed states is based on polaritons, which are mixtures of phonons and photons. Squeezing is achieved because of the correlation between $\pm\mathbf{k}$ mode phonons introduced by the incident (coherent or squeezed) phonons.

We have also briefly analyzed a potential detection method of phonon squeezed states. Experiments in quantum optics indicate that phase-sensitive methods—such as homodyne detection—are the best in detecting photon squeezed states. Therefore, we have proposed a detection scheme based on a reflected probe light and an ordinary phase-sensitive optical detector.

Like in the photon case [11], the experimental realization of phonon squeezed states might require years of work after its initial proposal. We hope that our effort will lead to more theoretical and experimental explorations in the area of phonon quantum noise manipulation.

Chapter 3

Quantum Phonon Optics: Modulating Quantum Fluctuations of Atomic Displacements

3.1 Introduction

3.1.1 Classical Incoherent-Phonon Optics

Classical phonon optics [24, 25, 26] has succeeded in producing many acoustic analogs of *classical optics*, such as phonon mirrors, phonon lenses, phonon filters, and even phonon microscopes [27] that can generate acoustic pictures with a resolution comparable to that of visible light microscopy. Most phonon optics experiments use heat pulses or superconducting transducers to generate *incoherent* phonons, which propagate ballistically in the crystal. These ballistic incoherent phonons can then be manipulated by the above-mentioned devices, just like in geometric optics.

3.1.2 Classical Coherent-Phonon Optics

Phonons can also be excited *phase-coherently.* For instance, coherent acoustic waves with frequencies of up to 10^{10}Hz can be generated by piezoelectric oscillators [28]. Lasers have also been used to generate coherent acoustic and optical phonons through stimulated Brillouin and Raman scattering experiments [29, 30, 31].

To detect the time-domain dynamic behavior of molecules and crystals, pump-probe techniques with picosecond laser pulses were developed by various groups (see [32] and references therein). One of these pump-probe schemes, Time-Resolved Coherent Anti-Stokes Raman Scattering (TRCARS) [33, 34], has been used to generate and observe coherent phonons in semiconductors. These experiments provide useful information on the dynamics

of the relevant phonon states and the electronic response to a nonlinear laser excitation. However, limited by its time-resolution of the order of 10^{-12} seconds, this technique (TR-CARS) cannot be used to make time-domain pictures of coherent phonons.

In recent years, it has been possible for the first time to track the phases of coherent optical phonons [35], due to the availability of femtosecond-pulse ultrafast lasers (with a pulse duration shorter than a phonon period) [36], and techniques that can measure optical reflectivity with accuracy of one part in 10^6 (see, e.g., Refs. [37, 38, 39]). Early on, the observations of the phases of coherent optical phonons were made in dyes and molecular crystals [40, 41, 42], and were explained using the theory of Impulsive Stimulated Raman Scattering (ISRS). More recently, coherent optical phonons were also generated and observed in metals [43], semiconductors [44, 45], and high temperature superconducting films [46]. Furthermore, femtosecond lasers have been used to generate coherent zone-folded acoustic phonons in superlattices [47].

The time-domain tracking techniques mentioned above provide quantitative information on the evolution of the dielectric properties of the solid, which reflect the phase dynamics of the ionic displacements. The dielectric function can be measured with high precision in reflectivity or transmission experiments [35].

The time-domain observation of coherent phonons has important implications in phonon physics. It provides a much better spectroscopic resolution compared to spontaneous Raman scattering for the study of low-frequency phonon modes. It also provides an opportunity to study the high-frequency phonon modes [52]. Tracking dephasing processes down to sub-picosecond time scales presents a unique insight into the interaction between specific phonon modes and the electronic continuum and other elementary excitations. Furthermore, the study of optically excited coherent phonons leads to a better understanding of symmetry in the lattice and the phonon-electron interaction [52]. It also provides a novel determination of the Debye-Waller factor, a test of the mode coupling theory [53], and a direct measurement of Raman tensor components [41].

Coherent phonons can also lead to changes in the physical properties of various systems. For instance, coherent phonons directly modulate the electron energy bands through a deformation potential and the electro-optic coupling [49]. Their behavior is important in connection with many lattice instabilities including structural phase transitions, chemical reactions, and melting [54]. For instance, it has also been proposed [48] to use coherent optical phonons to induce a Peierls distortion and thus generate charge-density-waves in

quantum wire networks. Coherent phonons can induce large amplitude atomic motion, therefore driving the phonon system out of equilibrium and providing a tool for micro-ferroelectric-domain switching [55]. The later opens the possibility of future optoelectronic control of micro-domains, which are considered a possible substitute for magnetic domains in memory chips.

Different generating mechanisms have been proposed to explain these coherent optical phonon experiments. One of these mechanisms, ISRS, is a Raman scattering process [41] which is valid for insulators, where no free carriers are present. There are also theories in which free carriers are important [49, 50, 51]. Among them, the theory of the Displacive Excitation of Coherent Phonons (DECP) [49] considers the displaced electronic distribution as the driving force for the phonons, and the theory of Ultrafast Screening of Surface Charge Field (USSCF) [44, 50] considers the free carrier current as the major driving force.

It is a difficult task to explain the detailed mechanisms on how coherent phonons are generated in several types of materials. Such an explanation requires simultaneous consideration of a number of interacting quantities including the exciting light field, the time-dependent distributions of electrons and holes, and the longitudinal optical phonon amplitude [56].

3.1.3 Coherent and Squeezed Quantum Phonon States: Modulating the Quantum Fluctuations of Atomic Displacements

In most situations, a classical description is adequate to describe macroscopic physical phenomena in condensed matter, where *thermal* noise is much larger than any *quantum* noise so that the later can be neglected. However, at low temperatures coherent effects (e.g., Bose-Einstein condensation of atoms [13]) and quantum noise can play a crucial role. For instance, Josephson junctions provide an example of macroscopic quantum coherent phenomenon, where quantum fluctuations can be important. Moreover, a recent study [15] shows that quantum noise in the atomic positions can indeed influence observable quantities (e.g., the Raman line-shape) even when temperatures are not very low. With these facts in mind, and prompted by the many interesting developments in *classical* phonon optics and the recent exciting results in coherent phonon experiments, we would like to explore some phonon analogs of *quantum* optics. Specifically, we want to study coherent and squeezed *quantum* phonon states.

There are several types of phonon quantum states mentioned in this paper. The phonon vacuum state refers to the state in which no phonon is excited. However, due to the

zero-point fluctuations of the atoms, the atomic displacement operator still has a finite uncertainty in this state. The phonon number state $|n\rangle$ describes the situation where exactly n phonons are excited. Also, the vacuum and number states are both eigenstates of a non-interacting phonon system. A phonon coherent state is a phase-coherent sum of all the phonon number states. It is a quantum state that can best describe the classical behavior of a system. In addition, the quantum fluctuations in a phonon coherent state are as small as the ones in the phonon vacuum state. Finally, a phonon squeezed state is a generalized phonon coherent state. The difference between them is that a squeezed state can have a smaller quantum noise than the coherent state level in one of the conjugate variables. Below, we will explain the properties of all the above quantum states in more detail.

The concepts of coherent and squeezed states were both first proposed in the context of quantum optics. The experimental advances during the early days of lasers led to extensive theoretical research, and eventually to the first systematic description of photon coherent states in the early sixties [7]. Years later, and after much research on the quantum fluctuation properties of coherent states, squeezed states of photons were theoretically proposed [8, 9]. Their experimental realization occurred about ten years later [10] and it has attracted widespread attention [11]. Squeezed states are interesting because they can have *smaller quantum noise than coherent states*, thus having a promising future in different applications ranging from gravitational wave detection to optical communications [11]. In addition, squeezed states form a new and exciting group of states and can provide unique insight into quantum mechanical fluctuations. Indeed, squeezed states are now being explored in a variety of non-quantum-optics systems, including classical squeezed states [16, 17].

In this chapter we study the dynamics and quantum fluctuation properties of coherent and squeezed phonon states. We have calculated the experimentally-observable time-evolution and fluctuations of the lattice amplitude operator $u(\pm\mathbf{q}) = b_{\mathbf{q}} + b^{\dagger}_{-\mathbf{q}} + b^{\dagger}_{\mathbf{q}} + b_{-\mathbf{q}}$ in various phonon states. We show that the averages $\langle u(\pm\mathbf{q})\rangle$ are sinusoidal functions of time in both coherent and squeezed states, but for squeezed states the fluctuation $\langle(\Delta u(\pm\mathbf{q}))^2\rangle$ is periodically smaller than its coherent state value 2, which is also the vacuum state noise level. Therefore, phonon squeezed states are periodically quieter than the vacuum state.

Our analytical results cannot be obtained without several simplifications of the most complete models. In particular, we study single-mode and two-mode phonon states throughout this paper, while in a generic crystal lattice, phonon modes are crowded together. How-

ever, as pointed out in Refs. [58, 59], a theory dealing only with a single mode or two modes is adequate when the detection scheme is sophisticated enough to choose the mode (or modes) of interest. Therefore, here we focus on such a single-mode and two-mode theory. This will serve as a first stepping stone to a more complete approach. In the text below, we will describe the approximations used and their ranges of validity. A more complete and realistic treatment is extremely hard to do *analytically* because of the complexities in the real lattice potential—e.g., its nonlinearities and anisotropies.

It is difficult to generate squeezed states because they have noise levels which are even lower than the one for the vacuum state. Indeed, the experimental and theoretical development of photon coherent and squeezed states took decades. Likewise, the experimental realization of phonon squeezed states might require years of further theoretical and experimental work. Nevertheless, we believe that theoretical results in quantum phonon optics can help the development of the corresponding experiments. We hope that our effort [18, 19, 20, 21], which is only a glimpse into a very rich and new field, will lead to more theoretical and experimental developments in the still unexplored area of quantum phonon optics and the "manipulation" of phonon quantum fluctuations.

3.1.4 Overview of this Chapter

The plan of the chapter is as follows. In Section 3.2 we list several analogies and differences between phonons and photons; these will be taken into account in our discussions. Since there are several differences between these two kinds of bosons, it is not possible to do a simple and straightforward transplant of ideas from quantum optics to phonon physics.

Section 3.3 introduces definitions and notation which will be used throughout this work. Furthermore, it studies the general properties of both coherent and squeezed phonon states.

The modulation of quantum fluctuations is, for the time being, nontrivial to realize in a laboratory setting. Thus, it is important to study not one but *several* alternative approaches to manipulate quantum fluctuations. In Sections 3.4 and 3.5, we propose four different methods to generate squeezed states. These approaches are based on a variety of physical processes, including three-phonon interactions, number-conserving single-mode phonon-phonon interactions, second-order Raman scattering, and photon-phonon interactions that lead to polaritons. In Section 3.6 we propose a possible detection scheme. Finally, Section 3.7 discusses several limitations of our proposals.

3.2 Analogies and Differences between Phonons and Photons

Coherent and squeezed states were initially introduced to describe photons [60, 61]. Here we are interested in applying these concepts to phonons. Although both photons and phonons are bosons, they do have significant differences, and the physics of squeezed states of light cannot be straightforwardly extended to phonons. For example, photons have zero mass, and all our results do have a *mass* in them. This mass cannot be set to zero, because it is often located in denominators. Thus, the straightforward $M \rightarrow 0$ limit does not work here. This is a very significant difference in the physics and the analytical results. Table 3.1 presents a brief comparison between phonons and photons. Below we mention a few important similarities and differences that are relevant to our study.

Photons are elementary particles with no internal structure, thus are sometimes called simple bosons. On the other hand, phonons describe the collective displacements of very many atoms in a crystal, and are thus sometimes described as composite bosons [62]. Phonons are bosons because of the commutation relation between the coordinate and momentum operators. Kohn and Sherrington [62] pioneered the research on composite bosons like phonons, excitons, etc., and classified them into two categories, with type-I referring to those bosons composed of an even number of fermions (such as ^{4}He atoms), and type-II referring to those that are collective excitations—such as phonons, excitons, magnons, etc. In this sense it is also possible to consider photons to be type-II composite bosons [62], because they are the energy quanta of electromagnetic field modes. Their commutation relation originates from the simple harmonic oscillators that are used to quantize the electromagnetic field. Essentially, both photons and phonons are field quanta: photons are quanta of a continuous field, while phonons are quanta of a discrete field.

Non-interacting phonons are used to describe harmonic crystal potentials. However, anharmonicity, which leads to phonon-phonon interactions, is always present. Some properties of solids, such as lattice heat conductivity and thermal expansion, solely depend on the anharmonic terms in the crystal potential. In other words, phonons in general interact with each other. For photons, the situation is somewhat different. In vacuum and at low intensity, photon interactions are so weak that the rule of linear superposition holds. However, in nonlinear media, photons are effectively interactive, with their interaction mediated by the atoms.

As mentioned above, phonons exist in discrete media. Therefore, phonons have cut-off frequencies, which put an upper-limit to their energy spectra. For a diatomic lattice, this

limit is of the order of 0.1 eV, which is in the infrared region. Photons, on the other hand, do not have such an upper bound for their energy. In addition, the discrete atomic lattice and the massive atoms lead to a finite zero-point fluctuation in the phonon field, while the continuous photon modes and the massless photons contribute to a divergent zero-point fluctuation in the photon field.

The dispersion relations for photons and phonons are qualitatively different. Photons in free space have a linear dispersion relation. On the other hand, phonons have complicated nonlinear dispersion relations which generally have several acoustic and optical branches. The acoustic branches are linear around the center of the first Brillouin zone, i.e., the $\mathbf{k} = 0$ point, which is at the continuum limit. When the quasi-wave-vector $\mathbf{k}$ is close to the first Brillouin zone boundary, ω saturates. The optical branches of the phonons have a different profile. Their dispersion relations are flat near $\mathbf{k} = 0$, where $\omega = \omega_0$. Furthermore, as $\mathbf{k}$ increases, ω decreases; indeed, the optical phonon dispersion relation can be even more complicated depending on the lattice structure. Compared to photons, with their simple linear dispersion relations, phonons have nonlinear dispersion relations that make it more difficult to satisfy both energy and momentum (in fact, quasi-momentum) conservation laws simultaneously.

The order of magnitude of the crystal cohesion energy determines that phonons have very low energies. Therefore, phonons can easily couple to many other excitations which are in a similar energy range, and be perturbed by thermal fluctuations even at low temperatures. All these couplings make phonon dynamics very dissipative. Due to its strong damping, coherent phonons have very short lifetimes ($\sim$ 1 picosecond for optical phonons, while larger for acoustic phonons) [35]. On the other hand, there exist many materials in which photons can propagate with little dissipation, and furthermore very long photon coherent times can be produced by lasers [60].

To summarize this brief comparison, we notice that the differences between phonons and photons can both help and hinder our effort to apply ideas originating in quantum optics to phonons. On the one hand, anharmonicity leads to nonlinear interactions between phonons, which can be helpful when we try to "mix" phonons. On the other hand, short phonon lifetimes and the strongly dissipative environment of phonons are negative factors. These will be taken into consideration when we work on the theory.

	Phonon	Photon
Type of boson	type-II composite	simple
Propagating media	discrete	continuous
Interactions	highly interactive	interactive in nonlinear media, noninteractive in linear media
Mass	massive	massless
Macroscopic description	wave equation for elastic continuum	Maxwell equations
Microscopic description	Schrödinger equation	Quantum Electrodynamics
Number of normal modes per allowed $\mathbf{k}$	$3p$ modes for each $\mathbf{k}$	2 modes for each $\mathbf{k}$
Dispersive ?	always: $\omega = \omega_s(\mathbf{k})$	not in vacuum: $\omega = ck$
Restriction on wave vector $\mathbf{k}$	confined to 1st Brillouin zone	arbitrary
Linear momentum	vanishes	non-zero
Spin	not defined	s = 1

Table 3.1: Comparison of several physical properties of phonons and photons

3.3 Phonon Quantum States: General Properties

3.3.1 Phonon Operators

In this section we introduce definitions and notation which will be used throughout this work. It is well known that phonons are energy quanta of the atomic oscillations in a perfect crystal. Under the harmonic approximation, the Hamiltonian for the vibrational degrees of freedom of a perfect and isolated lattice is

$$H_{\text{harmonic}} = \sum_{\mathbf{q}\lambda} \hbar\omega_{\mathbf{q}\lambda} \left(b^{\dagger}_{\mathbf{q}\lambda}\, b_{\mathbf{q}\lambda} + \frac{1}{2} \right), \tag{3.1}$$

which represents a series of independent oscillators. A phonon with quasi-momentum $\mathbf{p} = \hbar\mathbf{q}$ and branch subscript λ has energy $\epsilon_{\mathbf{q}\lambda} = \hbar\omega_{\mathbf{q}\lambda}$. The creation and annihilation operators for a phonon of momentum $\mathbf{q}$ in the branch λ are $b^{\dagger}_{\mathbf{q}\lambda}$ and $b_{\mathbf{q}\lambda}$. They satisfy the boson commutation relations:

$$[b_{\mathbf{q}'\lambda'},\ b^{\dagger}_{\mathbf{q}\lambda}] = \delta_{\mathbf{q}\mathbf{q}'}\delta_{\lambda\lambda'}\ , \quad [b_{\mathbf{q}\lambda},\ b_{\mathbf{q}'\lambda'}] = 0\ . \tag{3.2}$$

The lattice atomic displacements $u_{i\alpha}$ and velocities $\dot{u}_{i\alpha}$ are related to the phonon operators $b_{\mathbf{q}\lambda}$ and $b^{\dagger}_{\mathbf{q}\lambda}$ through the following relations:

$$u_{i\alpha} = \frac{1}{\sqrt{Nm}} \sum_{\mathbf{q}\lambda}^{N} U^{\lambda}_{\mathbf{q}\alpha} Q^{\lambda}_{\mathbf{q}} e^{i\mathbf{q}\cdot\mathbf{R}_i}$$

$$= \frac{1}{\sqrt{Nm}} \sum_{q_x>0\,\lambda}^{N} U^{\lambda}_{\mathbf{q}\alpha} \left(Q^{\lambda}_{\mathbf{q}} e^{i\mathbf{q}\cdot\mathbf{R}_i} + Q^{\lambda}_{-\mathbf{q}} e^{-i\mathbf{q}\cdot\mathbf{R}_i} \right)$$

$$= \frac{1}{\sqrt{Nm}} \sum_{\mathbf{q}\,\lambda}^{N} \sqrt{\frac{\hbar}{2\omega_{\mathbf{q}\lambda}}} \left(U^{\lambda}_{\mathbf{q}\alpha} e^{i\mathbf{q}\cdot\mathbf{R}_i} b_{\mathbf{q}\lambda} + U^{\lambda\,*}_{\mathbf{q}\alpha} e^{-i\mathbf{q}\cdot\mathbf{R}_i} b^{\dagger}_{\mathbf{q}\lambda} \right), \tag{3.3}$$

$$\dot{u}_{i\alpha} = \frac{-i}{\sqrt{Nm}} \sum_{\mathbf{q}\,\lambda}^{N} \sqrt{\frac{\hbar\omega_{\mathbf{q}\lambda}}{2}} \left(U^{\lambda}_{\mathbf{q}\alpha} e^{i\mathbf{q}\cdot\mathbf{R}_i} b_{\mathbf{q}\lambda} - U^{\lambda\,*}_{\mathbf{q}\alpha} e^{-i\mathbf{q}\cdot\mathbf{R}_i} b^{\dagger}_{\mathbf{q}\lambda} \right), \tag{3.4}$$

$$Q^{\lambda}_{\mathbf{q}} = \sqrt{\frac{\hbar}{2\omega_{\mathbf{q}\lambda}}} \left(b_{\mathbf{q}\lambda} + b^{\dagger}_{-\mathbf{q}\lambda} \right), \tag{3.5}$$

$$U^{\lambda\,*}_{-\mathbf{q}\alpha} = U^{\lambda}_{\mathbf{q}\alpha}. \tag{3.6}$$

Here $\mathbf{R}_i$ refers to the equilibrium lattice positions, α refers to a particular direction, and $Q^{\lambda}_{\mathbf{q}}$ is the normal-mode amplitude operator. The condition on the polarization vector $\mathbf{U}$ is a result of the requirement that the atomic displacement $u_{i\alpha}$ is Hermitian.

A physically interesting quantity is the Fourier transform of the atomic displacement. Since

$$\sum_{\mathbf{R}_i} \frac{e^{i\mathbf{q}\cdot\mathbf{R}_i}}{\sqrt{N}} \frac{e^{-i\mathbf{q}'\cdot\mathbf{R}_i}}{\sqrt{N}} = \delta_{\mathbf{q}\mathbf{q}'}, \tag{3.7}$$

we can use $e^{i\mathbf{q}\cdot\mathbf{R}_i}/\sqrt{N}$ as normalized orthogonal basis. Thus the Fourier transform of the atomic displacement takes the form

$$u_{\alpha}(\mathbf{q}) = \sum_{\mathbf{R}_i} u_{i\alpha} \frac{e^{-i\mathbf{q}\cdot\mathbf{R}_i}}{\sqrt{N}}$$

$$= \frac{1}{\sqrt{m}} \sum_{\lambda} U^{\lambda}_{\mathbf{q}\alpha} Q^{\lambda}_{\mathbf{q}} \tag{3.8}$$

$$= \sum_{\lambda} \sqrt{\frac{\hbar}{2m\omega_{\mathbf{q}\lambda}}} U^{\lambda}_{\mathbf{q}\alpha} \left(b_{\mathbf{q}\lambda} + b^{\dagger}_{-\mathbf{q}\lambda} \right), \tag{3.9}$$

which is directly related to the normal-mode amplitude $Q^{\lambda}_{\mathbf{q}}$. Notice that $u_{\alpha}(\mathbf{q})$ is not Hermitian, thus it cannot be observed. The quantity which is experimentally observable is the real part of $u_{\alpha}(\mathbf{q})$:

$$Re\left(u_{\alpha}(\mathbf{q})\right) = \sum_{\lambda} \sqrt{\frac{\hbar}{8m\omega_{\mathbf{q}\lambda}}} \left\{ U^{\lambda}_{\mathbf{q}\alpha} \left(b_{\mathbf{q}\lambda} + b^{\dagger}_{-\mathbf{q}\lambda} \right) + U^{\lambda\,*}_{\mathbf{q}\alpha} \left(b_{-\mathbf{q}\lambda} + b^{\dagger}_{\mathbf{q}\lambda} \right) \right\}. \tag{3.10}$$

For simplicity, hereafter we will drop the branch subscript λ, focusing on one particular branch. Our results can be easily generalized to the multi-branch situation. Now Eq. (3.10) is simplified to

$$Re\left(u_{\alpha}(\mathbf{q})\right) = \sqrt{\frac{\hbar}{8m\omega_{\mathbf{q}}}} \left\{ U_{\mathbf{q}\alpha} \left(b_{\mathbf{q}} + b^{\dagger}_{-\mathbf{q}} \right) + U^{*}_{\mathbf{q}\alpha} \left(b_{-\mathbf{q}} + b^{\dagger}_{\mathbf{q}} \right) \right\}. \tag{3.11}$$

Furthermore, let us assume that $U_{\mathbf{q}\alpha}$ is real. Eq. (3.11) can then be further simplified to

$$Re\left(u_\alpha(\mathbf{q})\right) = \frac{U_{\mathbf{q}\alpha}}{\sqrt{8m\omega_\mathbf{q}/\hbar}}\left(b_\mathbf{q} + b^\dagger_{-\mathbf{q}} + b_{-\mathbf{q}} + b^\dagger_\mathbf{q}\right) . \tag{3.12}$$

Thus, let us define a $\mathbf{q}$-mode dimensionless lattice amplitude operator $u(\pm\mathbf{q})$:

$$u(\pm\mathbf{q}) = b_\mathbf{q} + b^\dagger_{-\mathbf{q}} + b_{-\mathbf{q}} + b^\dagger_\mathbf{q} . \tag{3.13}$$

This operator contains essential information on the lattice dynamics, including quantum fluctuations. It is the phonon analog of the electric field quadrature operators in the photon case. The actual unit of $Re\left(u_\alpha(\mathbf{q})\right)$ is $\sqrt{\hbar/m\omega_\mathbf{q}}$. Using typical quantities such as $m \cong 10^{-26}$Kg, and $\omega_\mathbf{q} \cong 10^{13}$Hz, this unit $\sqrt{\hbar/m\omega_\mathbf{q}}$ is of the order of 0.3 Angstroms.

When $U_{\mathbf{q}\alpha} = |U_{\mathbf{q}\alpha}|e^{i\phi_{U_\mathbf{q}}}$ is complex, where $\phi_{U_\mathbf{q}}$ is a constant phase factor depending only on the lattice structure, the lattice amplitude operator has a generalized form

$$u_g(\pm\mathbf{q}) = \left(b_\mathbf{q} + b^\dagger_{-\mathbf{q}}\right)e^{i\phi_{U_\mathbf{q}}} + \left(b_{-\mathbf{q}} + b^\dagger_\mathbf{q}\right)e^{-i\phi_{U_\mathbf{q}}} . \tag{3.14}$$

Furthermore, an experimentally observable quantity which is related to the atomic displacements in the crystal can generally be expressed in terms of $Q^\lambda_\mathbf{q}$:

$$O = \sum_{\mathbf{q}\lambda} \frac{\partial O}{\partial Q^\lambda_\mathbf{q}} Q^\lambda_\mathbf{q} . \tag{3.15}$$

Due to the Hermiticity of the operator O and the relation $Q^\lambda_{-\mathbf{q}} = Q^{\lambda *}_\mathbf{q}$, we have the following constraint

$$\frac{\partial O}{\partial Q^\lambda_{-\mathbf{q}}} = \left(\frac{\partial O}{\partial Q^\lambda_\mathbf{q}}\right)^* . \tag{3.16}$$

Thus the operator O can be written as

$$\begin{aligned} O &= \sum_{\lambda, q_x>0}\left[\frac{\partial O}{\partial Q^\lambda_\mathbf{q}} Q^\lambda_\mathbf{q} + \left(\frac{\partial O}{\partial Q^\lambda_\mathbf{q}}\right)^* Q^{\lambda *}_\mathbf{q}\right] \\ &= \sum_{\lambda, q_x>0}\left|\frac{\partial O}{\partial Q^\lambda_\mathbf{q}}\right|\sqrt{\frac{\hbar}{2\omega_{\mathbf{q}\lambda}}}\left[\left(b_{\mathbf{q}\lambda} + b^\dagger_{-\mathbf{q}\lambda}\right)e^{i\Psi_{\mathbf{q}\lambda}} + \left(b_{-\mathbf{q}\lambda} + b^\dagger_{\mathbf{q}\lambda}\right)e^{-i\Psi_{\mathbf{q}\lambda}}\right] . \end{aligned} \tag{3.17}$$

Here $\Psi_{\mathbf{q}\lambda}$ is the phase of $\partial O/\partial Q^\lambda_\mathbf{q}$. An example of an experimentally observable quantity is the change in the crystal dielectric constant $\delta\epsilon$ due to the atomic displacement $Q^\lambda_\mathbf{q}$. It can be expressed as

$$\delta\epsilon = \sum_{\mathbf{q}\lambda} \frac{\partial\left(\delta\epsilon\right)}{\partial Q^\lambda_\mathbf{q}} Q^\lambda_\mathbf{q} . \tag{3.18}$$

Indeed, a widely used method to track the phases of coherent phonons [37, 38, 39] is based on the observation of the reflectivity modulation ΔR of the sample, which is linearly related to $\delta\epsilon$, the change in the dielectric constant due to lattice vibrations.

Equation (3.17) indicates that we can define a generalized lattice amplitude operator

$$u_G(\pm\mathbf{q}) = \left(b_{\mathbf{q}} + b^{\dagger}_{-\mathbf{q}}\right) e^{i\Psi_{\mathbf{q}}} + \left(b_{-\mathbf{q}} + b^{\dagger}_{\mathbf{q}}\right) e^{-i\Psi_{\mathbf{q}}}, \tag{3.19}$$

where the branch label λ has been dropped for simplicity. However, it can be easily shown that this generalized operator $u_G(\pm\mathbf{q})$ has the same fluctuation properties in phonon coherent and squeezed states as $u(\pm\mathbf{q})$. Moreover, the expectation values of $u_G(\pm\mathbf{q})$ and $u(\pm\mathbf{q})$ in these states have a phase difference equal to $\Psi_{\mathbf{q}\lambda}$. Indeed, in calculating the quantum fluctuation $\langle(\Delta u_G(\pm\mathbf{q}))^2\rangle$, the important terms are $\langle b_{\mathbf{q}} b^{\dagger}_{\mathbf{q}}\rangle$ and $\langle b_{\mathbf{q}} b_{-\mathbf{q}}\rangle$, where the phases cancel out with each other. Therefore, we will only use $u(\pm\mathbf{q})$ hereafter. All of our results on $u(\pm\mathbf{q})$ can be easily generalized to $u_g(\pm\mathbf{q})$ and $u_G(\pm\mathbf{q})$.

3.3.2 Phase Operator

Classically, the amplitude and phase of the atomic vibrations are conjugate variables. However, quantum mechanically, the phase operator is not well defined either in quantum optics or for phonons. Here, let us consider one particular definition of the phase operator borrowed from quantum optics [63] and calculate its expectation value in a phonon coherent state. The more straightforward definition of the phase operator by Dirac [64] is not Hermitian, while the definitions of the $\cos\hat{\phi}$ and $\sin\hat{\phi}$ operators by Susskind and Glogower [63] are Hermitian. The cosine of the phase operator [63] is defined as

$$\cos\hat{\phi} = \frac{1}{2}\left[a^{\dagger}\frac{1}{\sqrt{a^{\dagger}a+1}} + \frac{1}{\sqrt{a^{\dagger}a+1}}a\right]. \tag{3.20}$$

where a is the annihilation operator for the mode $\mathbf{k}$ phonon in consideration. Recall that the quantum state that most closely resembles the classical description is the coherent state. Let us now calculate the average of $\cos\hat{\phi}$ in a phonon coherent state $|\alpha\rangle$ in mode $\mathbf{k}$:

$$\begin{aligned}
\langle\cos\hat{\phi}\rangle &= \langle\alpha|\frac{1}{2}\left[a^{\dagger}\frac{1}{\sqrt{a^{\dagger}a+1}} + \frac{1}{\sqrt{a^{\dagger}a+1}}a\right]|\alpha\rangle \\
&= \frac{1}{2}\langle\alpha|\frac{\alpha^* + \alpha}{\sqrt{a^{\dagger}a+1}}|\alpha\rangle \\
&= \frac{1}{2}e^{-|\alpha|^2}\sum_{m,n}^{\infty}\frac{\alpha^{*m}\alpha^n}{\sqrt{m!n!}}\left(\alpha^* + \alpha\right)\langle m|\frac{1}{\sqrt{a^{\dagger}a+1}}|n\rangle \\
&= \mathrm{Re}\{\alpha\}\, e^{-|\alpha|^2}\sum_{n}\frac{|\alpha|^{2n}}{n!\sqrt{n+1}}.
\end{aligned} \tag{3.21}$$

When $|\alpha|$ is a very large number, the above sum takes the asymptotic expression

$$\sum_{n}\frac{|\alpha|^{2n}}{\sqrt{n+1}n!} \cong \frac{e^{|\alpha|^2}}{|\alpha|}.$$

Therefore,

$$\langle \cos\hat{\phi} \rangle \cong \cos\phi_\alpha \tag{3.22}$$

which clearly demonstrates that the expectation of the phase operator $\hat{\phi}$ is given by the phase ϕ_α of the coherent displacement $\alpha = |\alpha|e^{i\phi_\alpha}$. Furthermore, it will be shown later in Section 3.3.4 that the quantum phase ϕ_α of the coherent displacement α corresponds to the phase of a classical plane wave in the crystal. The coherent-state phase ϕ_α is determined by the mechanism of coherent phonon generation. For instance, if the coherent phonons are produced by impulsive Raman scattering [40], $\phi_\alpha = \pi/2$. If the coherent phonons are generated through a displacive mechanism [43], $\phi_\alpha = 0$. Therefore, a measurement of the phonon phase provides valuable information about the microscopic mechanism responsible for the production of coherent phonons.

3.3.3 Phonon Number States

The eigenstates of the harmonic phonon Hamiltonian, Eq. (3.1), are number states:

$$b_{\mathbf{q}} \mid n_{\mathbf{q}} \rangle = \sqrt{n_{\mathbf{q}}} \mid n_{\mathbf{q}} - 1 \rangle, \tag{3.23}$$

$$b_{\mathbf{q}}^{\dagger} \mid n_{\mathbf{q}} \rangle = \sqrt{n_{\mathbf{q}} + 1} \mid n_{\mathbf{q}} + 1 \rangle. \tag{3.24}$$

As noted before, phonons are intrinsically interactive and have a dissipative dynamics. Thus the number states and the simple harmonic Hamiltonian for independent oscillators are generally not sufficient to describe a phonon system. Furthermore, the phonon number and phase of the atomic vibrations are conjugate variables. Thus, due to the uncertainty principle, the phase is arbitrary when the phonon number is certain, as it is the case with any number state $|n_{\mathbf{q}}\rangle$. Therefore, in the number state representation, the following quantities vanish: the expectation values of the atomic displacement $\langle n_{\mathbf{q}}|u_{i\alpha}|n_{\mathbf{q}}\rangle$, velocity $\langle n_{\mathbf{q}}|\dot{u}_{i\alpha}|n_{\mathbf{q}}\rangle$, and $\mathbf{q}$-mode lattice amplitude $\langle n_{\mathbf{q}}|u(\pm\mathbf{q})|n_{\mathbf{q}}\rangle$:

$$\langle n_{\mathbf{q}}|u_{i\alpha}|n_{\mathbf{q}}\rangle = \langle n_{\mathbf{q}}|\dot{u}_{i\alpha}|n_{\mathbf{q}}\rangle = \langle n_{\mathbf{q}}|u(\pm\mathbf{q})|n_{\mathbf{q}}\rangle = 0. \tag{3.25}$$

These results do not imply that atoms never move and always remain at their equilibrium positions. Instead, they originate from the randomness in the phase of the atomic displacements.

This issue can be also looked at from another perspective. Number states are the eigenstates of an isolated system and thus they are appropriate when we deal with a system that does not interact with its environment. However, if we consider a subset of an interacting

system, for which energy is not a good quantum number anymore, number states are not the best choice. In fact, there exist states that can describe such a non-conserving system better. Coherent states [7] are in this category, and will be discussed in the next section.

3.3.4 Phonon Coherent States and Their Generation

In this section we study the dynamical and quantum fluctuation properties of phonon coherent states. We also briefly discuss the connection between phonon coherent states and the experimentally-observed coherent phonons. Typically, the dynamics of coherent phonons are described by using *classical* equations of motion, while here we present a *quantum* description of them. This is a necessary step before introducing phonon squeezed states.

Single-mode Phonon Coherent States

A single-mode phonon coherent state is an eigenstate of a phonon annihilation operator

$$b_{\mathbf{q}}|\beta_{\mathbf{q}}\rangle = \beta_{\mathbf{q}}|\beta_{\mathbf{q}}\rangle . \tag{3.26}$$

It can also be generated by applying a phonon displacement operator $D_{\mathbf{q}}(\beta_{\mathbf{q}})$ to the phonon vacuum state (where there is no phonon excited)

$$|\beta_{\mathbf{q}}\rangle = D_{\mathbf{q}}(\beta_{\mathbf{q}})|0\rangle = \exp\left(\beta_{\mathbf{q}} b_{\mathbf{q}}^{\dagger} - \beta_{\mathbf{q}}^{*} b_{\mathbf{q}}\right)|0\rangle = e^{-\frac{|\beta_{\mathbf{q}}|^2}{2}} \sum_{n_{\mathbf{q}}=0}^{\infty} \frac{\beta_{\mathbf{q}}^{n_{\mathbf{q}}}}{\sqrt{n_{\mathbf{q}}!}} |n_{\mathbf{q}}\rangle . \tag{3.27}$$

It can be seen from Eq. (3.27) that a phonon coherent state is a phase-coherent superposition of number states. Moreover, coherent states are a set of minimum-uncertainty states which are as noiseless as the vacuum state. Coherent states are also the set of quantum states that best describe classical harmonic oscillators. Indeed, these results are the phonon analog of the photon coherent states [7, 57, 65]. Appendix A presents a summary of some useful properties of photon coherent states.

A single-mode coherent state can be generated by the following Hamiltonian:

$$\begin{cases} H &= H_0 + V \\ H_0 &= \hbar\omega_{\mathbf{q}} \left(b_{\mathbf{q}}^{\dagger} b_{\mathbf{q}} + \frac{1}{2} \right) \\ V &= \lambda_{\mathbf{q}}^{*} e^{i\omega_{\mathbf{q}} t}\, b_{\mathbf{q}} + \lambda_{\mathbf{q}} e^{-i\omega_{\mathbf{q}} t}\, b_{\mathbf{q}}^{\dagger} \end{cases} \tag{3.28}$$

and an appropriate initial state (see Appendix A for further details). Here $\lambda_{\mathbf{q}}$ represents both the interaction strength between phonons and the external pump and the intensity magnitude of the pump. Also notice that the pump is on resonance with the phonon mode.

More specifically, if the initial state is a vacuum state, $|\psi(0)\rangle = |0\rangle$, then the state vector $|\psi\rangle$ becomes a single-mode coherent state thereafter

$$|\psi(t)\rangle = |\Lambda_{\mathbf{q}}(t)\, e^{-i\omega_{\mathbf{q}}t}\rangle\,, \tag{3.29}$$

$$\Lambda_{\mathbf{q}}(t) = -\left(\frac{i}{\hbar}\lambda_{\mathbf{q}}\right) t\,, \tag{3.30}$$

where $\Lambda_{\mathbf{q}}(t)$ is the coherent amplitude of mode $\mathbf{q}$. The linear divergence of $\Lambda_{\mathbf{q}}(t)$ with time t reflects the facts that no dissipation mechanism is present and that the external pump is working continuously. Here the initial state does not necessarily have to be a vacuum state. It can be an arbitrary coherent state because of the relation

$$D_{\mathbf{q}}(\alpha_{\mathbf{q}})\,|\beta_{\mathbf{q}}\rangle = e^{i\theta_{\mathbf{q}}}\,|\alpha_{\mathbf{q}} + \beta_{\mathbf{q}}\rangle\,, \tag{3.31}$$

where $\theta_{\mathbf{q}} = Im(\beta_{\mathbf{q}}\alpha_{\mathbf{q}}^{*})$ is an additional overall phase factor [65].

If the initial state is a single-mode coherent state

$$|\psi(0)\rangle = |\alpha_{\mathbf{q}}\rangle, \tag{3.32}$$

then the state vector at time t takes the form

$$|\psi(t)\rangle = |\,\{\Lambda_{\mathbf{q}}(t) + \alpha_{\mathbf{q}}\}\, e^{-i\omega_{\mathbf{q}}t}\rangle, \tag{3.33}$$

which is still a coherent state.

In a single-mode ($\mathbf{q}$) coherent state $|\Lambda_{\mathbf{q}}(t)\, e^{-i\omega_{\mathbf{q}}t}\rangle$, the time-dependent expectation value of the atomic displacement operator is

$$\langle u_{i\alpha}\rangle_{\rm coh} = \sqrt{\frac{2\hbar}{Nm\omega_{\mathbf{q}}}}\,|U_{\mathbf{q}\alpha}\Lambda_{\mathbf{q}}(t)|\cos(\mathbf{q}\cdot\mathbf{R}_i - \omega_{\mathbf{q}}t + \phi_{U_{\mathbf{q}}} + \phi_{\Lambda_{\mathbf{q}}}(t))\,. \tag{3.34}$$

Here the branch subscript λ has been dropped for simplicity, $U_{\mathbf{q}\alpha} = |U_{\mathbf{q}\alpha}|\exp(i\phi_{U_{\mathbf{q}}})$, and $\Lambda_{\mathbf{q}}(t) = |\Lambda_{\mathbf{q}}(t)|\exp(i\phi_{\Lambda_{\mathbf{q}}}(t))$. The time evolution of the expectation value of the lattice amplitude operator also takes the plane-wave form

$$\langle u(\pm\mathbf{q})\rangle_{\rm coh} = 2|\Lambda_{\mathbf{q}}|\cos(\omega_{\mathbf{q}}t + \phi_{\Lambda_{\mathbf{q}}}(t))\,. \tag{3.35}$$

Thus a single-mode phonon coherent state is a plane wave propagating in the crystal when $\phi_{\Lambda_{\mathbf{q}}}(t)$ does not depend on time.

The variance (also called "uncertainty", "fluctuations", or "noise") of the atomic displacement operator for a single-mode coherent state is

$$\langle(\Delta u_{i\alpha})^2\rangle_{\rm coh} \equiv \langle(u_{i\alpha})^2\rangle_{\rm coh} - \langle u_{i\alpha}\rangle^2_{\rm coh} = \sum_{\mathbf{q}}^{N}\frac{\hbar|U_{\mathbf{q}\alpha}|^2}{2Nm\omega_{\mathbf{q}\alpha}}\,. \tag{3.36}$$

Notice that all the modes that are not excited are in the vacuum state and thus all contribute to the noise in the form of zero-point fluctuations. This shows that a coherent state has the same noise as the vacuum state. Furthermore, this expression of the atomic displacement fluctuations gives a finite sum. On the other hand, the similar expression for the electric field fluctuation in a photon field diverges.

The uncertainty of the lattice amplitude operator for a single-mode coherent state is

$$\langle(\Delta u(\pm\mathbf{q}))^2\rangle_{\rm coh} \equiv \langle(u(\pm\mathbf{q}))^2\rangle_{\rm coh} - \langle u(\pm\mathbf{q})\rangle^2_{\rm coh} = 2\,. \tag{3.37}$$

Notice that, from the expressions of the noise $\langle(\Delta u_{i\alpha})^2\rangle_{\rm coh}$ and $\langle(\Delta u(\pm\mathbf{q}))^2\rangle_{\rm coh}$, it is impossible to know which state (if any) has been excited. On the other hand, this information is clearly present in the expression of the expectation value of the lattice amplitude $\langle u(\pm\mathbf{q})\rangle_{\rm coh}$.

Multi-mode Phonon Coherent States

A multi-mode coherent state is a coherent state with more than one mode. Since phonon modes are independent of each other, a multi-mode coherent state can be simply expressed as a product of a series of single-mode coherent states:

$$|\alpha_1, \alpha_2, \cdots, \alpha_n\rangle = |\alpha_1\rangle \otimes |\alpha_2\rangle \otimes \cdots \otimes |\alpha_n\rangle\,. \tag{3.38}$$

Theoretically, a multi-mode coherent state can be obtained from the following Hamiltonian:

$$\left\{\begin{array}{lcl} H &=& H_0 + V \\ H_0 &=& \sum_{\mathbf{q}} \hbar\omega_{\mathbf{q}} \left(b^\dagger_{\mathbf{q}} b_{\mathbf{q}} + \frac{1}{2}\right) \\ V &=& \sum_{\mathbf{q}} \left\{\lambda^*_{\mathbf{q}} e^{i\omega_{\mathbf{q}} t}\, b_{\mathbf{q}} + \lambda_{\mathbf{q}} e^{-i\omega_{\mathbf{q}} t}\, b^\dagger_{\mathbf{q}}\right\} \end{array}\right. \tag{3.39}$$

and an appropriate initial state. Here $\lambda_{\mathbf{q}}$ is the interaction strength between the phonon system and the external source. For simplicity, branch labels have been dropped.

Similar to the single-mode case, if the initial state is a vacuum state, $|\psi(0)\rangle = |0\rangle$, the state vector $|\psi\rangle$ will become a multi-mode coherent state thereafter,

$$|\psi(t)\rangle = \prod_{\mathbf{q}} \otimes\, |\Lambda_{\mathbf{q}}(t)\, e^{-i\omega_{\mathbf{q}} t}\rangle\,, \tag{3.40}$$

$$\Lambda_{\mathbf{q}}(t) = -\left(\frac{i}{\hbar}\lambda_{\mathbf{q}}\right) t\,, \tag{3.41}$$

where $\Lambda_{\mathbf{q}}(t)$ is the coherent amplitude of mode $\mathbf{q}$. If the initial state is a multi-mode coherent state

$$|\psi(0)\rangle = \prod_{\mathbf{q}} \otimes\, |\alpha_{\mathbf{q}}\rangle, \tag{3.42}$$

the state vector at time t will be

$$|\psi(t)\rangle = \prod_{\mathbf{q}} \otimes \, |\, \{\Lambda_{\mathbf{q}}(t) + \alpha_{\mathbf{q}}\}\, e^{-i\omega_{\mathbf{q}}t}\rangle, \tag{3.43}$$

which is still a coherent state.

We can now calculate the expectation values and quantum fluctuations of the atomic displacement and lattice amplitude operators. In a multi-mode coherent state $|\psi(t)\rangle = \prod_{\mathbf{q}} \otimes |\Lambda_{\mathbf{q}}(t)\, e^{-i\omega_{\mathbf{q}}t}\rangle$, the expectation value of the atomic displacement operator $u_{i\alpha}(t)$ is

$$\begin{aligned} \langle u_{i\alpha}(t)\rangle_{\rm coh} &= \frac{1}{\sqrt{Nm}} \sum_{\mathbf{q}}^{N} \sqrt{\frac{\hbar}{2\omega_{\mathbf{q}}}} \left\{ U_{\mathbf{q}\alpha}\, e^{i(\mathbf{q}\cdot\mathbf{R}_i - \omega_{\mathbf{q}}t)}\, \Lambda_{\mathbf{q}}(t) + U^{*}_{\mathbf{q}\alpha}\, e^{-i(\mathbf{q}\cdot\mathbf{R}_i - \omega_{\mathbf{q}}t)}\, \Lambda^{*}_{\mathbf{q}}(t) \right\} \\ &= \frac{1}{\sqrt{Nm}} \sum_{\mathbf{q}}^{N} \sqrt{\frac{2\hbar}{\omega_{\mathbf{q}}}}\, |U_{\mathbf{q}\alpha}\, \Lambda_{\mathbf{q}}(t)| \cos(\mathbf{q}\cdot\mathbf{R}_i - \omega_{\mathbf{q}}t + \phi_{U_{\mathbf{q}}} + \phi_{\Lambda_{\mathbf{q}}}(t)) \,, \end{aligned} \tag{3.44}$$

which is a sum of cosine functions. Here the branch subscript λ has been dropped, $U_{\mathbf{q}\alpha} = |U_{\mathbf{q}\alpha}| \exp(i\phi_{U_{\mathbf{q}}})$, and $\Lambda_{\mathbf{q}}(t) = |\Lambda_{\mathbf{q}}(t)| \exp(i\phi_{\Lambda_{\mathbf{q}}}(t))$. For a particular pair of $\pm\mathbf{q}$, the lattice amplitude operator $u(\pm\mathbf{q})$ is

$$\begin{aligned} \langle u(\pm\mathbf{q})\rangle_{\rm coh} &= \Lambda_{\mathbf{q}}(t)\, e^{-i\omega_{\mathbf{q}}t} + \Lambda^{*}_{\mathbf{q}}(t)\, e^{i\omega_{\mathbf{q}}t} + \Lambda_{-\mathbf{q}}(t)\, e^{-i\omega_{-\mathbf{q}}t} + \Lambda^{*}_{-\mathbf{q}}(t)\, e^{i\omega_{-\mathbf{q}}t} \\ &= 2\left\{ |\Lambda_{\mathbf{q}}(t)| \cos(\omega_{\mathbf{q}}t + \phi_{\Lambda_{\mathbf{q}}}(t)) + |\Lambda_{-\mathbf{q}}(t)| \cos(\omega_{-\mathbf{q}}t + \phi_{\Lambda_{-\mathbf{q}}}(t)) \right\} . \end{aligned} \tag{3.45}$$

In the special case where $|\Lambda_{-\mathbf{q}}| = |\Lambda_{\mathbf{q}}|$, and recalling that $\omega_{-\mathbf{q}} = \omega_{\mathbf{q}}$, the average of $u(\pm\mathbf{q})$ takes the simple form

$$\langle u(\pm\mathbf{q})\rangle_{\rm coh} = 4\, |\Lambda_{\mathbf{q}}| \cos\left(\frac{\phi_{\Lambda_{\mathbf{q}}}(t) - \phi_{\Lambda_{-\mathbf{q}}}(t)}{2} \right) \cos\left(\omega_{\mathbf{q}}t + \frac{\phi_{\Lambda_{\mathbf{q}}}(t) + \phi_{\Lambda_{-\mathbf{q}}}(t)}{2} \right) . \tag{3.46}$$

Moreover, if $\Lambda_{-\mathbf{q}} = \Lambda_{\mathbf{q}}$, then $u(\pm\mathbf{q})$ takes an even simpler form

$$\langle u(\pm\mathbf{q})\rangle_{\rm coh} = 4\, |\Lambda_{\mathbf{q}}| \cos(\omega_{\mathbf{q}}t + \phi_{\Lambda_{\mathbf{q}}}(t)) \,. \tag{3.47}$$

Therefore, in a multi-mode coherent state, $\langle u_{i\alpha}(t)\rangle_{\rm coh}$ and $\langle u(\pm\mathbf{q})\rangle_{\rm coh}$ are sinusoidal functions of time, instead of being zero like in a number state $|n_{\mathbf{q}}\rangle$.

In a multi-mode coherent state, the fluctuation of the atomic displacement operator takes the form

$$\langle (\Delta u_{i\alpha})^2 \rangle_{\rm coh} = \sum_{\mathbf{q}}^{N} \frac{\hbar |U_{\mathbf{q}\alpha}|^2}{2Nm\omega_{\mathbf{q}\alpha}} \,. \tag{3.48}$$

If the $\pm\mathbf{q}$ modes are both in a multi-mode coherent state, the fluctuation of the lattice amplitude operator becomes

$$\langle (\Delta u(\pm\mathbf{q}))^2 \rangle_{\rm coh} = 2 \,. \tag{3.49}$$

Therefore, if a phonon system is in either a single-mode or a multi-mode coherent state, the fluctuations of the atomic displacement operator $\langle(\Delta u_{i\alpha})^2\rangle_{\rm coh}$ and of the lattice amplitude operator $\langle(\Delta u(\pm\mathbf{q}))^2\rangle_{\rm coh}$ will be independent of time.

Equivalence of Quantum and Classical Coherent Phonons

Coherent phonons have been the subject of considerable interest in recent years, as pointed out in the introduction section of this chapter and in Ref. [35]. Experimentally, coherent optical phonons can be generated through optical interactions such as stimulated Raman scattering [60, 61]. Using a similar technique, coherent acoustic phonons have also been generated in zone-folded superlattices [12]. Typically, the dynamics of coherent phonons are described by using *classical* equations of motion. Here we present a *quantum* description and show that it is consistent with the classical one and, as an additional bonus, contains information on quantum fluctuations. An effective Hamiltonian for a coherent-phonon-generating process is

$$H_{\rm stimulated-Raman} = \hbar\omega_p b_p^\dagger b_p + \hbar\omega_{\mathbf{k}_1} a_{\mathbf{k}_1}^\dagger a_{\mathbf{k}_1} + \hbar\omega_{\mathbf{k}_2} a_{\mathbf{k}_2}^\dagger a_{\mathbf{k}_2} + \lambda\, b_p a_{\mathbf{k}_1} a_{\mathbf{k}_2}^\dagger + \lambda^*\, b_p^\dagger a_{\mathbf{k}_1}^\dagger a_{\mathbf{k}_2}, \quad (3.50)$$

where p refers to a Raman active phonon mode, $\mathbf{k}_1$ ($\mathbf{k}_2$) denotes the higher- (lower-) energy incident laser photons. In the context of spontaneous Raman scattering, where there is only one beam of incident photons, mode $\mathbf{k}_2$ is called the Stokes mode of the scattered (instead of incident) photons. However, in a stimulated Raman process, two incident laser beams are needed. The two incident photon modes have a frequency difference that is equal to the frequency of the Raman active phonon mode. Since in a stimulated Raman process both incident photon modes $\mathbf{k}_1$ and $\mathbf{k}_2$ are pumped into large amplitude coherent states, the creation and annihilation operators of these two modes can be treated as c-numbers. Hence in a mean-field (MF) approximation the Hamiltonian $H_{\rm stimulated-Raman}$ can be simplified to

$$H^{MF}_{\rm stimulated-Raman} = \hbar\omega_p\, b_p^\dagger b_p + \lambda_p e^{i\omega_p t} b_p + \lambda_p^* e^{-i\omega_p t} b_p^\dagger . \quad (3.51)$$

As we pointed out earlier in this section, the phonons will be in a coherent state starting from either a vacuum or a coherent state.

Coherent phonons can also be generated transiently by a femtosecond short pulse laser. A femtosecond pulse duration is much shorter than any phonon period and therefore acts as a delta-function driving force. It can produce coherent longitudinal optical (LO) phonons [39, 43, 45, 46]. We can make a very simplified calculation by replacing the coupling strength

$\lambda_p e^{i\omega_p t}$ with $\lambda_p(t) = A\delta(t - t_0)$ in Eq. (3.51), so that

$$H^{MF}_{\text{stimulated-Raman}} = \hbar\omega_p b_p^\dagger b_p + A\,\delta(t - t_0)\,b_p + A^*\,\delta(t - t_0)\,b_p^\dagger . \tag{3.52}$$

Here $A = |A|e^{i\phi_A}$ is a time-independent complex amplitude containing the information of the photon-phonon interaction and the coherent amplitude of the relevant modes in the incident optical pulse. We assume that the crystal is in the phonon vacuum state before it is hit by the laser pulse at $t = t_0$. Let us now consider the time-evolution of the phonons in the p mode.

To obtain the time-evolution operator for the phonon mode, we first change into the interaction picture, where the interaction-picture Hamiltonian takes the form

$$V_I(t) = \delta(t - t_0)\left[Ab_p e^{-i\omega_p t} + A^* b_p^\dagger e^{i\omega_p t}\right] . \tag{3.53}$$

Notice that this Hamiltonian is time-dependent. Thus, we cannot integrate the Schrödinger equation directly like we have done for the on-resonance cases. However, we can use the Magnus method [66] to calculate the time-evolution operator $U_I(t) = \exp(-iA_1 - iA_2 - iA_3 - \cdots)$ of the phonons (see Appendix A.2 for details). Since the Hamiltonian $V_I(t)$ above is linear in b_p and $b_p^\dagger$, all the commutators equal to or higher than third-order vanish. The second-order term A_2 can be calculated as follows

$$\begin{aligned}
A_2(t, t_0) &= \frac{1}{2!i\hbar}\int_{t_0}^{t} dt_2 \int_{t_0}^{t_2} dt_1\,[V_I(t_1), V_I(t_2)] \\
&= \frac{1}{2!i\hbar}\int_{t_0}^{t} dt_2 \int_{t_0}^{t_2} dt_1\,|A|^2\,\delta(t_1 - t_0)\,\delta(t_2 - t_0)\left[e^{i\omega_p(t_2 - t_1)} - e^{-i\omega_p(t_2 - t_1)}\right] \\
&= \frac{1}{\hbar}\int_{t_0}^{t} dt_2 \int_{t_0}^{t_2} dt_1\,|A|^2\,\delta(t_1 - t_0)\,\delta(t_2 - t_0)\,\sin\omega_p(t_2 - t_1) \\
&= 0 .
\end{aligned}$$

Therefore, only A_1 contributes to the time-evolution operator. $U_I(t)$ can thus be written as

$$\begin{aligned}
U_I(t, t_0) &= e^{-iA_1} \\
&= \exp\left(-\frac{i}{\hbar}\int_{t_0}^{t} d\tau\, V_I(\tau)\right) \\
&= \exp\left(-\frac{iA}{2\hbar}b_p e^{-i\omega_p t_0} - \frac{iA^*}{2\hbar}b_p^\dagger e^{i\omega_p t_0}\right) .
\end{aligned} \tag{3.54}$$

In other words, for $t > t_0$, the crystal is in a single-mode (if this phonon mode is the only Raman active mode) coherent state $|\Lambda_p e^{-i\omega_p t}\rangle$. The coherent phonon amplitude Λ_p from Eq. (3.30) is then

$$\Lambda_p = -\frac{iA^*}{2\hbar}\,e^{i\omega_p t_0} . \tag{3.55}$$

which is a constant complex number. Thus, a very short laser pulse conveniently provides a time-independent amplitude and a coherent phase (see, e.g., [41]). If $\mathbf{q}$ is the wave vector of the p mode, the state vector can be written as $|\Lambda_{\mathbf{q}} e^{-i\omega_{\mathbf{q}} t}\rangle$, where $\Lambda_{\mathbf{q}} = -iAe^{i\omega_{\mathbf{q}} t_0}/2\hbar$. For $t > t_0$, the average of the lattice amplitude operator in the state $|\Lambda_{\mathbf{q}} e^{-i\omega_{\mathbf{q}} t}\rangle \otimes |0_{-\mathbf{q}}\rangle$ becomes

$$\begin{aligned}
\langle u(\pm\mathbf{q})\rangle_{\text{coh}} &= \langle 0_{-\mathbf{q}}| \otimes \langle \Lambda_{\mathbf{q}}^* e^{i\omega_{\mathbf{q}} t}|\, u(\pm\mathbf{q})\, |\Lambda_{\mathbf{q}} e^{-i\omega_{\mathbf{q}} t}\rangle \otimes |0_{-\mathbf{q}}\rangle \\
&= \langle \Lambda_{\mathbf{q}}^* e^{i\omega_{\mathbf{q}} t}|\left(b_{\mathbf{q}} + b_{\mathbf{q}}^\dagger\right)|\Lambda_{\mathbf{q}} e^{-i\omega_{\mathbf{q}} t}\rangle \\
&= -\frac{i|A|}{2\hbar}\left\{e^{-i\omega_{\mathbf{q}}(t-t_0)+i\phi_A} - e^{i\omega_{\mathbf{q}}(t-t_0)-i\phi_A}\right\} \\
&= -\frac{|A|}{\hbar}\sin\left\{\omega_{\mathbf{q}}(t-t_0) - \phi_A\right\} . \qquad (3.56)
\end{aligned}$$

These longitudinal optical phonons can have a coherence time of about 50ps at 10K, and even longer at lower temperatures [35].

In the classical sense, "coherent" means a wave with a well-defined phase, or waves that can interfere with each other when superimposed. Here we have shown that the *single-mode coherent state of phonons generated by a short laser pulse is indeed a plane wave with a well-defined phase.* Thus, these phonons in a *quantum* coherent state are also coherent in a *classical* manner.

3.3.5 Phonon Squeezed States

In this section we study the dynamical and quantum fluctuation properties of various kinds of phonon squeezed states. These states are special because they periodically exhibit less quantum noise than phonon coherent states or the phonon vacuum state, both of which exhibit zero-point fluctuations.

Quadrature Squeezed States

In order to reduce quantum fluctuations to a level below the one for coherent phonons, we need to consider phonon squeezed states. Quadrature squeezed states are generalized coherent states [9, 58, 67]. Here "quadrature" refers to the dimensionless variables such as dimensionless coordinate and momentum. Compared to coherent states, squeezed ones can achieve smaller variances for one of the quadratures during certain time intervals, and are therefore helpful for modulating and decreasing quantum noise.

Phonon number states have the smallest possible noise in the phonon number, thus are an extreme form of squeezed states. However, they have no phase coherence, which is important in many situations. Figures 3.1 and 3.2 schematically illustrate several types

of phonon states, including vacuum, number, coherent and squeezed states. These figures are the phonon analogs of the illuminating schematic diagrams used for photons [68, 69]. Appendix B summarizes some definitions and useful results on quadrature squeezed states.

A single-mode quadrature phonon squeezed state is generated by applying a phonon squeezing operator $S_{\mathbf{q}}(\xi)$ and a phonon displacement operator $D_{\mathbf{q}}(\alpha_{\mathbf{q}})$ to a vacuum state

$$|\alpha_{\mathbf{q}}, \xi\rangle = D_{\mathbf{q}}(\alpha_{\mathbf{q}})\ S_{\mathbf{q}}(\xi)|0\rangle\,, \tag{3.57}$$

where

$$S_{\mathbf{q}}(\xi) = \exp\left(\frac{\xi^*}{2} b_{\mathbf{q}}^2 - \frac{\xi}{2} b_{\mathbf{q}}^{\dagger 2}\right)\,. \tag{3.58}$$

A two-mode quadrature phonon squeezed state is generated as follows

$$|\alpha_{\mathbf{q}_1},\ \alpha_{\mathbf{q}_2},\ \xi\rangle = D_{\mathbf{q}_1}(\alpha_{\mathbf{q}_1})\ D_{\mathbf{q}_2}(\alpha_{\mathbf{q}_2})\ S_{\mathbf{q}_1,\mathbf{q}_2}(\xi)\ |0\rangle\,, \tag{3.59}$$

$$S_{\mathbf{q}_1,\mathbf{q}_2}(\xi) = \exp(\xi^* b_{\mathbf{q}_1} b_{\mathbf{q}_2}\ - \xi\ b_{\mathbf{q}_1}^{\dagger} b_{\mathbf{q}_2}^{\dagger})\,. \tag{3.60}$$

Here $D_{\mathbf{q}}(\alpha_{\mathbf{q}})$ is the coherent state displacement operator with $\alpha_{\mathbf{q}} = |\alpha_{\mathbf{q}}|e^{i\phi}$, $S_{\mathbf{q}}(\xi)$ is the single-mode squeezing operator, $S_{\mathbf{q}_1,\mathbf{q}_2}(\xi)$ is the two-mode squeezing operator, and $\xi = re^{i\theta}$ is the complex squeezing factor with $r \geq 0$ and $0 \leq \theta < 2\pi$.

As shown in Ref. [58] and in Appendix B.3, the squeezing operator $S_{\mathbf{q}_1,\mathbf{q}_2}(\xi)$ can be produced by the following on-resonance Hamiltonian:

$$H_{\mathbf{q}_1,\mathbf{q}_2} = \hbar\omega_{\mathbf{q}_1} b_{\mathbf{q}_1}^{\dagger} b_{\mathbf{q}_1} + \hbar\omega_{\mathbf{q}_2} b_{\mathbf{q}_2}^{\dagger} b_{\mathbf{q}_2} + \zeta e^{-i(\omega_{\mathbf{q}_1}+\omega_{\mathbf{q}_2})t}\, b_{\mathbf{q}_1}^{\dagger} b_{\mathbf{q}_2}^{\dagger} + \zeta^* e^{i(\omega_{\mathbf{q}_1}+\omega_{\mathbf{q}_2})t}\, b_{\mathbf{q}_1} b_{\mathbf{q}_2}\,. \tag{3.61}$$

Its time-evolution operator has the form

$$U(t) = \exp\left(\frac{-iH_0 t}{\hbar}\right) \exp\left[\xi^*(t) b_{\mathbf{q}_1} b_{\mathbf{q}_2} - \xi(t) b_{\mathbf{q}_1}^{\dagger} b_{\mathbf{q}_2}^{\dagger}\right]\,, \tag{3.62}$$

$$H_0 = \hbar\omega_{\mathbf{q}_1} b_{\mathbf{q}_1}^{\dagger} b_{\mathbf{q}_1} + \hbar\omega_{\mathbf{q}_2} b_{\mathbf{q}_2}^{\dagger} b_{\mathbf{q}_2}$$

$$\xi(t) = \left(\frac{i}{\hbar}\zeta\right) t\,. \tag{3.63}$$

Here $\xi(t)$ is the squeezing factor and ζ is the strength of the interaction between the phonons and the external source (including the power of the external pump). This interaction allows the generation and absorption of two phonons at a time. The time-evolution operator $U(t)$ now factorizes into an unperturbed evolution operator $\exp(-iH_0 t/\hbar)$ and a two-mode $(\mathbf{q}_1, \mathbf{q}_2)$ squeezing operator $S_{\mathbf{q}_1,\mathbf{q}_2}(\xi) = \exp\left\{\xi(t) b_{\mathbf{q}_1}^{\dagger} b_{\mathbf{q}_2}^{\dagger} - \xi^*(t) b_{\mathbf{q}_1} b_{\mathbf{q}_2}\right\}$. If the two modes $\mathbf{q}_1$ and $\mathbf{q}_2$ are degenerate, the squeezing operator becomes a single-mode one. Notice that here the squeezing amplitude grows linearly with time. Such a divergence is due to the continuous pump and a lack of any dissipation mechanism. In an experimental situation,

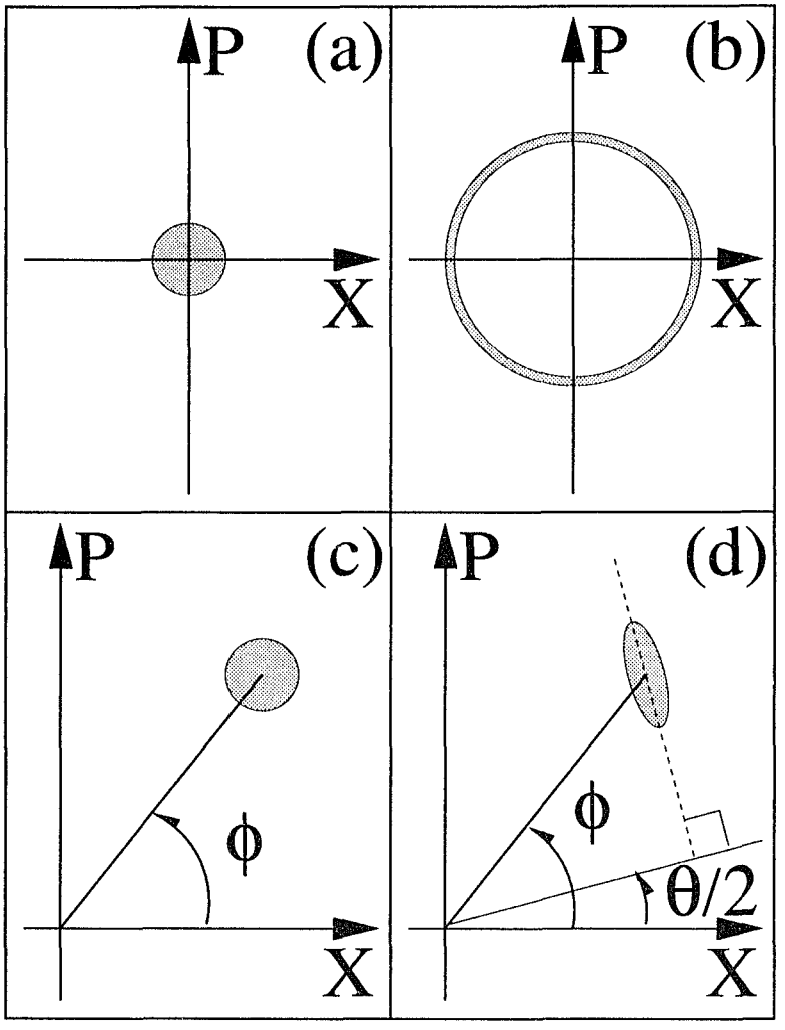

Figure 3.1: Schematic diagram of the uncertainty areas in the generalized coordinate and momentum ($X(\mathbf{q},-\mathbf{q})$, $P(\mathbf{q},-\mathbf{q})$) phase space of (a) the phonon vacuum state, (b) a phonon number state, (c) a phonon coherent state, and (d) a phonon squeezed state. Here $X(\mathbf{q},-\mathbf{q})$ and $P(\mathbf{q},-\mathbf{q})$ are the two-mode ($\pm\mathbf{q}$) coordinate and momentum operators defined in Section 3.3.1. They are direct generalizations of the single-mode coordinate and momentum operators. Notice that the phonon coherent state has the same uncertainty area as the vacuum state, and that both areas are circular, while the squeezed state has an elliptical uncertainty area. Therefore, in the direction parallel to the $\theta/2$ line, the squeezed state has a smaller noise than both the vacuum and coherent states.

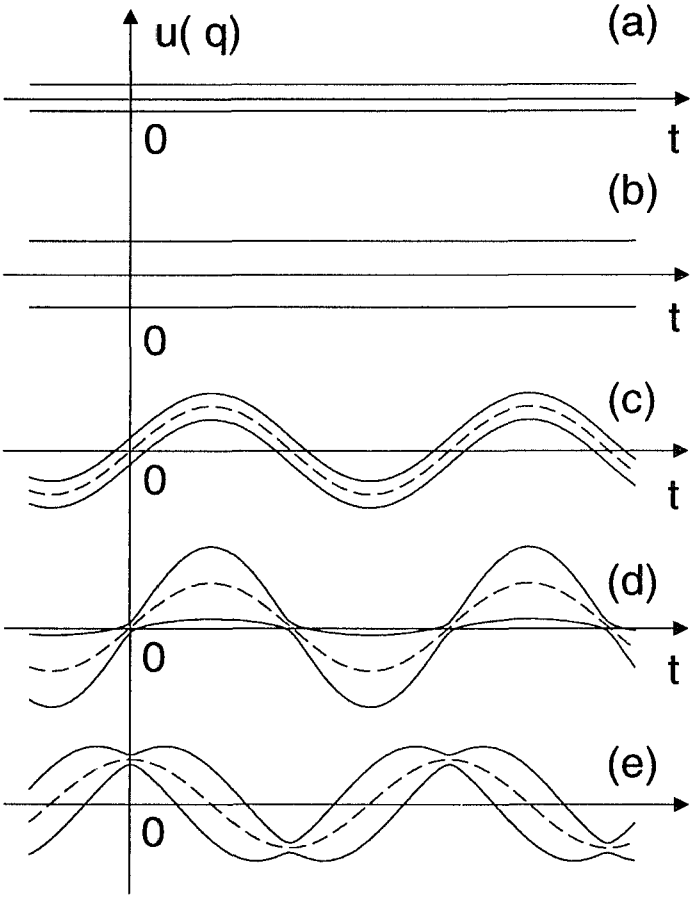

Figure 3.2: Schematic diagram of the time evolution of the expectation value and the fluctuation of the lattice amplitude operator $u(\pm\mathbf{q})$ in different states. Here dashed lines represent the average $\langle u(\pm\mathbf{q})\rangle(t)$, while solid lines represent the envelopes $\langle u(\pm\mathbf{q})\rangle(t) \pm \sqrt{\langle[\Delta u(\pm\mathbf{q})]^2\rangle(t)}$ which provide the upper and lower bounds for the fluctuations in $u(\pm\mathbf{q})(t)$. (a) The phonon vacuum state $|0\rangle$, where $\langle u(\pm\mathbf{q})\rangle = 0$ and $\langle[\Delta u(\pm\mathbf{q})]^2\rangle = 2$. (b) A phonon number state $|n_{\mathbf{q}}, n_{-\mathbf{q}}\rangle$, where $\langle u(\pm\mathbf{q})\rangle = 0$ and $\langle[\Delta u(\pm\mathbf{q})]^2\rangle = 2(n_{\mathbf{q}} + n_{-\mathbf{q}}) + 2$. (c) A single-mode phonon coherent state $|\alpha_{\mathbf{q}}\rangle$, where $\langle u(\pm\mathbf{q})\rangle = 2Re(\alpha_{\mathbf{q}} e^{-i\omega_{\mathbf{q}}t}) = 2|\alpha_{\mathbf{q}}|\cos\omega_{\mathbf{q}}t$, which means that $\alpha_{\mathbf{q}}$ is real, and $\langle[\Delta u(\pm\mathbf{q})]^2\rangle = 2$. (d) A single-mode phonon squeezed state $|\alpha_{\mathbf{q}} e^{-i\omega_{\mathbf{q}}t}, \xi(t)\rangle$, where the squeezing factor $\xi(t)$ satisfies $\xi(t) = re^{-2i\omega_{\mathbf{q}}t}$. Here, $\langle u(\pm\mathbf{q})\rangle = 2|\alpha_{\mathbf{q}}|\cos\omega_{\mathbf{q}}t$, which means that $\alpha_{\mathbf{q}}$ is real, and its fluctuation is $\langle[\Delta u(\pm\mathbf{q})]^2\rangle = 2(e^{-2r}\cos^2\omega_{\mathbf{q}}t + e^{2r}\sin^2\omega_{\mathbf{q}}t)$. (e) A single-mode phonon squeezed state, as in (d). Now the expectation value of u is $\langle u(\pm\mathbf{q})\rangle = 2|\alpha_{\mathbf{q}}|\sin\omega_{\mathbf{q}}t$, which means that $\alpha_{\mathbf{q}}$ is purely imaginary, and the fluctuation $\langle[\Delta u(\pm\mathbf{q})]^2\rangle$ has the same time-dependence as in (d). Notice that the squeezing effect now appears at the times when $\langle u(\pm\mathbf{q})\rangle$ reaches its maxima while in (d) the squeezing effect is present at the times when $\langle u(\pm\mathbf{q})\rangle$ is close to zero.

this initial linear growth in the squeezing factor will eventually be suppressed by dissipation which leads to increasing fluctuations.

For a single phonon mode, the quadrature operators are

$$\begin{cases} X(\mathbf{q}) &= (b_{\mathbf{q}} + b_{\mathbf{q}}^{\dagger})/\sqrt{2} \\ P(\mathbf{q}) &= -i(b_{\mathbf{q}} - b_{\mathbf{q}}^{\dagger})/\sqrt{2}\,. \end{cases} \tag{3.64}$$

For a two-mode ($\mathbf{q}_1$ and $\mathbf{q}_2$) situation, the phonon quadratures become

$$\begin{cases} X(\mathbf{q}_1, \mathbf{q}_2) &= \left(b_{\mathbf{q}_1} + b_{\mathbf{q}_1}^{\dagger} + b_{\mathbf{q}_2} + b_{\mathbf{q}_2}^{\dagger}\right)/2^{3/2} \\ P(\mathbf{q}_1, \mathbf{q}_2) &= \left(b_{\mathbf{q}_1} - b_{\mathbf{q}_1}^{\dagger} + b_{\mathbf{q}_2} - b_{\mathbf{q}_2}^{\dagger}\right)/(2^{3/2}i)\,. \end{cases} \tag{3.65}$$

Let us now consider a single-mode ($\mathbf{q}$) phonon squeezed state $|\alpha_{\mathbf{q}}, \xi\rangle$, where α is the coherent amplitude (equivalent to that in a coherent state), and $\xi(t)$ is a time-dependent complex squeezing factor $\xi(t) = re^{i\theta}$. The average value of the quadrature $X(\mathbf{q})$ is

$$\langle X(\mathbf{q})\rangle_{\rm sq} = \langle \alpha_{\mathbf{q}}, \xi | X(\mathbf{q}) | \alpha_{\mathbf{q}}, \xi\rangle = \sqrt{2}\, Re\,(\alpha_{\mathbf{q}})\,, \tag{3.66}$$

which is the same as for a single-mode ($\mathbf{q}$) coherent state $|\alpha_{\mathbf{q}}\rangle$. The variance of $X(\mathbf{q})$ for the single-mode phonon squeezed state $|\alpha_{\mathbf{q}}, \xi\rangle$ is

$$\langle (\Delta X(\mathbf{q}))^2\rangle_{\rm sq} = \langle \alpha_{\mathbf{q}}, \xi | (\Delta X(\mathbf{q}))^2 | \alpha_{\mathbf{q}}, \xi\rangle = \frac{1}{2}\left(e^{-2r}\cos^2\frac{\theta}{2} + e^{2r}\sin^2\frac{\theta}{2}\right)\,. \tag{3.67}$$

Similarly, in a two-mode phonon squeezed state $|\alpha_{\mathbf{q}_1}, \alpha_{\mathbf{q}_2}, \xi\rangle$, the average value of the quadrature $X(\mathbf{q}_1, \mathbf{q}_2)$ is

$$\langle X(\mathbf{q}_1, \mathbf{q}_2)\rangle_{\rm sq} = \langle \alpha_{\mathbf{q}_1}, \alpha_{\mathbf{q}_2}, \xi | X_2 | \alpha_{\mathbf{q}_1}, \alpha_{\mathbf{q}_2}, \xi\rangle = \frac{1}{\sqrt{2}} Re\,(\alpha_{\mathbf{q}_1} + \alpha_{\mathbf{q}_2})\,, \tag{3.68}$$

which is the same as in a two-mode coherent state $|\alpha_{\mathbf{q}_1}, \alpha_{\mathbf{q}_2}\rangle$, while the variance of $X(\mathbf{q}_1, \mathbf{q}_2)$ in a two-mode phonon squeezed state becomes

$$\langle (\Delta X(\mathbf{q}_1, \mathbf{q}_2))^2\rangle_{\rm sq} = \langle \alpha_{\mathbf{q}_1},\ \alpha_{\mathbf{q}_2},\ \xi | (\Delta X_2)^2 | \alpha_{\mathbf{q}_1},\ \alpha_{\mathbf{q}_2},\ \xi\rangle = \frac{1}{4}\left(e^{-2r}\cos^2\frac{\theta}{2} + e^{2r}\sin^2\frac{\theta}{2}\right)\,. \tag{3.69}$$

Both of the above variances can be smaller than their coherent state values, which are 1/2 and 1/4, respectively.

In the special case of $\mathbf{q}_2 = -\mathbf{q}_1$, the two-mode phonon quadrature operators have the simplified form

$$\begin{cases} X(\mathbf{q}, -\mathbf{q}) &= \left(b_{\mathbf{q}} + b_{\mathbf{q}}^{\dagger} + b_{-\mathbf{q}} + b_{-\mathbf{q}}^{\dagger}\right)/2^{3/2} \\ P(\mathbf{q}, -\mathbf{q}) &= \left(b_{\mathbf{q}} - b_{\mathbf{q}}^{\dagger} + b_{-\mathbf{q}} - b_{-\mathbf{q}}^{\dagger}\right)/(2^{3/2}i)\,. \end{cases} \tag{3.70}$$

Notice that $X(\mathbf{q},-\mathbf{q})$ takes the same form as the previously defined lattice amplitude operator $u(\pm\mathbf{q}) = b_{\mathbf{q}} + b^{\dagger}_{-\mathbf{q}} + b_{-\mathbf{q}} + b^{\dagger}_{\mathbf{q}}$, and both of them are proportional to the real part of the Fourier components $Q_{\mathbf{q}}$ (we have dropped the branch label λ) of the atomic displacement operators $u_{i\alpha}$, which is the physical quantity we are interested in. The two operators are only different by a constant factor of $1/2^{3/2}$:

$$u(\pm\mathbf{q}) = 2^{3/2} X(\mathbf{q},-\mathbf{q}) \quad \propto \quad Re\{Q_{\mathbf{q}}\}\,. \tag{3.71}$$

Therefore, the expectation value of $u(\pm\mathbf{q})$ in a two-mode $(\pm\mathbf{q})$ phonon squeezed state $|\alpha_{\mathbf{q}},\ \alpha_{-\mathbf{q}},\ \xi\rangle$ becomes

$$\langle u(\pm\mathbf{q})\rangle_{\rm sq} = 2Re\,(\alpha_{\mathbf{q}} + \alpha_{-\mathbf{q}})\,. \tag{3.72}$$

As shown in Eqs. (3.45) and (3.72), the expectation values of the lattice amplitude operator $u(\pm\mathbf{q})$ in both phonon coherent and squeezed states have the same sinusoidal dependence on time. However, the fluctuations of $u(\pm\mathbf{q})$ behave differently in coherent and squeezed states. As we have shown in Section 3.3.4, Eq. (3.49), the fluctuation of $u(\pm\mathbf{q})$ is a constant in a two-mode coherent state:

$$\langle(\Delta u(\pm\mathbf{q}))^2\rangle_{\rm coh} = 2\,. \tag{3.73}$$

On the other hand, if the phonon system is in a two-mode $(\pm\mathbf{q})$ squeezed state $|\alpha_{\mathbf{q}},\alpha_{-\mathbf{q}},\xi\rangle$ with squeezing factor $\xi = re^{i\theta}$, the fluctuation of $u(\pm\mathbf{q})$, which is linearly proportional to $\langle(\Delta X(\mathbf{q},-\mathbf{q}))^2\rangle$, becomes:

$$\langle(\Delta u(\pm\mathbf{q}))^2\rangle_{\rm sq} = 8\langle(\Delta X(\mathbf{q},-\mathbf{q}))^2\rangle_{\rm sq} \tag{3.74}$$

$$= 2\left(e^{-2r}\cos^2\frac{\theta}{2} + e^{2r}\sin^2\frac{\theta}{2}\right)\,. \tag{3.75}$$

Notice that the time dependence of the fluctuation $\langle(\Delta u(\pm\mathbf{q}))^2\rangle_{\rm sq}$ comes solely from the squeezing factor $\xi(t)$.

If one of the two $(\pm\mathbf{q})$ phonon modes is in a single-mode squeezed state $|\alpha_{\mathbf{q}},\xi\rangle$ with a squeezing factor of $\xi = re^{i\theta}$ and a coherent amplitude $\alpha_{\mathbf{q}} = |\alpha_{\mathbf{q}}|e^{i\phi}$, while the other mode is in an arbitrary coherent state $|\beta_{-\mathbf{q}}\rangle$, the lattice amplitude fluctuation will be

$$\langle(\Delta u(\pm\mathbf{q}))^2\rangle_{\rm coh+sq} = 1 + e^{-2r}\cos^2(\phi+\frac{\theta}{2}) + e^{2r}\sin^2(\phi+\frac{\theta}{2})\,, \tag{3.76}$$

which also depends on the phase ϕ of the coherent amplitude $\alpha_{\mathbf{q}}$ of the squeezed state. Notice that the only contribution of the arbitrary coherent state $|\beta_{-\mathbf{q}}\rangle$ is to add a constant background term of 1 to the fluctuation of $u(\pm\mathbf{q})$.

We have just considered two cases where squeezed states are involved in two modes of $\pm\mathbf{q}$; one where the system is in a two-mode ($\pm\mathbf{q}$) squeezed state $|\alpha_{\mathbf{q}}, \alpha_{-\mathbf{q}}, \xi\rangle$, and the other when the system is in a single-mode squeezed state $|\alpha_{\mathbf{q}}, \xi\rangle$ in the first mode and an arbitrary coherent state $|\beta_{-\mathbf{q}}\rangle$ in the second mode. In both of these cases, the uncertainties of the lattice amplitude operator $\langle(\Delta u(\pm\mathbf{q}))^2\rangle$, given by Eqs. (3.75) and (3.76), can be smaller than in coherent states (see, e.g., Figs. 3.1 and 3.2).

Squeezing Phonons within a Single-mode

Above, we have considered the ideal quadrature phonon squeezed states that are generated by one- or two-mode squeezing operator $S_{\mathbf{q}}(\xi)$ and $S_{\mathbf{q}_1,\mathbf{q}_2}(\xi)$. There are other types of pure phonon states with quadrature fluctuations periodically smaller than the coherent state value. An example of this is provided by the following single-mode phonon Hamiltonian,

$$H_2 = \hbar\omega_{\mathbf{q}}\, b^{\dagger}_{\mathbf{q}} b_{\mathbf{q}} + \hbar\lambda\, {b^{\dagger}_{\mathbf{q}}}^2 b^2_{\mathbf{q}}\,, \tag{3.77}$$

with an initial coherent state. Notice that this Hamiltonian provides an interaction that will not change the phonon number in mode $\mathbf{q}$. Of course, in thermal equilibrium the phonon number in any mode is not conserved. However, if we focus on a situation in which the phonon mode involved is a low-energy, long-lifetime acoustic mode, then in the *short-time limit* this number-conserving interaction potential can be dominant. For this special situation described by H_2, the fluctuations of the quadrature operators can be calculated analytically in the Heisenberg picture. From the equation $i\hbar d\hat{O}/dt = [\hat{O}, H]$, the time-dependent annihilation operator becomes

$$b_{\mathbf{q}}(t) = \exp\Big\{-i[\omega_{\mathbf{q}} + 2\lambda b^{\dagger}_{\mathbf{q}}(0) b_{\mathbf{q}}(0)]t\Big\}\; b_{\mathbf{q}}(0)\,. \tag{3.78}$$

Assuming the initial state to be a coherent state $|\alpha_{\mathbf{q}}\rangle$, the variance of the quadrature operator $X(\mathbf{q},t) = (b_{\mathbf{q}}(t) + b^{\dagger}_{\mathbf{q}}(t))/\sqrt{2}$ can then be calculated [70] and the result is,

$$\begin{aligned}\langle(\Delta X(\mathbf{q},t))^2\rangle_{\mathrm{sq}'} \;=\; & \frac{1}{2} Re\Big\{\alpha^2_{\mathbf{q}} \exp\Big(-2i\omega_{\mathbf{q}}t - 2i\lambda t + |\alpha_{\mathbf{q}}|^2(e^{-4i\lambda t} - 1)\Big) \\ & - \alpha^2_{\mathbf{q}} \exp\Big(-2i\omega_{\mathbf{q}}t + 2|\alpha_{\mathbf{q}}|^2(e^{-2i\lambda t} - 1)\Big)\Big\} \\ & + \frac{|\alpha_{\mathbf{q}}|^2}{2}\Big\{1 - \exp\Big(2|\alpha_{\mathbf{q}}|^2[\cos(2\lambda t) - 1]\Big)\Big\} + \frac{1}{2}\,.\end{aligned} \tag{3.79}$$

Here the subindex sq′ denotes squeezing by a number-conserving mechanism. Right after the anharmonic term is turned on, i.e., in the small-t limit, the above expression can be approximated by

$$\langle(\Delta X(\mathbf{q},t))^2\rangle_{\mathrm{sq}'} = \frac{1}{2} - 2|\alpha_{\mathbf{q}}|^2\lambda^2 t^2\left(1 + \frac{\omega_{\mathbf{q}}}{|\alpha_{\mathbf{q}}|^2\lambda}\right)\,, \tag{3.80}$$

which is smaller than its coherent state value $\langle(\Delta X(\mathbf{q},t))^2\rangle_{\rm coh} = 1/2$. Furthermore, since the expression (3.79) for $\langle(\Delta X(\mathbf{q},t))^2\rangle_{\rm sq'}$ is periodic in time, we can have a periodic squeezing effect in such a system.

The Hamiltonian H_2 in Eq. (3.77) can be generalized to the more anharmonic case

$$H_k = \hbar\omega_{\mathbf{q}}\, b^\dagger_{\mathbf{q}} b_{\mathbf{q}} + \hbar\lambda\,(b^\dagger_{\mathbf{q}} b_{\mathbf{q}})^k\,, \tag{3.81}$$

where k is an integer larger than two. Systems described by H_k conserve the number of phonons in a particular mode for any integer value of k. In general, the number of phonons is not conserved. Thus, we will only consider here the very-short-time limit of low-energy, long-lifetime acoustic phonons. In this very-short-time limit the number of phonons is approximately constant. For example, Tamura's calculations [74] indicate that some acoustic phonon lifetime are of the order of milliseconds.

In the Schrödinger picture, we can calculate the time-dependent variance of $X(\mathbf{q})$, but only numerically when $k > 2$. If the initial state is a coherent state, then the state vector at time t takes the form

$$\begin{aligned}
|\psi(t)\rangle &= e^{-iHt/\hbar}|\alpha_{\mathbf{q}}\rangle = \exp\left\{-i\omega_{\mathbf{q}} t b^\dagger_{\mathbf{q}} b_{\mathbf{q}} - i\lambda t (b^\dagger_{\mathbf{q}} b_{\mathbf{q}})^k\right\}|\alpha_{\mathbf{q}}\rangle \\
&= e^{-\frac{|\alpha_{\mathbf{q}}|^2}{2}} \sum_n \frac{(\alpha_{\mathbf{q}} e^{-i\omega_{\mathbf{q}} t})^n}{\sqrt{n!}} e^{-i\lambda t n^k}|n\rangle \\
&= e^{-\frac{|\alpha_{\mathbf{q}}(t)|^2}{2}} \sum_n \frac{\alpha_{\mathbf{q}}(t)^n}{\sqrt{n!}} e^{-i\phi_n}|n\rangle
\end{aligned} \tag{3.82}$$

where $\alpha_{\mathbf{q}}(t) = \alpha_{\mathbf{q}} e^{-i\omega_{\mathbf{q}} t}$ and $\phi_n = \lambda t n^k$. Compared to coherent states, this state is still a phase-coherent superposition of number states, and the number distribution is still Poissonian. The only difference is the phase factor $e^{-i\phi_n}$ in the sum. This factor will lead to a different superposition of number states, and thus to a squeezed state for quadrature operators.

Now that the state vector $|\psi(t)\rangle$ for the anharmonic Hamiltonian H_k is known, the variance of the quadrature operator $\langle\psi(t)|(\Delta X(\mathbf{q}))^2|\psi(t)\rangle$ can be calculated. The variances of the phonon operators in $|\psi(t)\rangle$ are

$$\begin{aligned}
\langle\psi(t)|b^2_{\mathbf{q}}|\psi(t)\rangle &= e^{-|\alpha_{\mathbf{q}}|^2} \sum_{m,n=0}^{\infty} \langle m| \frac{(\alpha^*_{\mathbf{q}} e^{i\omega_{\mathbf{q}} t})^m}{\sqrt{m!}} \frac{(\alpha_{\mathbf{q}} e^{-i\omega_{\mathbf{q}} t})^n}{\sqrt{n!}} e^{i(\phi_m - \phi_n)} \sqrt{n(n-1)}\,|n-2\rangle \\
&= e^{-|\alpha_{\mathbf{q}}|^2} \sum_{n=2}^{\infty} \frac{|\alpha_{\mathbf{q}}|^{2(n-2)}}{(n-2)!} \alpha^2_{\mathbf{q}} e^{-2i\omega_{\mathbf{q}} t} e^{i(\phi_{n-2} - \phi_n)} \\
&= \alpha^2_{\mathbf{q}} e^{-2i\omega_{\mathbf{q}} t} e^{-|\alpha_{\mathbf{q}}|^2} \sum_{n=0}^{\infty} \frac{|\alpha_{\mathbf{q}}|^{2n}}{n!} e^{-i(\phi_{n+2} - \phi_n)}\,,
\end{aligned} \tag{3.83}$$

$$\begin{aligned}
\langle\psi(t)|b_{\mathbf{q}}^{\dagger}b_{\mathbf{q}}|\psi(t)\rangle &= e^{-|\alpha_{\mathbf{q}}|^2}\sum_{m,n=0}^{\infty}\langle m|\frac{(\alpha_{\mathbf{q}}^{*}e^{i\omega_{\mathbf{q}}t})^m}{\sqrt{m!}}\frac{(\alpha_{\mathbf{q}}e^{-i\omega_{\mathbf{q}}t})^n}{\sqrt{n!}}e^{i(\phi_m-\phi_n)}n|n\rangle \\
&= e^{-|\alpha_{\mathbf{q}}|^2}\sum_{n=1}^{\infty}\frac{|\alpha_{\mathbf{q}}|^{2n}}{(n-1)!} \\
&= |\alpha_{\mathbf{q}}|^2 \qquad (3.84) \\
\langle\psi(t)|b_{\mathbf{q}}|\psi(t)\rangle &= e^{-|\alpha_{\mathbf{q}}|^2}\sum_{m,n=0}^{\infty}\langle m|\frac{(\alpha_{\mathbf{q}}^{*}e^{i\omega_{\mathbf{q}}t})^m}{\sqrt{m!}}\frac{(\alpha_{\mathbf{q}}e^{-i\omega_{\mathbf{q}}t})^n}{\sqrt{n!}}e^{i(\phi_m-\phi_n)}\sqrt{n-1}\,|n-1\rangle \\
&= e^{-|\alpha_{\mathbf{q}}|^2}\sum_{n=1}^{\infty}\frac{|\alpha_{\mathbf{q}}|^{2(n-1)}}{(n-1)!}\alpha_{\mathbf{q}}e^{-i\omega_{\mathbf{q}}t}e^{i(\phi_{n-1}-\phi_n)} \\
&= \alpha_{\mathbf{q}}e^{-i\omega_{\mathbf{q}}t}e^{-|\alpha_{\mathbf{q}}|^2}\sum_{n=0}^{\infty}\frac{|\alpha_{\mathbf{q}}|^{2n}}{n!}e^{-i(\phi_{n+1}-\phi_n)}\,. \qquad (3.85)
\end{aligned}$$

Therefore, the fluctuation of the single-mode quadrature operator $X(\mathbf{q}) = (b_{\mathbf{q}} + b_{\mathbf{q}}^{\dagger})/\sqrt{2}$ is

$$\begin{aligned}
\langle\psi(t)|(\Delta X(\mathbf{q}))^2|\psi(t)\rangle &= \frac{1}{2}\left\{\langle\psi(t)|(b_{\mathbf{q}}+b_{\mathbf{q}}^{\dagger})^2|\psi(t)\rangle - \langle\psi(t)|(b_{\mathbf{q}}+b_{\mathbf{q}}^{\dagger})|\psi(t)\rangle^2\right\} \\
&= Re\left\{\alpha_{\mathbf{q}}^2e^{-2i\omega_{\mathbf{q}}t}e^{-|\alpha_{\mathbf{q}}|^2}\sum_{n=0}^{\infty}\frac{|\alpha_{\mathbf{q}}|^{2n}}{n!}e^{-i(\phi_{n+2}-\phi_n)}\right\} + |\alpha_{\mathbf{q}}|^2 + \frac{1}{2} \\
&\quad -2\left\{Re\left[\alpha_{\mathbf{q}}e^{-i\omega_{\mathbf{q}}t}e^{-|\alpha_{\mathbf{q}}|^2}\sum_{n=0}^{\infty}\frac{|\alpha_{\mathbf{q}}|^{2n}}{n!}e^{-i(\phi_{n+1}-\phi_n)}\right]\right\}^2 . \qquad (3.86)
\end{aligned}$$

If at some specific times $\langle\psi(t)|(\Delta X(\mathbf{q}))^2|\psi(t)\rangle = \langle(\Delta X(\mathbf{q}))^2\rangle_{\mathrm{sq}'}$ reaches its minimum value $\langle(\Delta X(\mathbf{q}))^2\rangle_{\mathrm{sq}'} = e^{-r}/2$, which is less than $1/2$, then r is the maximum squeezing factor of $\langle(\Delta X(\mathbf{q}))^2\rangle_{\mathrm{sq}'}$. It measures how the variance decreases from the coherent state value $\langle(\Delta X(\mathbf{q}))^2\rangle_{\mathrm{coh}} = 1/2$.

Figure 3.3 presents some numerical results for the maximum squeezing exponent r, $\max\{r\}$. The general trend is that the squeezing effect is maximized by increasing the average phonon number $\langle n\rangle$ in the initial state. Furthermore, for larger values of the initial $\langle n\rangle$, the squeezing effect is larger for greater values of k, the degree of the nonlinearity in the potential. Thus, the squeezing effect is maximized by increasing both the nonlinearity in the potential and the initial average phonon number.

3.4 Generation of Phonon Squeezed States

In this section we discuss several possible ways to generate squeezed states of phonons. We first focus on the three-phonon parametric down-conversion and make a full description of the whole process, starting from the optical excitation of the optical phonon modes. Then we turn to another possible way of producing phonon squeezed states based on second-order

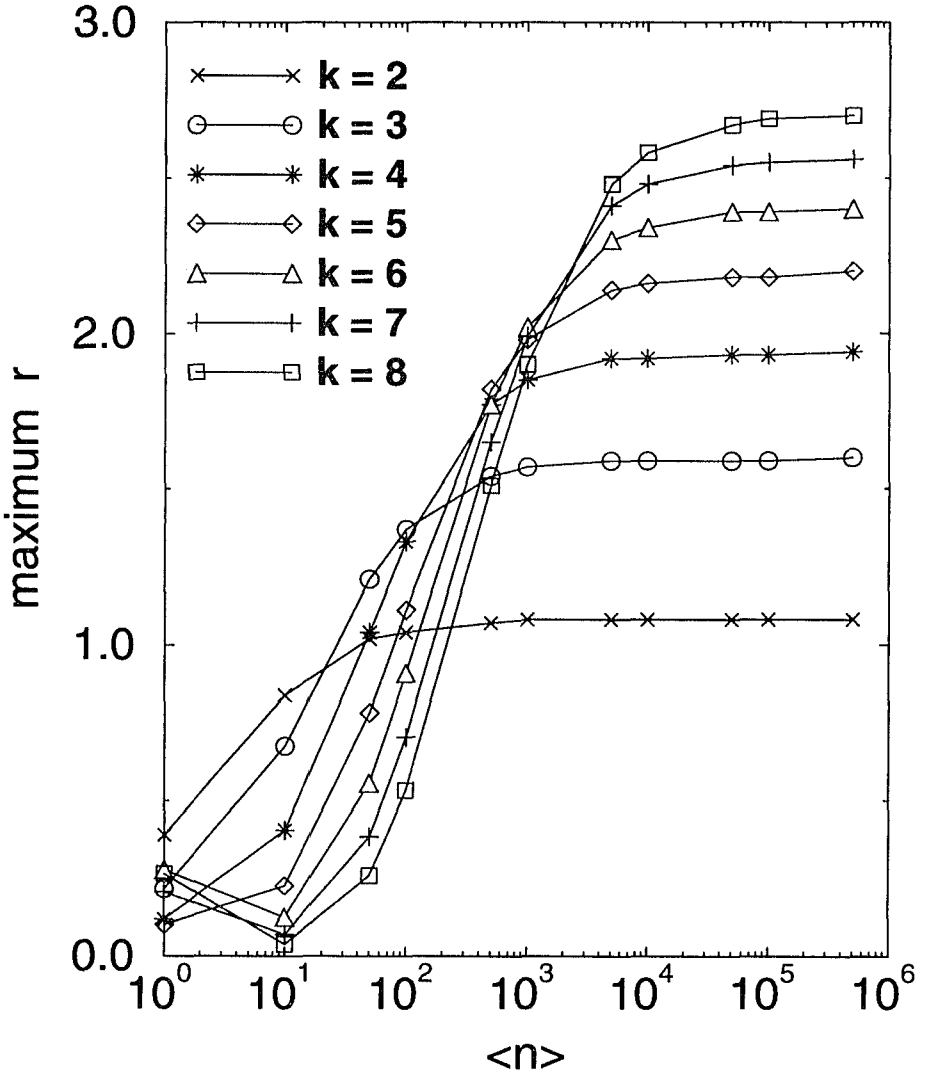

Figure 3.3: The maximum value of the squeezing exponent r, $\max\{r\}$, versus the initial average phonon number $\langle n \rangle$. This figure shows the squeezing effect in a phonon system with a potential $V_k \propto x^{2k}$. A larger k corresponds to a higher degree of nonlinearity in the potential energy. Notice that increasing the average phonon number $\langle n \rangle$ in the initial state leads to an increase in the maximum of r, but this rise in $\max\{r\}$ saturates at large $\langle n \rangle$. Also notice that, for a fixed and large $\langle n \rangle$, $\max\{r\}$ increases with the degree of nonlinearity k.

Raman scattering. We also re-analyze the simple short-time squeezing mechanism described in Section 3.3.5, applicable only for very short times, as another alternative way to generate phonon squeezed states. Finally, the effect of the continuum background is discussed.

3.4.1 Three-Phonon Parametric Amplification Process

Parametric Amplification Processes

A possible mechanism to generate phonon squeezed states is based on a three-phonon parametric down-conversion process (e.g., the decaying process LO phonon $\rightarrow$ two LA phonons, where LO refers to Longitudinal Optical, and LA refers to Longitudinal Acoustic). In a (nonlinear) parametric amplifier [60, 61], an input "signal" wave of frequency ω_s is mixed together with an intense "pump" wave of frequency ω_p. As a result of the parametric process, the input "signal" wave is amplified (called the output "signal" wave), accompanied by an "idler" output wave of frequency $\omega_i = \omega_p - \omega_s$ (see Fig. 3.4). Energy is transfered from the incident pump wave to both the output signal and idler waves.

Parametric processes exist in a variety of contexts and may manifest itself in different manners. They are typically called down-conversion processes when there is no amplification involved, and the input signal of frequency ω converts into two signals of frequency ω_1 and ω_2 which satisfy $\omega_1 + \omega_2 = \omega$. For example, if the pump and the idler are photon modes while the signal is made of phonons or excitons, the parametric process is called Raman scattering [60, 61]. In a Raman process the phonon mode is generally a Brillouin-Zone-center Longitudinal Optical (LO) mode. It does not necessarily have to have a finite population initially, as long as the phonon mode is Raman active. In other words, this parametric process can use the zero point fluctuation of the phonon mode as the input signal. Another example of a parametric process occurs when all the three waves are photon modes. This is referred to as a non-degenerate parametric process in the optics literature [60, 61]. Furthermore, if both the input signal and idler photons are in the same mode, so that $\omega_i = \omega_s$, then it is called a degenerate parametric process; its inverse induces second-harmonic generation [60, 61] since $\omega_p = \omega_i + \omega_s = 2\omega_s$.

Phonon Parametric Down-conversion

Here we would like to consider a phonon parametric down-conversion process where all the three modes are phonon modes. Such a process is based on three-phonon interactions. For all parametric processes, the pump wave must be very strong. This is because the generic parametric process is nonlinear and is weak in most cases—including phonon sys-

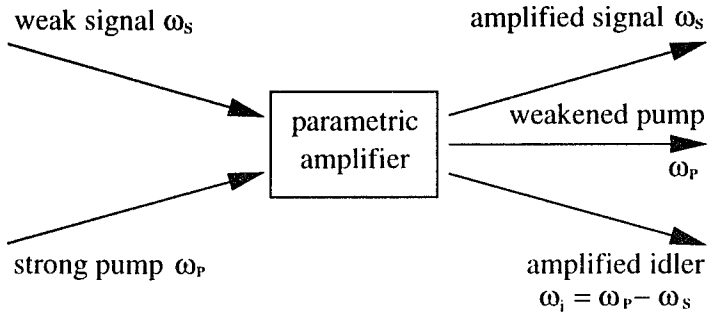

Figure 3.4: A schematic diagram of a nonlinear parametric amplification process, where the input signal is amplified because energy is transfered from the strong incident pump wave to both the output signal and the idler wave. The frequencies of the three waves are related by $\omega_p = \omega_s + \omega_i$. In our case, we have a strong pump of coherent optical phonons and a signal and an idler of acoustic phonons.

tems. Therefore, to realize a phonon parametric process, it is necessary to have a strong input of phonons in the pump mode.

Typically, three-phonon interactions are the dominant anharmonic processes in a phonon system and the lowest order perturbation to the harmonic Hamiltonian. We will neglect all the higher order interactions because they are generally much weaker than the third-order ones. Using the rotating wave approximation [6], which keeps the terms that can satisfy energy conservation, only terms like $b_s b_i b_p^\dagger$ and $b_s^\dagger b_i^\dagger b_p$ are left at the third-order. They lead to three-body interactions such as creating a pump mode phonon while annihilating two phonons in signal and idler modes respectively. If there is a degeneracy in the signal and idler modes, the aforementioned terms change to $b_s^2 b_p^\dagger$ and $b_s^{\dagger 2} b_p$. Below we will use the sub-indices s, i, and p to represent the "signal", "idler", and "pump" modes, respectively.

The simplest Hamiltonian with only three modes is

$$H_{3-\text{phonon}} = \hbar\omega_s b_s^\dagger b_s + \hbar\omega_i b_i^\dagger b_i + \hbar\omega_p b_p^\dagger b_p + \lambda^* b_s b_i b_p^\dagger + \lambda b_s^\dagger b_i^\dagger b_p, \tag{3.87}$$

with the energy conservation relation $\omega_s + \omega_i = \omega_p$. Similar to other parametric processes, we assume that the pump mode is classically driven into a coherent state $|\alpha_p e^{-i\omega_p t}\rangle$ of large amplitude and thus consider a mean field average over it. In other words, the creation and annihilation operators of the pump mode in the Hamiltonian are treated as c-numbers, $\alpha_p e^{-i\omega_p t}$ and $\alpha_p^* e^{i\omega_p t}$, instead of non-commuting operators. We can then consider the following simplified mean-field Hamiltonian

$$H_{3-\text{phonon}}^{MF} = \hbar\omega_s b_s^\dagger b_s + \hbar\omega_i b_i^\dagger b_i + \lambda^* \alpha_p^* e^{i\omega_p t} b_s b_i + \lambda \alpha_p e^{-i\omega_p t} b_s^\dagger b_i^\dagger . \tag{3.88}$$

The $\hbar\omega_p|\alpha_p|^2$ term is dropped from $H^{MF}_{3-\text{phonon}}$. In fact, a c-number term, even if time-dependent, does not affect quantum fluctuations. This can be seen by considering the following example Hamiltonian

$$H_{\text{ex}} = H_{\text{a}}(t) + F(t), \tag{3.89}$$

where $F(t)$ is a time-dependent scalar function. The corresponding state vector is

$$\begin{aligned} |\psi(t)\rangle_{\text{ex}} &= e^{-\frac{i}{\hbar}\int H_{\text{ex}}(\tau)d\tau}|\psi(0)\rangle_{\text{ex}} \\ &= e^{-\frac{i}{\hbar}\int F(\tau)d\tau}e^{-\frac{i}{\hbar}\int H_{\text{a}}(\tau)d\tau}|\psi(0)\rangle_{\text{ex}}. \end{aligned} \tag{3.90}$$

The time evolution operator $e^{-i\int H_{\text{ex}}(\tau)d\tau/\hbar}$ was split into two factors, because the exponential $e^{-i\int F(\tau)d\tau/\hbar}$ is an overall scalar phase factor which does not affect the expectation value of any operator. Since our purpose here is to calculate the quantum fluctuations and time averages of the lattice amplitude operator $u(\pm\mathbf{q})$, we can always drop any c-number term, time-dependent or not, from the Hamiltonian.

As discussed in Appendix B.3, the Hamiltonian $H^{MF}_{3-\text{phonon}}$ in Eq. (3.88) can generate two-mode quadrature squeezed states from a coherent state in both the signal and idler modes. The squeezing factor is

$$\xi(t) = \frac{i}{\hbar}\lambda\,\alpha_p\,t\,, \tag{3.91}$$

where α_p is the absolute value of the coherent amplitude of the pump mode. Notice that here the idler mode is not really "idle" because it plays an active role in the squeezing process, and is one of the modes of the two-mode squeezed state.

More Complete Description of the Three-Phonon Interaction Process

Using the Hamiltonian $H_{3-\text{phonon}}$, it is possible to generate a two-mode quadrature squeezed acoustic phonon state in the output signal and idler modes by pumping the pump mode into a coherent state of large amplitude. This pumping process can be realized by using two lasers to illuminate a crystal. With appropriate laser frequencies and directions, coherent *optical* phonons of the pump mode can be generated through, for example, stimulated Raman scattering (provided that the pump mode is Raman active), as we described in Section 3.3.4, and as discussed, e.g., in Ref. [35].

Thus the Hamiltonian for the whole process initiated by the Raman scattering is (see

Fig. 3.5)

$$\begin{cases} H_{\text{parametric}} &= H_0 + H_{\text{Raman}} + H_{\text{anharmonic}} \\ H_0 &= \hbar\omega_{\mathbf{k}_1} a^\dagger_{\mathbf{k}_1} a_{\mathbf{k}_1} + \hbar\omega_{\mathbf{k}_2} a^\dagger_{\mathbf{k}_2} a_{\mathbf{k}_2} + \sum_{\mathbf{q}} \hbar\omega_{\mathbf{q}} b^\dagger_{\mathbf{q}} b_{\mathbf{q}} \\ H_{\text{Raman}} &= \eta a_{\mathbf{k}_1} a^\dagger_{\mathbf{k}_2} b^\dagger_{\mathbf{q}_p} + \eta^* a^\dagger_{\mathbf{k}_1} a_{\mathbf{k}_2} b_{\mathbf{q}_p} \\ H_{\text{anharmonic}} &= \lambda_{\mathbf{q}_s\mathbf{q}_i} b_{\mathbf{q}_p} b^\dagger_{\mathbf{q}_s} b^\dagger_{\mathbf{q}_i} + \lambda^*_{\mathbf{q}_s\mathbf{q}_i} b^\dagger_{\mathbf{q}_p} b_{\mathbf{q}_s} b_{\mathbf{q}_i} \\ & \quad + \sum_{\mathbf{q}'\mathbf{q}''} (\lambda_{\mathbf{q}'\mathbf{q}''} b_{\mathbf{q}_p} b^\dagger_{\mathbf{q}'} b^\dagger_{\mathbf{q}''} + \lambda^*_{\mathbf{q}'\mathbf{q}''} b^\dagger_{\mathbf{q}_p} b_{\mathbf{q}'} b_{\mathbf{q}''}) \,. \end{cases} \tag{3.92}$$

Here a and b refer to photon and phonon operators, respectively. The higher- (lower-) energy incident photon mode is labeled as $\mathbf{k}_1$ ($\mathbf{k}_2$), and the lower-energy photon mode is generally called Stokes mode in the context of Raman scattering. The sums over $\mathbf{q}'$ and $\mathbf{q}''$ in $H_{\text{anharmonic}}$ represent decay channels other than the special one with acoustic signal and idler modes. In general, the lower energy phonons are Longitudinal Acoustic (LA) ones because the pump mode phonons are longitudinal optical phonons.

We now consider two mean field averages in order to simplify an otherwise analytically intractable problem. The first mean field is over the photons. The photons in the incident modes $\mathbf{k}_1$ and $\mathbf{k}_2$ (often denoted by "laser" and "Stokes" light) originate from two lasers. For a reason that will be apparent in the next few paragraphs, we assume that the photons in both modes are in ultrashort pulses with respective amplitudes $\alpha_{\mathbf{k}_1}$ and $\alpha_{\mathbf{k}_2}$. After averaging over the photon modes $\mathbf{k}_1$ and $\mathbf{k}_2$, the Hamiltonian becomes

$$\begin{cases} H'_{\text{parametric}} &= H'_0 + H'_{\text{Raman}} + H_{\text{anharmonic}} \\ H'_0 &= \hbar\omega_{\mathbf{k}_1} |\alpha_{\mathbf{k}_1}|^2 + \hbar\omega_{\mathbf{k}_2} |\alpha_{\mathbf{k}_2}|^2 + \sum_{\mathbf{q}} \hbar\omega_{\mathbf{q}} b^\dagger_{\mathbf{q}} b_{\mathbf{q}} \\ H'_{\text{Raman}} &= \eta |\alpha_{\mathbf{k}_1} \alpha_{\mathbf{k}_2}| \delta(t - t_0) b^\dagger_{\mathbf{q}_p} + \eta^* |\alpha_{\mathbf{k}_1} \alpha_{\mathbf{k}_2}| \delta(t - t_0) b_{\mathbf{q}_p} \\ H_{\text{anharmonic}} &= \lambda_{\mathbf{q}_s\mathbf{q}_i} b_{\mathbf{q}_p} b^\dagger_{\mathbf{q}_s} b^\dagger_{\mathbf{q}_i} + \lambda^*_{\mathbf{q}_s\mathbf{q}_i} b^\dagger_{\mathbf{q}_p} b_{\mathbf{q}_s} b_{\mathbf{q}_i} \\ & \quad + \sum_{\mathbf{q}'\mathbf{q}''} (\lambda_{\mathbf{q}'\mathbf{q}''} b_{\mathbf{q}_p} b^\dagger_{\mathbf{q}'} b^\dagger_{\mathbf{q}''} + \lambda^*_{\mathbf{q}'\mathbf{q}''} b^\dagger_{\mathbf{q}_p} b_{\mathbf{q}'} b_{\mathbf{q}''}) \,. \end{cases} \tag{3.93}$$

Here the pump mode phonon frequency $\omega_{\mathbf{q}_p}$ is the frequency difference of the two photon modes $\omega_{\mathbf{q}_p} = \omega_{\mathbf{k}_1} - \omega_{\mathbf{k}_2}$. Such an equality can always be achieved with a photon pulse, which is wide-band. In addition, since photon wave vectors are very small compared to phonons', we assume that the pump mode LO phonons have a wave-vector $\mathbf{q}_p \cong 0$.

The second mean field average is over the pump mode longitudinal optical phonons. As we discussed in the last part of Section 3.3.4, LO phonons produced by coherent or stimulated Raman scattering with an ultrashort pulse are in *constant* amplitude coherent states. This pump mode phonon coherent state $|\beta_0 e^{-i\omega_{\mathbf{q}_p} t}\rangle$ satisfies $\langle \beta_0 e^{-i\omega_{\mathbf{q}_p} t} | b_{\mathbf{q}_p} | \beta_0 e^{-i\omega_{\mathbf{q}_p} t} \rangle = \beta_0 e^{-i\omega_{\mathbf{q}_p} t}$. Here we use $H'_0 + H'_{\text{Raman}}$ to determine β_0, and then substitute β_0 back into $H'_{\text{parametric}}$ to obtain $H''_{\text{parametric}}$. Since these LO phonons are in coherent states, the results from the average over the pump mode phonons are c-numbers with a well-behaved time-dependence. Moreover, if the three-phonon process is a normal process (in which the

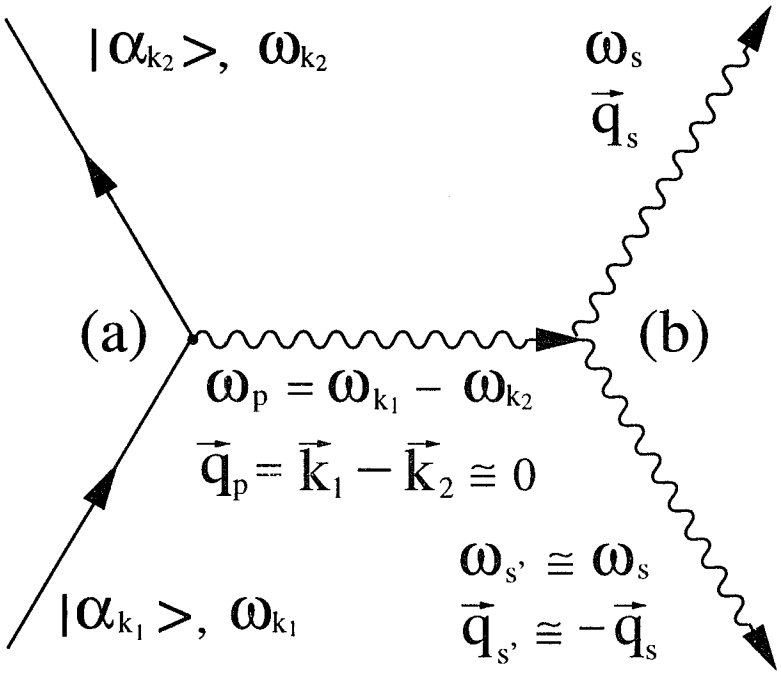

Figure 3.5: A schematic diagram of a three-phonon parametric downconversion process. Here (a) refers to a stimulated Raman scattering and (b) to a three-phonon anharmonic scattering process. The subscript $\mathbf{k}_1$ ($\mathbf{k}_2$) refers to the higher- (lower-) energy incident coherent photons. The arrows indicate the directions of the photon and phonon momentum vectors. A typical process is as follows: a photon in mode $\mathbf{k}_1$ interacts with the phonon system and emits one optical phonon in the pump mode of frequency ω_p, while the photon itself is scattered into mode $\mathbf{k}_2$; the generated pump mode optical phonon proceeds in the crystal, interacts with the lower-energy phonon modes through the three-phonon interaction, and eventually splits into two acoustic phonons in modes s and s'. Notice that the pump mode optical phonons have an almost-zero wave vector, so that the two lower-energy acoustic phonon modes have nearly opposite wave vectors $\pm\mathbf{q}_s$. The latter can be in a two-mode phonon squeezed state for appropriate initial states. Notice that this figure is not to scale. The appropriate scale in the figure would make all four lines of photons and phonons (excluding the horizontal wavy line corresponding to the pump mode optical phonon) vertical and almost parallel with each other. For the sake of clarity, we have increased the angle between the vertical lines.

quasi-momentum is conserved $\mathbf{q}_p = \mathbf{q}_i + \mathbf{q}_s$), we then have a special constraint on the resulting phonon wave vectors $\mathbf{q}_i \cong -\mathbf{q}_s$ because $\mathbf{q}_p \cong 0$. After these operations, the Hamiltonian can be simplified to

$$\left\{\begin{array}{lcl} H''_{\text{parametric}} & = & H''_0 + H''_{\text{Raman}} + H'_{\text{anharmonic}} \\ H''_0 & = & \hbar\omega_{\mathbf{k}_1}|\alpha_{\mathbf{k}_1}|^2 + \hbar\omega_{\mathbf{k}_2}|\alpha_{\mathbf{k}_2}|^2 + \hbar\omega_{\mathbf{q}_p}|\beta_0(t)|^2 + \sum_{\mathbf{q}} \hbar\omega_{\mathbf{q}} b^\dagger_{\mathbf{q}} b_{\mathbf{q}} \\ H''_{\text{Raman}} & = & \eta|\alpha_{\mathbf{k}_1}\alpha_{\mathbf{k}_2}|e^{-i\omega_{\mathbf{q}_p}t}\beta_0^* + \eta^*|\alpha_{\mathbf{k}_1}\alpha_{\mathbf{k}_2}|e^{i\omega_{\mathbf{q}_p}t}\beta_0 \\ H'_{\text{anharmonic}} & = & \lambda_{\mathbf{q}_s\mathbf{q}_i}\beta_0 e^{-i\omega_{\mathbf{q}_p}t} b^\dagger_{\mathbf{q}_s} b^\dagger_{\mathbf{q}_i} + \lambda^*_{\mathbf{q}_s\mathbf{q}_i}\beta_0^* e^{i\omega_{\mathbf{q}_p}t} b_{\mathbf{q}_s} b_{\mathbf{q}_i} \\ & & + \sum_{\mathbf{q}'\mathbf{q}''}(\lambda_{\mathbf{q}'\mathbf{q}''}\beta_0(t) b^\dagger_{\mathbf{q}'} b^\dagger_{\mathbf{q}''} + \lambda^*_{\mathbf{q}'\mathbf{q}''}\beta_0^*(t) b_{\mathbf{q}'} b_{\mathbf{q}''}) \,. \end{array}\right. \tag{3.94}$$

Now we drop all the c-number terms, based on the argument presented in Eqs. (3.89)–(3.90), because they will not affect the calculations of the fluctuations and expectation values of the lattice amplitude operator. In addition, we also drop all the phonon modes involved in the decay channels other than the special one consisting of the signal modes, considering them only weakly coupled to the pump mode; i.e., we assume $\lambda_{\mathbf{q}'\mathbf{q}''} \ll \lambda_{\mathbf{q}_s\mathbf{q}_i}$. The Hamiltonian now becomes

$$\begin{aligned} H'''_{\text{parametric}} &= \hbar\omega_{\mathbf{q}_s} b^\dagger_{\mathbf{q}_s} b_{\mathbf{q}_s} + \hbar\omega_{-\mathbf{q}_s} b^\dagger_{-\mathbf{q}_s} b_{-\mathbf{q}_s} \\ &\quad + \lambda_{\mathbf{q}_s,-\mathbf{q}_s}\beta_0 e^{-i\omega_{\mathbf{q}_p}t} b^\dagger_{\mathbf{q}_s} b^\dagger_{-\mathbf{q}_s} + \lambda^*_{\mathbf{q}_s,-\mathbf{q}_s}\beta_0^* e^{i\omega_{\mathbf{q}_p}t} b_{\mathbf{q}_s} b_{-\mathbf{q}_s}, \end{aligned} \tag{3.95}$$

where $\beta_0 e^{-i\omega_{\mathbf{q}_p}t}$ is the coherent amplitude of the pump mode LO phonons. Here we have implicitly assumed that the Raman scattering process is much stronger than the anharmonic scattering. According to the discussions in Section 3.3.5, the two-mode LA phonon system will evolve into a two-mode squeezed state $|\alpha_{\mathbf{q}_s}, \alpha_{-\mathbf{q}_s}, \xi(t)\rangle$ from an initial coherent or vacuum state, with a squeezing factor given by

$$\xi(t) = \frac{i}{\hbar}\lambda_{\mathbf{q}_s,-\mathbf{q}_s}\beta_0\, t\,. \tag{3.96}$$

The state $|\alpha_{\mathbf{q}_s}, \alpha_{-\mathbf{q}_s}, \xi(t)\rangle$ is exactly the one we used to calculate the expectation values and quantum fluctuations of the lattice amplitude operator $u(\pm\mathbf{q})$ in Section 3.3.5. It is a two-mode phonon squeezed state with a squeezing factor $\xi(t)$. Notice that to obtain this squeezed state, the pump mode has to be in a constant amplitude coherent state, which is in turn a result of the ultrashort pulse coherent photon pump. If the input photon modes are in coherent states, then the pump mode optical phonons will be in a coherent state with an amplitude growing linearly with time. With such a pump mode phonon state, we will not be able to obtain a time-evolution operator in the form of squeezing operator. Therefore, a crucial condition for the realization of a phonon squeezed state through our parametric process is that the photons come in as a pulse. The linear divergence in the squeezing

operator will not materialize in a real system, because various dissipation mechanisms are present in an experiment, so that the fluctuations generated by these processes will rapidly overshadow the intrinsic quantum noise in the phonon modes. Nevertheless, the squeezing effect should be dominant during the short initial moment.

In summary, we have just considered generating two-mode LA phonon squeezed states $|\alpha_{\mathbf{q}_s}, \alpha_{-\mathbf{q}_s}, \xi(t)\rangle$ by using the three-phonon anharmonic interaction. The higher-energy LO phonon mode, which is called the "pump" mode, is driven into a coherent state through a stimulated Raman scattering by a strong photon pulse. This mode in turn is used as a pump in the parametric amplification process involving itself and the two lower-energy LA phonon modes ($\pm\mathbf{q}_s$), the signal and the idler. Both of these modes can here be called "signal" because the "idler" mode is not really "idle"; indeed, it is actively involved in the squeezing process. We have shown that the LA phonons in the two signal modes ($\pm\mathbf{q}_s$) are in a two-mode squeezed state before relaxation if (i) the LO pump mode is in a coherent state and (ii) we can neglect the other decay channels.

3.4.2 Two-Phonon Raman Scattering Process

So far, we have only used first-order Raman scattering to generate coherent phonons. If we consider a second-order stimulated Raman process (see Fig. 3.6), the Hamiltonian can be written as

$$\begin{cases} H^{(2)}_{\text{Raman}} &= H_0 + H_{\text{int}} \\ H_0 &= \hbar\omega_{\mathbf{k}_1} a^\dagger_{\mathbf{k}_1} a_{\mathbf{k}_1} + \hbar\omega_{\mathbf{k}_2} a^\dagger_{\mathbf{k}_2} a_{\mathbf{k}_2} + \sum_{\mathbf{q}_s} \hbar\omega_{\mathbf{q}_s} b^\dagger_{\mathbf{q}_s} b_{\mathbf{q}_s} \\ H_{\text{int}} &= \sum_{\mathbf{q}_s} g_{\mathbf{q}_s} a_{\mathbf{k}_1} a^\dagger_{\mathbf{k}_2} b^\dagger_{\mathbf{q}_s} b^\dagger_{-\mathbf{q}_s}, \end{cases} \tag{3.97}$$

where $g_{\mathbf{q}_s}$ is the second-order Raman interaction constant. A mean field theory over the two incident coherent photon modes $\mathbf{k}_1$ (higher-energy) and $\mathbf{k}_2$ (lower-energy) produces the following Hamiltonian for the two excited acoustic phonon modes ($\pm\mathbf{q}_s$)

$$H^{(2)}_{\text{Raman-MF}} = \hbar\omega_{\mathbf{q}_s}(b^\dagger_{\mathbf{q}_s} b_{\mathbf{q}_s} + b^\dagger_{-\mathbf{q}_s} b_{-\mathbf{q}_s}) + c_{\mathbf{q}_s}(t)\, b^\dagger_{\mathbf{q}_s} b^\dagger_{-\mathbf{q}_s} + c^*_{\mathbf{q}_s}(t)\, b_{\mathbf{q}_s} b_{-\mathbf{q}_s}, \tag{3.98}$$

where $c_{\mathbf{q}_s}(t) = \langle g_{\mathbf{q}_s} a_{\mathbf{k}_1} a^\dagger_{\mathbf{k}_2} \rangle$ and has a time-dependent factor of $e^{-i(\omega_{\mathbf{q}_s}+\omega_{-\mathbf{q}_s})t}$, and the c-number terms obtained from the mean field average over $\hbar\omega_{\mathbf{k}_1} a^\dagger_{\mathbf{k}_1} a_{\mathbf{k}_{q_1}}$ and $\hbar\omega_{\mathbf{k}_2} a^\dagger_{\mathbf{k}_2} a_{\mathbf{k}_2}$ have been dropped because they do not contribute to the amplitude averages and fluctuations, as we saw above in this section. Thus, from the previous discussion in Section 3.3.5, $H^{(2)}_{\text{Raman-MF}}$ can generate two-mode squeezed states in these acoustic phonon modes. If for any reason the first-order Raman scattering is either very weak or prohibited, the second-order stimulated Raman scattering process can be used to generate two-mode

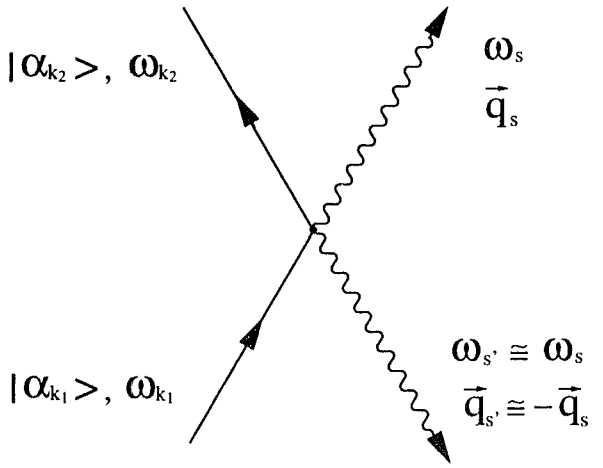

Figure 3.6: A stimulated second-order Raman scattering process. The subscript $\mathbf{k}_1$ ($\mathbf{k}_2$) represents the higher- (lower-) energy incident coherent photons. The arrows show the directions of the corresponding photon and phonon momenta. The incoming coherent photon beams are about parallel to each other. The actual physical process is as follows: an incident photon in mode $\mathbf{k}_1$ interacts with a solid, producing two acoustic phonons, and leaves in mode $\mathbf{k}_2$. For appropriate choice of initial photon and phonon states, the acoustic phonons can be in a two-mode squeezed state. Notice that there are also additional incoming photons in mode $\mathbf{k}_2$, therefore this mode becomes stronger after the interaction, at the expense of mode $\mathbf{k}_1$. Also notice that the vector sum of the two phonon momenta is the difference of the input and output photon momentum vectors. Since photon wave vectors are generally much smaller than the phonon ones $|\mathbf{k}_i| \ll |\mathbf{q}_s|$, the two acoustic phonon modes have nearly opposite wave vectors $\pm\mathbf{q}_s$. Similar to Fig. 3.5, this figure is not to scale. The appropriate scale in the figure would make all four lines of photons and phonons vertical and almost parallel with each other. For the sake of clarity, we have increased the angle between them.

phonon quadrature squeezed states $|\alpha_{\mathbf{q}_s}, \alpha_{-\mathbf{q}_s}, \xi(t)\rangle$. In this process, the incident photons should be in coherent states. They do not need to be in a pulse. In other words, we can generate phonon squeezed states with continuous incident photons through a second-order Raman process.

3.4.3 Short-time Squeezing Mechanism in a Single Phonon Mode

As discussed in the last part of Section 3.3.5, another way to generate short-lived squeezed phonons is through a special kind of anharmonic process that conserves the number of phonons in a certain low energy, *long lifetime* acoustic mode, as in the following Hamiltonian

$$H_k = \hbar\omega b^\dagger b + \hbar\lambda(b^\dagger b)^k. \tag{3.99}$$

The interaction in H_k comes from the potential $V_k = g_k x^{2k}$, where $k = 2, 3, \ldots$. Here we consider the short-time limit, and assume that there are phase-space restrictions that elimi-

nate all other processes coming from V_k, so that the phonon-number-conserving potential of H_k is the dominant interaction. According to the discussions in Section 3.3.5, such a Hamiltonian produces periodic squeezing in this single mode, provided that the initial phonon state is a coherent state. To realize such a process, the crystal must have a potential of the form V_k, with the lower-order terms in the potential either vanishing or very weak. Ferroelectric crystals are potential candidates because their atomic interaction energies can be modeled by a harmonic term plus an anharmonic term of the form $V_2 = g_2 x^4$ (see, e.g., Ref. [55]). If the coherent initial state is generated through an optical method such as stimulated Brillouin scattering, very low temperatures are needed so that the thermal occupation of the phonon mode is negligible compared to the optically excited population.

Of course, in general the number of phonons is not conserved. Thus, this mechanism for low-energy, long-lifetime acoustic modes might play a role only for very short times (compared to the lifetime of the particular mode in consideration) when the number of phonons is approximately constant.

3.4.4 The Continuum Background and the Finite Lifetime of Phonons

Calculation of the Phonon Decay Constant

A real three-phonon process must satisfy both energy and quasi-momentum conservation laws. In three dimensions, these constraints produce four equations: one for energy conservation, and three for quasi-momentum conservation. If the energy and quasi-momentum of the initial phonon and the dispersion relations for the outgoing phonons are known, there will be six unknown variables: all six components of the quasi-wave-vectors of the two phonons produced. Thus, there are two unconstrained degrees of freedom [72]. In general, they form a surface in momentum space. In special situations, this surface can degenerate into a line, a point, or even totally disappear. In our calculation on three-phonon interactions presented above, we focused on a special term and did not consider the effect of other terms on the solution surface; this is somewhat oversimplified. Unless we have a very degenerate situation, where only one channel exists for three-phonon decay, all the modes are qualitatively equivalent and thus none of them should be disregarded. Even in this extremely degenerate case, it is still difficult to single out only one decaying mode, because the higher order terms might be non-negligible. To partly remedy this shortcoming, let us now consider the general situation. The complete Hamiltonian is

$$H_{\text{3M-continuum}} = \hbar\omega_p\, b_p^\dagger b_p + \sum_s \hbar\omega_s\, b_s^\dagger b_s$$

$$+ \sum_{s,s',\mathbf{G}} \left\{ \lambda_{ss'} \, b_s b_{s'} b_p^\dagger \, \delta(\mathbf{q}_s + \mathbf{q}_{s'} + \mathbf{G} - \mathbf{q}_p) + h.\,c. \right\}, \quad (3.100)$$

where the δ-functions enforce the conservation of quasi-momentum, $\mathbf{G}$ are reciprocal lattice vectors, and the sum runs over all the final states of the possible three-phonon processes originating from the pump mode optical phonons. Here "pump mode" refers to the same mode we studied in Section 3.4.1 on the three-phonon parametric downconversion process. In the situation considered now, there is no real pumping actually happening.

In this section we focus on the decay of phonon modes regardless of their actual state. More precisely, we will calculate the decay constant of the input pump mode (labeled by the subscript "p" in Eq. (3.100)) due to the three-phonon interaction of strength $\lambda_{ss'}$ with lower-energy phonon modes (labeled by the subscripts "s" and "s'" in Eq. (3.100)). Here we choose our system to consist only of the pump mode phonons, and consider all the lower-energy phonon modes together as a reservoir. A system phonon is created by absorbing a pair of phonons from the reservoir, and is annihilated by emitting a pair of phonons into the reservoir. For simplicity let us consider only the normal process, in which $\mathbf{G} = 0$. The Hamiltonian can now be written as

$$\begin{cases} H_T &= H_P + H_R + V_I \\ H_P &= \hbar\omega_p \, b_p^\dagger b_p \\ H_R &= \sum_r \hbar\omega_r \, b_r^\dagger b_r \\ V_I &= \sum_{r,r'} \left\{ \lambda_{rr'} \, b_r b_{r'} b_p^\dagger + h.\,c. \right\}. \end{cases} \quad (3.101)$$

Here P refers to the system consisting of the pump mode phonons, while p refers to the pump mode; R denotes the reservoir consisting of the lower-energy phonons, while r denotes the reservoir phonon modes; and V_I is the interaction between the system P and the reservoir R.

To study the decay of the system phonons in P into reservoir phonons in R, we first use the interaction picture to eliminate the fast rotating part of the density matrix. The Schrödinger equation for the density operator P_{PR} of both the system and the reservoir is

$$\frac{\partial P_{PR}}{\partial t} = -\frac{i}{\hbar} \left[V_I(t - t_0), \, P_{PR} \right], \quad (3.102)$$

where

$$V_I(\tau) = e^{-i(H_P + H_R)\tau/\hbar} \, V_I \, e^{i(H_P + H_R)\tau/\hbar} \quad (3.103)$$

is the interaction between the system and the reservoir in the interaction picture.

Assuming that the interaction V_I between the system H_P and the reservoir H_R can be considered as a perturbation, and after taking a coarse-graining approximation (for further

details, see Appendix C), the Schrödinger equation for the reduced density operator for the system in the interaction picture becomes

$$\begin{aligned}\dot{\rho}(t) \;\cong\; & -\frac{i}{\hbar\tau}\int_0^\tau d\tau'\; tr_r\left\{V_I(\tau')P_{PR}(t)\right\} \\ & -\frac{1}{\hbar^2\tau}\int_0^\tau d\tau'\int_0^{\tau'} d\tau''\, tr_r\left\{V_I(\tau')V_I(\tau'')P_{PR}(t) - V_I(\tau')P_{PR}(t)V_I(\tau'')\right\} \\ & +h.c. \end{aligned} \tag{3.104}$$

Here the iteration has been cut off after second-order terms; ρ is the interaction-picture reduced density operator $\rho(t) \equiv tr_r\{P_{PR}(t)\}$; the trace tr_r is over all the reservoir variables; and $\tau = t - t_0$. Using techniques similar to the ones employed in Appendix A.2 to derive Eq. (A.24), the interaction can be explicitly written as

$$V_I(\tau) = \hbar b_p^\dagger F(\tau) + \hbar b_p F^\dagger(\tau) \tag{3.105}$$

$$F(\tau) = -i\sum_{r,r'}\lambda_{rr'}\, b_r b_{r'}\, e^{i(\omega_p-\omega_r-\omega_{r'})\tau} \tag{3.106}$$

If we assume that the reservoir is always in thermal equilibrium and has a wide bandwidth (as described in many quantum optics textbooks, e.g., [6]), the above Schrödinger equation, Eq. (3.104), can be simplified into a master equation for the system (for a derivation, see Appendix C),

$$\dot{\rho}(t) = -(\Gamma+\gamma)\left(b_p^\dagger b_p\rho - b_p\rho b_p^\dagger\right) - \Gamma\left(\rho b_p^\dagger b_p - b_p^\dagger\rho b_p\right) + h.c. \tag{3.107}$$

$$\begin{aligned}\Gamma = & \frac{\pi}{\hbar^2}\int_{0,\omega\neq\omega_p/2}^{\omega_p} d\omega\, D(\omega)\,|\lambda(\omega,\omega_p-\omega)|^2\, n_\omega n_{\omega_p-\omega} \\ & +\frac{\pi}{\hbar^2}D(\omega_p/2)\,|\lambda(\omega_p/2,\omega_p/2)|^2\,(n_{\omega_p/2}^2 - n_{\omega_p/2})\end{aligned} \tag{3.108}$$

$$\begin{aligned}\gamma = & \frac{\pi}{\hbar^2}\int_{0,\omega\neq\omega_p/2}^{\omega_p} d\omega\, D(\omega)\,\delta\omega\,|\lambda(\omega,\omega_p-\omega)|^2\,(n_\omega + n_{\omega_p-\omega}+1) \\ & +\frac{\pi}{\hbar^2}D(\omega_p/2)\,\delta\omega\,|\lambda(\omega_p/2,\omega_p/2)|^2\,(2n_{\omega_p/2}+1)\,.\end{aligned} \tag{3.109}$$

Here $D(\omega)$ is the density of states for reservoir phonons in the frequency range $(\omega,\omega+d\omega)$, and $\delta\omega$ is the line-width of the $\omega_p/2$-mode in the reservoir. $\lambda(\omega,\omega_p-\omega)$ is the three-phonon interaction strength between the system mode at frequency ω_p and the two lower-energy modes in the reservoir at frequencies ω and $\omega_p-\omega$, respectively. $\lambda(\omega,\omega_p-\omega)$ can be obtained directly from $\lambda_{rr'}$. Any possible degeneracy at the relevant frequencies has been taken into account in the density of states $D(\omega)$. The number n_ω is the thermal equilibrium number of phonons at frequency ω in the reservoir. It satisfies the Planck distribution $n_\omega = 1/(\exp(\hbar\omega/k_BT)-1)$, where T is the reservoir temperature. The constant Γ can be

considered as the rate for the phonons in the reservoir to recombine into system phonons; while $\Gamma + \gamma$ is the rate for system phonons to split into reservoir phonons. The difference γ is the net rate for the system phonons to decay into thermal phonons in the reservoir.

With this master equation, we can calculate the decay of the average population $\langle b_p^\dagger b_p \rangle$ and the coherent amplitude $\langle (b_p^\dagger + b_p) \rangle$ of a single-mode coherent state of the system. The time-evolution of the average population is given by

$$\frac{d\langle b_p^\dagger b_p \rangle}{dt} = -2\gamma \langle b_p^\dagger b_p \rangle + 2\Gamma \,, \tag{3.110}$$

while the average of the lattice amplitude satisfies the relation

$$\frac{d\langle (b_p^\dagger + b_p) \rangle}{dt} = -\gamma \langle (b_p^\dagger + b_p) \rangle \,. \tag{3.111}$$

Notice that the population $\langle b_p^\dagger b_p \rangle$ decays twice as fast (2γ versus γ) as the lattice amplitude $\langle (b_p^\dagger + b_p) \rangle$. This occurs because $b_p^\dagger b_p$ is quadratic and has the same dimensions as the square of the linear operator $b_p^\dagger + b_p$, and the decay mechanism for both is the same anharmonic interaction.

Let us denote by γ_1 the decay constant for the average population $\langle b_p^\dagger b_p \rangle$, and γ_2 as the decay constant for the average lattice amplitude $\langle (b_p^\dagger + b_p) \rangle$. Our calculation here indicates that $\gamma_1 = 2\gamma_2 = 2\gamma$. However, this is not true in general, because γ_2 can also contain contributions from dephasing processes such as elastic collisions between phonons and impurities, which destroy the coherence but will not affect the population very much. Therefore, the two decay constants can differ much less than a factor of two. However, in many materials phonons decay mainly through anharmonic processes. Elastic events that can change the phase of coherent phonon waves while leaving the population unchanged are much weaker than the inelastic ones (see, e.g., [35]).

In Ref. [73] it is pointed out that both the three-phonon interaction and the four-phonon interaction contribute to the phonon self-energy in the same order. However, the four-phonon interaction does not contribute to the phonon lifetime. It only gives the relevant phonon mode an energy shift. Therefore, our calculation of the phonon lifetime presented here, with only a three-phonon interaction, is a reasonable lowest-order estimate.

In the above calculation we assumed that the density matrix can be factorized into a product of two density matrices: the system's and the reservoir's. This is exact for a short period of time right at the beginning, but is only approximate afterwards because of the interaction between the system and the reservoir. Indeed, this approximation is good

when the interaction is weak. In addition, because of the relatively long lifetime of the lower-energy acoustic phonons, the reservoir is not always in thermal equilibrium. This will also introduce corrections to our results. Nevertheless, as it is the case in the quantum optics literature where similar approximations arise, we can consider our calculation to be a first-order approximation that gives a qualitatively correct estimate to the decay of phonons.

Physical Consequences of the Phonon Decay

Through the simple calculation presented above, we are able to show that, by coupling the pump mode phonons (the system) to a continuum of states (the reservoir), these high energy phonons lose their coherence as they proceed through the crystal. This loss of phonon coherence will introduce an additional noise, which we need to overcome to generate squeezed phonon states in the lower energy phonon modes. This noise can be easily modeled by using a Langevin equation for the pump mode phonons. Indeed, the approaches based on the Langevin and master equations are equivalent to each other [6]. Both of them describe a system interacting with a reservoir. A Langevin equation describes the time evolution of a particular dynamical variable, such as the annihilation operator b_p; while the master equation models the evolution of the density matrix of the system. The effect of the reservoir is to give rise to a decay constant *and* a noise term in the Langevin equation, while it only leads to a decay factor in the master equation. This additional noise term in the Langevin equation helps to preserve the commuting property of the dynamical variable. Otherwise, if there is only a decay term without a noise term, the commutator $[b_p, b_p^\dagger]$ will vanish instead of being equal to 1.

Physically, the effect of the finite phonon lifetime is to introduce fluctuations into the number of phonons in the pump mode. The coherence in this mode will then be either entirely or partially lost and the average amplitude of the pump mode $\beta_0(t)$ (see Eq. (3.95)) will not be a quantity with a periodic time-dependence. This irregularity will in turn affect $\xi(t)$, the squeezing factor. If $\beta_0(t)$ is a periodic function of time, $\xi(t)$ will also be periodic. If $\beta_0(t)$ changes with time aperiodically, the integration will fluctuate around zero and $\xi(t)$ will lose its periodicity. This will make the squeezed states undetectable, since the squeezing measurements are generally phase-sensitive (e.g., performed every period) and require the squeezing to be periodic [58].

It is known that the lifetimes of optical phonons are very short, generally of the order of one nanosecond to one picosecond [33]. The lifetimes of the lower-level modes, which are

most probably acoustic modes, should also be taken into consideration. However, they are much longer than the optical ones (up to milliseconds) [74, 75, 76], so that we can neglect them in the present discussion. In addition, phonons in a crystal are not only coupled with each other through anharmonic interactions, but are also coupled with electrons, impurities, etc. Here we will not go in detail about these processes. Instead, we just point out that mass-defect scattering—e.g., due to isotopic impurities—provides an important phonon-decay mechanism in many materials. However, this effect can be eliminated by using materials with a very low concentration of isotopic defects, such as diamond.

3.5 Polaritons and the Squeezing of the Lattice Amplitude

Squeezed states can be generated not only through phonon-phonon interactions, as we have discussed in previous sections, but also through phonon-photon interactions such as the one present in polaritons. When an ionic crystal is illuminated by light, there can be a strong coupling between photons and the local polarization of the crystal in the form of transverse optical (TO) phonons. Photons and phonons are thus not separable anymore. Instead, we have to consider the pair as a single entity, known as a polariton [78]. Here phonon and photon have the same wave vector, so we use $\mathbf{k}$ to denote both of them. In this section we study the squeezing of quantum noise in the atomic displacements of polaritons. The essential idea can be summarized as follows. The incident photons induce transverse optical phonons in the solid through the dipole interaction and introduce a correlation between the $\pm\mathbf{k}$ TO phonon modes. This correlation can produce suppression of quantum noise in the atomic displacements of the lattice.

3.5.1 Diagonalization of the Polariton Hamiltonian

Let us consider the simplest Hamiltonian describing polaritons; following the approach of Madelung [78],

$$\begin{aligned} H_{\text{polariton}} &= \sum_{\mathbf{k}} \Big\{ E_{1\mathbf{k}}\, a_{\mathbf{k}}^{\dagger}\, a_{\mathbf{k}} + E_{2\mathbf{k}}\, b_{\mathbf{k}}^{\dagger}\, b_{\mathbf{k}} \\ &\quad + E_{3\mathbf{k}} \left(a_{\mathbf{k}}^{\dagger} b_{\mathbf{k}} - a_{\mathbf{k}} b_{\mathbf{k}}^{\dagger} - a_{\mathbf{k}} b_{-\mathbf{k}} + a_{-\mathbf{k}}^{\dagger} b_{\mathbf{k}}^{\dagger} \right) \Big\} , \end{aligned} \tag{3.112}$$

where

$$E_{1\mathbf{k}} = \hbar c k \tag{3.113}$$

$$E_{2\mathbf{k}} = \hbar \omega_0 \sqrt{1+\chi} \tag{3.114}$$

$$E_{3\mathbf{k}} = i\left(\frac{\hbar^2 ck\omega_0\chi}{4\sqrt{1+\chi}}\right)^{1/2}. \tag{3.115}$$

Here $\mathbf{k}$ is the wave vector for both photons and phonons, ω_0 is the bare phonon frequency, and χ is the dimensionless dielectric susceptibility of the crystal, defined by

$$\chi\omega_0^2\varepsilon_0\mathbf{E} = \ddot{\mathbf{P}} + \omega_0^2\mathbf{P}\,,$$

where $\mathbf{E}$ is the electric field of the incoming light and $\mathbf{P}$ is the polarization due to transverse optical phonons in the crystal. In the Hamiltonian $H_{\text{polariton}}$, the two free oscillator sums correspond to free photons and free phonons, while the mixing terms come from the interaction $\mathbf{E}\cdot\mathbf{P}$ between photons and phonons. Notice that the phonon energy $E_{2\mathbf{k}}$ has been corrected, as ω_0 is substituted by $\omega_0\sqrt{1+\chi}$, so that we have "dressed" phonons.

To diagonalize the polariton Hamiltonian, we introduce a set of polariton operators $\alpha_{\mathbf{k}}$ through a canonical transformation,

$$\alpha_{i\mathbf{k}} = w_i\, a_{\mathbf{k}} + x_i\, b_{\mathbf{k}} + y_i\, a^\dagger_{-\mathbf{k}} + z_i\, b^\dagger_{-\mathbf{k}}\,, \qquad i = 1,2\,. \tag{3.116}$$

It is required that in the representation of $\alpha_{\mathbf{k}}$,

$$H'_{\text{polariton}} = \sum_{\mathbf{k}}\left[E^{(1)}_{\mathbf{k}}\left(\alpha^\dagger_{1\mathbf{k}}\,\alpha_{1\mathbf{k}} + \frac{1}{2}\right) + E^{(2)}_{\mathbf{k}}\left(\alpha^\dagger_{2\mathbf{k}}\,\alpha_{2\mathbf{k}} + \frac{1}{2}\right)\right]. \tag{3.117}$$

The sub-indices $i = 1\,,2$ specify the two polariton branches, with different dispersion relations $E^{(1)}_{\mathbf{k}}$ and $E^{(2)}_{\mathbf{k}}$. The transformation matrix elements w_i, x_i, y_i, z_i are determined by requiring that the $\alpha_{i\mathbf{k}}$'s satisfy boson commutation relations,

$$[\alpha_{i\mathbf{k}}\,,\ \alpha^\dagger_{j\mathbf{k}'}] = \delta_{ij}\delta_{\mathbf{k}\mathbf{k}'}\,, \quad [\alpha_{i\mathbf{k}}\,,\ \alpha_{j\mathbf{k}'}] = 0\,, \tag{3.118}$$

so that

$$[\alpha_{i\mathbf{k}}\,,\ H] = E^{(i)}_{\mathbf{k}}\,\alpha_{i\mathbf{k}}\,, \tag{3.119}$$

which is true if the two different polariton branches are independent of each other. We have shown in Appendix D.1 how to derive all the transformation matrix elements (w_i, x_i, y_i, z_i) and the polariton energies $E^{(1)}_{\mathbf{k}}$ and $E^{(2)}_{\mathbf{k}}$.

3.5.2 Time-Evolution of the Phonon and Photon Operators

The time-evolution of the TO phonon and photon operators can be computed after the transformation between polaritons $\alpha_{i\mathbf{k}}$ and photon-phonons ($a_{\mathbf{k}}$ and $b_{\mathbf{k}}$) is known. The calculations are done in the Heisenberg picture, where the operators evolve with time. To calculate the time-evolution of the phonon operators, we first go to the polariton representation

to find the time-dependence of the polaritons, then transform back to the photon-phonon representation.

In the polariton representation, the Hamiltonian $H'_{\rm polariton}$ describes two independent harmonic oscillators. From the Heisenberg equation

$$i\,\hbar\frac{d\hat{O}}{dt} = [\hat{O},\ H]\,, \tag{3.120}$$

we can obtain

$$\alpha_{1\mathbf{k}}(t) \;=\; \alpha_{1\mathbf{k}}(0)\; e^{-iE^{(1)}_{\mathbf{k}}\,t/\hbar}\,, \tag{3.121}$$

$$\alpha_{2\mathbf{k}}(t) \;=\; \alpha_{2\mathbf{k}}(0)\; e^{-iE^{(2)}_{\mathbf{k}}\,t/\hbar}\,. \tag{3.122}$$

The canonical transformation from the photon and phonon operators $a_{\mathbf{k}}$, $b_{\mathbf{k}}$ to the polariton operators $\alpha_{\mathbf{k}}$ can be written in a matrix form:

$$\alpha = \mathbf{A}\cdot\mathbf{a}\,, \tag{3.123}$$

and the inverse transformation is

$$\mathbf{a} = \mathbf{A}^{-1}\cdot\alpha\,, \tag{3.124}$$

where

$$\alpha = \begin{pmatrix} \alpha_{1\mathbf{k}} \\ \alpha_{2\mathbf{k}} \\ \alpha^{\dagger}_{1,-\mathbf{k}} \\ \alpha^{\dagger}_{2,-\mathbf{k}} \end{pmatrix}, \qquad \mathbf{A} = \begin{pmatrix} w_1 & x_1 & y_1 & z_1 \\ w_2 & x_2 & y_2 & z_2 \\ y_1^* & z_1^* & w_1^* & x_1^* \\ y_2^* & z_2^* & w_2^* & x_2^* \end{pmatrix}, \qquad \mathbf{a} = \begin{pmatrix} a_{\mathbf{k}} \\ b_{\mathbf{k}} \\ a^{\dagger}_{-\mathbf{k}} \\ b^{\dagger}_{-\mathbf{k}} \end{pmatrix}. \tag{3.125}$$

The α vector at time t is

$$\alpha(t) = \begin{pmatrix} \alpha_{1\mathbf{k}}(t) \\ \alpha_{2\mathbf{k}}(t) \\ \alpha^{\dagger}_{1,-\mathbf{k}}(t) \\ \alpha^{\dagger}_{2,-\mathbf{k}}(t) \end{pmatrix} = \begin{pmatrix} e^{-iE^{(1)}_{\mathbf{k}}t/\hbar} & 0 & 0 & 0 \\ 0 & e^{-iE^{(2)}_{\mathbf{k}}t/\hbar} & 0 & 0 \\ 0 & 0 & e^{iE^{(1)}_{-\mathbf{k}}t/\hbar} & 0 \\ 0 & 0 & 0 & e^{iE^{(2)}_{-\mathbf{k}}t/\hbar} \end{pmatrix} \times \begin{pmatrix} \alpha_{1\mathbf{k}}(0) \\ \alpha_{2\mathbf{k}}(0) \\ \alpha^{\dagger}_{1,-\mathbf{k}}(0) \\ \alpha^{\dagger}_{2,-\mathbf{k}}(0) \end{pmatrix}$$

$$= \mathbf{U}_{\alpha}(t)\alpha(0). \tag{3.126}$$

Thus $\mathbf{a}(t)$ is

$$\mathbf{a}(t) = \mathbf{A}^{-1}\,\alpha(t) = \mathbf{A}^{-1}\,\mathbf{U}_{\alpha}(t)\,\mathbf{A}\,\mathbf{a}(0)\,. \tag{3.127}$$

In other words, we can now express $a_{\mathbf{k}}(t)$, $b_{\mathbf{k}}(t)$, etc., as linear functions of $a_{\mathbf{k}}(0)$, $b_{\mathbf{k}}(0)$, etc.

3.5.3 Computation of the Variances in the Polariton System

Our goal is to compute the fluctuations of the lattice amplitude operator $u(\pm\mathbf{k},t) = b_{\mathbf{k}}(t) + b^{\dagger}_{-\mathbf{k}}(t) + b_{-\mathbf{k}}(t) + b^{\dagger}_{\mathbf{k}}(t)$, which is an observable. According to Eq. (3.49) in Section 3.3.4, the variances of this operator in a two-mode ($\pm\mathbf{k}$) coherent state $|\alpha_{\mathbf{q}}, \alpha_{-\mathbf{q}}\rangle$ is

$$\langle(\Delta u(\pm\mathbf{q}))^2\rangle_{\rm coh} = 2\,. \tag{3.128}$$

Therefore, if at any given time we obtain a value less than 2, the quantum noise of the lattice amplitude of the relevant mode is squeezed below the minimum uncertainty value given by the vacuum state.

From Eq. (3.127) we get

$$b_{\mathbf{k}}(t) + b^{\dagger}_{-\mathbf{k}}(t) = A_1(t)a_{\mathbf{k}}(0) + A_2(t)b_{\mathbf{k}}(0) + A_3(t)a^{\dagger}_{-\mathbf{k}}(0) + A_4(t)b^{\dagger}_{-\mathbf{k}}(0)\,, \tag{3.129}$$

$$b_{-\mathbf{k}}(t) + b^{\dagger}_{\mathbf{k}}(t) = A^*_1(t)a^{\dagger}_{\mathbf{k}}(0) + A^*_2(t)b^{\dagger}_{\mathbf{k}}(0) + A^*_3(t)a_{-\mathbf{k}}(0) + A^*_4(t)b_{-\mathbf{k}}(0)\,, \tag{3.130}$$

where $A_i(t)$ (they are not the elements of the transformation matrix $\mathbf{A}$) are time-dependent complex functions determined by the transformation matrices $\mathbf{A}$, $\mathbf{A}^{-1}$, and $\mathbf{U}_{\alpha}(t)$. Photons and TO phonons are initially independent, so that terms like $\langle a_{\mathbf{k}}b_{\mathbf{k}}\rangle - \langle a_{\mathbf{k}}\rangle\langle b_{\mathbf{k}}\rangle$ are zero. The fluctuation of $u(\pm\mathbf{k},t)$ is

$$\begin{aligned}
\langle(\Delta u(\pm\mathbf{k},t))^2\rangle &= \langle\psi(0)|\,(\Delta u(\pm\mathbf{k},t))^2\,|\psi(0)\rangle \\
&= A_1^2(t)\langle(\Delta a_{\mathbf{k}})^2\rangle + A_2^2(t)\langle(\Delta b_{\mathbf{k}})^2\rangle + A_3^2(t)\langle(\Delta a^{\dagger}_{-\mathbf{k}})^2\rangle + A_4^2(t)\langle(\Delta b^{\dagger}_{-\mathbf{k}})^2\rangle \\
&\quad + A^{*\,2}_1(t)\langle(\Delta a^{\dagger}_{\mathbf{k}})^2\rangle + A^{*\,2}_2(t)\langle(\Delta b^{\dagger}_{\mathbf{k}})^2\rangle + A^{*\,2}_3(t)\langle(\Delta a_{-\mathbf{k}})^2\rangle \\
&\quad + A^{*\,2}_4(t)\langle(\Delta b_{-\mathbf{k}})^2\rangle + 2A_1(t)A^*_3(t)\left(\langle a_{\mathbf{k}}a_{-\mathbf{k}}\rangle - \langle a_{\mathbf{k}}\rangle\langle a_{-\mathbf{k}}\rangle\right) \\
&\quad + 2A_3(t)A^*_1(t)\left(\langle a^{\dagger}_{\mathbf{k}}a^{\dagger}_{-\mathbf{k}}\rangle - \langle a^{\dagger}_{\mathbf{k}}\rangle\langle a^{\dagger}_{-\mathbf{k}}\rangle\right) \\
&\quad + 2A_2(t)A^*_4(t)\left(\langle b_{\mathbf{k}}b_{-\mathbf{k}}\rangle - \langle b_{\mathbf{k}}\rangle\langle b_{-\mathbf{k}}\rangle\right) \\
&\quad + 2A_4(t)A^*_2(t)\left(\langle b^{\dagger}_{\mathbf{k}}b^{\dagger}_{-\mathbf{k}}\rangle - \langle b^{\dagger}_{\mathbf{k}}\rangle\langle b^{\dagger}_{-\mathbf{k}}\rangle\right) \\
&\quad + 2|A_1(t)|^2\left(\langle a^{\dagger}_{\mathbf{k}}a_{\mathbf{k}}\rangle - \langle a^{\dagger}_{\mathbf{k}}\rangle\langle a_{\mathbf{k}}\rangle\right) + 2|A_2(t)|^2\left(\langle b^{\dagger}_{\mathbf{k}}b_{\mathbf{k}}\rangle - \langle b^{\dagger}_{\mathbf{k}}\rangle\langle b_{\mathbf{k}}\rangle\right) \\
&\quad + 2|A_3(t)|^2\left(\langle a^{\dagger}_{-\mathbf{k}}a_{-\mathbf{k}}\rangle - \langle a^{\dagger}_{-\mathbf{k}}\rangle\langle a_{-\mathbf{k}}\rangle\right) \\
&\quad + 2|A_4(t)|^2\left(\langle b^{\dagger}_{-\mathbf{k}}b_{-\mathbf{k}}\rangle - \langle b^{\dagger}_{-\mathbf{k}}\rangle\langle b_{-\mathbf{k}}\rangle\right) \\
&\quad + |A_1(t)|^2 + |A_2(t)|^2 + |A_3(t)|^2 + |A_4(t)|^2\,.
\end{aligned} \tag{3.131}$$

Notice that all the expectation values in Eq. (3.131) such as $\langle b^{\dagger}_{-\mathbf{k}}b_{-\mathbf{k}}\rangle$ are the shorthanded version of terms like $\langle\psi(0)|b^{\dagger}_{-\mathbf{k}}(0)b_{-\mathbf{k}}(0)|\psi(0)\rangle$.

The initial state $|\psi(0)\rangle$ includes both photon and phonon initial states. We have done numerical calculations on several different combinations of initial states and analyzed their effects on the time-evolution of the lattice amplitude variances. The results are summarized below.

When the initial photon state is a coherent state and the initial TO phonon state is either a vacuum or a coherent state, the fluctuation of $u(\pm\mathbf{k},t)$ is (The subindices "coh" and "vac" refer to "coherent" and "vacuum" respectively. The first subindex refers to the initial photon state while the second subindex refers to the initial phonon state.)

$$\langle(\Delta u(\pm\mathbf{k},t))^2\rangle_{\text{coh+vac}} = |A_1(t)|^2 + |A_2(t)|^2 + |A_3(t)|^2 + |A_4(t)|^2 \,. \tag{3.132}$$

Our numerical results show that there is a squeezing effect in $u(\pm\mathbf{k})$.

When the initial state is a photon squeezed state in mode $\mathbf{k}$ (with squeezing factor $\xi = re^{i\theta}$) and photon vacuum state in mode $-\mathbf{k}$, and a phonon vacuum state in both modes $\pm\mathbf{k}$, the fluctuation then becomes

$$\begin{aligned}\langle(\Delta u(\pm\mathbf{k},t))^2\rangle_{\text{smsq+vac}} &= |A_1(t)|^2\left(e^{-2r}\cos^2\frac{\Phi}{2} + e^{2r}\sin^2\frac{\Phi}{2}\right) \\ &\quad +|A_2(t)|^2 + |A_3(t)|^2 + |A_4(t)|^2 \,,\end{aligned} \tag{3.133}$$

where $\Phi = \theta + 2\arg\{A_1(t)\}$ and the subindex "smsq" stands for "single-mode squeezed" state. We have done numerical calculations for the two cases $\theta = 0$ and $\theta = 2t$ (assuming $\omega_{\text{photon}} = ck = 1$), and the results are that there are squeezing effects in both cases.

When the initial state is a photon squeezed state in mode $\mathbf{k}$ (with squeezing factor $\xi = re^{i\theta}$) and photon vacuum state in mode $-\mathbf{k}$, and a thermal phonon state in both modes $\pm\mathbf{k}$, then the fluctuation becomes

$$\begin{aligned}\langle(\Delta u(\pm\mathbf{k},t))^2\rangle_{\text{smsq+thm}} &= |A_1(t)|^2\left(e^{-2r}\cos^2\frac{\Phi}{2} + e^{2r}\sin^2\frac{\Phi}{2}\right) + |A_2(t)|^2 + |A_3(t)|^2 \\ &\quad +|A_4(t)|^2 + 2\langle n_{\pm\mathbf{k}}\rangle(|A_2(t)|^2 + |A_4(t)|^2) \,,\end{aligned} \tag{3.134}$$

where $\Phi = \theta + 2\arg\{A_1(t)\}$, and $\langle n_{\pm\mathbf{k}}\rangle$ is the thermal distribution of the relevant mode phonons,

$$\langle n_{\pm\mathbf{k}}\rangle = \frac{1}{e^{\hbar\omega_{\pm\mathbf{k}}/kT} - 1} \,. \tag{3.135}$$

Numerical calculations show that there are squeezing effects below a particular temperature determined by the frequency of the phonons (in $\langle n_{\pm\mathbf{k}}\rangle$), the time-dependence of phase θ, and the susceptibility χ of the lattice.

When the initial state is a two-mode ($\pm\mathbf{k}$) photon squeezed state (with squeezing factor $\xi = re^{i\theta}$), and vacuum phonon state in both modes $\pm\mathbf{k}$, then the fluctuation becomes

$$\begin{aligned}\langle(\Delta u(\pm\mathbf{k},t))^2\rangle_{\text{tmsq+vac}} &= \frac{1}{2}\left\{e^{2r}\left[(|A_1(t)|-|A_3(t)|)^2+4|A_1(t)A_3(t)|\sin^2\frac{\theta+\Theta}{2}\right]\right.\\ &\quad\left.+\,e^{-2r}\left[(|A_1(t)|-|A_3(t)|)^2+4|A_1(t)A_3(t)|\cos^2\frac{\theta+\Theta}{2}\right]\right\}\\ &\quad+(|A_2(t)|^2+|A_4(t)|^2)\,, \qquad (3.136)\end{aligned}$$

where $\Theta = \arg\{A_1(t)\} - \arg\{A_3(t)\}$. Numerical results show that there is a very weak squeezing effect for the lattice amplitude operator $u(\pm\mathbf{k},t)$ when $\chi > 0.3$.

All the above results are summarized in Table 3.2, and some numerical examples are shown in Figs. 3.7 and 3.8. Throughout the course of our calculations we have assumed that the two polariton branches are independent from each other. This assumption turns out to be a limiting factor of our approach. In our polariton transformation, the commutation relation between $\alpha_{1\mathbf{k}}$ and $\alpha^\dagger_{2\mathbf{k}}$ should be zero if the two modes are truly independent, while in fact the commutator is nonzero (see Appendix D.2). This shows that the polariton operators we construct (Eq. (3.116)), following standard textbooks such as Madelung's [78], are in fact weakly interactive. However, as discussed in Appendix D.2, it is reasonable to use them as a first-order approximation.

$t=0$ photons	$t=0$ phonons	Squeezed $u(\pm\mathbf{k})$?
CS($\pm$k)	CS($\pm$k)	yes (no) if $\chi >$ ($\leq$) 0.1
SMSS(k), VS($-$k)	VS($\pm$k)	yes (no) if $\chi >$ ($\leq$) 0.1
SMSS(k), VS($-$k)	TS($\pm$k)	yes if $T < T_s(\chi)$
TMSS($\pm$k)	VS($\pm$k)	weak (no) if $\chi >$ ($\leq$) 0.1

Table 3.2: Different combinations of $t = 0$ initial states (modes $\pm\mathbf{k}$) for the polariton approach to lattice amplitude squeezing and the corresponding effects in the fluctuations of the lattice amplitude operator $u(\pm\mathbf{k})$. Here CS(k), VS(k), TS(k), SMSS(k), TMSS($\pm$k) refer, respectively, to coherent, vacuum, thermal, single-mode and two-mode squeezed states in the modes inside the parentheses, k, $-$k, or $\pm$k. $T_s(\chi)$ is the temperature below which squeezing is obtained (see Fig. 4). By squeezing we mean that the quantum noise of the relevant variable is below its corresponding vacuum state value.

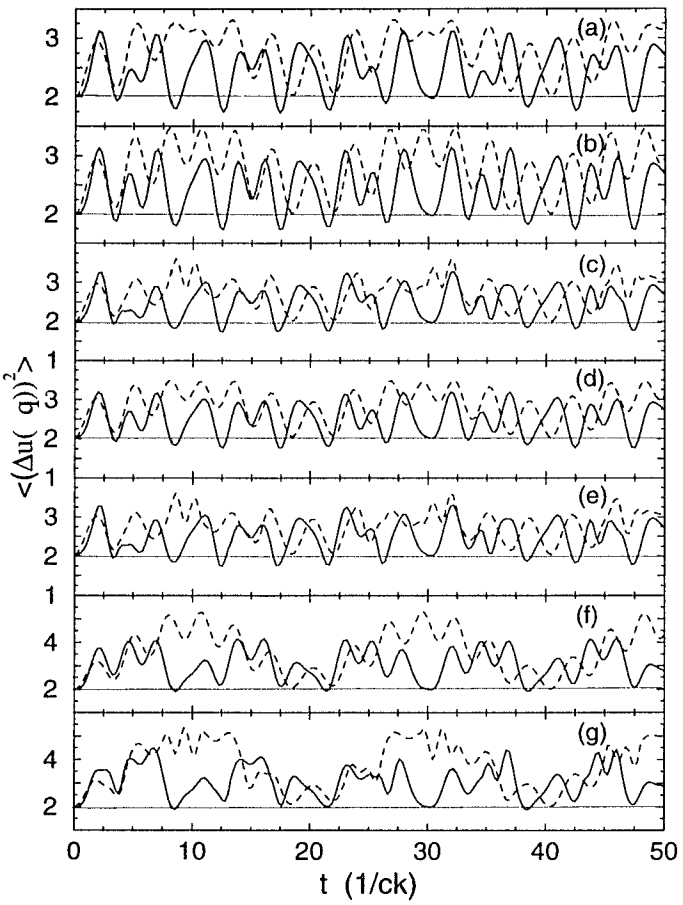

Figure 3.7: Calculated fluctuation $\langle u(\pm\mathbf{k})\rangle(t)$ of the lattice amplitude versus time for different combinations of photon and phonon initial states using a polariton mechanism for lattice amplitude squeezing. Dashed (solid) lines correspond to a susceptibility of $\chi = 0.1$ (0.4). Here χ is a dimensionless dielectric susceptibility, and time is measured in units of $1/ck$, where ck is the free photon frequency. Our calculations here focus on the case where ck is close to ω_0, the bare phonon frequency. A typical value of ω_0 for optical phonons is 10THz, therefore a typical time in our case is 0.1 picosecond. The horizontal lines at $\langle(\Delta u(\pm\mathbf{k}))^2\rangle = 2$ correspond to the noise level of coherent states. Thus, any time the fluctuation satisfies $\langle(\Delta u(\pm\mathbf{k}))^2\rangle < 2$, the state is squeezed. Different combinations of initial states were considered. (a) Coherent photon and phonon states. (b) Single-mode squeezed state in photon mode $\mathbf{k}$ with squeezing factor $\xi = 0.1$ and a vacuum state in the photon mode $-\mathbf{k}$; both phonon modes are in the vacuum state. (c) Same combination of states as in (b), but here $\xi = 0.1e^{2it}$ (recall that the unit of time is $1/ck$). (d) Single-mode squeezed state in photon mode $\mathbf{k}$ with squeezing factor $\xi = re^{i\theta}$, where $r = 0.1$ and $\theta = 0$, vacuum state in the $-\mathbf{k}$ photon mode, and both phonon modes in a thermal state with temperature $T = 25K$ (the bare phonon frequency is 10THz). (e) Same combination of states as in (d), but here $\theta = 2t$. (f) Two-mode ($\pm\mathbf{k}$) squeezed state for the photons, with squeezing factor $\xi = re^{i\theta}$, where $r = 0.1$ and $\theta = 0$, vacuum state for the two phonon modes. (g) Same combination of states as in (f), but here $\theta = 2t$.

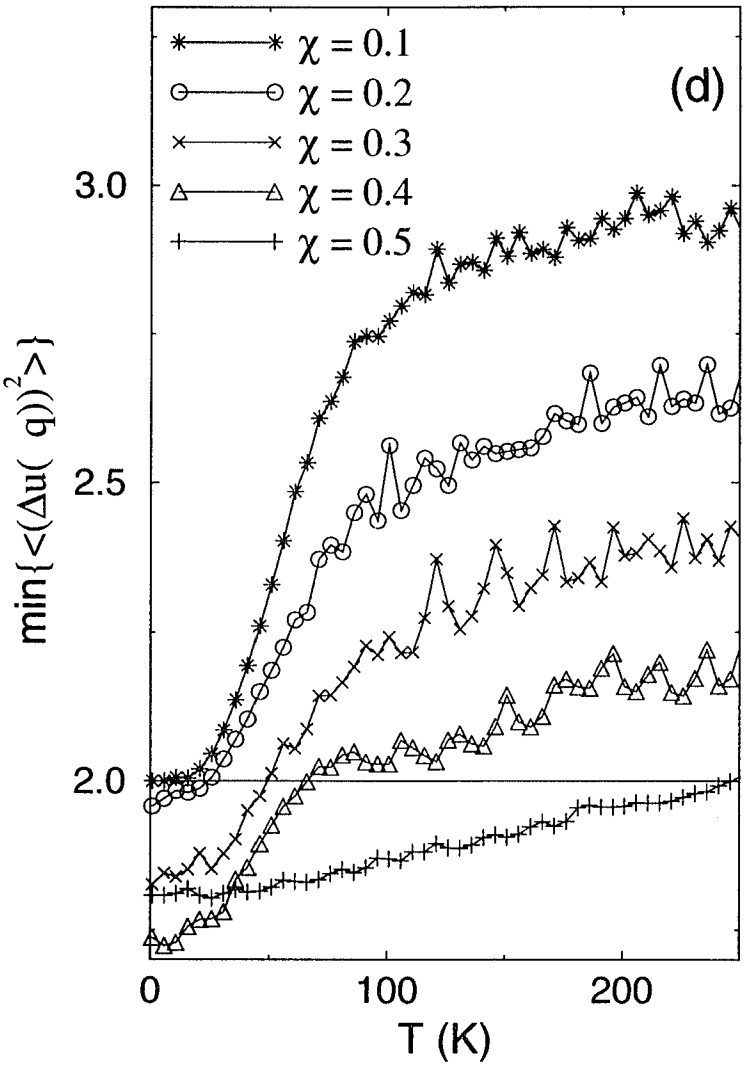

Figure 3.8: Temperature dependence of the *minimum* fluctuation $\min\{\langle(\Delta u[\pm\mathbf{k})]^2\rangle\}$ in the dimensionless lattice amplitude operator $u(\pm\mathbf{k})$ using a polariton mechanism for lattice amplitude squeezing. The phonon frequency is 10 THz. The initial states are: single-mode squeezed state in photon mode $\mathbf{k}$, vacuum state in photon mode $-\mathbf{k}$, and thermal state in both $(\pm\mathbf{k})$ phonon modes. The squeezing factor is $\xi = 0.1e^{2it}$. Squeezing can exist up to a temperature $T_s(\chi)$. For example, when $\chi = 0.2$, squeezing effects vanish when $T \gtrsim 25$ K. On the other hand, for stronger photon-phonon interaction (e.g., $\chi = 0.5$), the squeezing effects can be obtained up to $T \approx 250$K. At first sight, this temperature might seem very large and thermal effects might seem to dominate all the fluctuations in the system. Indeed, this is the case for the low energy acoustic phonons. However, the polariton mechanism squeezes optical (not acoustic) phonons. The energy of optical phonons is around 10TeraHertz, too large to be affected by thermal fluctuations. Indeed, the optical phonons considered here are excited by the incident laser beam.

3.6 Suggested Detection Schemes

As summarized in Appendix E.1, it is possible to directly detect a single-mode squeezed state, although it might not be the best method to measure quadrature squeezing effects. In a phonon system, direct detection would involve phonon counting. There are two kinds of phonon counters: superconducting tunnel junction bolometers and vibronic detectors [24, 77]. Superconducting tunnel junction bolometers are the most widely used; however, they are wide-band detectors. Phonons with similar energies to the squeezed ones can also be detected, therefore causing unwanted noise. Another kind of phonon counters are based on the vibronic band absorption present in certain materials [77]. These phonon counters can detect a particular frequency, and therefore may be more suitable in detecting single-mode squeezed states, although their efficiency is not very high.

To detect photon squeezed states, phase-sensitive schemes such as homodyne and heterodyne detectors are used most often because of their ability to lock their phases with the electric field of the measured state. These are summarized in Appendices E.2, E.3, and E.4. There appears to be no available phase-sensitive detection method for phonons. A promising candidate might be measuring the intensity of a reflected probe light [37, 38, 46]. This method has already been used to detect phonon amplitudes, since the reflectivity is linearly related to the atomic displacements in a crystal [37, 38, 46]. The displacements' Fourier components at the relevant frequency, or the value of the lattice amplitude operator, can be extracted by making a Fourier analysis on the sample reflectivity. If squeezing should happen, its effect will be contained in the Fourier components of the reflectivity, and therefore in (the Fourier components of) the intensity of the reflected light. In this manner the information on the squeezing effect in the phonons is also carried by the reflected light in the form of squeezing of the photon intensity. We can then use a standard optical detection method to determine whether the related light is squeezed or not. One shortcoming of this method is that it is not direct. In the measurement there can be noise added into the signal, such as the intensity fluctuation of the original probe light, the noise coming from the finite efficiency of the reflected light to pick up the signals in the phonons, etc. Needless to say, further research needs to be done on how to realize this phase-sensitive detection scheme, and we hope that our initial proposals stimulate further theoretical and experimental work on this problem.

3.7 Discussion

From Eq. (3.75) in Section 3.3.5 it is clear that phonon squeezing depends on both the absolute value r and the phase θ of the squeezing factor $\xi(t) = re^{i\theta}$. The explicit result is,

$$\langle(\Delta u(\pm\mathbf{q}))^2\rangle_{\rm sq} = 2\left(e^{-2r}\cos^2\frac{\theta}{2} + e^{2r}\sin^2\frac{\theta}{2}\right). \tag{3.137}$$

Only when θ is close to 0 is noise suppressed in the lattice amplitude operator. This means that in order to suppress the noise, the squeezing factor $\xi(t)$ has to have a dominant positive real part ($\cos\theta > \tanh r$). The squeezing factor obtained from the three-phonon process is

$$\xi(t) = \frac{i}{\hbar}\int_0^t \lambda\,\beta_0(\tau)\,e^{i(\omega_s+\omega_i)\tau}d\tau\,, \tag{3.138}$$

where the real number λ is the strength of the interaction and β_0 is the amplitude of the phonon coherent state in the pump mode. From this expression for $\xi(t)$ we can see that the squeezing effect only appears during certain time intervals. If $\beta_0(t)$ does not depend on time or has a periodic dependence on time, squeezing will be periodic in time, which makes a phase-sensitive detection easier to achieve.

According to the discussions in Section 3.4.4, the finite-lifetime of the pump mode phonons does not favor the generation of squeezed states. Thus, one may wonder whether an extremely degenerate case, where only one special phonon decay channel exists, might solve this problem. Unfortunately, it does not. The vanishing of the third-order terms simultaneously introduces the fourth- and higher-order anharmonic terms because of the following argument. A high-energy phonon can decay into N lower-energy phonons, where $N = 2, 3, 4, \cdots$, because of the anharmonicity in the lattice interaction. The decay rate is determined by both the strength of the interaction and the accessible phase space for the decay to take place (which is limited by polarization considerations, and the conservation of energy and quasi-momentum). In general, the larger N is, the smaller the accessible phase space available for each one of the decaying phonon modes. Thus, a high-energy phonon generally has a higher probability of decaying into two lower-energy phonons (corresponding to the third-order anharmonic interaction) than to three or more phonons. These higher-order terms are therefore neglected in our approximation. However, if the third-order anharmonic term has only one accessible phase point, its significance will be very much weakened so that the higher-order anharmonic terms can become important. If these higher-order terms dominate the problem, they will play the same role as we assigned to the vanished third-order terms. Namely, they will behave as a reservoir and give rise to a finite

lifetime for the pump mode phonons. Therefore, the very unlikely degenerate situation (where the third-order terms have only one accessible point in phase space) may not be helpful in providing a better experimental environment for the generation and observation of squeezed phonon states.

In addition, to make the various schemes (including those using phonon-phonon interactions and phonon-photon interactions) work, there are some noise problems that must be overcome. First, any attempt to generate or detect squeezed states should be at low temperatures to avoid thermal noise in the crystal. For instance, the energy of a 10THz optical phonon corresponds to a temperature of about 100K. Therefore, the experiment might have to be carried out at a temperature well below 100K, such as 10K or lower. Besides thermal noise, there is also noise generated by the optical interactions. The fluctuations in the laser intensity and in the interaction between the laser and the crystal has to be very small, so that it will not suppress the noise reduction process in the generation of squeezed acoustic phonons. In fact, one possible way to reduce the noise coming from the laser beam is by using a beam of squeezed photons. Another problem is the incoherence in the procedure itself, like the finite lifetime of the pump mode phonons. We need to use phonon modes with lifetimes as long as possible.

Due to a variety of reasons, squeezing effects are not easy to observe. On the one hand, thermal noise is much larger than quantum noise in many experiments. On the other hand, even when quantum noise is dominant, the squeezing effect might be overlooked because the measurements focus on other aspects of the system. However, the difficulties in observing reduction in the quantum noise do not imply that the squeezing effect is rare (see, e.g., [11, 16]). On the contrary, it is quite general: any diagonalizable system can be "squeezed" in some manner by an appropriate choice of initial states. For example, consider a free oscillator

$$H = a^\dagger a\,, \tag{3.139}$$

and let us define,

$$d = \mu a + \nu a^\dagger\,, \tag{3.140}$$

where μ and ν are complex scalars. In order for d to be a boson operator, μ and ν must satisfy the relation $|\mu|^2 - |\nu|^2 = 1$. Then the Hamiltonian becomes

$$H = (|\mu|^2 + |\nu|^2)d^\dagger d - (\mu\nu {d^\dagger}^2 + \mu^*\nu^* d^2) + |\nu|^2\,. \tag{3.141}$$

The generalized "displacement" $(d + d^\dagger)/\sqrt{2}$ is a mixture of the original displacement $(a +$

$a^\dagger)/\sqrt{2}$ and momentum $-i(a-a^\dagger)/\sqrt{2}$. If we are interested in a quantity such as $(d+d^\dagger)/\sqrt{2}$ and it is observable, the squeezing effect can be obtained when the initial state is a coherent state of mode "d", i.e., $d|\delta\rangle = \delta|\delta\rangle$. On the other hand, such a hybrid quantity $(d+d^\dagger)/\sqrt{2}$ might not be physically interesting and/or observable. In other words, the squeezing effect is only relevant when it is related to the observables.

3.8 Conclusions

In this chapter we have investigated the dynamics and quantum fluctuation properties of phonon coherent and squeezed states. In particular, we calculated the experimentally observable time-evolution and fluctuation of the lattice amplitude operator $u(\pm\mathbf{q}) = b_\mathbf{q} + b^\dagger_{-\mathbf{q}} + b^\dagger_\mathbf{q} + b_{-\mathbf{q}}$. We showed that the $\langle u(\pm\mathbf{q})\rangle(t)$ are sinusoidal functions of time in both coherent and squeezed states, but the fluctuation $\langle(\Delta u(\pm\mathbf{q}))^2\rangle(t)$ in a squeezed phonon state is periodically smaller than its coherent state value 2, which is also the vacuum state noise level. Therefore, phonon squeezed states are periodically quieter than the vacuum state.

We have discussed four different approaches to generate phonon squeezed states. These approaches are based on a variety of physical processes, including three-phonon interactions, short-time single-mode phonon-phonon interactions, second-order Raman scattering, and photon-phonon interactions that lead to polaritons.

First, we considered a three-phonon scattering process when the higher-energy LO phonon mode is coherently pumped with an ultrashort photon pulse. We showed that the two lower-energy LA phonon modes can be in a two-mode phonon quadrature squeezed state given appropriate initial conditions. We achieved this by dealing separately with (i) the optical excitation of the pump mode LO phonons and (ii) the anharmonic scattering of the pump mode LO phonons into the lower-energy LA phonons.

We also demonstrated that certain types of nonlinear phonon-phonon interaction can be used to generate single-mode squeezed states in a low-energy, long-lifetime acoustic phonon mode. Numerical results show that with this mechanism, the squeezing effect is maximized by increasing both the average initial phonon number in the mode and the nonlinearity in the interaction potential.

The two different mechanisms mentioned above—the three-phonon parametric amplification and the short-time single-mode approach—generate squeezed states through phonon-phonon interactions. We also considered two alternative approaches based on photon-

phonon interactions: a second-order Raman scattering process, and a polariton mechanism.

We treated the second-order Raman process in a similar fashion as the three-phonon parametric amplification process. In other words, assuming that the photons involved are in coherent states, we take a mean field average over the photon operators. This approximation enables us to obtain a two-mode phonon Hamiltonian. Given an initial vacuum or coherent state, the phonons in these two modes evolve into a two-mode phonon quadrature squeezed state. Here the incident photons for the Raman process do not have to be in a pulse but can also originate from a continuous-wave laser.

In the polariton approach to squeezing, we calculate the atomic displacement part of a polariton with various combinations of initial photon and transverse optical phonon states, and prove that the fluctuations of the associated lattice amplitude operator can be squeezed to various degrees for different combinations of initial states and large enough ($\chi > 0.1$) interaction strength. The effect is more pronounced for large values of the dimensionless dielectric susceptibility χ ($\chi > 10$). More specifically, squeezing effects in $u(\pm\mathbf{k})$ are relatively strong for either one of the following two sets of initial states: (i) photon and phonon coherent states, or (ii) single-mode photon squeezed state and phonon vacuum state. For instance, the maximum squeezing exponent r is 0.015 when the incident photon state has a squeezing factor $\xi = 0.1e^{2ickt}$ (where ck is the photon frequency). On the other hand, with an initial two-mode photon squeezed state and two-mode phonon vacuum state, the squeezing effect in $u(\pm\mathbf{k})$ is weak. We have also used initial conditions with a single-mode photon squeezed state and thermal states in the two phonon modes. Our numerical results show that squeezing effects are quickly overshadowed by the thermal noise for small χ, while for large χ ($\gtrsim 0.5$) the squeezing effect can exist up to $T \approx 250$K.

We have also briefly analyzed several potential detection methods of phonon squeezed states. Experiments in quantum optics indicate that phase-sensitive methods—such as homodyne detection—are the best in detecting photon squeezed states. Therefore, we have proposed a detection scheme based on a reflected probe light and an ordinary phase-sensitive optical detector.

Chapter 4

Squeezed States in Josephson Junctions

This chapter presents a summary of our ideas and results on squeezed states in Josephson junctions [21, 22]; these are discussed in detail in Chapter 5. We study quantum fluctuation properties of Josephson junctions in the limit of large coupling and small charging energies. We consider Josephson junctions coupled to one or several of the following circuit elements: a capacitor, an inductor (in a superconducting ring), and an applied current source. These can have ground states which are either squeezed vacuum or coherent states. Finally, we calculate the uncertainties of their canonical quantum mechanical momentum (charge) and coordinate (phase).

4.1 Hamiltonians for System Configurations Containing a Josephson Junction.

Here we study the quantum noise originating from the non-vanishing commutator between the phase and the charge number.

We first consider the Hamiltonian $H_1 = Q^2/2C - E_J \cos\phi$ for an isolated junction near its ground state at temperature $T = 0$, with capacitance C. The operators Q and ϕ satisfy $[\phi, Q] = 2ie$. Since $Q = e^* n = 2en$ and $E_C = 4e^2/C$, H_1 takes the form $H_1 = 2e^2 n^2/C - E_J \cos\phi = E_C\, n^2/2 - E_J \cos\phi$, where $[\phi, n] = i$. Here we only consider the coherent Cooper pair tunneling and neglect quasi-particle tunneling and shunting Ohmic resistance, which actually originates from the quasiparticle tunneling.

When a JJ is current-biased, it can still be described by an effective Hamiltonian: $H_2 = E_C\, n^2/2 - E_J \cos\phi + I\Phi_0\phi/2\pi$, where I is the biasing current and $\Phi_0 = h/2e$.

When a JJ is in a superconducting loop with an external flux $\Phi_e = \Phi_0\phi_e/2\pi$, the

Hamiltonian has the form $H_3 = E_C\, n^2/2 - E_J \cos\phi + \Phi_0^2(\phi - \phi_e)^2/8\pi^2 L$, where L is the inductance of the loop. In the special case when $\Phi_e = 0$, H_3 takes the simplified form $H_4 = E_C n^2/2 - E_J \cos\phi + \Phi_0^2\phi^2/8\pi^2 L$.

For a JJ with $E_J \gg E_C$, we expand the $\cos\phi$ term at a potential minimum ϕ_m as: $\cos\phi = \cos(\phi_m + \phi_{\rm local}) \cong (1 - \phi_{\rm local}^2/2 + \phi_{\rm local}^4/24)\cos\phi_m - (\phi_{\rm local} - \phi_{\rm local}^3/6)\sin\phi_m$. Here $\phi_{\rm local} = \phi - \phi_m$ is a small number. In doing so, we substitute the periodic potential with a parabolic-type potential in the phase-representation. We thus put our emphasis on the local properties of the phase ϕ instead of its transport properties. This kind of approximation has been used in a variety of problems, including spin-density waves [90] and Josephson junction arrays [91]. Needless to say, phase variations during a tunneling event do affect the local properties of a junction and give rise to larger fluctuations. However, in the limit when $T = 0$ and $E_J \gg E_C$, transport effects are small, so that we can neglect them as a first order approximation.

When there is a biasing current I, the system is in the so-called "washboard" potential. When I is large enough ($I\Phi_0 \gg \sqrt{E_J E_C}$), any localized state is unstable; i.e., the phase of the system will inevitably tunnel from one local potential minimum to another. However, when I is small ($I\Phi_0 \ll \sqrt{E_J E_C}$), so that the lifetime of a metastable state is long compared to the characteristic time inside the potential well, we can study the properties of the metastable state at the potential minima as if it were a localized state.

In order to further simplify the problem, we introduce an annihilation operator

$$a = \left\{ (E_{Ji}/E_C)^{1/4}\, \phi_{\rm local} + i\,(E_C/E_{Ji})^{1/4}\, n \right\} / \sqrt{2}\,, \tag{4.1}$$

where i refers to one of the four different configurations. The E_{Ji}'s are summarized in Table 5.1. In the short time limit, the third or higher-order terms in a and $a^\dagger$ are negligible. Such an approximation greatly simplifies the Hamiltonians in the various cases. The four simplified Hamiltonians belong to two groups; the first group (denoted by H_A) includes H_1 and H_4, with a free oscillator term and two quadratic perturbation terms: $H_A = \hbar\omega a^\dagger a + \beta a^2 + \beta^* a^{\dagger\,2}$. The second group (denoted by H_B) includes H_2 and H_3, which have two additional linear terms: $H_B = \hbar\omega a^\dagger a + \alpha a + \alpha^* a^\dagger + \beta a^2 + \beta^* a^{\dagger\,2}$. The corresponding parameters for each of the four different configurations are summarized in Table 5.2. Below we will find that these linear terms lead to higher-energy ground states for the relevant systems.

4.2 Ground and Excited States of Various Hamiltonians

The ground state of the Hamiltonian H_A is

$$|\text{ground}\rangle_A = S^{-1}(\xi)|0\rangle_a = S(-\xi)|0\rangle_a\,, \tag{4.2}$$

where $|0\rangle_a$ is the vacuum state in the a-representation, and $S(\xi)$ is a squeezing operator [11]: $S(\xi) = \exp\left(\xi^* a^2/2 - \xi a^{\dagger 2}/2\right)$, and $\xi = se^{i\theta}$ is a complex squeezing factor. The physical meaning of $S(\xi)$ is described in Figs. 1.1 and 1.2. Briefly, the squeezing operator acting on the vacuum or a coherent state periodically reduces or "squeezes" the uncertainty of one of the conjugate coordinates (e.g., n and ϕ, or x and p) below its coherent state or vacuum state value. Therefore, the ground state of H_A is a squeezed vacuum state with a squeezing factor of $-\xi$. The intuitive picture is the following. The dominant ϕ^2 term in the original H_1 and H_4 provides a confining harmonic oscillator potential (represented by the $a^\dagger a$ term in H_A), which produces minimum fluctuations allowed by the uncertainty principle in the canonical conjugate coordinates. It is the (smaller) ϕ^4 term in the original H_1 and H_4 (which gives rise to the a^2 and $a^{\dagger 2}$ terms in H_A) that induces modulations on the fluctuations of the conjugate variables, therefore leads to the squeezing effect. Higher-order terms will also contribute to this modulation of the quantum fluctuations, but they are neglected here because their effects are relatively small at the short time limit. The ground state fluctuations for H_1 are

$$\langle(\Delta\phi_{\text{local}})^2\rangle = \sqrt{E_C/4E_J}\, e^{2s_1}\,, \tag{4.3}$$

$$\langle(\Delta n)^2\rangle = \sqrt{E_J/4E_C}\, e^{-2s_1}\,, \tag{4.4}$$

and the magnitudes s_i of the squeezing factors for the four different cases considered here are summarized in Table 5.2. Figure 5.3a is a schematic demonstration of the ground state fluctuations of H_A in the ϕ-n phase space.

The excited states of the Hamiltonian H_A are

$$|\text{excited}\rangle_A = |n\rangle_b = b^{\dagger n}|0\rangle_b/\sqrt{n!} = S(-\xi)|n\rangle_a\,. \tag{4.5}$$

In other words, the excited states of H_A are not the number states in the a-representation, $|n\rangle_a$, nor the number states $|n\rangle_n$ in the charge-number representation, where the Cooper-pair number is a good quantum number. Instead, $|\text{excited}\rangle_A$ is a "squeezed" version of the number states $|n\rangle_a$. The fluctuations of the charge-number and phase operators are:

$$\langle(\Delta\phi_{\text{local}})^2\rangle = \frac{\lambda}{2}(2n+1)\left(e^{-2s}\cos^2\frac{\theta}{2} + e^{2s}\sin^2\frac{\theta}{2}\right),$$

$$\langle(\Delta n)^2\rangle = \frac{\lambda}{2}(2n+1)\left(e^{-2s}\sin^2\frac{\theta}{2} + e^{2s}\cos^2\frac{\theta}{2}\right).$$

Therefore, in the excited states of H_A, the fluctuations in the charge number and phase are modulated because of the correction in the harmonic oscillator potential. Whether the noises will be larger or smaller depends on the phase angle θ of the squeezing operator ξ.

The ground state of H_B can be expressed as

$$|\text{ground}\rangle_B \cong D_a\left(-\frac{\alpha^* - 2\alpha\delta e^{i(\phi_\nu - \phi_\mu)}}{\hbar\omega}\right) S_a(-\xi)|0\rangle_a\,, \tag{4.6}$$

which is a squeezed coherent state in the "a" representation (i.e., $a|0\rangle_a = 0$), with $\xi = \delta$. Here $D_a(\alpha) = \exp(\alpha a^\dagger - \alpha^* a)$ is a displacement operator in the "a" representation. Now, for instance, the local phase and number operators for H_2 have the following properties

$$\begin{aligned}
\langle\phi_{\text{local}}\rangle &= -(4E_C/E_{J2})^{1/4}\,\alpha_2(1+4\delta_2)/\hbar\omega_2\,,\\
\langle(\Delta\phi_{\text{local}})^2\rangle &= \{E_C/4E_{J2}\}^{1/2}\,e^{2s_2}\,,\\
\langle n\rangle &= 0\,,\\
\langle(\Delta n)^2\rangle &= \{E_{J2}/4E_C\}^{1/2}\,e^{-2s_2}\,.
\end{aligned}$$

The relevant parameters here are all summarized in the Table, while Fig. 5.3b gives a phase space representation of the ground state fluctuations of H_B. The excited eigenstates of H_B can be obtained in a similar manner as for H_A. They are the number states in the c-representation

$$|\text{excited}\rangle_B = D_a\left(-\frac{\alpha^* - 2\alpha\delta e^{i(\phi_\nu - \phi_\mu)}}{\hbar\omega}\right) S_a(-\xi)|n\rangle_a. \tag{4.7}$$

Therefore, the excited states of H_B are displaced and squeezed number states in the a-representation.

4.3 Discussion

The key parameter $\lambda = \sqrt{E_J/E_C}$ does not lead to squeezing directly, and so far cannot be tuned at will in most experiments. However, λ does provide a powerful control over quantum noise. By adjusting the value of λ, it is possible to redistribute the noise in both n and ϕ. This is very important because the number n and the phase ϕ are observable quantities.

Here we have focused on four model Hamiltonians describing different ways to couple a Josephson junction to its environment. Needless to say, this list is not exhaustive. However,

these basic cases constitute a first step towards the study of more complicated and hybrid-mode interactions with the environment. To include a heat reservoir is beyond the scope of this thesis.

The approximations used here are valid in the limit of $T = 0$, $E_J \gg E_C$, and a very small biasing current. The states considered here are either the ground state or the low-energy excited states. If the above conditions are not satisfied, other effects can be important. The real quantum noise of the junction also includes contributions from the quasiparticles and other environmental degrees of freedom. Whether our results will provide the most important contribution depends on the relative strength of the dissipation and the thermal energy to the Josephson coupling constant E_J.

By replacing a periodic potential with a localized one, we are using localized states to represent "snapshots" of the extended states. Therefore, to improve our results, we need to either change to an extended-state basis, or at least take into account the fluctuations caused by the tunneling events.

4.4 Conclusion

In this work, we have investigated the quantum fluctuation properties of a Josephson junction in several different circuit configurations. Specifically, we considered the limit of large Josephson coupling energy and small charging energy, so that the JJs are in the nearly-localized regime. This limit can be easily realized for large S-I-S junctions. It is analogous to the tight-binding limit for electrons in a crystal.

The approximate ground states of a Josephson junction in a variety of situations are obtained. In particular, the ground state is a squeezed vacuum state for either an isolated junction in a potential minimum or a junction in a superconducting ring without external flux and in the global potential minimum. On the other hand, if the junction is current-biased, or there is an external flux through the superconducting ring, the ground state is a squeezed coherent state. In both of the above cases, we have calculated the corresponding fluctuations of the charge and phase difference over the junction in these states. The squeezing factors are determined by the parameter $\lambda = \sqrt{E_J/E_C}$, where E_J is the Josephson coupling energy and E_C is the charging energy of the junction. The squeezing effect is strong when λ is small. Since our working limit is at large λ, a compromise should be reached in order to both preserve the effectiveness of our approximation and maximize the squeezing effect. The excited states of a Josephson junction in different circumstances are

also obtained. We show that these excited states are similar to the number states of a simple harmonic oscillator but with different fluctuation properties.

Chapter 5

Quantum Noise and Squeezed States in Josephson Junctions

5.1 Introduction

5.1.1 Motivation

During the past decade, squeezed states of light [11] have attracted much attention in the atomic-molecular-optical physics community. In these states, the quantum fluctuations of one of the canonical variables (e.g., the electric field) can be squeezed below its vacuum-state value at the expense of increasing the quantum fluctuations of its conjugate variable. Examples of canonical conjugate variables are the position x and momentum p of a particle confined in one dimension, the electric field intensity and phase for light, as well as the charge number difference n and phase difference ϕ for a superconducting Josephson junction. The use of squeezed states for the exploitation of the limits of the uncertainty principle provides nearly noiseless optical measurements [79], unique opportunities for the study of QED (e.g., enhance the lifetime of atomic excited states), higher signal-to-noise ratio for gravitational wave detectors [69], and the promise of improved optical information transmission [11]. These and many other applications of squeezed states are described in [69], [11], [57], and references therein.

Is it possible to control quantum fluctuations in condensed matter systems, in analogy to these optical situations? We have explored this question in several condensed matter examples [18, 19, 20]. Indeed, quantum fluctuations can produce important measurable effects [15] in these systems even when temperatures are not very low. Moreover, other non-quantum-optics analogs of squeezed states are now being vigorously investigated by several groups [16].

The modulation of the quantum fluctuations in the photon field is made possible by the

very high precision achieved by optical measurements. Although most condensed matter experiments do not produce such high-accuracy results, two exceptions to this rule are the quantum Hall effect and the Josephson effect. For instance, the most precise measurement of energy levels has been achieved not in the traditional context of atomic-optical physics, but with superconducting tunneling Josephson junctions [23], to an astounding accuracy of three parts in 10^{19}. Furthermore, Josephson junctions are currently been used in an increasingly large number of applications involving high-precision measurements [80], Indeed, the goal of several single-electron transport devices [81] is to operate in the limiting case where fluctuations in junction charge number N are totally suppressed for all times (i.e., $\Delta N = 0$). For instance, the quantum pump proposed by Qian Niu [81, 82] acts like a "controlled conveyor belt" or "turnstile" of electrons, where electrons are transported by a time-dependent electric field. This remarkable device might provide an accurate standard of current. In Niu's quantum pump, ΔN is always zero since the time-dependent electric field produces a constant current of electrons. Thus the phase is totally undetermined, and both conjugate variables can be treated as classical quantities. Here, we are interested in studying quantum noise and JJs are ideal candidates for the possible manipulation of quantum fluctuations.

Here we explore the quantum fluctuation properties of a Josephson junction, and therefore point out a possible way of manipulating the accuracy limitations imposed by quantum noise. In light of the recent advances in micro-fabrication and the general interest in the possible control and minimization of quantum noise, we ask the following question: how do quantum fluctuations affect Cooper pair tunneling in a Josephson junction? To answer this, we need to first compute its quantum fluctuations and understand how they behave in different physical situations involving Josephson junctions. This is indeed the problem we focus on here. We would like to develop a theory of the quantum mechanical squeezed states in Josephson junctions, and identify and list their properties. In particular, we diagonalize several Hamiltonians corresponding to different configurations containing Josephson junctions, find their eigenstates, and calculate the corresponding fluctuations. We also construct the time-evolution operators for the various cases considered here. From them, and with different initial states, we calculate the time evolution of the variances of the conjugate variables of the system. These provide a measure of the quantum fluctuations of the charge and the phase difference of the Josephson junction.

5.1.2 Quantum Noise

There are various kinds of quantum noise. If a pair of quantum variables do not commute with each other, the product of the variances of these two quantities has a lower limit which is determined by the uncertainty principle. This kind of quantum noise, originating from the non-vanishing commutator of the conjugate variables, is an intrinsic property of an isolated system. However, no physical system is truly isolated; no matter how a system is chosen, it always has an environment to interact with. Furthermore, all the environmental degrees of freedom are ultimately governed by quantum mechanics and often involve non-commuting variables. Therefore, each degree of freedom has its own quantum noise due to the uncertainty principle, and this noise is also embodied in the system variables due to the interaction between the system and the environment; this kind of fluctuation can be considered as external to the system.

Another kind of quantum noise is shot noise. It originates from the discreteness of the carriers in the transport phenomena. For example, the tunneling events of quasi-particles in a Josephson junction are mostly uncorrelated and random. Such randomness naturally introduces a noise into the tunneling current, which is shot noise.

In this chapter (and the whole thesis) we only deal with the first kind of quantum noise—the intrinsic one originating from the non-vanishing commutator of the conjugate variables. The shot noise can be disregarded because of the coherence in the supercurrent of a Josephson junction. We also neglect the coupling of the junction to its environment. In addition, we focus our attention on the zero temperature case, so that no quasiparticle is excited, and no thermal noise is involved. We expect that our results will still persist at sufficiently low (but finite) temperatures.

5.1.3 Summary of This Chapter

In this chapter, we study the intrinsic quantum fluctuations of the charge and phase of a Josephson junction in various circumstances. Section 5.1 explains the motivation of this study. In Section 5.2 we consider a Josephson junction in a variety of situations, i.e., coupled to one or several of the following circuit elements: a capacitor, an inductor (in a superconducting ring), and an applied current-source. The Hamiltonian for each case is constructed. We use the small-phase approximation (described in Section 5.2) because we work in the strong coupling limit and treat the metastable states as nearly localized. In Section 5.3 we find the second quantized forms of the Hamiltonians. We then proceed to solve for the

ground and excited states near the potential minima of the various configurations that were described in Section 5.4. The corresponding ground states are squeezed vacuum or coherent states, while the excited states are a class of squeezed number states. In Section 5.5 we calculate the quantum fluctuations of the phase ϕ and Cooper pair number n over the junction for all the cases considered. We also construct the approximate time evolution operators for the configurations described in Section 5.6. In Section 5.7 we present another approach to study this problem: the rotating wave approximation. This is basically also a first-order perturbation in energy. Section 5.8 presents a discussion and also lists several open problems in the field. Finally, Section 5.9 summarizes the conclusions for the chapter.

Appendices A, B, F, and G are related to this chapter. Appendices A and B summarize some properties of squeezed and coherent states. Appendix F presents a brief review of the quantized LC circuit model, and Appendix G presents derivations of results used in the main body of the chapter.

5.2 Hamiltonians for System Configurations Containing a Josephson Junction

5.2.1 General Cases

A Josephson junction [83, 84, 85] is a weak link between two superconductors. A supercurrent can tunnel through it without any dissipation. The supercurrent I and the phase difference ϕ between the two superconductors satisfy the following equations

$$I = I_0 \sin\phi\,, \tag{5.1}$$

$$\frac{d\phi}{dt} = \frac{2e}{\hbar}V\,. \tag{5.2}$$

Here I_0 is a critical current, below which only the supercurrent exists at $T = 0$; and V is the voltage drop over the junction when quasiparticle tunneling exists.

Josephson junctions are generally damped systems, especially if quasiparticles are involved. Furthermore, in the Josephson equations the phase difference ϕ is treated as a classical quantity instead of a quantum mechanical operator. However, in the limit of zero temperature and small current, the system is dissipationless. Therefore, it is possible in this limit to write an effective Hamiltonian for an ideal junction.

Here we treat the phase difference ϕ as an operator, and we also include in our effective Hamiltonian its conjugate variable, the charge number n, in the form of charging energy. We want to study the quantum noise originating from the non-vanishing commutator between

the phase and the charge number.

We first consider an isolated junction (i.e., decoupled from its environment) near its ground state, at temperature $T = 0$. A capacitance is always present in Josephson junctions, especially in small-area ones (see, e.g., [86, 87], and references therein). A standard model [85, 89] for a simple Josephson junction is an ideal junction in parallel with a capacitor C. Its Hamiltonian is,

$$H_1 = \frac{Q^2}{2C} - E_J \cos\phi\,, \tag{5.3}$$

where the operators Q and ϕ satisfy the commutation relation

$$[\phi,\, Q] = 2ie\,. \tag{5.4}$$

Rewriting Q as $Q = e^* n = 2en$ and $E_C = 4e^2/C$, H_1 takes the form

$$\begin{aligned} H_1 &= \frac{4e^2}{C}\frac{n^2}{2} - E_J \cos\phi \\ &= \frac{E_C}{2} n^2 - E_J \cos\phi\,, \end{aligned} \tag{5.5}$$

where

$$[\phi,\, n] = i\,. \tag{5.6}$$

Here we only consider the coherent Cooper pair tunneling and neglect quasi-particle tunneling and shunting Ohmic resistance, which actually originates from the quasiparticle tunneling.

When a Josephson junction is current-biased, the system is no longer closed. However, it can still be described by an effective Hamiltonian, with an additional linear interaction term:

$$H_2 = \frac{E_C}{2} n^2 - E_J \cos\phi + \frac{I\Phi_0}{2\pi}\phi\,. \tag{5.7}$$

Here I is the biasing current and $\Phi_0 = h/2e$ is the superconducting flux quantum in the MKS units.

When a Josephson junction is in a superconducting loop with an external flux $\Phi_e = \Phi_0\phi_e/2\pi$, the Hamiltonian has the form

$$H_3 = \frac{E_C}{2} n^2 - E_J \cos\phi + \frac{\Phi_0^2}{8\pi^2 L}(\phi - \phi_e)^2\,, \tag{5.8}$$

where L is the inductance of the loop. In the special case when the external flux vanishes, the Hamiltonian takes the simplified form

$$H_4 = \frac{E_C}{2} n^2 - E_J \cos\phi + \frac{\Phi_0^2}{8\pi^2 L}\phi^2\,. \tag{5.9}$$

These different configurations are summarized in Table 5.1.

Case #	System	Hamiltonian
1	Isolated JJ	$H_1 = \frac{E_C}{2} n^2 - E_J \cos\phi$
2	Current-biased JJ	$H_2 = \frac{E_C}{2} n^2 - E_J \cos\phi - E_S\phi$
3	JJ in an SC ring with an external magnetic flux	$H_3 = \frac{E_C}{2} n^2 + \Phi^2/2L - E_J \cos\phi$
4	JJ in an SC ring without external magnetic flux and at the global potential minimum	$H_4 = \frac{E_C}{2} n^2 + \frac{(\Phi-\Phi_x)^2}{2L} - E_J \cos\phi$

Table 5.1: The four different configurations of a Josephson Junction in an LC Circuit considered in Chapters 4 and 5. Here JJ refers to Josephson Junction, SC refers to Super-Conducting, Φ is the magnetic flux through a superconducting ring, while ϕ is the phase difference between the two superconducting leads of a Josephson junction. These two quantities are related by $\Phi = \Phi_0(\phi/2\pi)$, where Φ_0 is the flux quantum $\Phi_0 = h/2e$. It can be proved from the Josephson equations that the superconducting phase difference ϕ here is equivalent to the phase on the capacitor, which is defined in Appendix F. Therefore, it is not a coincidence that they have the same relation to the magnetic flux. In H_2, $E_S = hI/2e$, where I is the biasing current of the junction.

5.2.2 Form of the Hamiltonians near a Potential Minimum

Motivation for the Small Phase Approximation

In this section, we investigate the intrinsic quantum fluctuation properties of the various Hamiltonians described in the previous section. For this purpose, we focus on the localized or nearly-localized states of a Josephson junction, and neglect its tunneling features. Below we consider each individual physical situation.

In the case of an isolated single junction, the problem is similar to that of an electron in a periodic potential, with E_J corresponding to the strength of the potential and E_C corresponding to the inverse mass of the electron. The eigenstates of such a periodic system are Bloch states. However, when an electron is in a deep potential well, it will be tightly bound to that site most of the time. Therefore, even though an electron in a periodic potential is always in an extended state, for deep enough potential wells we can consider its localized regime in the tight-binding limit. Similarly, for a Josephson junction with $E_J \gg E_C$, we can expand the $\cos\phi$ term at a potential minimum. In doing so, we substitute the periodic potential with a parabolic-type potential in the phase-representation. We thus put our emphasis on the local properties of the phase ϕ instead of its transport properties. This kind of approximation has been used in a variety of problems, including spin-density

waves [90] and Josephson junction arrays [91]. Needless to say, phase variations during a tunneling event do affect the local properties of a junction and give rise to larger fluctuations. However, in the limit when $T = 0$ and $E_J \gg E_C$, transport effects are small, so that we can neglect them to a first order approximation.

When there is a biasing current, the system is in the so-called "washboard" potential. When the biasing current is large enough, any localized state is unstable; i.e., the phase of the system will inevitably tunnel from one local potential minimum to another. However, when the biasing current is small $I\Phi_0 \ll \sqrt{E_J E_C}$, so that the lifetime of a metastable state is long compared to the characteristic time inside the potential well, we can study the properties of the metastable state at the potential minima as if it were a localized state.

When there is a superconducting ring associated with the Josephson junction, the situation is somewhat different. Now the potential is a parabolic one modulated by a sinusoidal term. There is a definite potential minimum, and the quantum fluctuation properties around this global minimum are of interest.

In summary, to study the intrinsic quantum fluctuation properties of a Josephson junction, it is physically justified to expand the interaction potential term around a local (or a global) minimum. The analytical solution of the full problem, without approximations, is quite difficult and would require a much more numerical approach, which is beyond the scope of this work.

Single Junction: Isolated or Current-Biased

For a single isolated junction, there is an infinite number of potential minima, which are all equivalent to each other. We expand the potential energy around $\phi = 0$:

$$H_1 = \frac{E_C}{2} n^2 - E_J \left(1 - \frac{1}{2}\phi^2 + \frac{1}{24}\phi^4\right) . \tag{5.10}$$

When the junction is current-biased, the sinusoidal potential is tilted and becomes the well-known "washboard" potential.

$$V_2 = -E_J \cos\phi + \frac{I\Phi_0}{2\pi}\phi . \tag{5.11}$$

Again, there is an infinite number of equivalent local potential minima, ϕ_{m2}; and any one of them satisfies

$$\left.\frac{\partial V_2}{\partial \phi}\right|_{\phi_{m2}} = \left.\left(E_J \sin\phi + \frac{I\Phi_0}{2\pi}\right)\right|_{\phi_{m2}} = 0 , \tag{5.12}$$

$$\left.\frac{\partial^2 V_2}{\partial \phi^2}\right|_{\phi_{m2}} = E_J \cos\phi\,|_{\phi_{m2}} > 0 . \tag{5.13}$$

In other words,

$$\sin\phi_{m2} = -\frac{I\Phi_0}{2\pi E_J}, \tag{5.14}$$

$$\cos\phi_{m2} = \sqrt{1-\left(\frac{I\Phi_0}{2\pi E_J}\right)^2}. \tag{5.15}$$

Now we can expand the potential energy V_2 around ϕ_{m2} to investigate properties of the localized states. Writing $\phi = \phi_{m2} + \phi_{\rm local}$, the potential is then expanded as

$$\begin{aligned} V_2 &= -E_J\cos(\phi_{m2}+\phi_{\rm local}) + \frac{I\Phi_0}{2\pi}(\phi_{m2}+\phi_{\rm local}) \\ &= -E_J(\cos\phi_{m2}\cos\phi_{\rm local} - \sin\phi_{m2}\sin\phi_{\rm local}) + \frac{I\Phi_0}{2\pi}(\phi_{m2}+\phi_{\rm local}). \end{aligned} \tag{5.16}$$

Since we are concerned with quantum states in the vicinity of a local potential minimum, the variable $\phi_{\rm local}$ is a small quantity. Therefore we use the following expansions

$$\cos\phi_{\rm local} = 1 - \frac{1}{2}\phi_{\rm local}^2 + \frac{1}{24}\phi_{\rm local}^4, \tag{5.17}$$

$$\sin\phi_{\rm local} = \phi_{\rm local} - \frac{1}{6}\phi_{\rm local}^3. \tag{5.18}$$

Here we have taken higher-order corrections into account so that the nonlinear feature of the sinusoidal functions can be described better. The potential now takes the form

$$\begin{aligned} V_2 &= -E_J\left\{\left(1-\frac{1}{2}\phi_{\rm local}^2+\frac{1}{24}\phi_{\rm local}^4\right)\cos\phi_{m2} - \left(\phi_{\rm local}-\frac{1}{6}\phi_{\rm local}^3\right)\sin\phi_{m2}\right\} \\ &\quad + \frac{I\Phi_0}{2\pi}(\phi_{m2}+\phi_{\rm local}) \\ &= \left(-E_J\cos\phi_{m2}+\frac{I\Phi_0}{2\pi}\phi_{m2}\right) + \frac{1}{2}(E_J\cos\phi_{m2})\phi_{\rm local}^2 - \frac{1}{6}(E_J\sin\phi_{m2})\phi_{\rm local}^3 \\ &\quad - \frac{1}{24}(E_J\cos\phi_{m2})\phi_{\rm local}^4 \\ &= \left(-E_J\cos\phi_{m2}+\frac{I\Phi_0}{2\pi}\phi_{m2}\right) + \frac{E_J}{2}\sqrt{1-\left(\frac{I\Phi_0}{2\pi E_J}\right)^2}\phi_{\rm local}^2 + \frac{I\Phi_0}{12\pi}\phi_{\rm local}^3 \\ &\quad - \frac{E_J}{24}\sqrt{1-\left(\frac{I\Phi_0}{2\pi E_J}\right)^2}\phi_{\rm local}^4. \end{aligned} \tag{5.19}$$

The constant term (which is a function of ϕ_{m2}) gives the value of the local potential minimum, while the terms related to $\phi_{\rm local}$ determine the quantum fluctuation properties of the metastable states at the minimum. It can be seen that these later terms are only related to E_J and I, while the actual value of ϕ_{m2} is irrelevant.

Notice that the fourth-order term in the Hamiltonian has a negative sign, which at first sight might appear to be a non-stabilizing term. Recall that in the standard Landau

argument for phase transitions, a free energy is expanded in terms of powers of the order parameter, and only the first powers are kept (assuming a small value of the order parameter close to T_c). There, the ϕ^4 term provides stability when the ϕ^2 term is not stable, i.e., when the coefficient of ϕ^2 is either zero or negative. In our case, we have a dynamic model instead of a statistical model. The coefficients in our Hamiltonians are all microscopic constants that do not depend on temperature (to first order approximation), and the coefficient of ϕ^2 (i.e., E_J) does not change sign. These are significantly different from the standard Landau phenomenology for phase transitions. Indeed, in the small-ϕ approximation, the ϕ^2 term of the JJ energy expansion in ϕ provides stability to the $\phi = 0$ solution.

The essential idea of our approach is as follows. The dominant ϕ^2 term provides a confining harmonic oscillator potential, which produces *time-independent* fluctuations in the canonical conjugate coordinates. It is the (smaller) ϕ^4 term that induces *time-dependent* modulations on the fluctuations of the conjugate variables. Higher-order terms (e.g., ϕ^6, and ϕ^8) *also* modulate in time the time-independent harmonic fluctuations, but since these higher-order terms are much smaller than the (already small) ϕ^4 term, we will ignore them here. Notice that even for the large-ϕ case when $\phi = 1$, the ϕ^4 term is 12 times *smaller* than the ϕ^2 case (see Eq. (5.10)). Thus, the small-ϕ limit we use here is robust for a relatively wide range of values of ϕ.

Josephson Junction in a Superconducting Ring

When a Josephson junction is in a superconducting ring, the situation is different. Now the potential is a parabola modulated by a cosine function in ϕ-space. Therefore, there generally exists a global potential minimum, where the state is localized. Furthermore, if the system falls into one of the local potential minima, it tends to eventually relax into the global one. Otherwise, these local metastable potential minima should have similar quantum fluctuation properties as in the case of the washboard potential. Now let us take a closer look at the relevant Hamiltonians.

If there is an external flux $\Phi_e = \Phi_0\phi_e/2\pi$ through the superconducting ring, the Hamiltonian is

$$H_3 = \frac{E_C}{2}n^2 + V_3\,, \tag{5.20}$$

$$V_3 = -E_J\cos\phi + \frac{\Phi_0^2}{8\pi^2 L}(\phi - \phi_e)^2\,. \tag{5.21}$$

The potential minima are at ϕ_{m3} where $\partial V/\partial\phi|_{\phi_{m3}} = 0$ and $\partial^2 V/\partial\phi^2|_{\phi_{m3}} > 0$. In other words, ϕ_{m3} satisfies $E_J\sin\phi_{m3} + \Phi_0^2(\phi_{m3} - \phi_e)/4\pi^2 L = 0$ and $E_J\cos\phi_{m3} + \Phi_0^2/4\pi^2 L > 0$.

In the neighborhood of ϕ_{m3}, the phase can be expressed as $\phi = \phi_{m3} + \phi_{\rm local}$. The potential then has the form

$$\begin{aligned} V_3 &= -E_J \cos(\phi_{m3} + \phi_{\rm local}) + \frac{\Phi_0^2}{8\pi^2 L}(\phi_{m3} + \phi_{\rm local} - \phi_e)^2 \\ &= -E_J \left(\cos\phi_{m3} \cos\phi_{\rm local} - \sin\phi_{m3} \sin\phi_{\rm local}\right) \\ &\quad + \frac{\Phi_0^2}{8\pi^2 L}\left\{(\phi_{m3} - \phi_e)^2 + 2(\phi_{m3} - \phi_e)\phi_{\rm local} + \phi_{\rm local}^2\right\} . \end{aligned} \tag{5.22}$$

Now we again expand $\cos\phi_{\rm local}$ and $\sin\phi_{\rm local}$ as in Eq. (5.14) and (5.15); the potential V_3 can then be simplified to

$$\begin{aligned} V_3 &= \left\{-E_J \cos\phi_{m3} + \frac{\Phi_0^2}{8\pi^2 L}(\phi_{m3} - \phi_e)^2\right\} + \frac{1}{2}\left(E_J \cos\phi_{m3} + \frac{\Phi_0^2}{4\pi^2 L}\right)\phi_{\rm local}^2 \\ &\quad - \frac{1}{6}\left(E_J \sin\phi_{m3}\right)\phi_{\rm local}^3 - \frac{1}{24}\left(E_J \cos\phi_{m3}\right)\phi_{\rm local}^4 , \end{aligned} \tag{5.23}$$

while

$$E_J \sin\phi_{m3} = -(\phi_{m3} - \phi_e)\Phi_0^2/4\pi^2 L , \tag{5.24}$$

$$E_J \cos\phi_{m3} > -\Phi_0^2/4\pi^2 L . \tag{5.25}$$

Therefore, the Hamiltonian for a Josephson junction in a superconducting ring threaded with an external flux Φ_e takes the simplified form

$$\begin{aligned} H_3 &= \frac{E_C}{2}n^2 + \left\{-E_J \cos\phi_{m3} + \frac{\Phi_0^2}{8\pi^2 L}(\phi_{m3} - \phi_e)^2\right\} + \frac{1}{2}\left(E_J \cos\phi_{m3} + \frac{\Phi_0^2}{4\pi^2 L}\right)\phi_{\rm local}^2 \\ &\quad - \frac{1}{6}\left(E_J \sin\phi_{m3}\right)\phi_{\rm local}^3 - \frac{1}{24}\left(E_J \cos\phi_{m3}\right)\phi_{\rm local}^4 . \end{aligned} \tag{5.26}$$

When the external flux through the ring is zero, the form of the Hamiltonian will remain the same, but the equations satisfied by ϕ_{m4} are different:

$$E_J \sin\phi_{m4} = -\frac{\Phi_0^2}{4\pi^2 L}\phi_{m4} , \tag{5.27}$$

$$E_J \cos\phi_{m4} > -\frac{\Phi_0^2}{4\pi^2 L} . \tag{5.28}$$

Furthermore, it can be seen from the above equations that $\phi_{m4} = 0$ is the global potential energy minimum. The expansion around this point is even simpler than around a metastable point:

$$H_4 = \frac{E_C}{2}n^2 - E_J + \frac{1}{2}\left(E_J + \frac{\Phi_0^2}{4\pi^2 L}\right)\phi_{\rm local}^2 - \frac{1}{24}E_J\phi_{\rm local}^4 , \tag{5.29}$$

$$\phi_{m4} = 0 . \tag{5.30}$$

Notice that the third-order term in $\phi_{\rm local}$ has vanished. Indeed, from the form of the original potential, it can be seen that the external flux only shifts the position of the minimum of the parabolic potential. If $\Phi_e = 0$, the global minimum of the total potential is at $\phi = 0$. Moreover, the change of Φ_e does not directly affect the quantum fluctuation properties of the total potential because it only leads to a horizontal shift in the parabolic part of the potential.

5.3 Second Quantized form

5.3.1 Single Isolated Junction

Let us first consider a free oscillator,

$$H_1 = \frac{E_C}{2}n^2 + \frac{E_J}{2}\phi^2 - \frac{E_J}{24}\phi^4 - E_J. \tag{5.31}$$

We introduce a pair of creation and annihilation operators

$$a_1 = \frac{1}{\sqrt{2}}\left\{\left(\frac{E_J}{E_C}\right)^{1/4}\phi + i\left(\frac{E_C}{E_J}\right)^{1/4}n\right\}, \tag{5.32}$$

$$a_1^\dagger = \frac{1}{\sqrt{2}}\left\{\left(\frac{E_J}{E_C}\right)^{1/4}\phi - i\left(\frac{E_C}{E_J}\right)^{1/4}n\right\}, \tag{5.33}$$

and also the following definitions

$$\hbar\omega_1 = \sqrt{E_J E_C}, \tag{5.34}$$

$$\lambda_1 = \sqrt{\frac{E_J}{E_C}}, \tag{5.35}$$

so that

$$\phi = \frac{1}{\sqrt{2}}\left(\frac{E_C}{E_J}\right)^{1/4}(a_1 + a_1^\dagger) = \frac{1}{\sqrt{2\lambda_1}}(a_1 + a_1^\dagger), \tag{5.36}$$

$$n = \frac{1}{i\sqrt{2}}\left(\frac{E_J}{E_C}\right)^{1/4}(a_1 - a_1^\dagger) = -i\sqrt{\frac{\lambda_1}{2}}(a_1 - a_1^\dagger). \tag{5.37}$$

Notice that the number states for a_1 and $a_1^\dagger$ are not the Cooper-pair-number eigenstates. Instead, they are the eigenstates of the operator $a_1^\dagger a_1$. In the a-representation, the charge-number operator n plays a role which is similar to the momentum in a simple harmonic oscillator (see Appendix F). The Hamiltonian for an isolated single junction now takes the form

$$H_1 = \hbar\omega_1\left(a^\dagger a + \frac{1}{2}\right) - \frac{\hbar\omega_1}{96\lambda_1}(a + a^\dagger)^4$$

$$= \hbar\omega_1 \left(1 - \frac{1}{8\lambda_1}\right) a^\dagger a - \frac{\hbar\omega_1}{16\lambda_1}\left(a^2 + a^{\dagger 2}\right)$$
$$-\frac{\hbar\omega_1}{96\lambda_1}\left(a^{\dagger 4} + 4a^{\dagger 3}a + 6a^{\dagger 2}a^2 + 4a^\dagger a^3 + a^4\right) + \text{constant}. \quad (5.38)$$

From its definition, ω_1 is the plasma frequency of the junction and our quantum here [83]. The lowest-order terms of H_1 are proportional to a_1^2 and $a_1^{\dagger 2}$, and there is no linear term.

5.3.2 Current-Biased Junction

In the cases of a current-biased junction and a junction within a superconducting ring, the Hamiltonians are more complicated because of the linear shifts in the potentials produced by the current and the flux.

For a current-biased junction, in the vicinity of any local potential minimum, the Hamiltonian is

$$H_2 = \frac{E_C}{2}n^2 + \frac{E_J}{2}\sqrt{1 - \left(\frac{I\Phi_0}{2\pi E_J}\right)^2}\,\phi_{\text{local}}^2 + \frac{I\Phi_0}{12\pi}\phi_{\text{local}}^3 - \frac{E_J}{24}\sqrt{1 - \left(\frac{I\Phi_0}{2\pi E_J}\right)^2}\,\phi_{\text{local}}^4, \quad (5.39)$$

where we have already dropped the constant term, which does not affect the quantum noise. To take into account the shift in the potential, we redefine the Josephson coupling energy as

$$E_{J2} = E_J\sqrt{1 - \left(\frac{I\Phi_0}{2\pi E_J}\right)^2}. \quad (5.40)$$

The eigenfrequency of the system and the junction parameter then have to be redefined as

$$\omega_2 = \frac{1}{\hbar}\sqrt{E_{J2}E_C}, \quad (5.41)$$

$$\lambda_2 = \sqrt{\frac{E_{J2}}{E_C}}, \quad (5.42)$$

and the creation and annihilation operators become

$$a_2 = \frac{1}{\sqrt{2}}\left\{\left(\frac{E_{J2}}{E_C}\right)^{1/4}\phi_{\text{local}} + i\left(\frac{E_C}{E_{J2}}\right)^{1/4} n\right\}, \quad (5.43)$$

$$a_2^\dagger = \frac{1}{\sqrt{2}}\left\{\left(\frac{E_{J2}}{E_C}\right)^{1/4}\phi_{\text{local}} - i\left(\frac{E_C}{E_{J2}}\right)^{1/4} n\right\}, \quad (5.44)$$

so that

$$\phi_{\text{local}} = \frac{1}{\sqrt{2}}\left(\frac{E_C}{E_{J2}}\right)^{1/4}(a_2 + a_2^\dagger), \quad (5.45)$$

$$n = \frac{1}{i\sqrt{2}}\left(\frac{E_{J2}}{E_C}\right)^{1/4}(a_2 - a_2^\dagger). \quad (5.46)$$

Now the Hamiltonian H_2 takes the form

$$\begin{aligned} H_2 &= \hbar\omega_2\left(a_2^\dagger a_2+\frac{1}{2}\right)+\frac{I\Phi_0}{24\sqrt{2}\pi}\left(\frac{E_C}{E_{J2}}\right)^{3/4}\left(a_2+a_2^\dagger\right)^3-\frac{E_C}{96}\left(a_2+a_2^\dagger\right)^4 \qquad (5.47)\\ &= \hbar\omega_2\left(a_2^\dagger a_2+\frac{1}{2}\right)+\frac{I\Phi_0}{8\sqrt{2}\pi\lambda_2^{3/2}}\left(a_2^\dagger+a_2\right)-\frac{\hbar\omega_2}{32\lambda_2}\left\{8a_2^\dagger a_2+1+2\left(a_2^{\dagger 2}+a_2^2\right)\right\}\\ &\quad+\frac{I\Phi_0}{24\sqrt{2}\pi\lambda_2^{3/2}}\left(a_2^{\dagger 3}+3a_2^{\dagger 2}a_2+3a_2^\dagger a_2+a_2^3\right)\\ &\quad-\frac{\hbar\omega_2}{96\lambda_2}\left(a_2^{\dagger 4}+4a_2^{\dagger 3}a_2+6a_2^{\dagger 2}a_2^2+4a_2^\dagger a_2^3+a_2^4\right)\\ &= \hbar\omega_2\left(1-\frac{1}{8\lambda_2}\right)a_2^\dagger a_2+\frac{I\Phi_0}{8\sqrt{2}\pi\lambda_2^{3/2}}\left(a_2^\dagger+a_2\right)-\frac{\hbar\omega_2}{16\lambda_2}\left(a_2^{\dagger 2}+a_2^2\right)\\ &\quad+\text{constant}+\text{higher order terms}. \qquad (5.48)\end{aligned}$$

The difference between H_1 and H_2 lies in the linear term in H_2, which represents a driving force (the effect of the biasing current).

5.3.3 Josephson Junction in a Superconducting Ring

When the Josephson junction is in a superconducting ring, the situation is somewhat similar to the current-biased junction. Recall that the Hamiltonian (with an external flux) is

$$\begin{aligned} H_3 &= \frac{E_C}{2}n^2+\frac{1}{2}\left(E_J\cos\phi_{m3}+\frac{\Phi_0^2}{4\pi^2L}\right)\phi_{\text{local}}^2-\frac{1}{6}\left(E_J\sin\phi_{m3}\right)\phi_{\text{local}}^3\\ &\quad-\frac{1}{24}\left(E_J\cos\phi_{m3}\right)\phi_{\text{local}}^4+\text{constant}, \qquad (5.49)\end{aligned}$$

where ϕ_{m3} satisfies

$$E_J\sin\phi_{m3}=-\frac{\Phi_0^2}{4\pi^2L}(\phi_{m3}-\phi_e). \qquad (5.50)$$

Consequently, the renormalized Josephson coupling energy and the eigenfrequency of the system are

$$\begin{aligned} E_{J3} &= E_J\cos\phi_{m3}+\frac{\Phi_0^2}{4\pi^2L}, \qquad (5.51)\\ \omega_3 &= \frac{1}{\hbar}\sqrt{E_CE_{J3}}, \qquad (5.52)\\ \lambda_3 &= \sqrt{\frac{E_{J3}}{E_C}}. \qquad (5.53)\end{aligned}$$

The creation and annihilation operators are now defined as

$$\begin{aligned} a_3 &= \frac{1}{\sqrt{2}}\left\{\left(\frac{E_{J3}}{E_C}\right)^{1/4}\phi_{\text{local}}+i\left(\frac{E_C}{E_{J3}}\right)^{1/4}n\right\}, \qquad (5.54)\\ a_3^\dagger &= \frac{1}{\sqrt{2}}\left\{\left(\frac{E_{J3}}{E_C}\right)^{1/4}\phi_{\text{local}}-i\left(\frac{E_C}{E_{J3}}\right)^{1/4}n\right\}, \qquad (5.55)\end{aligned}$$

so that $\phi_{\rm local}$ and n can be expressed as

$$\phi_{\rm local} = \frac{1}{\sqrt{2}}\left(\frac{E_C}{E_{J3}}\right)^{1/4}\left(a_3+a_3^\dagger\right), \tag{5.56}$$

$$n = \frac{1}{i\sqrt{2}}\left(\frac{E_{J3}}{E_C}\right)^{1/4}\left(a_3-a_3^\dagger\right). \tag{5.57}$$

The Hamiltonian H_3 is now

$$\begin{aligned} H_3 &= \hbar\omega_3\left(a_3^\dagger a_3+\frac{1}{2}\right) - \frac{\hbar\omega_3}{12\sqrt{2\lambda_3}}\frac{E_J\sin\phi_{m3}}{E_J\cos\phi_{m3}+\Phi_0^2/4\pi^2L}\left(a_3^\dagger+a_3\right)^3 \\ &\quad -\frac{\hbar\omega_3}{96\lambda_3}\frac{E_J\cos\phi_{m3}}{E_J\cos\phi_{m3}+\Phi_0^2/4\pi^2L}\left(a_3+a_3^\dagger\right)^4 \qquad (5.58) \\ &= \hbar\omega_3\left(a_3^\dagger a_3+\frac{1}{2}\right) - \frac{\hbar\omega_3}{4\sqrt{2\lambda_3}}\frac{E_J\sin\phi_{m3}}{E_{J3}}\left(a_3^\dagger+a_3\right) \\ &\quad -\frac{\hbar\omega_3}{96\lambda_3}\frac{E_J\cos\phi_{m3}}{E_{J3}}\left\{12a_3^\dagger a_3+3+6\left(a_3^{\dagger 2}+a_3^2\right)\right\} \\ &\quad -\frac{\hbar\omega_3}{12\sqrt{2\lambda_3}}\frac{E_J\sin\phi_{m3}}{E_{J3}}\left(a_3^{\dagger 3}+3a_3^{\dagger 2}a_3+3a_3^\dagger a_3+a_3^3\right) \\ &\quad -\frac{\hbar\omega_3}{96\lambda_3}\frac{E_J\cos\phi_{m3}}{E_{J3}}\left(a_3^{\dagger 4}+4a_3^{\dagger 3}a_3+6a_3^{\dagger 2}a_3^2+4a_3^\dagger a_3^3+a_3^4\right) \\ &= \hbar\omega_3\left(1-\frac{E_J\cos\phi_{m3}}{8\lambda_3E_{J3}}\right)a_3^\dagger a_3 - \frac{\hbar\omega_3E_J\sin\phi_{m3}}{4\sqrt{2\lambda_3}E_{J3}}\left(a_3^\dagger+a_3\right) \\ &\quad -\frac{\hbar\omega_3E_J\cos\phi_{m3}}{16\lambda_3E_{J3}}\left(a_3^{\dagger 2}+a_3^2\right)+\text{constant}+\text{higher order terms}. \qquad (5.59) \end{aligned}$$

If the external flux through the superconducting ring vanishes, we can still use all the definitions and formulae above, by simply substituting ϕ_e by 0. However, if we further limit our focus onto the global minimum, the expressions for the Hamiltonian H_4 and the relevant quantities become more compact because in this case $\phi_{m4}=0$. We thus have

$$E_{J4} = E_J+\frac{\Phi_0^2}{4\pi^2L}, \tag{5.60}$$

$$\omega_4 = \frac{1}{\hbar}\sqrt{E_CE_{J4}}, \tag{5.61}$$

$$\lambda_4 = \sqrt{\frac{E_{J4}}{E_C}}, \tag{5.62}$$

$$\cos\phi_{m4} = 1, \tag{5.63}$$

$$a_4 = \frac{1}{\sqrt{2}}\left\{\left(\frac{E_{J4}}{E_C}\right)^{1/4}\phi_{\rm local}+i\left(\frac{E_C}{E_{J4}}\right)^{1/4}n\right\}, \tag{5.64}$$

$$\phi_{\rm local} = \frac{1}{\sqrt{2}}\left(\frac{E_C}{E_{J4}}\right)^{1/4}\left(a_4+a_4^\dagger\right), \tag{5.65}$$

$$n = \frac{1}{i\sqrt{2}}\left(\frac{E_{J4}}{E_C}\right)^{1/4}\left(a_4-a_4^\dagger\right), \tag{5.66}$$

$$H_4 = \hbar\omega_4\left(1-\frac{E_J}{8\lambda_4E_{J4}}\right)a_4^\dagger a_4 - \frac{\hbar\omega_4E_J}{16\lambda_4E_{J4}}(a_4^{\dagger 2}+a_4^2) \tag{5.67}$$

$$+\text{constant}+\text{higher order terms}. \tag{5.68}$$

The parameters for all the above configurations are summarized in Table 5.2.

5.3.4 Approximate Form of the Hamiltonians

From the Schrödinger equation, the state vector of an arbitrary system (with a time-independent Hamiltonian) can be formally written as

$$|\psi(t)\rangle = e^{iHt/\hbar}|\psi(0)\rangle\,. \tag{5.69}$$

In general, $|\psi(t)\rangle$ can be expanded in a coherent state basis:

$$|\psi(t)\rangle = \int d^2\alpha\, d^2\beta\, |\alpha\rangle\langle\alpha|e^{iHt/\hbar}|\beta\rangle\langle\beta|\psi(0)\rangle\,. \tag{5.70}$$

In the short-time limit, $e^{i\int Ht/\hbar} \cong 1 + iHt/\hbar$. Furthermore, let us restrict ourself to the cases when $|\psi(0)\rangle$ is the ground state or a low-energy excited state. When this condition is true, $\langle\beta|\psi(0)\rangle$ should have its largest value for small $|\beta|$. Since t is small, $|\psi(t)\rangle$ should not be too different from $|\psi(0)\rangle$. Therefore, the above integral is significant only when $|\alpha|$ is small. With both α and β small, i.e., $|\alpha| \ll 1$ and $|\beta| \ll 1$, $\langle\alpha|\left(a^{\dagger 3} + a^3\right)|\beta\rangle \cong \max\{|\alpha|^3, |\beta|^3\} \ll \max\{|\alpha|^2, |\beta|^2\} \cong \langle\alpha|\left(a^{\dagger 2} + a^2\right)|\beta\rangle$. In addition, the higher order terms also have very small coefficients. Therefore, as a first-order approximation, we can drop all the terms that are to third or higher-orders in a and $a^\dagger$. Such an approximation greatly simplifies the Hamiltonians in the various cases. For instance, the Hamiltonian for the single isolated junction becomes

$$H_1 = \hbar\omega_1\left(1 - \frac{1}{8\lambda_1}\right)a_1^\dagger a_1 - \frac{\hbar\omega}{16\lambda_1}\left(a_1^2 + a_1^{\dagger 2}\right)\,. \tag{5.71}$$

The Hamiltonian of the current-biased junction takes the form

$$H_2 = \hbar\omega_2\left(1 - \frac{1}{8\lambda_2}\right)a_2^\dagger a_2 + \frac{I\Phi_0}{8\sqrt{2}\pi\lambda_2^{3/2}}\left(a_2^\dagger + a_2\right) - \frac{\hbar\omega_2}{16\lambda_2}\left(a_2^{\dagger 2} + a_2^2\right)\,. \tag{5.72}$$

The Hamiltonian of a Josephson junction in a superconducting ring becomes

$$H_3 = \hbar\omega_3\left(1 - \frac{E_J\cos\phi_{m3}}{8\lambda_3 E_{J3}}\right)a_3^\dagger a_3 - \frac{\hbar\omega_3 E_J\sin\phi_{m3}}{4\sqrt{2\lambda_3}E_{J3}}\left(a_3^\dagger + a_3\right) - \frac{\hbar\omega_3 E_J\cos\phi_{m3}}{16\lambda_3 E_{J3}}\left(a_3^{\dagger 2} + a_3^2\right)\,. \tag{5.73}$$

Finally, when there is no external flux through the ring, and we consider only the global potential minimum, the Hamiltonian is

$$H_4 = \hbar\omega_4\left(1 - \frac{E_J}{8\lambda_4 E_{J4}}\right)a_4^\dagger a_4 - \frac{\hbar\omega_4 E_J}{16\lambda_4 E_{J4}}\left(a_4^{\dagger 2} + a_4^2\right)\,. \tag{5.74}$$

	Case 1	Case 2	Case 3	Case 4
Effective JJ coupling E_{Ji}	$E_{J1} = E_J$	$E_{J2} = E_J\sqrt{1-\left(\frac{I\Phi_0}{2\pi E_J}\right)^2}$	$E_{J3} = E_J\cos\phi_{m3} + \Phi_0^2/4\pi^2 L$	$E_{J4} = E_J + \Phi_0^2/4\pi^2 L$
Energy quantum $\hbar\omega_i$	$\hbar\omega_1 = \sqrt{E_J E_C}$	$\hbar\omega_2 = \sqrt{E_{J2} E_C}$	$\hbar\omega_3 = \sqrt{E_{J3} E_C}$	$\hbar\omega_4 = \sqrt{E_{J4} E_C}$
JJ parameter λ_i	$\lambda_1 = \sqrt{E_J/E_C}$	$\lambda_2 = \sqrt{E_{J2}/E_C}$	$\lambda_3 = \sqrt{E_{J3}/E_C}$	$\lambda_4 = \sqrt{E_{J4}/E_C}$
nonlinearity parameter δ_i	$\delta_1 = 1/16\lambda_1$	$\delta_2 = 1/16\lambda_2$	$\delta_3 = E_J\cos\phi_{m3}/16\lambda_3 E_{J3}$	$\delta_4 = \sqrt{E_J^2 E_C/E_{J4}^3}/16$
Renormalized frequency ω	$\omega_1(1-2\delta_1)$	$\omega_2(1-2\delta_2)$	$\omega_3(1-2\delta_3)$	$\omega_4(1-2\delta_4)$
Linear coefficient α_i	0	$\alpha_2 = I\Phi_0/8\sqrt{2}\pi\lambda_2^{3/2}$	$\alpha_3 = -\hbar\omega_3 E_J\sin\phi_{m3}/4\sqrt{2\lambda_3}E_{J3}$	0
Displacement factor d_i	0	$-\alpha_2(1+2\delta_2)/\hbar\omega_2$	$-\alpha_3(1+2\delta_3)/\hbar\omega_3$	0
Quadratic coefficient β_i	$-\delta_1$	$-\delta_2$	$-\delta_3$	$-\delta_4$
|Squeezing factor| $= s_i$	δ_1	δ_2	δ_3	δ_4

Table 5.2: The parameters for the different Josephson junction configurations considered in Chapters 4 and 5. In the table, E_J is the Josephson coupling energy for an ideal junction; E_C is the charging energy associated with the relevant junction; $\Phi_0 = h/2e$ is the superconducting magnetic flux quantum; ϕ_{m3} is the phase of a local potential minimum for case 3; L is the inductance of the superconducting ring; and finally, I is the biasing current for case 2.

The four simplified Hamiltonians belong to two groups. The first group (denoted by H_A) includes H_1 and H_4, with a free oscillator term and two second-order perturbation terms. The second group (denoted by H_B) includes H_2 and H_3, which have two linear terms in addition to the free oscillator term and the second-order perturbation terms. Below we will find that these linear terms lead to higher-energy ground states for the relevant systems.

Why the four diverse situations we originally considered can be simplified into only two categories? The reason lies in the special form of the Josephson coupling energy. Although each one of these Hamiltonians has its particular character, they all share the charging and Josephson coupling energy terms. When E_J is the dominant energy scale in the system, the Josephson coupling is the governing factor in all of these systems, which leads to similar properties. More specifically, the linear and quadratic energy terms are more of global importance. If we focus on a local potential minimum, the special features should mostly be determined by the sinusoidal function.

5.4 Ground and Excited States of Various Hamiltonians

In this section we focus on the ground states of the various systems we are interested in.

5.4.1 Ground and Excited States of the Hamiltonians H_1 and H_4

The Hamiltonian H_1 for an isolated junction and H_4 for a junction in a superconducting ring (at zero flux) at the global potential minimum have the same form H_A:

$$H_A = \hbar\omega a^\dagger a + \beta a^2 + \beta^* a^{\dagger 2}\,. \tag{5.75}$$

This Hamiltonian can be easily diagonalized by introducing operators b and $b^\dagger$:

$$b = \mu a + \nu a^\dagger\,, \tag{5.76}$$

$$b^\dagger = \mu^* a^\dagger + \nu^* a\,. \tag{5.77}$$

From these expressions we obtain

$$b^\dagger b = (|\mu|^2 + |\nu|^2)a^\dagger a + \mu\nu^* a^2 + \mu^*\nu a^{\dagger 2} + |\nu|^2\,. \tag{5.78}$$

Therefore, if we require that

$$\beta = \frac{\hbar\omega\mu\nu^*}{|\mu|^2 + |\nu|^2}\,, \tag{5.79}$$

the Hamiltonian H_A is diagonalized to

$$H_A = \frac{\hbar\omega}{|\mu|^2 + |\nu|^2} b^\dagger b - \frac{\hbar\omega|\nu|^2}{|\mu|^2 + |\nu|^2}\,. \tag{5.80}$$

To satisfy the boson commutator $[b, b^\dagger] = 1$, μ and ν must satisfy the equality

$$|\mu|^2 - |\nu|^2 = 1\,. \tag{5.81}$$

From this equation and Eq. (5.79), we can solve for the transformation coefficients μ and ν up to a global phase factor:

$$\begin{aligned}
|\mu|^2 &= \frac{1}{2\sqrt{1-4\delta^2}} + \frac{1}{2} \\
&\cong 1 + \delta^2\,, && (5.82)\\
|\nu|^2 &= \frac{1}{2\sqrt{1-4\delta^2}} - \frac{1}{2} \\
&\cong \delta^2\,, && (5.83)\\
|\mu|^2 + |\nu|^2 &= \frac{1}{\sqrt{1-4\delta^2}} \\
&\cong 1 + 2\delta^2\,, && (5.84)\\
\phi_\mu - \phi_\nu &= \phi_\beta + 2m\pi\,, && (5.85)\\
\delta &= \frac{|\beta|}{\hbar\omega}\,. && (5.86)
\end{aligned}$$

Here m is an arbitrary integer, and δ is a small quantity because the perturbation terms are much smaller than the free oscillator term. Now the Hamiltonian takes on the simpler form

$$\begin{aligned}
H_A &= \hbar\omega\sqrt{1-4\delta^2}\; b^\dagger b - \frac{1}{2}\hbar\omega\left(1 - \sqrt{1-4\delta^2}\right) \\
&\cong \hbar\omega(1-2\delta^2)\; b^\dagger b - \hbar\omega\delta^2\,. && (5.87)
\end{aligned}$$

The ground state of this Hamiltonian satisfies

$$b|0\rangle_b = 0\,. \tag{5.88}$$

A squeezing operator $S(\xi)$ [11, 58] can be introduced to represent the transformation between b and a:

$$S(\xi) = \exp\left(\frac{\xi^*}{2}a^2 - \frac{\xi}{2}a^{\dagger 2}\right)\,, \tag{5.89}$$

where $\xi = se^{i\theta}$ is a complex squeezing factor. Its physical meaning is described in [58] and also in Figs. 5.1 and 5.2. Briefly, the squeezing operator acting on the vacuum or a coherent state periodically reduces or "squeezes" the uncertainty of one of the conjugate coordinates (e.g., n and ϕ, or x and p) below its minimum uncertainty or coherent-state value. It can be easily shown that

$$S^{-1}(\xi)\, a\, S(\xi) = a\cosh s - a^\dagger e^{i\theta}\sinh s\,. \tag{5.90}$$

Therefore, if we let

$$\mu = \cosh s\,, \tag{5.91}$$

$$\nu = -e^{i\theta}\sinh s\,, \tag{5.92}$$

then

$$b = S^{-1}(\xi)\,a\,S(\xi)\,. \tag{5.93}$$

Together with Eqs. (5.82) and (5.83), we can express the squeezing factor ξ in terms of δ and ϕ_β:

$$s = \operatorname{arccosh}\mu\,, \tag{5.94}$$

$$\theta = -\phi_\beta - \pi\,. \tag{5.95}$$

Recall that the ground state of the system satisfies $b|0\rangle_b = 0$, thus

$$S^{-1}(\xi)\,a\,S(\xi)|0\rangle_b = 0\,, \tag{5.96}$$

which leads to

$$a\,\{S(\xi)|0\rangle_b\} = 0\,. \tag{5.97}$$

In other words, $S(\xi)|0\rangle_b$ is the vacuum state for a:

$$S(\xi)|0\rangle_b = |0\rangle_a\,, \tag{5.98}$$

or $|0\rangle_b = S^{-1}(\xi)|0\rangle_a$. Namely, the ground state of the Hamiltonian H_A is

$$|\text{ground}\rangle_A = S^{-1}(\xi)|0\rangle_a = S(-\xi)|0\rangle_a\,, \tag{5.99}$$

where $|0\rangle_a$ is the vacuum state in the a-representation. In other words, the ground state of H_A is a squeezed vacuum state with a squeezing factor of $-\xi$. Intuitively, the dominant ϕ^2 term in the original H_1 and H_4 provides a confining harmonic oscillator potential (represented by the $a^\dagger a$ term in H_A), which produces the minimum fluctuations allowed by the uncertainty principle in the canonical conjugate coordinates. It is the (smaller) ϕ^4 term in the original H_1 and H_4 (which gives rise to the a^2 and $a^{\dagger 2}$ terms) that induces modulations on the fluctuations of the conjugate variables, therefore leading to the squeezing effect.

The excited states of the Hamiltonian H_A are number states in the b-representation:

$$|\text{excited}\rangle_A = |n\rangle_b = \frac{b^{\dagger n}}{\sqrt{n!}}|0\rangle_b\,. \tag{5.100}$$

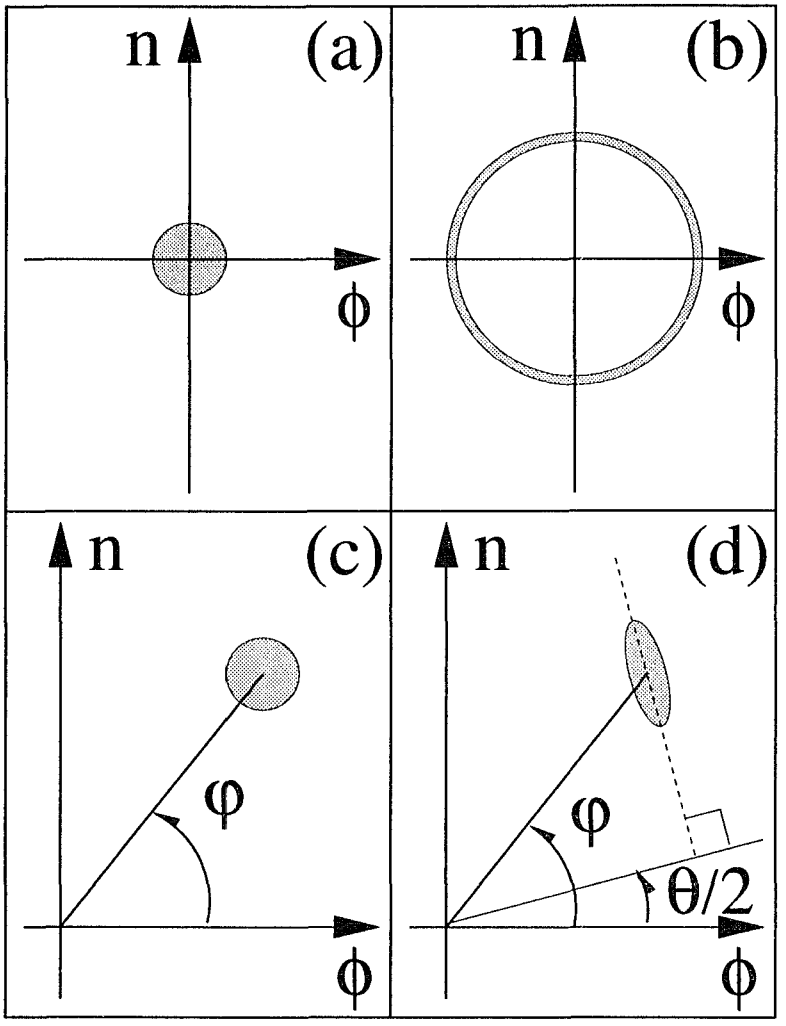

Figure 5.1: Schematic diagram of the uncertainty areas in the phase difference and charge number (ϕ, n) phase space of: (a) the vacuum state, (b) a "number" state, (c) a coherent state, and (d) a squeezed state. In these diagrams, the phases are measured in units of $(E_C/E_J)^{1/4}$, while the charge numbers in units of $(E_J/E_C)^{1/4}$. In addition, the "number" state here is not an eigenstate of the charge number operator n. It is actually an eigenstate of the harmonic part of the Hamiltonians. Notice that the coherent state has the same uncertainty area as the vacuum state, and that both areas are circular, while the squeezed state has an elliptical uncertainty area. Therefore, in the direction parallel to the $\theta/2$ line, the squeezed state has a smaller noise than both the vacuum and coherent states.

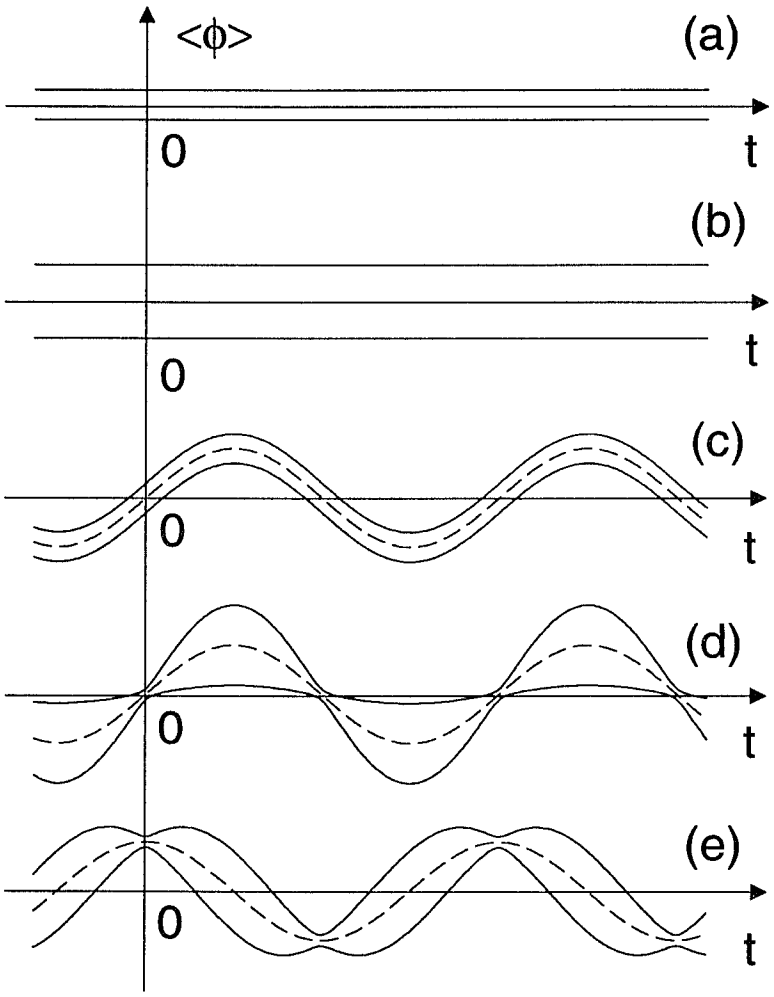

Figure 5.2: Schematic diagram of the time evolution of both the expectation value $\langle\phi\rangle(t)$ and the fluctuation $\langle(\Delta\phi)^2\rangle(t)$ of the phase operator ϕ for different states: vacuum (a), number (b), coherent (c), as well as squeezed (d) and (e). Here dashed lines represent $\langle\phi\rangle(t)$, while solid lines represent the envelopes $\langle\phi\rangle \pm \sqrt{\langle(\Delta\phi)^2\rangle}$, which provide the upper and lower bounds for the fluctuating quantity $\phi(t)$. (a) For the vacuum state $|0\rangle$, $\langle\phi\rangle(t) = 0$ and $\langle(\Delta\phi)^2\rangle(t) = 2\sqrt{E_C/E_J}$. (b) For a number state $|n\rangle$, $\langle\phi\rangle(t) = 0$ and $\langle(\Delta\phi)^2\rangle(t) = 2n+1$. (c) For a coherent state $|\alpha\rangle$, $\langle\phi\rangle(t) = 2Re(\alpha e^{-i\omega t}) = 2|\alpha|\cos\omega t$, which means that α is real, and $\langle(\Delta\phi)^2\rangle(t) = 2$. (d) For a squeezed state $|\alpha e^{-i\omega t}, \xi(t)\rangle$, where the squeezing factor $\xi(t)$ satisfies $\xi(t) = re^{-2i\omega t}$, $\langle\phi\rangle(t) = 2|\alpha|\cos\omega t$, which means that α is real, and its fluctuation is $\langle(\Delta\phi)^2\rangle(t) = 2(e^{-2r}\cos^2\omega t + e^{2r}\sin^2\omega t)$. (e) A squeezed state, as in (d). Now the expectation value of ϕ is $\langle\phi\rangle(t) = 2|\alpha|\sin\omega t$, which means that α is purely imaginary, and the fluctuation $\langle(\Delta\phi)^2\rangle$ has the same time-dependence as in (d). Notice that the squeezing effect now appears at the times when $\langle\phi\rangle(t)$ reaches its maxima while in (d) the squeezing effect is present at the times when $\langle\phi\rangle(t)$ is close to zero.

Since $b^\dagger$ is related to $a^\dagger$ by $b^\dagger = S^{-1}(\xi)a^\dagger S(\xi)$, the excited states of H_A can be simplified as

$$\begin{aligned} |\text{excited}\rangle_A &= \frac{1}{\sqrt{n!}}\left(S^{-1}(\xi)a^\dagger S(\xi)\right)^n S^{-1}(\xi)|0\rangle_a \\ &= \frac{1}{\sqrt{n!}} S^{-1}(\xi)\, a^{\dagger n}|0\rangle_a \\ &= S^{-1}(\xi)|n\rangle_a \\ &= S(-\xi)|n\rangle_a\,. \end{aligned} \tag{5.101}$$

In other words, the excited states of H_A are not the number states in the a-representation, $|n\rangle_a$, nor the number states $|n\rangle_n$ in the charge-number representation, where the Cooper-pair number is a good quantum number. Instead, $|\text{excited}\rangle_A$ is a "squeezed" version of the number states $|n\rangle_a$ (see Section 5.5.3 for more details).

For the isolated-junction Hamiltonian H_1, the parameters in H_A should be substituted by

$$\omega = \omega_1\left(1 - \frac{1}{8\lambda_1}\right), \tag{5.102}$$

$$\beta = -\frac{\hbar\omega_1}{16\lambda_1}, \tag{5.103}$$

$$\delta_1 = \frac{|\beta|}{\hbar\omega_1} = \frac{1}{16\lambda_1 - 2}. \tag{5.104}$$

In the large-ratio limit, $\lambda_1 = \sqrt{E_J/E_C} \gg 1$, between the Josephson coupling energy and the charging energy, the quantity $\delta_1 \cong 1/16\lambda_1 \ll 1$ is very small. Therefore,

$$|\mu|^2 \cong 1 + \delta_1^2 \cong 1 + \left(\frac{1}{16\lambda_1}\right)^2, \tag{5.105}$$

$$|\nu|^2 \cong \delta_1^2 \cong \left(\frac{1}{16\lambda_1}\right)^2. \tag{5.106}$$

Notice that the phase of β is π, so that we can set $\phi_\mu = 0$ and $\phi_\nu = \pi$. Furthermore, the squeezing factor is

$$\begin{aligned} \xi_1 &= s_1 \cong \delta_1 \\ &= \frac{1}{16\lambda_1} = \frac{1}{16}\sqrt{\frac{E_C}{E_J}}, \end{aligned} \tag{5.107}$$

with the phase angle of ξ_1 satisfying $\theta_1 = 0$.

For H_4, which is the Hamiltonian of a Josephson junction at the global potential minimum in a superconducting loop without external flux, the parameters are

$$\omega = \omega_4\left(1 - \frac{E_J}{8\lambda_4 E_{J4}}\right), \tag{5.108}$$

$$\beta = -\frac{\hbar\omega_4 E_J}{16\lambda_4 E_{J4}}. \tag{5.109}$$

Thus, now we have

$$\delta_4 \cong \frac{E_J E_C^{1/2}}{16 E_{J4}^{3/2}} = \frac{1}{16}\sqrt{\frac{E_J^2 E_C}{E_{J4}^3}}\,, \tag{5.110}$$

and the squeezing factor becomes

$$\xi_4 = \delta_4 \cong \frac{1}{16}\sqrt{\frac{E_J^2 E_C}{E_{J4}^3}}\,, \tag{5.111}$$

with the phase angle of ξ_4 satisfying $\theta_4 = 0$.

5.4.2 Ground and Excited States of the Hamiltonians H_2 and H_3

Recall that the Hamiltonian H_2 describes a current-biased Josephson junction and H_3 a Josephson junction in a superconducting ring with external flux. Both H_2 and H_3 have the similar form H_B:

$$H_B = \hbar\omega a^\dagger a + \alpha a + \alpha^* a^\dagger + \beta a^2 + \beta^* a^{\dagger 2}\,. \tag{5.112}$$

Systems represented by H_2 are diagonalizable, as in the the case of H_A. Again, we can introduce a pair of operators b and $b^\dagger$:

$$b = \mu a + \nu a^\dagger\,, \tag{5.113}$$

$$b^\dagger = \mu^* a^\dagger + \nu^* a\,. \tag{5.114}$$

Namely, $b = S^{-1}(-\xi)\, a\, S(-\xi)$, where $S(-\xi) = \exp(-\xi^* a^2/2 + \xi a^\dagger/2)$ is a squeezing operator and $-\xi = s e^{i(\theta+\pi)}$ is the squeezing factor; ξ is related to μ and ν by $\mu = \cosh s$ and $\nu = -e^{i\theta}\sinh s$. If we define

$$\delta = \frac{|\beta|}{\hbar\omega}\,, \tag{5.115}$$

μ and ν then satisfy

$$|\mu|^2 \cong 1 + \delta^2\,, \tag{5.116}$$

$$|\nu|^2 \cong \delta^2\,, \tag{5.117}$$

$$\phi_\mu - \phi_\nu = \phi_\beta\,. \tag{5.118}$$

The Hamiltonian can thus be simplified to

$$\begin{aligned} H_B &= \frac{\hbar\omega}{|\mu|^2+|\nu|^2} b^\dagger b - \frac{\hbar\omega|\nu|^2}{|\mu|^2+|\nu|^2} + (\alpha\mu^* - \alpha^*\nu^*)b + (\alpha^*\mu - \alpha\nu)b^\dagger \\ &\cong \hbar\omega(1-2\delta^2)b^\dagger b - \hbar\omega\delta^2 + \gamma b + \gamma^* b^\dagger\,, \end{aligned} \tag{5.119}$$

where

$$\gamma = \alpha\mu^* - \alpha^*\nu^*\,. \tag{5.120}$$

Now we introduce the operator c which diagonalizes H_B

$$c = b + \frac{\gamma^*}{\hbar\omega}(1 + 2\delta^2)\,, \tag{5.121}$$

so that

$$c^\dagger c = b^\dagger b + \frac{\gamma}{\hbar\omega}(1 + 2\delta^2)b + \frac{\gamma^*}{\hbar\omega}(1 + 2\delta^2)b^\dagger + \left\{\frac{|\gamma|}{\hbar\omega}(1 + 2\delta^2)\right\}^2\,, \tag{5.122}$$

and

$$H_B = \hbar\omega(1 - 2\delta^2)c^\dagger c - \hbar\omega\delta^2 - \frac{|\gamma|^2}{\hbar\omega}(1 + 2\delta^2)\,. \tag{5.123}$$

The ground state of this Hamiltonian satisfies

$$c|0\rangle_c = 0\,. \tag{5.124}$$

If we define a displacement operator D as

$$D_b(\eta) = \exp\left(\eta b^\dagger - \eta^* b\right)\,, \tag{5.125}$$

which "displaces" b by η

$$D_b^{-1}(\eta)\, b\, D_b(\eta) = b + \eta\,, \tag{5.126}$$

we can express the operator c as

$$\begin{aligned} c &= D_b^{-1}\left(\frac{\gamma^*}{\hbar\omega'}\right) b\, D_b\left(\frac{\gamma^*}{\hbar\omega'}\right) \\ &= D_b^{-1}\left(\frac{\gamma^*}{\hbar\omega'}\right) S_a^{-1}(-\xi)\, a\, S_a(-\xi)\, D_b\left(\frac{\gamma^*}{\hbar\omega'}\right)\,, \end{aligned} \tag{5.127}$$

where

$$\omega' = \omega(1 - 2\delta^2)\,. \tag{5.128}$$

Thus

$$D_b^{-1}(\gamma^*/\hbar\omega')\, b\, D_b(\gamma^*/\hbar\omega')\, |0\rangle_c = 0\,, \tag{5.129}$$

or

$$b\,\{D_b(\gamma^*/\hbar\omega')\, |0\rangle_c\} = 0\,. \tag{5.130}$$

Therefore,

$$D_b(\gamma^*/\hbar\omega')\, |0\rangle_c = |0\rangle_b\,. \tag{5.131}$$

In other words,

$$|0\rangle_c = D_b^{-1}\left(\frac{\gamma^*}{\hbar\omega'}\right)|0\rangle_b\,. \tag{5.132}$$

According to the discussion in the previous section

$$|0\rangle_b = S_a^{-1}(\xi)|0\rangle_a \,. \tag{5.133}$$

Therefore, the ground state of H_B can be expressed as

$$|\text{ground}\rangle_B = |0\rangle_c = D_b^{-1}\left(\frac{\gamma^*}{\hbar\omega'}\right) S_a^{-1}(\xi)|0\rangle_a \,. \tag{5.134}$$

Recall that $D^{-1}(\eta) = D(-\eta)$ and $S^{-1}(\xi) = S(-\xi)$. Thus the ground state of H_B is

$$\begin{aligned} |0\rangle_c &= D_b\left(-\frac{\gamma^*}{\hbar\omega'}\right) S_a(-\xi)|0\rangle_a \\ &= D_a\left(-\frac{1+2\delta^2}{\hbar\omega}\left[\alpha^*(|\mu|^2+|\nu|^2) - 2\alpha\mu^*\nu\right]\right) S_a(-\xi)|0\rangle_a \\ &\cong D_a\left(-\frac{\alpha^* - 2\alpha\delta e^{i(\phi_\nu - \phi_\mu)}}{\hbar\omega}\right) S_a(-\xi)|0\rangle_a \,, \end{aligned} \tag{5.135}$$

which is a squeezed coherent state in the "a" representation, with $\xi = \delta$.

The excited eigenstates of H_B can be obtained in a similar manner as for H_A. They are the number states in the c-representation

$$|\text{excited}\rangle_B = |n\rangle_c \tag{5.136}$$

$$\begin{aligned} &= \frac{\left(c^\dagger\right)^n}{\sqrt{n!}}|0\rangle_c \\ &= \frac{1}{\sqrt{n!}}\left[D_b^{-1}\left(\frac{\gamma^*}{\hbar\omega'}\right) S_a^{-1}(\xi) a^\dagger S_a(\xi) D_b\left(\frac{\gamma^*}{\hbar\omega'}\right)\right]^n D_b^{-1}\left(\frac{\gamma^*}{\hbar\omega'}\right) S_a^{-1}(\xi)|0\rangle_a \\ &= D_b^{-1}\left(\frac{\gamma^*}{\hbar\omega'}\right) S_a^{-1}(\xi)\frac{a^{\dagger\, n}}{\sqrt{n!}}|0\rangle_a \\ &= D_b^{-1}\left(\frac{\gamma^*}{\hbar\omega'}\right) S_a^{-1}(\xi)|n\rangle_a \\ &= D_b\left(-\frac{\gamma^*}{\hbar\omega'}\right) S_a(-\xi)|n\rangle_a \,. \end{aligned} \tag{5.137}$$

Therefore, the excited states of H_B are displaced and squeezed number states in the a-representation.

In the case of H_2, which describes a current-biased Josephson junction, the parameters are

$$\omega = \omega_2\left(1 - \frac{1}{8\lambda_2}\right) , \tag{5.138}$$

$$\alpha = \frac{I\Phi_0}{8\sqrt{2}\pi\lambda_2^{3/2}} , \tag{5.139}$$

$$\beta = -\frac{\hbar\omega_2}{16\lambda_2} . \tag{5.140}$$

Consequently, $\alpha^* = \alpha$, $\phi_\beta = \pi$, and $\phi_\nu = \pi$. If we define $\delta_2 = |\beta|/\hbar\omega = 1/(16\lambda_2 - 2) \cong 1/16\lambda_2$, which is a very small quantity, the squeezing factor ξ_2 has the form

$$\xi_2 = \delta_2 = \frac{1}{16\lambda_2}, \tag{5.141}$$

and the displacement d is

$$\begin{aligned} d_2 &= -\frac{\alpha^* - 2\alpha\delta e^{i(\phi_\nu - \phi_\mu)}}{\hbar\omega} \\ &= -\frac{\alpha_2}{\hbar\omega_2}(1 + 4\delta_2). \end{aligned} \tag{5.142}$$

In the case of H_3, which describes a Josephson junction in a superconducting ring with an external flux, the parameters are

$$\omega = \omega_3 \left(1 - \frac{E_J}{8\lambda_3 E_{J3}} \cos\phi_{m3}\right), \tag{5.143}$$

$$\alpha = -\frac{\hbar\omega_3 E_J}{4\sqrt{2\lambda_3} E_{J3}} \sin\phi_{m3}, \tag{5.144}$$

$$\beta = -\frac{\hbar\omega_3 E_J}{16\lambda_3 E_{J3}} \cos\phi_{m3}, \tag{5.145}$$

$$\delta_3 = \frac{|\beta|}{\hbar\omega_3} \cong \frac{E_J \cos\phi_{m3}}{16\lambda_3 E_{J3}}. \tag{5.146}$$

Here δ_3 is again a very small quantity. The squeezing factor is now

$$\xi_3 = \delta_3 = \frac{E_J \cos\phi_{m3}}{16\lambda_3 E_{J3}}, \tag{5.147}$$

and the displacement d now becomes

$$\begin{aligned} d_3 &= -\frac{\alpha^* - 2\alpha\delta e^{i(\phi_\nu - \phi_\mu)}}{\hbar\omega} \\ &= \frac{E_J \sin\phi_{m3}}{4\sqrt{2\lambda_3} E_{J3}}(1 + 4\delta_3) = d_3. \end{aligned} \tag{5.148}$$

5.5 Expectation Values and Fluctuations of the Number and Phase Operators

In the previous section we have obtained approximate ground state wavefunctions by neglecting the higher-order terms in the JJ interaction. Now we compute the quantum fluctuations for the phase and charge number in these approximate ground and excited states.

5.5.1 Squeezed Vacuum State

Let us first consider H_1 and H_4, for which the ground state can be written in the form $|\text{ground}\rangle = S(-\xi)|0\rangle$, which is a squeezed vacuum state. Recall that

$$S^{-1}(\xi)\, a\, S(\xi) = a\cosh s - a^\dagger e^{i\theta}\sinh s\,, \tag{5.149}$$

$$S^{-1}(-\xi)\, a\, S(-\xi) = a\cosh s + a^\dagger e^{i\theta}\sinh s\,, \tag{5.150}$$

where $\xi = se^{i\theta}$. In a squeezed vacuum state $|0,-\xi\rangle = S(-\xi)|0\rangle$, we can calculate the fluctuation

$$\begin{aligned}\langle[\Delta(a+a^\dagger)]^2\rangle &= \langle(a+a^\dagger)^2\rangle - \langle(a+a^\dagger)\rangle^2 &(5.151)\\ &= \langle 0|S^{-1}(-\xi)(a^{\dagger 2}+a^2+2a^\dagger a+1)S(-\xi)|0\rangle\\ &= e^{i\theta}\sinh s\cosh s + e^{-i\theta}\sinh s\cosh s + 1 + 2\sinh^2 s\\ &= e^{-2s}\sin^2\frac{\theta}{2} + e^{2s}\cos^2\frac{\theta}{2}\,. &(5.152)\end{aligned}$$

On the other hand,

$$\begin{aligned}\langle[\Delta(a-a^\dagger)]^2\rangle &= \langle(a-a^\dagger)^2\rangle - \langle(a-a^\dagger)\rangle^2 &(5.153)\\ &= \langle 0|S^{-1}(\xi)(a^{\dagger 2}+a^2-2a^\dagger a-1)S(\xi)|0\rangle\\ &= e^{i\theta}\sinh s\cosh s + e^{-i\theta}\sinh s\cosh s - 1 - 2\sinh^2 s\\ &= -e^{-2s}\cos^2\frac{\theta}{2} - e^{2s}\sin^2\frac{\theta}{2}\,. &(5.154)\end{aligned}$$

For an isolated single junction, the phase and number operators are related to a and $a^\dagger$ by

$$\phi = \frac{1}{\sqrt{2}}\left(\frac{E_C}{E_J}\right)^{1/4}(a+a^\dagger) = \frac{1}{\sqrt{2\lambda}}(a+a^\dagger)\,, \tag{5.155}$$

$$n = \frac{1}{i\sqrt{2}}\left(\frac{E_J}{E_C}\right)^{1/4}(a-a^\dagger) = -i\sqrt{\frac{\lambda}{2}}(a-a^\dagger)\,. \tag{5.156}$$

Therefore, the ground state fluctuations for an isolated single junction are

$$\begin{aligned}\langle(\Delta\phi_{\text{local}})^2\rangle &= \frac{1}{2\lambda_1}\langle[\Delta(a+a^\dagger)]^2\rangle\\ &= \frac{1}{2\lambda_1}\left(e^{-2s_1}\cos^2\frac{\theta_1}{2} + e^{2s_1}\sin^2\frac{\theta_1}{2}\right)\\ &= \sqrt{\frac{E_C}{4E_J}}\,e^{2s_1}\,, &(5.157)\\ \langle(\Delta n)^2\rangle &= -\frac{\lambda_1}{2}\langle[\Delta(a-a^\dagger)]^2\rangle\end{aligned}$$

$$= \frac{\lambda_1}{2}\left(e^{-2s_1}\sin^2\frac{\theta_1}{2} + e^{2s_1}\cos^2\frac{\theta_1}{2}\right)$$
$$= \sqrt{\frac{E_J}{4E_C}}\, e^{-2s_1}\,, \tag{5.158}$$

where

$$\lambda_1 = \sqrt{\frac{E_J}{E_C}}\,, \tag{5.159}$$
$$\theta_1 = 0\,, \tag{5.160}$$
$$s_1 = \frac{1}{16\lambda_1}\,. \tag{5.161}$$

For a Josephson junction in a superconducting ring, with no external flux and at the global potential minimum, the local phase and number operators are

$$\begin{aligned}\phi_{\rm local} &= (E_C/4E_{J4})^{1/4}(a+a^\dagger)\\ n &= -i\,(E_{J4}/4E_C)^{1/4}(a-a^\dagger)\,.\end{aligned} \tag{5.162}$$

The Hamiltonian of this system is H_4, which has the same ground state as H_1 for the isolated single junction case. Thus the ground state fluctuations are

$$\begin{aligned}\langle(\Delta\phi_{\rm local})^2\rangle &= \frac{1}{2\lambda_4}\langle[\Delta(a+a^\dagger)]^2\rangle\\ &= \sqrt{\frac{E_C}{4E_{J4}}}\left(e^{-2s_4}\cos^2\frac{\theta_4}{2} + e^{2s_4}\sin^2\frac{\theta_4}{2}\right)\\ &= \sqrt{\frac{E_C}{4E_{J4}}}\, e^{2s_4}\,, \qquad (5.163)\\ \langle(\Delta n)^2\rangle &= -\frac{\lambda_4}{2}\langle[\Delta(a-a^\dagger)]^2\rangle\\ &= \sqrt{\frac{E_{J2}}{4E_C}}\left(e^{-2s_4}\sin^2\frac{\theta_4}{2} + e^{2s_4}\cos^2\frac{\theta_4}{2}\right)\\ &= \sqrt{\frac{E_{J4}}{4E_C}}\, e^{-2s_4}\,, \qquad (5.164)\end{aligned}$$

where

$$E_{J4} = E_J + \frac{\Phi_0^2}{4\pi^2 L}\,, \tag{5.165}$$
$$\theta_4 = 0\,, \tag{5.166}$$
$$s_4 = \frac{1}{16}\sqrt{\frac{E_J^2 E_C}{E_{J4}^3}}\,. \tag{5.167}$$

Figure 5.3(a) schematically illustrates the uncertainty area of a squeezed vacuum state. Both the average values of charge number n and phase difference ϕ vanish. The uncertainty

area in the n-ϕ phase space is squeezed along the n-direction, which indicates smaller fluctuations for the charge number n compared to the zeroth-order approximation where the $\cos\phi$ term is expanded to the second-order in ϕ.

5.5.2 Squeezed Coherent State

In the case of the current-biased junction, the ground state takes the form of $|\text{ground}\rangle_B$

$$|\text{ground}\rangle_2 = D_a\left(-\frac{\alpha_2(1+2\delta_2)}{\hbar\omega_2}\right) S_a(-\xi_2)|0\rangle_a\,, \tag{5.168}$$

which is a squeezed coherent state. We can calculate the expectations and fluctuations:

$$\langle(a_2+a_2^\dagger)\rangle = -\frac{2\alpha_2(1+2\delta_2)}{\hbar\omega_2}\,, \tag{5.169}$$

$$\langle[\Delta(a_2+a_2^\dagger)]^2\rangle = e^{-2s_2}\sin^2\frac{\theta_2}{2} + e^{2s_2}\cos^2\frac{\theta_2}{2}\,, \tag{5.170}$$

$$\langle(a_2-a_2^\dagger)\rangle = 0\,, \tag{5.171}$$

$$\langle[\Delta(a_2-a_2^\dagger)]^2\rangle = -e^{-2s_2}\cos^2\frac{\theta_2}{2} - e^{2s_2}\sin^2\frac{\theta_2}{2}\,. \tag{5.172}$$

Here $-\xi_2 = s_2 e^{i(\theta_2+\pi)}$ is the squeezing factor.

The local phase and number operators now have the following properties

$$\begin{aligned}\langle\phi_{\text{local}}\rangle &= \frac{1}{\sqrt{2}}\left(\frac{E_C}{E_{J2}}\right)^{1/4}\langle(a+a^\dagger)\rangle \\ &= -\left(\frac{4E_C}{E_{J2}}\right)^{1/4}\frac{\alpha_2}{\hbar\omega_2}(1+2\delta_2)\,, \end{aligned}\tag{5.173}$$

$$\begin{aligned}\langle(\Delta\phi_{\text{local}})^2\rangle &= \frac{1}{2\lambda_2}\langle[\Delta(a+a^\dagger)]^2\rangle \\ &= \sqrt{\frac{E_C}{4E_{J2}}}\left(e^{-2s_2}\sin^2\frac{\theta_2}{2} + e^{2s_2}\cos^2\frac{\theta_2}{2}\right) \\ &= \sqrt{\frac{E_C}{4E_J\sqrt{1-(I\Phi_0/2\pi E_J)^2}}}\,e^{2s_2}\,, \end{aligned}\tag{5.174}$$

$$\begin{aligned}\langle n\rangle &= \frac{1}{i\sqrt{2}}\left(\frac{E_{J2}}{E_C}\right)^{1/4}\langle(a-a^\dagger)\rangle \\ &= -\frac{1}{i\sqrt{2}}\left(\frac{E_{J2}}{E_C}\right)^{1/4}\frac{\alpha_2-\alpha_2^*}{\hbar\omega_2'} = 0\,, \end{aligned}\tag{5.175}$$

$$\begin{aligned}\langle(\Delta n)^2\rangle &= -\frac{\lambda_2}{2}\langle[\Delta(a-a^\dagger)]^2\rangle \\ &= \sqrt{\frac{E_{J2}}{4E_C}}\left(e^{-2s_2}\cos^2\frac{\theta_2}{2} + e^{2s_2}\sin^2\frac{\theta_2}{2}\right) \\ &= \sqrt{\frac{E_J\sqrt{1-(I\Phi_0/2\pi E_J)^2}}{4E_C}}\,e^{-2s_2}\,, \end{aligned}\tag{5.176}$$

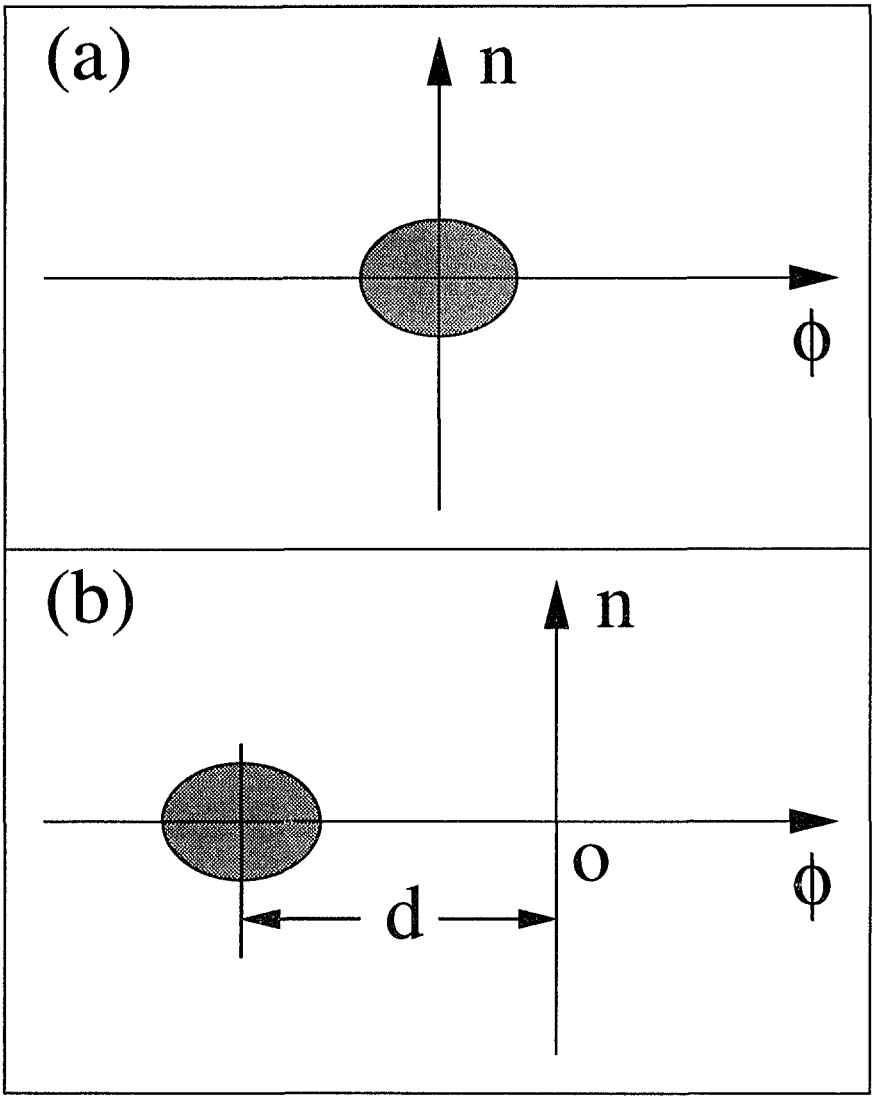

Figure 5.3: Schematic diagram of the uncertainty area in the phase difference and charge number (ϕ, n) phase space of (a) the ground states of H_1 and H_4 (which are squeezed vacuum states), and (b) the ground state of H_2 and H_3 (which are squeezed coherent states). The units for ϕ and n are $(E_C/E_J)^{1/4}$ and $(E_J/E_C)^{1/4}$, respectively. It can be seen from the diagram (a) that the uncertainty of the charge number n is squeezed by a factor of $1/16\lambda$, where $\lambda = \sqrt{E_J/E_C}$. In (b) the uncertainty area has been displaced away from the origin by an amount d, because linear driving terms are present in both H_2 and H_3. Again, the uncertainty of the charge number n is squeezed by a factor $s = 1/16\lambda$, with $\lambda = \sqrt{E_J/E_C}$. The displacement d from the origin is $-\sqrt{2}\alpha(1 + 2\delta)/\hbar\omega$, where α is the coefficient of the linear driving term, and δ reflects the relative strength of the nonlinear correction terms.

where

$$E_{J2} = E_J\sqrt{1-\left(\frac{I\Phi_0}{2\pi E_J}\right)^2}, \tag{5.177}$$

$$\hbar\omega_2 = \sqrt{E_{J2}E_C}, \tag{5.178}$$

$$\lambda_2 = \sqrt{\frac{E_{J2}}{E_C}}, \tag{5.179}$$

$$\alpha_2 = \frac{I\Phi_0}{8\sqrt{2}\pi\lambda_2^{3/2}}, \tag{5.180}$$

$$\theta_2 = 0, \tag{5.181}$$

$$s_2 = \frac{1}{16\lambda_2}. \tag{5.182}$$

In the case of Josephson junction in a superconducting ring with external flux, the ground state is similar to that of the current-biased junction. The parameters are different, so that the expectation values and fluctuations of the local phase and number operators become

$$\begin{aligned}\langle\phi_{\rm local}\rangle &= \frac{1}{\sqrt{2}}\left(\frac{E_C}{E_{J3}}\right)^{1/4}\langle a_3+a_3^\dagger\rangle \\ &= -\left(\frac{4E_C}{E_{J3}}\right)^{1/4}\frac{\alpha_3}{\hbar\omega_3}(1+2\delta_3),\end{aligned} \tag{5.183}$$

$$\begin{aligned}\langle(\Delta\phi_{\rm local})^2\rangle &= \frac{1}{2}\sqrt{\frac{E_C}{E_{J3}}}\langle[\Delta(a_3+a_3^\dagger)]^2\rangle \\ &= \frac{1}{2}\sqrt{\frac{E_C}{E_{J3}}}\left(e^{-2s_3}\sin^2\frac{\theta_3}{2}+e^{2s_3}\cos^2\frac{\theta_3}{2}\right) \\ &= \frac{1}{2}\sqrt{\frac{E_C}{E_{J3}}}\,e^{2s_3},\end{aligned} \tag{5.184}$$

$$\begin{aligned}\langle n\rangle &= \frac{1}{i\sqrt{2}}\left(\frac{E_{J3}}{E_C}\right)^{1/4}\langle a_3-a_3^\dagger\rangle \\ &= -\frac{1}{i\sqrt{2}}\left(\frac{E_{J3}}{E_C}\right)^{1/4}\frac{(1+2\delta_3)(\alpha_3^*-\alpha_3)}{\hbar\omega_3} \\ &= 0,\end{aligned} \tag{5.185}$$

$$\begin{aligned}\langle(\Delta n)^2\rangle &= -\frac{1}{2}\sqrt{\frac{E_{J3}}{E_C}}\langle[\Delta(a_3-a_3^\dagger)]^2\rangle \\ &= \frac{1}{2}\sqrt{\frac{E_{J3}}{E_C}}\left(e^{-2s_3}\cos^2\frac{\theta_3}{2}+e^{2s_3}\sin^2\frac{\theta_3}{2}\right) \\ &= \frac{1}{2}\sqrt{\frac{E_{J3}}{E_C}}\,e^{2s_3},\end{aligned} \tag{5.186}$$

where L is the inductance of the superconducting ring, ϕ_{m3} is the phase of the local mini-

mum, and

$$E_{J3} = E_J \cos\phi_{m3} + \frac{\Phi_0^2}{4\pi^2 L}, \tag{5.187}$$

$$\hbar\omega_3 = \sqrt{E_{J3}E_C}, \tag{5.188}$$

$$\lambda_3 = \sqrt{\frac{E_{J3}}{E_C}}, \tag{5.189}$$

$$\alpha_3 = \frac{E_J E_C \sin\phi_{m3}}{4\sqrt{2}E_{J3}}, \tag{5.190}$$

$$s_3 \cong \frac{E_J \cos\phi_{m3}}{16\lambda_3 E_{J3}}, \tag{5.191}$$

$$\theta_3 = 0. \tag{5.192}$$

Figure 5.3(b) schematically illustrates the uncertainty area of a squeezed coherent state. The finite $\langle\phi\rangle$ in this state represents the asymmetry in the potential energy. The uncertainty area has the same shape and orientation as that of the squeezed vacuum state considered in the last section, because these two cases share the same nonlinear potential of $\cos\phi$.

5.5.3 The Excited States

Recall that the excited states for H_A are

$$|n,\xi\rangle = S(-\xi)|n\rangle_a . \tag{5.193}$$

It can be shown that

$$S^{-1}(-\xi)aS(\xi) = a\cosh s + a^\dagger e^{i\theta}\sinh s, \tag{5.194}$$

$$S^{-1}(-\xi)a^\dagger S(\xi) = a^\dagger\cosh s + ae^{-i\theta}\sinh s, \tag{5.195}$$

where $\xi = se^{i\theta}$. Therefore, the matrix elements can be calculated as

$$\langle(a+a^\dagger)\rangle = 0, \tag{5.196}$$

$$\begin{aligned}\langle(a+a^\dagger)^2\rangle &= \langle n,\xi|(a+a^\dagger)^2|n,\xi\rangle \\ &= \langle n|S^{-1}(-\xi)(a+a^\dagger)^2S(\xi)|n\rangle \\ &= \langle n|\left\{a\left(\cosh s + e^{-i\theta}\sinh s\right) + a^\dagger\left(\cosh s + e^{i\theta}\sinh s\right)\right\}^2|n\rangle \\ &= \left(\cosh s + e^{-i\theta}\sinh s\right)\left(\cosh s + e^{i\theta}\sinh s\right)\langle n|(aa^\dagger + a^\dagger a)|n\rangle \\ &= (2n+1)\left(e^{-2s}\sin^2\frac{\theta}{2} + e^{2s}\cos^2\frac{\theta}{2}\right), \end{aligned} \tag{5.197}$$

$$\begin{aligned}\langle(a-a^\dagger)^2\rangle &= \langle n,\xi|\,(a-a^\dagger)^2\,|n,\xi\rangle \\ &= -(2n+1)\left(e^{-2s}\cos^2\frac{\theta}{2} + e^{2s}\sin^2\frac{\theta}{2}\right). \end{aligned} \tag{5.198}$$

We can then compute the fluctuations of the charge-number and phase operators:

$$\begin{aligned}\langle(\Delta\phi)^2\rangle &= \frac{\lambda}{2}\langle(a+a^\dagger)^2\rangle \\ &= \frac{\lambda}{2}(2n+1)\left(e^{-2s}\sin^2\frac{\theta}{2}+e^{2s}\cos^2\frac{\theta}{2}\right), \qquad (5.199)\\ \langle(\Delta n)^2\rangle &= -\frac{\lambda}{2}\langle(a-a^\dagger)^2\rangle \\ &= \frac{\lambda}{2}(2n+1)\left(e^{-2s}\cos^2\frac{\theta}{2}+e^{2s}\sin^2\frac{\theta}{2}\right). \qquad (5.200)\end{aligned}$$

On the other hand, in a pure number state (again, not the charge-number eigenstates) in the a-representation, the fluctuations of the number and phase are

$$\begin{aligned}\langle(\Delta\phi)^2\rangle &= \frac{\lambda}{2}\langle n|(a+a^\dagger)^2|n\rangle \\ &= \frac{\lambda}{2}(2n+1), \qquad (5.201)\\ \langle(\Delta n)^2\rangle &= -\frac{\lambda}{2}\langle n|(a-a^\dagger)^2|n\rangle \\ &= \frac{\lambda}{2}(2n+1). \qquad (5.202)\end{aligned}$$

Therefore, in the excited states of H_A, the fluctuations in the charge number and phase are modulated because of the correction in the harmonic oscillator potential. Whether the noises will be larger or smaller depends on the phase angle θ of the squeezing operator ξ.

In the excited states of H_B, the expectation values such as $\langle(a+a^\dagger)\rangle$ do not vanish because the states are displaced. For example,

$$\begin{aligned}{}_c\langle n|\left(a+a^\dagger\right)|n\rangle_c &= {}_a\langle n|S_a^{-1}(-\xi)D_a^{-1}(-\zeta)\left(a+a^\dagger\right)D_a(-\zeta)S(-\xi)|n\rangle_a \\ &= {}_a\langle n|S_a^{-1}(-\xi)\left(a+a^\dagger-\zeta-\zeta^*\right)S(-\xi)|n\rangle_a \\ &= -(\zeta+\zeta^*). \qquad (5.203)\end{aligned}$$

On the other hand, the fluctuations of $a+a^\dagger$ in the excited states of H_B take the same form as that in the excited states of H_A:

$$\begin{aligned}{}_c\langle n|\left(a+a^\dagger\right)^2|n\rangle_c &= {}_a\langle n|S_a^{-1}(-\xi)D_a^{-1}(-\zeta)\left(a+a^\dagger\right)^2D_a(-\zeta)S(-\xi)|n\rangle_a \\ &= {}_a\langle n|S_a^{-1}(-\xi)\left(a+a^\dagger-\zeta-\zeta^*\right)^2S_a(-\xi)|n\rangle_a \\ &= {}_a\langle n|S_a^{-1}(-\xi)\left(a+a^\dagger\right)^2S_a(-\xi)|n\rangle_a+(\zeta+\zeta^*)^2, \qquad (5.204)\end{aligned}$$

so that

$$\begin{aligned}{}_c\langle n|\left[\Delta\left(a+a^\dagger\right)\right]^2|n\rangle_c &= {}_a\langle n|S_a^{-1}(-\xi)\left(a+a^\dagger\right)^2S_a(-\xi)|n\rangle_a \\ &= (2n+1)\left(e^{-2s}\sin^2\frac{\theta}{2}+e^{2s}\cos^2\frac{\theta}{2}\right), \qquad (5.205)\end{aligned}$$

where $-\xi = se^{i(\theta+\pi)}$ is the squeezing factor. It is thus evident that the displacement operation in the excited states of H_B is irrelevant to the fluctuation properties.

5.6 Time Evolution Operators of the Various Hamiltonians

In the previous sections we have obtained the eigenstates of a Josephson junction in various configurations. With the help of these eigenstates we can expand any initial state in terms of these eigenstates and study its time-evolution. However, this approach can be quite complicated for an arbitrary initial state. An easier way is to first find the time-evolution operator $U(t,t_0)$ of the particular Hamiltonian, and then calculate the transformation $U^\dagger(t,t_0)f(a,a^\dagger)U(t,t_0)$.

5.6.1 Time Evolution Operator of H_A

The Hamiltonian H_A encompasses both H_1 (for an isolated Josephson junction) and H_4 (for a Josephson junction in a superconducting ring without external flux and at the global potential minimum):

$$\begin{aligned} H_A &= \hbar\omega a^\dagger a + \beta a^2 + \beta^* a^{\dagger 2} \\ &= H_0 + V_A\,, \end{aligned} \tag{5.206}$$

where

$$H_0 = \hbar\omega a^\dagger a\,, \tag{5.207}$$

$$V_A = \beta a^2 + \beta^* a^{\dagger 2}\,. \tag{5.208}$$

To obtain a factorized time-evolution operator, so that each term has a special meaning (such as the displacement and squeezing operators), the general practice is to first change to the interaction picture to eliminate the free oscillator term in the Hamiltonian, and then solve the Schrödinger equation for $U_I(t,t_0)$ in the interaction picture. The free-oscillator time-evolution operator $U_0(t)$ is

$$U_0(t) = e^{-iH_0 t/\hbar} = e^{-i\omega t a^\dagger a}\,. \tag{5.209}$$

In the interaction picture, the Schrödinger equation becomes

$$i\hbar\frac{\partial}{\partial t}U_I(t) = V_I(t)\,U_I(t), \tag{5.210}$$

$$|\psi(t)\rangle_I = U_I(t)\,|\psi(0)\rangle_I, \tag{5.211}$$

$$|\psi(t)\rangle_S = U_0(t)\,|\psi(0)\rangle_I, \tag{5.212}$$

$$\begin{aligned} V_I(t) &= U_0^{-1}(t)\,V_A\,U_0(0) \\ &= e^{i\omega t a^\dagger a}\,\beta\,a^2\,e^{-i\omega t a^\dagger a} + h.c., \end{aligned} \tag{5.213}$$

where $U_I(t)$ is the time-evolution operator in the interaction picture, and the subscript S refers to the Schrödinger picture. Recall that for a single mode

$$\begin{aligned} ae^{\beta a^\dagger a} &= a\sum_{n=0}^{\infty}\frac{\beta^n}{n!}(a^\dagger a)^n = \sum_{n=0}^{\infty}\frac{\beta^n}{n!}(a^\dagger a+1)^n a \\ &= e^{\beta(a^\dagger a+1)}a = e^{\beta a^\dagger a}ae^{\beta}, \end{aligned} \tag{5.214}$$

V_I can thus be simplified to

$$V_I(t) = \beta a^2 e^{-2i\omega t} + \beta^* a^{\dagger 2} e^{2i\omega t}. \tag{5.215}$$

Formally, the time-evolution operator can be written as

$$U_I(t) = T\exp\left\{-\frac{i}{\hbar}\int_{t_0}^{t} V_I(\tau)d\tau\right\}, \tag{5.216}$$

where T is the time-ordering operator. This expression cannot be easily simplified because $V_I(t)$ is time-dependent; thus, in general, $V_I(t)$'s at different times do not commute with each other. One way to circumvent this problem is to divide the time interval $[t_0, t]$ into a large amount of small intervals, so that in each of the intervals $V_I(t)$ is approximately a constant. Thus the Schrödinger equation can be integrated in each of the intervals and the time-evolution operator during that period can be obtained by direct integration. Since the time-evolution operator $U(t_0, t)$ satisfies $U(t_0, t) = U(t_0, t_1)\,U(t_1, t)$, we can therefore obtain $U_I(t_0, t) = U_I(t_0, t_1)\,U_I(t_1, t_2)\cdots U_I(t_n, t)$. Such an approach may be useful when a numerical computation is the sole purpose; although the efficiency of such an algorithm might not be very high. Analytically, this approach does not simplify the problem.

To obtain an analytical expression for any function of the creation and annihilation operators, we can first transform into the b-representation, in which H_A is diagonalized: $H_A = \hbar\omega_b\,b^\dagger b$. Here we have dropped a constant. Thus the time-evolution operator of the system in the b-representation is simply

$$U_b(t_0, t) = e^{-i\omega_b t\,b^\dagger b} = R_b(\theta), \tag{5.217}$$

where $\theta = \omega_b t$. Therefore, the expectation value of a polynomial $f(a, a^\dagger)$ of a and $a^\dagger$ is

$$\langle\Phi(t)|f(a,a^\dagger)|\Phi(t)\rangle = \langle\Phi(t_0)|U^\dagger(t_0,t)\,f(a,a^\dagger)\,U(t_0,t)|\Phi(t_0)\rangle \tag{5.218}$$

$$= \langle\Phi(t_0)|e^{i\omega_b t\,b^\dagger b}\,f(a,a^\dagger)\,e^{-i\omega_b t\,b^\dagger b}|\Phi(t_0)\rangle \tag{5.219}$$

$$= \langle\Phi(t_0)|R_b^\dagger(\theta)\,f(a,a^\dagger)\,R_b(\theta)|\Phi(t_0)\rangle. \tag{5.220}$$

Let us now consider how to simplify the expression in between the state vectors. Recall that

$$a = S_b^\dagger(s,\phi)\, b\, S_b(s,\phi) \tag{5.221}$$

$$a^\dagger = S_b^\dagger(s,\phi)\, b^\dagger\, S_b(s,\phi)\,, \tag{5.222}$$

where

$$S_b(s,\phi) = \exp\left\{\frac{s}{2}\left(e^{-2i\phi}b^2 - e^{2i\phi}b^{\dagger 2}\right)\right\} \tag{5.223}$$

is a single-mode squeezing operator in the b-representation, $0 \le s < \infty$ and $-\pi/2 \le \phi \le \pi/2$. We can thus express the function f in terms of b and $b^\dagger$. More specifically,

$$\begin{aligned} f(a,a^\dagger) &= f\left(S_b^\dagger(s,\phi)\, b\, S_b(s,\phi),\, S_b^\dagger(s,\phi)\, b^\dagger\, S_b(s,\phi)\right) \\ &= S_b^\dagger(s,\phi)\, f(b,\, b^\dagger)\, S_b(s,\phi)\,, \end{aligned} \tag{5.224}$$

since $S_b^\dagger(s,\phi)\, S_b(s,\phi) = 1$. Now we have

$$\begin{aligned} U^\dagger(t_0,t)\, f(a,a^\dagger)\, U(t_0,t) &= R_b^\dagger(\theta)\, S_b^\dagger(s,\phi)\, f(b,b^\dagger)\, S_b(s,\phi)\, R_b(\theta) \\ &= R_b^\dagger(\theta)\, S_b^\dagger(s,\phi)\, R_b(\theta)\, R_b^\dagger(\theta)\, f(b,b^\dagger)\, R_b(\theta)\, R_b^\dagger(\theta)\, S_b(s,\phi)\, R_b(\theta) \\ &= \left\{R_b^\dagger(\theta)\, S_b^\dagger(s,\phi)\, R_b(\theta)\right\}\left\{R_b^\dagger(\theta)\, f(b,\, b^\dagger)\, R_b(\theta)\right\} \\ &\quad \times \left\{R_b^\dagger(\theta)\, S_b(s,\phi)\, R_b(\theta)\right\}\,. \end{aligned} \tag{5.225}$$

Since operators S and R satisfy [92]

$$R_b^\dagger(\theta)\, S_b(s,\phi)\, R_b(\theta) = S_b(s,\phi+\theta) \tag{5.226}$$

$$R_b^\dagger(\theta)\, b\, R_b(\theta) = be^{-i\theta}\,, \tag{5.227}$$

so that

$$R_b^\dagger(\theta)\, f(b,\, b^\dagger)\, R_b(\theta) = f(R_b^\dagger(\theta)\, b\, R_b(\theta),\, R_b^\dagger(\theta)\, b^\dagger\, R_b(\theta)) \tag{5.228}$$

$$= f(be^{-i\theta},\, b^\dagger e^{i\theta})\,, \tag{5.229}$$

we can therefore simplify the original expression Eq. (5.225) as

$$\begin{aligned} U^\dagger(t_0,t)\, f(a,\, a^\dagger)\, U(t_0,t) &= \left\{R_b^\dagger(\theta)\, S_b^\dagger(s,\phi)\, R_b(\theta)\right\}\left\{R_b^\dagger(\theta)\, f(b,\, b^\dagger)\, R_b(\theta)\right\} \\ &\quad \times \left\{R_b^\dagger(\theta)\, S_b(s,\phi)\, R_b(\theta)\right\} \\ &= S_b^\dagger(s,\phi+\theta)\, f(be^{-i\theta},\, b^\dagger e^{i\theta})\, S_b(s,\phi+\theta) \\ &= f\left[S_b^\dagger(s,\phi+\theta)\, be^{-i\theta}\, S_b(s,\phi+\theta),\right. \\ &\qquad \left. S_b^\dagger(s,\phi+\theta)\, b^\dagger e^{i\theta}\, S_b(s,\phi+\theta)\right]\,. \end{aligned} \tag{5.230}$$

Since the parameters of the squeezing operator S have been changed (ϕ becomes $\phi+\theta$), now $S_b^\dagger(s,\phi+\theta)\, b\, S_b(s,\phi+\theta)$ is not equal to a anymore. However, it can still be expressed as a linear combination of a and $a^\dagger$:

$$\begin{aligned} S_b^\dagger(s,\phi+\theta)\, b\, S_b(s,\phi+\theta) &= b\cosh s - b^\dagger e^{2i(\phi+\theta)}\sinh s \\ &= \left(a\cosh s - a^\dagger e^{2i\phi}\sinh s\right)\cosh s \\ &\quad + \left(a^\dagger\cosh s - a e^{-2i\phi}\sinh s\right) e^{2i(\phi+\theta)}\sinh s \\ &= a\cosh^2 r - a^\dagger e^{2i\phi}\sinh s\cosh s \\ &\quad + a^\dagger e^{2i(\phi+\theta)}\sinh s\,\cosh s - a e^{2i\theta}\sinh^2 r \\ &= a\left(\cosh^2 r - e^{2i\theta}\sinh^2 r\right) \\ &\quad + a^\dagger e^{2i\phi}\sinh s\,\cosh s\left(1-e^{2i\theta}\right) . \end{aligned} \tag{5.231}$$

In particular, if $\theta = 0$,

$$a\left(\cosh^2 s - e^{2i\theta}\sinh^2 s\right) + a^\dagger e^{2i\phi}\sinh s\,\cosh s\left(1-e^{2i\theta}\right) = a\,. \tag{5.232}$$

Therefore, $U^\dagger(t_0,t)f(a,a^\dagger)U(t_0,t)$ now becomes a polynomial of a and $a^\dagger$ and is easier to handle. Taking H_1 as an example, we obtain

$$s = \frac{1}{16\lambda_1} \tag{5.233}$$

$$\phi = 0 \tag{5.234}$$

$$\begin{aligned} \theta &= \omega_b t \cong \omega_1 t\left(1-\frac{1}{16\lambda_1}\right)\left(1-2\delta_1^2\right) \\ &\cong \omega_1 t\left(1-\frac{1}{16\lambda_1}\right) . \end{aligned} \tag{5.235}$$

Here we have only kept terms up to first order in $\delta = 1/16\lambda_1$. Substituting these parameters into expressions [5.230] and [5.231], the expectation value of function f at any time t can then be calculated with an arbitrary initial state.

5.6.2 Time Evolution Operator of H_B

The time-evolution operator for H_B, which describes both H_2 (for a current-biased junction) and H_3 (for a Josephson junction in a superconducting ring driven by external magnetic flux), can be obtained similarly. We first separate the Hamiltonian H_B into a free oscillator part H_0 and a correction V_B,

$$\begin{aligned} H_B &= \hbar\omega a^\dagger a + \alpha a + \alpha^* a^\dagger + \beta a^2 + \beta^* a^{\dagger 2} \\ &= H_0 + V_B\,, \end{aligned} \tag{5.236}$$

where

$$H_0 = \hbar\omega a^\dagger a\,, \tag{5.237}$$

$$V_B = \alpha a + \alpha^* a^\dagger + \beta a^2 + \beta^* a^{\dagger 2}\,. \tag{5.238}$$

Again, if we transform into the interaction picture, we will only be able to obtain a time-evolution operator that is either a formal time-ordered expression, or a product of time-evolution operators at each small time increment. To achieve a more analytical expression, we will now follow the approach we have taken for H_A. In other words, we will transform into a representation in which H_B is diagonalized (that is, the c-representation we discussed in Section 5.4), obtain the time-evolution operator in that representation, do the calculations there, and then transform back to the a-representation. This procedure is presented below.

In the c-representation, H_B is diagonalized $H_B = \hbar\omega_c c^\dagger c$; here we have dropped a constant. The time-evolution operator of the system in the c-representation is then simply

$$U_c(t_0, t) = e^{-i\omega_c t c^\dagger c} = R_c(\theta)\,, \tag{5.239}$$

where $\theta = \omega_c t$.

The transformation from the a-representation to the c-representation is given by

$$b = S_a^\dagger(s,\phi)\, a\, S_a(s,\phi) \tag{5.240}$$

$$c = D_b^\dagger(\alpha)\, b\, D_b(\alpha)\,. \tag{5.241}$$

The inverse transformations are

$$a = S_b(s,\phi)\, b\, S_b^\dagger(s,\phi) \tag{5.242}$$

$$b = D_c^\dagger(-\alpha)\, c\, D_c(-\alpha)\,. \tag{5.243}$$

Therefore,

$$a = S_b(s,\phi)\, D_c^\dagger(-\alpha)\, c\, D_c(-\alpha)\, S_b^\dagger(s,\phi)\,. \tag{5.244}$$

From $b = c - \alpha$, we can express $S_b(s,\phi)$ in terms of c

$$\begin{aligned}
S_b(s,\phi) &= \exp\left\{\frac{s}{2}\left(e^{-2i\phi}b^2 - e^{2i\phi}b^{\dagger 2}\right)\right\} \\
&= \exp\left\{\frac{s}{2}\left[e^{-2i\phi}(c-\alpha)^2 - e^{2i\phi}(c^\dagger - \alpha^*)^2\right]\right\} \\
&= \exp\left\{\frac{s}{2}\left[e^{-2i\phi}(c^2 - 2\alpha c + \alpha^2) - e^{2i\phi}(c^{\dagger 2} - 2\alpha^* c^\dagger + \alpha^{*2})\right]\right\} \\
&= \exp\left\{\frac{s}{2}\left[e^{-2i\phi}c^2 - e^{2i\phi}c^{\dagger 2}\right] + s\left[e^{2i\phi}\alpha^* c^\dagger - e^{-2i\phi}\alpha c\right]\right. \\
&\qquad \left. + \frac{s}{2}\left[e^{-2i\phi}\alpha^2 - e^{2i\phi}\alpha^{*2}\right]\right\}\,.
\end{aligned} \tag{5.245}$$

Using the result we derived in Appendix B.4, this operator can be factorized:

$$\begin{aligned} S_b(s,\phi) &= \exp\left\{\frac{s}{2}\left[e^{-2i\phi}c^2 - e^{2i\phi}c^{\dagger 2}\right] + r\left[e^{2i\phi}\alpha^* c^\dagger - e^{-2i\phi}\alpha c\right] + \frac{s}{2}\left[e^{-2i\phi}\alpha^2 - e^{2i\phi}\alpha^{*2}\right]\right\} \\ &= D_c(\beta)\, S_c(s,\phi)\, e^\gamma\,, \end{aligned} \tag{5.246}$$

where β and γ are complex numbers determined from α, r, and ϕ. In particular, γ is pure imaginary. Therefore,

$$\begin{aligned} a &= e^\gamma\, D_c(\beta)\, S_c(s,\phi)\, D_c^\dagger(-\alpha)\, c\, D_c(-\alpha)\, S_c^\dagger(s,\phi)\, D_c^\dagger(\beta)\, e^{-\gamma} \\ &= D_c(\beta)\, S_c(s,\phi)\, D_c^\dagger(-\alpha)\, c\, D_c(-\alpha)\, S_c^\dagger(s,\phi)\, D_c^\dagger(\beta)\,. \end{aligned} \tag{5.247}$$

To calculate the expectation value of $f(a,a^\dagger)$, we have

$$\langle\Phi(t)|\, f(a,a^\dagger)\,|\Phi(t)\rangle = \langle\Phi(0)|\, U^\dagger(t_0,t)\, f(a,a^\dagger)\, U(t_0,t)\,|\Phi(0)\rangle \tag{5.248}$$

$$\begin{aligned} &= \langle\Phi(0)|R_c^\dagger(\theta)\, f(a,a^\dagger)\, R_c(\theta)|\Phi(0)\rangle \\ &= \langle\Phi(0)|R_c^\dagger(\theta)\, f\Big[D_c(\beta)S_c(s,\phi)D_c^\dagger(-\alpha)\, c\, D_c(-\alpha)D_c^\dagger(\beta)S_c^\dagger(s,\phi), \\ &\qquad D_c(\beta)S_c(s,\phi)D_c^\dagger(-\alpha)\, c^\dagger\, D_c(-\alpha)D_c^\dagger(\beta)S_c^\dagger(s,\phi)\Big]\, R_c(\theta)|\Phi(0)\rangle \\ &= \langle\Phi(0)|R_c^\dagger(\theta)\, D_c(\beta)\, S_c(r,\phi)\, D_c^\dagger(-\alpha) \\ &\quad \times f(c,\, c^\dagger)\, D_c(-\alpha)\, S_c^\dagger(s,\phi)\, D_c^\dagger(\beta)\, R_c(\theta)|\Phi(0)\rangle\,. \end{aligned} \tag{5.249}$$

Since operators S, D, and R satisfy [92]

$$R_c^\dagger(\theta)\, S_c(s,\phi)\, R_c(\theta) = S_c(s,\phi+\theta) \tag{5.250}$$

$$R_c^\dagger(\theta)\, D_c(\alpha)\, R_b(\theta) = D_c\left(\alpha e^{i\theta}\right) \tag{5.251}$$

$$R_b^\dagger(\theta)\, b\, R_b(\theta) = be^{-i\theta}\,, \tag{5.252}$$

the above matrix element can be further simplified to

$$\begin{aligned} &\langle\Phi(t)|\, f(a,a^\dagger)\,|\Phi(t)\rangle \\ &= \langle\Phi(0)|\, D_c(\beta e^{i\theta})\, S_c(s,\phi+\theta)\, D_c^\dagger(-\alpha e^{i\theta}) \times f(ce^{-i\theta},\, c^\dagger e^{i\theta}) \\ &\quad \times D_c(-\alpha e^{i\theta})\, S_c^\dagger(s,\phi+\theta)\, D_c^\dagger(\beta e^{i\theta})\,|\Phi(0)\rangle \\ &= \langle\Phi(0)|f\Big[D_c(\beta e^{i\theta})\, S_c(s,\phi+\theta)\, D_c^\dagger(-\alpha e^{i\theta})\, ce^{-i\theta}\, D_c(-\alpha e^{i\theta})\, S_c^\dagger(s,\phi+\theta)\, D_c^\dagger(\beta e^{i\theta}), \\ &\quad D_c(\beta e^{i\theta})\, S_c(s,\phi+\theta)\, D_c^\dagger(-\alpha e^{i\theta})\, c^\dagger e^{i\theta}\, D_c(-\alpha e^{i\theta})\, S_c^\dagger(s,\phi+\theta)\, D_c^\dagger(\beta e^{i\theta})\Big]\,|\Phi(0)\rangle\,. \end{aligned} \tag{5.253}$$

Since

$$D_c(\beta e^{i\theta})\, c\, D_c^\dagger(\beta e^{i\theta}) = c - \beta e^{i\theta} \tag{5.254}$$

$$S_c(r,\phi+\theta)\, c\, S_c^\dagger(s,\phi+\theta) = c\cosh s + c^\dagger e^{i(\phi+\theta)}\sinh s\,, \tag{5.255}$$

the kernel of the above quantum average can thus be expressed as a polynomial of c and $c^\dagger$, which in turn are linear functions of a and $a^\dagger$. In other words, the kernel of Eq. (5.253) is also a polynomial of a and $a^\dagger$, whose matrix elements can be calculated in a straightforward manner.

5.7 Rotating Wave Approximation

In the previous sections, we solved for the approximate eigenstates of the various configurations involving Josephson junctions. In this section we study the problem using a very different approach. Here we use the standard (see, e.g., [6]) rotating wave approximation (RWA) which enforces energy conservation—since the contribution to the energy correction from the non-number-conserving terms vanishes. This approach give us a complementary viewpoint on the fluctuation properties of a Josephson junction. The results obtained are consistent with our previous calculations. Again, we consider the small-phase approximation and focus on the bottom of a local potential minimum.

For an isolated Josephson junction, from Eq. (5.38), after dropping the constant terms which only produce an unimportant energy shift, we obtain the following Hamiltonian

$$H_1 = \hbar\omega_1 \left(1 - \frac{1}{16\lambda_1}\right) a^\dagger a - \frac{\hbar\omega_1}{16\lambda_1} \left(a^\dagger a\right)^2 . \tag{5.256}$$

In Appendix G we demonstrate that the RWA is only valid when $\langle a^\dagger a\rangle$ is small. Since throughout this chapter the system is near its ground state, the above condition for the RWA is always satisfied. Similarly, the Hamiltonian H_2 for the current-biased junction can be simplified from Eq. (5.47) into the form

$$H_2 = \hbar\omega_2 \left(1 - \frac{1}{16\lambda_2}\right) a^\dagger a - \frac{\hbar\omega_2}{16\lambda_2} \left(a^\dagger a\right)^2 + \gamma(a + a^\dagger) , \tag{5.257}$$

with

$$\gamma = -\frac{I\Phi_0}{8\sqrt{2}\pi\lambda_2^{3/2}} . \tag{5.258}$$

From now on, let us drop the subscripts and focus on the general properties of the Hamiltonians.

5.7.1 Factorization of the Time Evolution Operator (TEO)

TEO of a Free Oscillator

To simplify the notation, let us first introduce

$$\mu = \omega\left(1 - \frac{1}{16\lambda}\right) , \tag{5.259}$$

$$\nu = -\frac{\omega}{16\lambda}. \tag{5.260}$$

The time evolution operators for the free oscillators of cases (1) (an isolated Josephson junction) and (4) (a Josephson junction in a superconducting ring with no external flux, at the global potential minimum) are already in factorized form, making the calculations straightforward. For example, for H_1,

$$\begin{aligned} |\Psi_1(t)\rangle_S &= U_1(t)|\Psi_1(0)\rangle_S = \exp\left(-\frac{i}{\hbar}\int_0^t H_1 d\tau\right)|\Psi_1(0)\rangle_S \\ &= e^{-i\mu t a^\dagger a} e^{i\nu t (a^\dagger a)^2}|\Psi_1(0)\rangle_S , \end{aligned} \tag{5.261}$$

where $|\Psi_1\rangle_S$ is the Schrödinger-picture state and $U_1(t)$ is the time evolution operator for free oscillators [valid for both cases (1) and (4)].

TEO of a Linearly-Driven Junction

The time-evolution operators for the case (2) (linearly-driven Josephson junction) and (3) (Josephson junction in a superconducting ring with an external flux), $U_2(t)$ and $U_3(t)$, are much more complicated since these systems have interactions. We use the interaction picture to derive the factorized time evolution operator. The linear term is treated as the interaction. The full Hamiltonian H_2 is split as

$$H_2 = H_1 + H_I , \tag{5.262}$$

$$H_1 = \hbar\mu\, a^\dagger a - \hbar\nu\,(a^\dagger a)^2 , \tag{5.263}$$

$$H_I = \gamma\,(a + a^\dagger). \tag{5.264}$$

The Schrödinger equation is

$$i\hbar\frac{\partial}{\partial t}|\Psi_2\rangle_S = H_2|\Psi_2\rangle_S , \tag{5.265}$$

where $|\Psi_2\rangle_S$ is the Schrödinger-picture state for a linearly-driven junction. It can be proved that approximately (see Appendix B),

$$\begin{aligned} |\Psi_2(t)\rangle_S &= U_2(t)\,|\Psi_2(0)\rangle_S = \exp\left(-\frac{i}{\hbar}\int_0^t H_2 d\tau\right)|\Psi_2(0)\rangle_S \\ &\cong e^{-iH_1 t/\hbar} e^{\eta a^\dagger - a\eta^*}|\Psi_2(0)\rangle_S , \end{aligned} \tag{5.266}$$

where

$$\eta = \frac{\gamma}{\hbar\omega}\frac{1 - e^{i(1-a^\dagger a/8\lambda)\omega t}}{1 - a^\dagger a/8\lambda}. \tag{5.267}$$

Notice that the operator η does not commute with either a or $a^\dagger$. Therefore, the transformation matrix (or displacement operator) $\exp(\eta a^\dagger - a\eta^*)$ cannot be directly factorized.

To simplify the problem of factorizing $U_2(t)$, we first expand the numerator and denominator of η to zeroth order in $a^\dagger a$ (i.e., we take $a^\dagger a/8\lambda \sim 0$), and consider the small-time limit, in which $\omega t < 1$. Thus, to zeroth order in $a^\dagger a/8\lambda$, the TEO becomes

$$U_2^{(0)}(t) = \exp\left\{-i\mu t a^\dagger a + i\nu t (a^\dagger a)^2\right\} \exp\left(\eta_0 a^\dagger - \eta_0^* a\right) , \tag{5.268}$$

where

$$\eta_0 = \frac{\gamma}{\hbar\omega}\left(1 - e^{i\omega t}\right) . \tag{5.269}$$

To check the accuracy of the above approximation, we also expand η to the next higher order (i. e. , first order) in $a^\dagger a/8\lambda$, so that now the TEO becomes

$$\begin{aligned} U_2^{(1)}(t) &= \exp\left\{i\omega t\left(1 - \frac{1}{16\lambda}\right) a^\dagger a - i\frac{\omega t}{16\lambda}(a^\dagger a)^2\right\} \\ &\quad \times \exp\left\{(\eta_0 + \eta_1)a^\dagger - (\eta_0 + \eta_1)^* a + \eta_1 {a^\dagger}^2 a - \eta_1^* a^\dagger a^2\right\} , \end{aligned} \tag{5.270}$$

where

$$\eta_0 = \frac{\gamma}{\hbar\omega}(1 - e^{i\omega t}) , \tag{5.271}$$

$$\eta_1 = \frac{\gamma}{8\lambda\hbar\omega}[1 - e^{i\omega t}(1 - i\omega t)] . \tag{5.272}$$

According to the Baker-Hausdorff formula [6], $e^{A+B} = e^A e^B e^{[A,B]/2}$, if $[A,[A,B]] = [B,[A,B]] = 0$. However, the later condition does not hold in this case, where $A = (\eta_0 + \eta_1)a^\dagger - (\eta_0 + \eta_1)^* a$ and $B = \eta_1 {a^\dagger}^2 a - \eta_1^* a^\dagger a^2$. Nevertheless, higher-order terms, like $[A,B]$, $[A,[A,B]]$, etc., are at most $O(\eta_0\eta_1)$ and thus smaller than the terms that are $O(\eta_0)$ or $O(\eta_1)$, since $|\eta_0| < 1$ and $|\eta_1| < 1$. Therefore, we only consider the dominant terms, which are $\sim O(\eta_0)$ and $O(\eta_1)$, and factorize the exponential of $U_2^{(1)}(t)$ as $e^{A+B} \cong e^A e^B$. Now, $U_2^{(1)}(t)$ becomes

$$\begin{aligned} U_2^{(1)}(t) &= \exp\left\{i\omega t\left(1 - \frac{1}{16\lambda}\right) a^\dagger a - i\frac{\omega t}{16\lambda}(a^\dagger a)^2\right\} \exp\left\{\eta_1 {a^\dagger}^2 a - \eta_1^* a^\dagger a^2\right\} \\ &\quad \times \exp\left\{(\eta_0 + \eta_1)a^\dagger - (\eta_0 + \eta_1)^* a\right\} , \end{aligned} \tag{5.273}$$

which has a more factorized form. These results, derived for H_2, also apply *mutatis mutandis* to H_3

5.7.2 Calculation of the Quantum Fluctuations

Free Oscillator Case

The state vector for a free oscillator can then be expressed as

$$|\psi_1(t)\rangle = e^{-i\mu t a^\dagger a} e^{-i\nu t (a^\dagger a)^2} |\psi_1(0)\rangle . \tag{5.274}$$

Thus, given an initial state, the state vector at any future time is determined. A special initial state is a coherent state, namely,

$$|\psi_1(0)\rangle = |\alpha\rangle = e^{-\frac{|\alpha|^2}{2}} \sum_{n=0}^{\infty} \frac{\alpha^n}{\sqrt{n!}} |n\rangle \,. \tag{5.275}$$

A coherent state [6] is an eigenstate of the annihilation operator, $a|\alpha\rangle = \alpha|\alpha\rangle$. It can also be generated by acting a displacement operator on a vacuum state, $|\alpha\rangle = D(\alpha)|0\rangle$, where the displacement operator is $D(\alpha) = \exp(\alpha a^\dagger - \alpha^* a)$. See Appendix A for further explanations. Now the state vector of the free oscillator with an initial coherent state is

$$\begin{aligned} |\psi_1^{\rm coh}(t)\rangle &= e^{-\frac{|\alpha|^2}{2}} \sum_{n=0}^{\infty} \frac{\alpha^n}{\sqrt{n!}} e^{-i\mu t a^\dagger a} e^{-i\nu t (a^\dagger a)^2} |n\rangle \\ &= e^{-\frac{|\alpha|^2}{2}} \sum_{n=0}^{\infty} \frac{\alpha^n}{\sqrt{n!}} e^{-i\mu t n} e^{-i\nu t n^2} |n\rangle \,. \end{aligned} \tag{5.276}$$

The canonical coordinate and momentum are defined as

$$X = \frac{1}{\sqrt{2}}(a + a^\dagger) \,, \tag{5.277}$$

$$P = \frac{1}{\sqrt{2}\, i}(a - a^\dagger) \,. \tag{5.278}$$

X and P are dimensionless quadrature operators. They are related to n and ϕ by

$$X = \left(\frac{E_J}{E_C}\right)^{1/4} \phi \,, \tag{5.279}$$

$$P = \left(\frac{E_C}{E_J}\right)^{1/4} n \,. \tag{5.280}$$

So the fluctuations of the phase and charge number are

$$\langle (\phi_{\rm local})^2 \rangle = \sqrt{\frac{E_C}{E_J}}\, \langle (\Delta X)^2 \rangle = \frac{1}{\lambda} \langle (\Delta X)^2 \rangle \,, \tag{5.281}$$

$$\langle (\Delta n)^2 \rangle = \sqrt{\frac{E_J}{E_C}}\, \langle (\Delta P)^2 \rangle = \lambda \langle (\Delta P)^2 \rangle \,. \tag{5.282}$$

Now that we have the state vector $|\psi_1(t)\rangle$, we can calculate the fluctuations of X and P:

$$\langle (\Delta X)^2 \rangle_1 = \langle X^2 \rangle_1 - \langle X \rangle_1^2 \tag{5.283}$$

$$\begin{aligned} &= \frac{1}{2}(1 + 2|\alpha|^2) + e^{-|\alpha|^2} \sum_{n=0}^{\infty} \frac{|\alpha|^{2n+2}}{n!} \cos(2\mu t + 4(n+1)\nu t) \\ &\quad -2 \left\{ e^{-|\alpha|^2} \sum_{n=0}^{\infty} \frac{|\alpha|^{2n+1}}{n!} \cos(\mu t + (2n+1)\nu t) \right\}^2 \end{aligned} \tag{5.284}$$

$$\langle(\Delta P)^2\rangle_1 = \langle P^2\rangle_1 - \langle P\rangle_1^2 \tag{5.285}$$

$$= \frac{1}{2}(1+2|\alpha|^2) - e^{-|\alpha|^2}\sum_{n=0}^{\infty}\frac{|\alpha|^{2n+2}}{n!}\cos(2\mu t + 4(n+1)\nu t)$$
$$-2\left\{e^{-|\alpha|^2}\sum_{n=0}^{\infty}\frac{|\alpha|^{2n+1}}{n!}\sin(\mu t + (2n+1)\nu t)\right\}^2 \tag{5.286}$$

This calculation can be numerically carried out when α, ω, and λ are given. We have done so and we conclude that there is a squeezing effect when $\alpha \neq 0$, i.e., when the initial state is a coherent state; but there is no squeezing when the initial state is a vacuum state.

According to the above results for $\langle(\Delta X)^2\rangle_1$ and $\langle(\Delta P)^2\rangle_1$, a large-area junction, which has large E_J and small E_C, should have small fluctuations in phase and large fluctuations in particle number. On the other hand, a small-area junction has smaller Josephson coupling and smaller junction capacitance (which means a larger charging energy E_C); therefore it should have larger phase fluctuations but smaller number fluctuations. All these conclusions are qualitatively consistent with experiments. Further experimental studies, with thermal and environmental noise smaller than the intrinsic quantum noise, are needed to quantitatively verify the above results.

Linearly-Driven Josephson Junctions

In this section we derive some analytical results for the fluctuations of the phase and charge number of a linearly-driven Josephson junction. Recall that the corresponding state vector is approximately

$$|\psi_2(t)\rangle = e^{-i\mu t a^\dagger a}e^{-i\nu t(a^\dagger a)^2}e^{\eta_0 a^\dagger - \eta_0^* a}|\psi_2(0)\rangle\,, \tag{5.287}$$

where $\eta_0 = \gamma(1-e^{i\omega t})/\hbar\omega$, $\lambda = \sqrt{E_J/E_C}$, and $\gamma = -E_S/\sqrt{2\lambda}$. The later parameter, γ, reflects the relative strength of the external driving current, which acts like a "force".

We calculate the fluctuations with two different initial states: vacuum state and coherent state. If the initial state is a vacuum state, the state vector is

$$|\psi_2^{\rm vac}(t)\rangle = e^{-i\mu t a^\dagger a}e^{-i\nu t(a^\dagger a)^2}e^{\eta_0 a^\dagger - \eta_0^* a}|0\rangle$$
$$= e^{-i\mu t a^\dagger a}e^{-i\nu t(a^\dagger a)^2}|\eta_0\rangle\,. \tag{5.288}$$

On the other hand, we can also use a coherent state as the initial state. As an example, we use an initial coherent state $|\xi\rangle$ with $\xi = 1$. The state vector now becomes

$$|\psi_2^{\rm coh}(t)\rangle = e^{-i\mu t a^\dagger a}e^{-i\nu t(a^\dagger a)^2}e^{\eta_0 a^\dagger - \eta_0^* a}|1\rangle\,. \tag{5.289}$$

Coherent states exhibit the following property

$$D(\eta_0)|\xi\rangle = e^{i\delta}|\eta_0 + \xi\rangle\,, \tag{5.290}$$

where δ is a real number related to η_0 and ξ. In other words, δ is just a phase which will not affect the calculation of the expectation values. Thus we can drop this constant phase, and the state vector takes the form

$$|\psi_2^{\rm coh}(t)\rangle = e^{-i\mu t a^\dagger a} e^{-i\nu t a^\dagger a)^2}|1 + \eta_0\rangle\,. \tag{5.291}$$

For both of these initial states, $|\psi_2^{\rm vac}(t)\rangle$ and $|\psi_2^{\rm coh}(t)\rangle$, the fluctuations are given by

$$\begin{aligned}\langle(\Delta X)^2\rangle_2 &= \frac{1}{2} + |\zeta|^2 + e^{-|\zeta|^2}\sum_{n=0}^{\infty}\frac{|\zeta|^{2n+2}}{n!}\cos(2\phi_\zeta - 2\mu t - 4\nu t(n+1)) \\ &\quad -2\left\{e^{-|\zeta|^2}\sum_{n=0}^{\infty}\frac{|\zeta|^{2n+1}}{n!}\cos(\phi_\zeta - \mu t - \nu t(2n+1))\right\}^2\,, \qquad (5.292)\\ \langle(\Delta P)^2\rangle_2 &= \frac{1}{2} + |\zeta|^2 - e^{-|\zeta|^2}\sum_{n=0}^{\infty}\frac{|\zeta|^{2n+2}}{n!}\cos(2\phi_\zeta - 2\mu t - 4\nu t(n+1)) \\ &\quad -2\left\{e^{-|\zeta|^2}\sum_{n=0}^{\infty}\frac{|\zeta|^{2n+1}}{n!}\sin(\phi_\zeta - \mu t - \nu t(2n+1))\right\}^2\,. \qquad (5.293)\end{aligned}$$

When the initial state is a vacuum state, $|0\rangle$, the parameters ζ and ϕ_ζ in $\langle(\Delta X)^2\rangle_2$ and $\langle(\Delta P)^2\rangle_2$ become

$$\zeta^{\rm vac} = \eta_0 = \frac{\gamma}{\hbar\omega}(1 - e^{i\omega t})\,, \tag{5.294}$$

$$\phi_\zeta^{\rm vac} = \arctan\left(\frac{\sin\omega t}{\cos\omega t - 1}\right) = \pi/2 + \omega t/2\,. \tag{5.295}$$

However, if the initial state is the coherent state $|1\rangle$, the parameters are,

$$\zeta^{\rm coh} = 1 + \eta_0 = 1 + \frac{\gamma}{\hbar\omega}(1 - e^{i\omega t})\,, \tag{5.296}$$

$$\phi_\zeta^{\rm coh} = \arctan\left(\frac{\sin\omega t}{\cos\omega t - 1 - \hbar\omega/\gamma}\right)\,. \tag{5.297}$$

These results, derived for case (2), also apply for case (3). We have carried out the numerical calculation of the above fluctuations but found no squeezing effect in either X or P when the initial state is a vacuum state. On the other hand, with an initial coherent state, we have found squeezing effects over a wide range of values of λ. The results are presented in Fig. 5.4, where solid lines correspond to initial coherent states and dotted lines to an initial vacuum state.

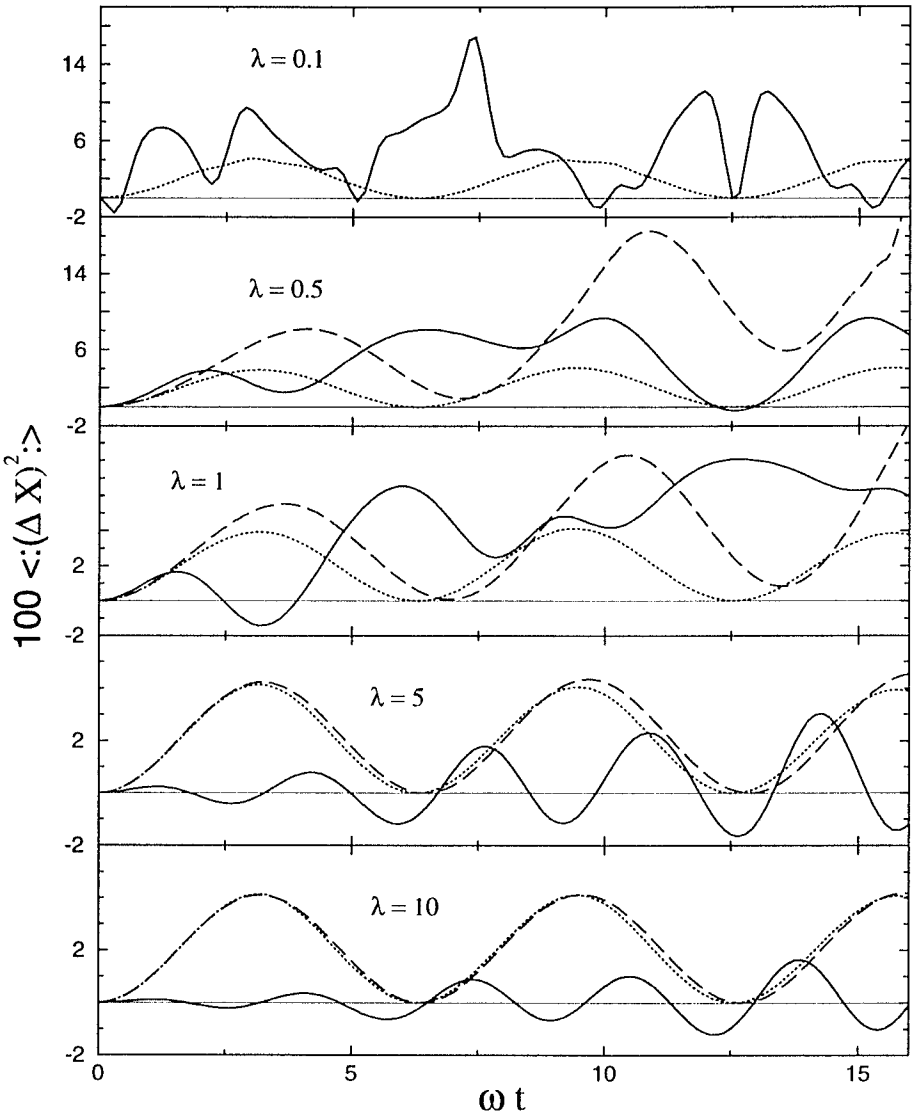

Figure 5.4: Time evolution of the variances of the quadrature phase difference in the linearly-driven Josephson junctions, using the rotating wave approximation. The products are normal ordered and the quadrature phase is $X = (E_J/E_C)^{1/4}\phi$. The squeezing or reduction of the quadrature phase fluctuations is reached whenever its normal-ordered variance falls below zero. The solid lines represent results obtained with a zeroth-order approximation in $a^\dagger a/8\lambda$ and with an initial coherent state. The dotted lines are results obtained with the same approximation but with an initial vacuum state. The dashed lines use the first-order approximation in $a^\dagger a/8\lambda$ and with an initial vacuum state. The fluctuations $\langle(\Delta X)^2\rangle(t)$ and $\langle(\Delta P)^2\rangle(t)$ for the first-order approximation in $a^\dagger a/8\lambda$, and starting from an initial coherent state, are indistinguishable from the zeroth-order results (at least for small times). This indicates that our approximation is robust and works well when in the regime $0.5 < \lambda < 5$, where $\lambda = \sqrt{E_J/E_C}$.

First order Correction for the Linearly-Driven Case

For the linearly-driven junction cases (2) and (3), and with an initial vacuum state, we have also calculated the fluctuations of the canonical conjugate variables by expanding η to first order in $a^\dagger a/8\lambda$. In other words, now

$$\begin{aligned} \eta &= \frac{\gamma}{\hbar\omega}\frac{1-e^{i(1-a^\dagger a/8\lambda)\omega t}}{1-a^\dagger a/8\lambda} \\ &\cong \eta_0 + \eta_1 a^\dagger a\,, \end{aligned} \tag{5.298}$$

where

$$\eta_0 = \frac{\gamma}{\hbar\omega}(1-e^{i\omega t})\,, \tag{5.299}$$

$$\eta_1 = \frac{\gamma}{8\lambda\hbar\omega}\left[1-e^{i\omega t}(1-i\omega t)\right]\,. \tag{5.300}$$

The formal displacement operator can now be simplified as:

$$\begin{aligned} e^{\eta a^\dagger - a\eta^\dagger} &\cong e^{(\eta_0 a^\dagger - \eta_0{}^* a)+\eta_1 a^\dagger a a^\dagger - \eta_1^* a a^\dagger a} \\ &\cong e^{\eta_1 a^{\dagger 2} a - \eta_1^* a^\dagger a^2} e^{(\eta_0+\eta_1)a^\dagger - (\eta_0+\eta_1)^* a} \\ &\cong (1+\eta_1 a^{\dagger 2} a - \eta_1^* a^\dagger a^2)\, D(\eta_0+\eta_1)\,. \end{aligned} \tag{5.301}$$

Where in the last line we have kept the dominant terms of the first exponential factor.

If the initial state is a vacuum state, we will have a state vector

$$\begin{aligned} |\psi_2^{\rm vac}(t)\rangle_S &\cong e^{-i\mu t a^\dagger a} e^{-i\nu t (a^\dagger a)^2}(1+\eta_1 a^{\dagger 2} a - \eta_1^* a^\dagger a^2)\, D(\eta_0+\eta_1)\,|0\rangle \\ &= e^{-i\mu t a^\dagger a} e^{-i\nu t (a^\dagger a)^2}(1+\eta_1 a^{\dagger 2} a - \eta_1^* a^\dagger a^2)|\eta_0+\eta_1\rangle\,. \end{aligned} \tag{5.302}$$

The numerical evaluation of the fluctuations $\langle(\Delta X)^2\rangle_2$ and $\langle(\Delta P)^2\rangle_2$ does not show a qualitative difference from the zeroth-order approximation (see Fig. 5.4, in which these results are shown in dashed lines), which demonstrates that the approximation we make for η is robust. The fluctuations for large values of t show an abnormal increase in magnitude because of the limitations of the small-time approximation. Therefore, we will only focus on the zeroth-order approximation, keeping in mind that we should remain in the small-time regime ($\omega t \sim 1$).

Physical Significance of the Initial States

Now let us look at the rotating wave approximation to this problem more closely. It is clear that when we take the small phase approximation, we have already implicitly assumed that

the states are localized. Thus our approach is better suited for the situations where E_J is relatively large.

As shown above, with an initial vacuum state we cannot reach a squeezed state at any time. The reason can be seen from the squeezing mechanism considered here. The fourth-order terms in the creation and annihilation operators are responsible for the redistribution of phase, which in turn leads to a squeezing effect. To make this term more effective, a large number of quanta are needed, because each one of the fourth-order terms involves four quanta at a time. An initial vacuum state cannot satisfy this condition, thus preventing the formation of squeezed states. On the other hand, an initial coherent state does have a nonzero average number of quanta, therefore making it possible for squeezed states to be generated.

5.8 Discussions and Open Problems

As we mentioned before, a key parameter in a Josephson junction is $\lambda = \sqrt{E_J/E_C}$. This parameter does not lead to squeezing directly, and so far cannot be tuned at will in most experiments. However, λ does provide a powerful control over quantum noise. By adjusting the value of λ, it is possible to redistribute the noise in both n (the tunneling Cooper pair number) and ϕ (the phase difference between the two sides of the junction). This is very important because the number n and the phase ϕ are observable quantities.

Here we have focused on four model Hamiltonians describing different ways to couple a Josephson junction to its environment. Needless to say, this list is not exhaustive, although we believe that these basic cases constitute a first step towards the study of more complicated and hybrid-mode interactions with the environment. Other interactions with the environment can be considered. For example, a thermal reservoir can be represented by a series of harmonic oscillators and introduce a linear coupling. Such a model was used to discuss dissipation in tunneling events (see Ref. [93] and references therein).

Recently, another Hamiltonian was proposed [95] in which the coupling between a Josephson junction and an external electromagnetic mode is contained in the quasicharge. Such an interaction can give rise to modulation of supercurrent through the junction. However, in this approach the phase difference over a Josephson junction is treated as an exactly measurable classical quantity, whose fluctuation comes solely from the driving external electromagnetic field. A more complete treatment has to consider both the external noise and the intrinsic quantum fluctuation we have discussed in this paper.

We did not include a heat reservoir in any of the cases considered in this paper, assuming that the noise due to the exchange with the environment is relatively weak. With a reservoir, a better approach would be to solve a quantum Langevin equation for a relevant variable such as the phase difference. This is beyond the scope of this work.

Throughout this paper, we have used two major approximations: we treat Josephson junctions as ideal and consider their quantum states to be localized. These approximations are valid in the limit of $T = 0$, $E_J \gg E_C$, and a very small biasing current. The states considered here should be either the ground states or the low-energy excited states. If the above conditions are not satisfied, other effects can be important.

Recall that the Josephson coupling energy is a sinusoidal function of the phase difference across the junction. In our treatment, we choose one of the potential minima and expand the whole potential around this minimum in a Taylor series up to the fourth-order terms. Such an expansion and truncation provides a potential that can localize wavefunctions. The expansion is a good representation of the original potential only around the potential minimum. Furthermore, by replacing a periodic potential with a localized one, we are using localized states to represent "snapshots" of the extended states. Therefore, to improve our results, we need to either change to an extended-state basis, or at least take into account the fluctuations caused by the tunneling events.

We can consider the effect of the periodicity from another point of view. From elementary quantum mechanics, a band structure will form in the energy spectrum as a result of a periodic potential. In Josephson junctions, the periodicity in the original sinusoidal potential transforms the discrete energy levels we obtained to a series of bands [85, 89]. The corresponding states are Bloch states. When $E_J \gg E_C$, the lowest-energy bands are very narrow and highly degenerate, and the energy spectrum is very similar to a localized oscillator, which is what we obtained from our approximations.

Real junctions are not ideal. A commonly-used model for them is the resistively-shunted junction model [83], in which the junction is represented by an ideal junction in parallel with a capacitor and a resistor. The damping of a non-ideal junction comes from the resistor. Microscopically, this dissipation originates from the interaction between Cooper pairs and their environmental degrees of freedom and also the excitation of quasiparticles. Therefore, the real quantum noise of the junction also includes contributions from the quasiparticles and other environmental degrees of freedom. Whether our results will provide the most important contribution depends on the relative strength of the dissipation and the thermal

energy to the Josephson coupling constant E_J.

To go beyond the approximations used in this work, it would be interesting to study the interplay between the intra-potential-well fluctuation and the inter-potential-well tunneling. To relate the Bloch states to the localized states studied here would also be an interesting subject. Such a comparison would clearly show whether our results, which are based on an approximation, contain most of the relevant information in the Bloch states, which are the exact solution to the periodic potential problem. In addition, to describe the quantum noise in a more complete manner, it is also important to study the shot noise from the quasiparticle tunneling and the white noise (or colored noise, to be more general) of the environment. Another very interesting topic is the possible manipulation of the quantum fluctuations in n and ϕ. Notice that in this paper we have only discussed the variation of the quantum noises due to the nonlinearity of the Josephson coupling energy $\cos\phi$. No external tuning was considered. Therefore, an open problem would be to consider an external mechanism that would control the level of quantum noise in a given variable, similar to our work on phonons [18, 19, 20], where the incoming coherent light pumps optical phonons into a parametric amplification process through a Raman mechanism. These optically excited coherent optical phonons can then convert into squeezed acoustic phonons through an anharmonic interaction.

5.9 Conclusions

In this chapter, we investigate the quantum fluctuation properties of a Josephson junction in several different configurations. Specifically, we work in the limit of large Josephson coupling energy and small charging energy, so that the junctions are in the nearly-localized regime. This limit can be easily realized for the large S-I-S junctions. It is analogous to the tight-binding limit for electrons in a crystal. Furthermore, we expand the $E_J\cos\phi$ Josephson coupling energy around $\phi = 0$ to fourth order in $\Delta\phi$, since we work in the nearly-localized regime. Such an expansion enables us to solve for the eigenstates analytically.

We also obtain the approximate ground states of a Josephson junction in a variety of configurations. In particular, the ground state is a squeezed vacuum state for either an isolated junction in a potential minimum or a junction in a superconducting ring without external flux and in the global potential minimum. On the other hand, if the junction is current-biased, or there is an external flux through the superconducting ring, the ground state is a squeezed coherent state. In both of the above cases, we calculate the corresponding

fluctuations of the charge and phase difference over the junction in these states. The squeezing factors are determined by the parameter $\lambda = \sqrt{E_J/E_C}$, where E_J is the Josephson coupling energy and E_C is the charging energy of the junction. The squeezing effect is strong when λ is small. Since our working limit is at large λ, a compromise should be reached in order to both preserve the effectiveness of our approximation and maximize the squeezing effect.

The excited states of a Josephson junction in different circumstances are also obtained. We show that these excited states are similar to the number states of a simple harmonic oscillator but with different fluctuation properties.

One can think of the squeezing effect intuitively in terms of the expanded $\cos\phi$ term. The second-order term in the expansion provides a harmonic potential, which has constant quantum fluctuations in its eigenstates. The fourth-order term introduces a time-dependent modulation to these states, thus also modulates the intrinsic quantum noise in the states.

We have also studied the time evolution of quantum fluctuations of a Josephson junction under the rotating wave approximation, which enforces energy conservation. When calculating the fluctuations of the canonical momentum and coordinate in the free oscillator cases (e.g., a Josephson junction coupled to a capacitor or a superconducting ring) and in the linearly driven cases (e.g., a current biased junction), we find that in the small-phase, small-time limit, there is squeezing when we have an initial coherent state, and no squeezing if we have an initial vacuum state.

According to the calculations for $\langle(\Delta\phi)^2\rangle$ and $\langle(\Delta n)^2\rangle$, a large-area junction, which has large E_J and small E_C, should have small fluctuations in phase and large fluctuations in particle number. On the other hand, a small-area junction has smaller Josephson coupling and smaller junction capacitance (which means a larger charging energy E_C); thus it should have larger phase fluctuations but smaller number fluctuations. Therefore, our calculations of $\langle(\Delta\phi)^2\rangle$ and $\langle(\Delta n)^2\rangle$ provide results qualitatively consistent with experiments. Further experimental studies, with thermal and environmental noise smaller than the intrinsic quantum noise, are needed to quantitatively verify our results.

Chapter 6

Conclusions

This thesis cuts through different sub-areas of physics: quantum optics and condensed matter. The proposals contained in it open a new area of research: the control of quantum fluctuations in condensed matter systems. Here we theoretically study the quantum fluctuation properties of two condensed matter systems: phonons and Josephson junctions. In particular, we investigate several approaches for the generation and detection of squeezed states in these systems.

We first study coherent and squeezed quantum states of phonons. The latter allow the possibility of modulating the quantum fluctuations of atomic displacements below the zero-point quantum noise level of coherent states. The expectation values and quantum fluctuations of both the atomic displacement and the lattice amplitude operators are calculated in these states—in most cases analytically. We also study the possibility of generating squeezed phonon states using a variety of different approaches, including a three-phonon parametric down-conversion, a second-order Raman process, a short-time single-mode squeezing mechanism, and a polariton-based approach. The first two are based on phonon-phonon interactions, while the last two exploit photon-phonon interactions. Furthermore, we analyze several possible detection schemes, point out their advantages and disadvantages, and propose one based on reflectivity measurements.

For the Josephson junctions, we study their quantum fluctuation properties in the limit of large coupling and small charging energies, when the eigenstates of the systems can be treated approximately as being localized. We consider Josephson junctions in a variety of circuit configurations, e.g., coupled to one or several of the following elements: a capacitor, an inductor (in a superconducting ring), and an applied current source. By solving their effective Schrödinger equations for a range of parameters, we obtain squeezed vacuum and coherent states as the ground states of a Josephson junction in several of these configura-

tions. We calculate the uncertainties of its canonical momentum (charge) and coordinate (phase), and also study the time-evolution of an arbitrary operator of the Josephson junction system given an arbitrary initial state. Furthermore, the time evolution and quantum fluctuations of the conjugate variables (phase and charge) are studied using the rotating wave approximation, where we also find that, in a certain regime of parameters, the quantum fluctuations of the charge and phase difference over the junction can be squeezed below their coherent-state values.

Appendix A

Coherent States

A.1 Coherence and Photon Coherent States

The nth-order correlation function of a photon system is defined as

$$G^{(n)}_{\mu_1\cdots\mu_{2n}}(x_1, x_2, \ldots, x_{2n}) = Tr\left\{\rho E^{(-)}_{\mu_1}(x_1)\cdots E^{(-)}_{\mu_n}(x_n) E^{(+)}_{\mu_{n+1}}(x_{n+1})\cdots E^{(+)}_{\mu_{2n}}(x_{2n})\right\}, \quad \text{(A.1)}$$

where the superscripts $(\pm)$ refer to the positive and negative frequency components of the electric field $\mathbf{E}$, and E_{μ_i} refers to the μ_ith spatial component of $\mathbf{E}$,

$$\mathbf{E}^{(+)}(\mathbf{r}, t) = i\sum_{\mathbf{k}} \sqrt{\frac{\hbar\omega_{\mathbf{k}}}{2}}\, a_{\mathbf{k}}\, \mathbf{u}_{\mathbf{k}}(\mathbf{r})\, e^{-i\omega_{\mathbf{k}} t}, \quad \text{(A.2)}$$

$$\mathbf{E}^{(-)}(\mathbf{r}, t) = -i\sum_{\mathbf{k}} \sqrt{\frac{\hbar\omega_{\mathbf{k}}}{2}}\, a^{\dagger}_{\mathbf{k}}\, \mathbf{u}^{*}_{\mathbf{k}}(\mathbf{r})\, e^{i\omega_{\mathbf{k}} t}. \quad \text{(A.3)}$$

The nth-order coherence is defined as the factorization of up to the nth-order correlation function $G^{(n)}_{\mu_1\cdots\mu_{2n}}$. If the state is an eigenstate of the annihilation operators $a_{\mathbf{k}}$, the correlation functions can be factorized straightforwardly. Therefore, these eigenstates are introduced as the basis for the quantum description of coherent light. They are called coherent states [7].

A single-mode coherent state $|\alpha\rangle$ is an eigenstate of the annihilation operator a:

$$a|\alpha\rangle = \alpha|\alpha\rangle, \quad \text{(A.4)}$$

where $\alpha = |\alpha|e^{i\phi}$ is an arbitrary complex number. An equivalent expression is

$$|\alpha\rangle = D(\alpha)|0\rangle, \quad \text{(A.5)}$$

$$D(\alpha) = \exp(\alpha a^{\dagger} - \alpha^{*} a). \quad \text{(A.6)}$$

The displacement operator $D(\alpha)$ transforms the annihilation operator a as

$$D^{-1}(\alpha)\, a\, D(\alpha) = a + \alpha. \quad \text{(A.7)}$$

In the number state basis, a coherent state can be expressed as,

$$|\alpha\rangle = e^{-\frac{|\alpha|^2}{2}} \sum_n \frac{\alpha^n}{\sqrt{n!}} |n\rangle , \tag{A.8}$$

and the probability distribution of the coherent state in the number state basis is

$$|\langle n|\alpha\rangle|^2 = \frac{\alpha^{2n} e^{-|\alpha|^2}}{n!} , \tag{A.9}$$

which is a Poisson distribution.

In the coordinate and momentum representations, the wavefunctions of a coherent state $|\alpha\rangle$ are

$$\langle q|\alpha\rangle = \left(\frac{\omega}{\pi\hbar}\right)^{1/4} \exp\left(-\left[\sqrt{\frac{\omega}{2\hbar}} q - \alpha\right]^2\right) , \tag{A.10}$$

$$\langle p|\alpha\rangle = \left(\frac{1}{\pi\hbar\omega}\right)^{1/4} \exp\left(-\left[\sqrt{\frac{1}{2\hbar\omega}} p + i\alpha\right]^2\right) . \tag{A.11}$$

Therefore, a coherent state is a Gaussian wave packet in both coordinate and momentum spaces.

The generalized coordinate and momentum q and p (which satisfy the commutator $[q, p] = i\hbar$) can be expressed in terms of a and $a^\dagger$,

$$q = \sqrt{\frac{\hbar}{2\omega}} (a + a^\dagger) , \tag{A.12}$$

$$p = -i\sqrt{\frac{\hbar\omega}{2}} (a - a^\dagger) . \tag{A.13}$$

Their variances in a coherent state satisfy

$$\langle (\Delta p)^2 \rangle_{\rm coh} \times \langle (\Delta q)^2 \rangle_{\rm coh} = \frac{1}{4} \hbar^2 , \tag{A.14}$$

which is at the lower limit of the Heisenberg uncertainty relation. In other words, a coherent state is a minimum-uncertainty state. If we define dimensionless quadrature operators X and P as

$$X = \frac{1}{\sqrt{2}} (a + a^\dagger) = (\omega/\hbar)^{1/2} \, q, \tag{A.15}$$

$$P = -\frac{i}{\sqrt{2}} (a - a^\dagger) = (\hbar\omega)^{-1/2} \, p, \tag{A.16}$$

there will be a circular uncertainty region in the complex α plane for any coherent state,

$$\langle (\Delta X)^2 \rangle_{\rm coh} = \langle (\Delta P)^2 \rangle_{\rm coh} = \frac{1}{2} . \tag{A.17}$$

The uncertainties in an arbitrary coherent state are the same as in the vacuum state, which means that coherent states are as quiet as the vacuum. Fig. 1.1 graphically illustrates such a circular uncertainty region for a coherent state.

A.2 Derivation of the Coherent Phonon Displacement Operator

In Appendix A on coherent states, a displacement operator $D(\alpha) = \exp(\alpha a^\dagger - \alpha^* a)$ was used to generate a coherent state $|\alpha\rangle = D(\alpha)|0\rangle$. Such an operator can be explicitly derived for phonons starting from the following Hamiltonian

$$\begin{cases} H_{\text{coherent}} &= H_0 + V \\ H_0 &= \sum_{\mathbf{q}} \hbar\omega_{\mathbf{q}} \left(b_{\mathbf{q}}^\dagger b_{\mathbf{q}} + \frac{1}{2}\right) \\ V &= \sum_{\mathbf{q}} \left\{\lambda_{\mathbf{q}}\, e^{-i\omega_{\mathbf{q}} t}\, b_{\mathbf{q}}^\dagger + \lambda_{\mathbf{q}}^*\, e^{i\omega_{\mathbf{q}} t}\, b_{\mathbf{q}}\right\}, \end{cases} \tag{A.18}$$

which represents an ensemble of independent phonons H_0 interacting via V with an external source, such as a beam of light. Notice that the external pump is on resonance with the relevant phonon mode. Here the strength of the interaction is given by the $\lambda_{\mathbf{q}}(t)$s, which are smooth functions of time. A convenient way to find the time-evolution operator of this system is to first change to the interaction picture. The transformation matrix is

$$U_0 = e^{-iH_0 t/\hbar} = e^{-i\sum_{\mathbf{q}} \omega_{\mathbf{q}} t (b_{\mathbf{q}}^\dagger b_{\mathbf{q}} + \frac{1}{2})}. \tag{A.19}$$

In the interaction picture, the Schrödinger equation becomes

$$i\hbar \frac{\partial}{\partial t} U_I = V_I U_I, \tag{A.20}$$

$$|\psi(t)\rangle_I = U_I |\psi(0)\rangle_I, \tag{A.21}$$

$$\begin{aligned} V_I &= U_0^{-1} V U_0 \\ &= \sum_{\mathbf{q}} \left\{ e^{it/\hbar \sum_{\mathbf{q}} \hbar\omega_{\mathbf{q}} (b_{\mathbf{q}}^\dagger b_{\mathbf{q}} + \frac{1}{2})}\, \lambda_{\mathbf{q}}(t)\, b_{\mathbf{q}}^\dagger\, e^{-it/\hbar \sum_{\mathbf{q}} \hbar\omega_{\mathbf{q}} (b_{\mathbf{q}}^\dagger b_{\mathbf{q}} + \frac{1}{2})} + h.c. \right\}, \end{aligned} \tag{A.22}$$

where U_I is the time-evolution operator in the interaction picture. Recall that for a single mode

$$\begin{aligned} a e^{\beta a^\dagger a} &= a \sum_{n=0}^{\infty} \frac{\beta^n}{n!} (a^\dagger a)^n = \sum_{n=0}^{\infty} \frac{\beta^n}{n!} (a^\dagger a + 1)^n a \\ &= e^{\beta(a^\dagger a + 1)} a = e^{\beta a^\dagger a} a e^{\beta}, \end{aligned} \tag{A.23}$$

so that V_I can be simplified to

$$V_I = \sum_{\mathbf{q}} \left(\lambda_{\mathbf{q}}\, b_{\mathbf{q}}^\dagger + h.c.\right), \tag{A.24}$$

which is time-independent. The equation for U_I thus becomes

$$\frac{\partial}{\partial t} U_I(t) = -\frac{i}{\hbar} \sum_{\mathbf{q}} \left\{\lambda_{\mathbf{q}}\, b_{\mathbf{q}}^\dagger + h.c.\right\} U_I(t). \tag{A.25}$$

This differential equation can be integrated directly, because the factor before $U_I(t)$ on the right hand side of the equation commutes with $U_I(t)$. The solution is

$$U_I(t) = \prod_{\mathbf{q}} \exp\left\{\Lambda_{\mathbf{q}}(t)\, b_{\mathbf{q}}^\dagger - \Lambda_{\mathbf{q}}^*(t)\, b_{\mathbf{q}}\right\}, \tag{A.26}$$

$$\Lambda_{\mathbf{q}}(t) = -\frac{i}{\hbar}\lambda_{\mathbf{q}}\, t\,. \tag{A.27}$$

So $U_I(t)$ is a multi-mode displacement operator in the interaction picture. It is a generalization of the single-mode case where $D(\alpha) = \exp(\alpha a^\dagger - \alpha^* a)$. Here the magnitude of the coherent displacement grows linearly with time. Such a linear growth (which will be eventually suppressed in any real experiment) originates from the continuous pumping and our neglect of any dissipation mechanism.

Changing back to the Schrödinger picture, the time-evolution operator $U_S(t)$ (so that $|\psi(t)\rangle = U_S(t)|\psi(0)\rangle$) will have an additional free oscillator term in it

$$U_S(t) = \prod_{\mathbf{q}} \exp(-i\omega_{\mathbf{q}} t b_{\mathbf{q}}^\dagger b_{\mathbf{q}}) \exp\left\{\Lambda_{\mathbf{q}}(t)\, b_{\mathbf{q}}^\dagger - \Lambda_{\mathbf{q}}^*(t)\, b_{\mathbf{q}}\right\}. \tag{A.28}$$

If the initial state is a vacuum state $|0\rangle$, the state vector at time t will be

$$\begin{aligned} |\psi(t)\rangle &= U_S(t)|0\rangle \\ &= \prod_{\mathbf{q}} \exp\left\{-i\omega_{\mathbf{q}} t b_{\mathbf{q}}^\dagger b_{\mathbf{q}}\right) \exp(\Lambda_{\mathbf{q}}(t)\, b_{\mathbf{q}}^\dagger - \Lambda_{\mathbf{q}}^*(t)\, b_{\mathbf{q}}\Big\}|0\rangle \\ &= \prod_{\mathbf{q}} \exp(-i\omega_{\mathbf{q}} t b_{\mathbf{q}}^\dagger b_{\mathbf{q}})|\Lambda_{\mathbf{q}}(t)\rangle \\ &= \prod_{\mathbf{q}} \otimes |\Lambda_{\mathbf{q}}(t)\, e^{-i\omega_{\mathbf{q}} t}\rangle\,. \end{aligned} \tag{A.29}$$

Therefore the effect of the free-oscillator time-evolution operator $e^{-i\omega_{\mathbf{q}} t b_{\mathbf{q}}^\dagger b_{\mathbf{q}}}$ is to make the coherent displacement vector $|\Lambda_{\mathbf{q}}(t)\rangle$ rotate around the origin in the $(X, P) = (Re\{\alpha\}, Im\{\alpha\})$ phase space. The state vector $|\Lambda_{\mathbf{q}}(t)\, e^{-i\omega_{\mathbf{q}} t}\rangle$ is still a coherent state.

In the cases when the external pump is not on resonance with the relevant phonon mode, so that $\lambda_{\mathbf{q}} e^{-i\omega_{\mathbf{q}} t}$ in Eq. (A.18) is replaced by $\lambda_{\mathbf{q}}(t)$ with an arbitrary time-dependence, the time-evolution operator for the $\mathbf{q}$ mode in the interaction picture can be written as

$$U_{\mathbf{q}}(t_0, t) = T \exp\left\{-\frac{i}{\hbar}\int_{t_0}^{t} V_I(\mathbf{q}, \tau) d\tau\right\} \tag{A.30}$$

$$V_I(\mathbf{q}, \tau) = \lambda_{\mathbf{q}}(\tau)\, b_{\mathbf{q}}^\dagger + \lambda_{\mathbf{q}}^*(\tau)\, b_{\mathbf{q}}\,, \tag{A.31}$$

where T is the time-ordering operator. Since this Hamiltonian is time-dependent, we cannot integrate the Schrödinger equation directly like we have done in the on-resonance cases. A

general approach we can take to explicitly write out the time-evolution operator is the Magnus method [66]. According to the Magnus approach, $U_I(t)$ can be expressed as

$$U_I(t) = \exp\left[-iA_1(t,t_0) - iA_2(t,t_0) - iA_3(t,t_0) + \dots\right], \tag{A.32}$$

where (dropping the mode label $\mathbf{q}$)

$$A_1(t,t_0) = \frac{1}{\hbar}\int_{t_0}^{t} dt_1 V_I(t_1) \tag{A.33}$$

$$A_2(t,t_0) = \frac{1}{2!i\hbar}\int_{t_0}^{t} dt_2 \int_{t_0}^{t_2} dt_1 \left[V_I(t_1), V_I(t_2)\right] \tag{A.34}$$

$$A_3(t,t_0) = \frac{1}{3!i^2\hbar}\int_{t_0}^{t} dt_3 \int_{t_0}^{t_3} dt_2 \int_{t_2}^{t_0} dt_1 \left\{\left[V_I(t_1),\left[V_I(t_2),V_I(t_3)\right]\right] + \left[\left[V_I(t_1),V_I(t_2)\right],V_I(t_3)\right]\right\}. \tag{A.35}$$

Since our Hamiltonian $V_I(t)$ here is linear in $b_{\mathbf{q}}$ and $b_{\mathbf{q}}^{\dagger}$, the commutators (like the ones in A_3) equal to or higher than third-order all vanish. The second-order term A_2 can be calculated but will only give a global phase factor which is irrelevant when we calculate any expectation value.

Due to the fact that $V_I(t)$ is linear in $b_{\mathbf{q}}$ and $b_{\mathbf{q}}^{\dagger}$, we can obtain the time-evolution operator by directly solving the Schrödinger equation. In the interaction picture, the Schrödinger equation is (dropping the mode subscript $\mathbf{q}$, because we are treating a single-mode problem)

$$i\hbar\frac{\partial}{\partial t}|\Psi(t)\rangle = V_I(t)|\Psi(t)\rangle, \tag{A.36}$$

$$V_I(t) = \lambda(t)\,b^{\dagger} + \lambda^*(t)\,b. \tag{A.37}$$

Let us now make a transformation,

$$|\Psi(t)\rangle = \exp\left(\frac{1}{i\hbar}\int_0^t V_I(\tau)d\tau\right)|\Psi'(t)\rangle, \tag{A.38}$$

and substitute it into the Schrödinger equation. Thus we get

$$i\hbar\left[\frac{\partial}{\partial t}e^{\frac{1}{i\hbar}\int_0^t V_I(\tau)d\tau}\right]|\Psi'(t)\rangle + i\hbar e^{\frac{1}{i\hbar}\int_0^t V_I(\tau)d\tau}\frac{\partial}{\partial t}|\Psi'(t)\rangle = V_I(t)e^{\frac{1}{i\hbar}\int_0^t V_I(\tau)d\tau}|\Psi'(t)\rangle. \tag{A.39}$$

Let

$$A = \frac{1}{i\hbar}\int_0^t V_I(\tau)d\tau, \tag{A.40}$$

$$B = \frac{\partial A}{\partial t} = \frac{1}{i\hbar}V_I(t). \tag{A.41}$$

Thus $[A,B] = c$ where c is a c-number. We need to simplify the expression $\partial e^A/\partial t$, which can be expressed as

$$\frac{\partial}{\partial t}e^A = \frac{\partial}{\partial t}\sum_{n=0}^{\infty}\frac{A^n}{n!}. \tag{A.42}$$

It can be easily shown that

$$\frac{\partial}{\partial t}A^n = nBA^{n-1} + \frac{n(n-1)}{2}cA^{n-2}, \tag{A.43}$$

therefore,

$$\frac{\partial}{\partial t}e^A = \left(B + \frac{c}{2}\right)e^A. \tag{A.44}$$

The Schrödinger equation can thus be greatly simplified to

$$i\hbar|\Psi'(t)\rangle = -\frac{c(t)}{2}|\Psi'(t)\rangle. \tag{A.45}$$

The equation can now be integrated, and the results are

$$|\Psi'(t)\rangle = \exp\left\{-\frac{1}{2i\hbar}\int_0^t c(\tau)d\tau\right\}|\Psi'(0)\rangle, \tag{A.46}$$

and

$$|\Psi(t)\rangle = \exp\left\{-\frac{1}{2i\hbar}\int_0^t c(\tau)d\tau\right\}\exp\left\{\frac{1}{i\hbar}\int_0^t V_I(\tau)d\tau\right\}|\Psi(0)\rangle. \tag{A.47}$$

Therefore, the state $|\Psi(t)\rangle$ is a coherent state if the initial state is a vacuum or coherent state. The global phase factor is not important because it will cancel out when we calculate any expectation value.

Appendix B

Quadrature Squeezed States

Quadrature squeezed states are generalized coherent states [9, 10, 11, 58, 67, 70]. The error circle in phase space for coherent states becomes an ellipse for quadrature squeezed states, so that the variance of one of the quadratures can be smaller than the coherent state value. This is schematically illustrated in Figs. 1.1 and 1.2. This property makes the squeezed states useful in situations where we need to observe one of the quadratures with very high accuracy.

B.1 Single-mode Quadrature Squeezed States

A single-mode squeezed state is generated by a squeezing operator $S(\xi)$ as follows

$$|\alpha, \xi\rangle = D(\alpha)\, S(\xi)\, |0\rangle\,, \tag{B.1}$$

$$S(\xi) = \exp\left(\frac{\xi^*}{2} a^2 - \frac{\xi}{2} a^{\dagger 2}\right), \tag{B.2}$$

where $D(\alpha)$ is the coherent state displacement operator with $\alpha = |\alpha| e^{i\phi}$, $S(\xi)$ is the single-mode squeezing operator, and $\xi = r e^{i\theta}$ is a complex number, with $r \geq 0$, $0 \leq \theta < 2\pi$. The annihilation operator is transformed by the squeezing operator as follows

$$S^{-1}(\xi)\, a\, S(\xi) = a \cosh r - a^\dagger e^{i\theta} \sinh r\,. \tag{B.3}$$

With the help of the above transformation, it can be proved that in a squeezed state,

$$\langle (\Delta X)^2 \rangle_{\rm sq} = \frac{1}{2}\left(e^{-2r} \cos^2\frac{\theta}{2} + e^{2r} \sin^2\frac{\theta}{2}\right), \tag{B.4}$$

$$\langle (\Delta P)^2 \rangle_{\rm sq} = \frac{1}{2}\left(e^{-2r} \sin^2\frac{\theta}{2} + e^{2r} \cos^2\frac{\theta}{2}\right), \tag{B.5}$$

$$\langle (\Delta X)^2 \rangle_{\rm sq} \langle (\Delta P)^2 \rangle_{\rm sq} = \frac{1}{4}\left(1 + \sin^2\theta \sinh^2 2r\right) \geq \frac{1}{4}\,. \tag{B.6}$$

Notice that the variances are independent of the coherent amplitude α. In particular, when $\theta = 0$, the above relations become

$$\langle(\Delta X)^2\rangle_{\rm sq} = \frac{1}{2}e^{-2r}, \tag{B.7}$$

$$\langle(\Delta P)^2\rangle_{\rm sq} = \frac{1}{2}e^{2r}, \tag{B.8}$$

$$\langle(\Delta X)^2\rangle_{\rm sq}\langle(\Delta P)^2\rangle_{\rm sq} = \frac{1}{4}, \tag{B.9}$$

where the minimum uncertainty relation is satisfied while $\langle(\Delta X)^2\rangle_{\rm sq}$ can be smaller than $1/2$.

The average number of particles in a single-mode squeezed state is

$$\langle\hat{n}\rangle_{\rm sq} = |\alpha|^2 + \sinh^2 r\,. \tag{B.10}$$

Assuming that $\langle\hat{n}\rangle_{\rm sq}$ is far larger than $\sinh^2 r$ (i.e., $|\alpha|^2 \gg 0$ and the state is highly excited above the vacuum state), we can calculate similar relations for the number-phase (n, ψ) conjugate variables,

$$\langle(\Delta\hat{n})^2\rangle_{\rm sq} = |\alpha|^2\left(e^{-2r}\cos^2(\phi - \frac{\theta}{2}) + e^{2r}\sin^2(\phi - \frac{\theta}{2})\right), \tag{B.11}$$

$$\langle(\Delta\hat{\psi})^2\rangle_{\rm sq} = \frac{1}{4|\alpha|^2}\left(e^{-2r}\sin^2\left(\phi - \frac{\theta}{2}\right) + e^{2r}\cos^2\left(\phi - \frac{\theta}{2}\right)\right). \tag{B.12}$$

Here $\hat{n}$ is the number operator and $\hat{\psi}$ is the phase operator defined as the angle, measured from the origin, spanned by the uncertainty area [58]. Here we denote operators with tilde to distinguish between scalar angles (such as θ and ϕ) and the phase operator $\hat{\psi}$. In the case $|\alpha|^2 \gg 0$, we can see that for $\phi = \theta/2$,

$$\langle(\Delta\hat{n})^2\rangle_{\rm sq} = |\alpha|^2 e^{-2r}, \tag{B.13}$$

$$\langle(\Delta\hat{\psi})^2\rangle_{\rm sq} = \frac{1}{4|\alpha|^2}e^{2r}, \tag{B.14}$$

$$\tag{B.15}$$

thus the fluctuation in the number operator $\hat{n}$ is squeezed. For $\phi = \theta/2 + \pi/2$,

$$\langle(\Delta\hat{n})^2\rangle_{\rm sq} = |\alpha|^2 e^{2r}, \tag{B.16}$$

$$\langle(\Delta\hat{\psi})^2\rangle_{\rm sq} = \frac{1}{4|\alpha|^2}e^{-2r}, \tag{B.17}$$

$$\tag{B.18}$$

so that the fluctuation in the phase operator $\hat{\psi}$ is squeezed. In either case,

$$\langle(\Delta\hat{n})^2\rangle_{\rm sq}\langle(\Delta\hat{\psi})^2\rangle_{\rm sq} = \frac{1}{4}\,, \tag{B.19}$$

which agrees with the minimum uncertainty relation.

In the three special cases considered above ($\theta = 0$, $\phi = \theta/2$, and $\phi = \theta/2 + \pi/2$), the uncertainty for one of the quadratures is smaller than the coherent state value.

B.2 Two-mode Quadrature Squeezed States

It is also possible to generate two-mode quadrature squeezed states [58],

$$|\alpha_{\mathbf{q}_1},\, \alpha_{\mathbf{q}_2},\, \xi\rangle = D_{\mathbf{q}_1}(\alpha_{\mathbf{q}_1})\, D_{\mathbf{q}_2}(\alpha_{\mathbf{q}_2})\, S_{\mathbf{q}_1,\mathbf{q}_2}(\xi)\, |0\rangle\,, \tag{B.20}$$

$$S_{\mathbf{q}_1,\mathbf{q}_2}(\xi) = \exp\left(\xi^* a_{\mathbf{q}_1} a_{\mathbf{q}_2} - \xi a^\dagger_{\mathbf{q}_1} a^\dagger_{\mathbf{q}_2}\right), \tag{B.21}$$

where the Ds are still displacement operators, and $S_{\mathbf{q}_1,\mathbf{q}_2}(\xi)$ is the two-mode squeezing operator, where $\xi = re^{i\theta}$. It will transform the creation and annihilation operators as follows

$$S^{-1}_{\mathbf{q}_1,\mathbf{q}_2}(\xi)\, a_{\mathbf{q}_1}\, S_{\mathbf{q}_1,\mathbf{q}_2}(\xi) = a_{\mathbf{q}_1} \cosh r - a^\dagger_{\mathbf{q}_2}\, e^{i\theta} \sinh r\,, \tag{B.22}$$

$$S^{-1}_{\mathbf{q}_1,\mathbf{q}_2}(\xi)\, a_{\mathbf{q}_2}\, S_{\mathbf{q}_1,\mathbf{q}_2}(\xi) = a_{\mathbf{q}_2} \cosh r - a^\dagger_{\mathbf{q}_1}\, e^{i\theta} \sinh r\,. \tag{B.23}$$

For the two-mode squeezed state, the generalized quadrature operators are defined as

$$X_{\mathbf{q}_1,\mathbf{q}_2} = \left(a_{\mathbf{q}_1} + a^\dagger_{\mathbf{q}_1} + a_{\mathbf{q}_2} + a^\dagger_{\mathbf{q}_2}\right)/2^{3/2} \tag{B.24}$$

$$P_{\mathbf{q}_1,\mathbf{q}_2} = \left(a_{\mathbf{q}_1} - a^\dagger_{\mathbf{q}_1} + a_{\mathbf{q}_2} - a^\dagger_{\mathbf{q}_2}\right)/2^{3/2} \tag{B.25}$$

Using the above relations, we find that

$$\langle(\Delta X_{\mathbf{q}_1,\mathbf{q}_2})^2\rangle_{\rm sq} = \frac{1}{4}\left(e^{-2r}\cos^2\frac{\theta}{2} + e^{2r}\sin^2\frac{\theta}{2}\right), \tag{B.26}$$

$$\langle(\Delta P_{\mathbf{q}_1,\mathbf{q}_2})^2\rangle_{\rm sq} = \frac{1}{4}\left(e^{-2r}\sin^2\frac{\theta}{2} + e^{2r}\cos^2\frac{\theta}{2}\right). \tag{B.27}$$

Therefore, the variance of one of the quadrature operators can decrease while the other one simultaneously increases to satisfy the uncertainty principle.

B.3 Derivation of the Quadrature Squeezing Operator

In this Appendix we prove that the Hamiltonian $H_{\mathbf{q}_1,\mathbf{q}_2}$ of Eq. (3.61) can generate a two-mode quadrature squeezed state in modes $\mathbf{q}_1$ and $\mathbf{q}_2$ from either a vacuum state $|0\rangle$ or a coherent state $|\alpha_{\mathbf{q}_1}, \alpha_{\mathbf{q}_2}\rangle$. Let us consider now the following two-mode Hamiltonian,

$$\begin{cases} H_{\mathbf{q}_1,\mathbf{q}_2} = H_0 + V_{\mathbf{q}_1,\mathbf{q}_2} \\ H_0 = \hbar\omega_{\mathbf{q}_1} b^\dagger_{\mathbf{q}_1} b_{\mathbf{q}_1} + \hbar\omega_{\mathbf{q}_2} b^\dagger_{\mathbf{q}_2} b_{\mathbf{q}_2} \\ V_{\mathbf{q}_1,\mathbf{q}_2} = \zeta\, e^{-i(\omega_{\mathbf{q}_1}+\omega_{\mathbf{q}_2})t} b^\dagger_{\mathbf{q}_1} b^\dagger_{\mathbf{q}_2} + \zeta^*\, e^{i(\omega_{\mathbf{q}_1}+\omega_{\mathbf{q}_2})t} b_{\mathbf{q}_1} b_{\mathbf{q}_2}\,. \end{cases} \tag{B.28}$$

where the external pump is on resonance with the driven system. In the interaction picture, $V_{\mathbf{q}_1,\mathbf{q}_2}$ becomes V_I:

$$V_I = \zeta\, b^\dagger_{\mathbf{q}_1} b^\dagger_{\mathbf{q}_2} + \zeta^*\, b_{\mathbf{q}_1} b_{\mathbf{q}_2}\,. \tag{B.29}$$

Now the interaction becomes independent of time, so that U_I, the time-evolution operator in the interaction picture, can be integrated out as

$$U_I = \exp\left\{\xi^*(t)\, b_{\mathbf{q}_1} b_{\mathbf{q}_2} - \xi(t)\, b^\dagger_{\mathbf{q}_1} b^\dagger_{\mathbf{q}_2}\right\}, \tag{B.30}$$

$$\xi(t) = \frac{i}{\hbar}\zeta\, t, \tag{B.31}$$

and the state vector in the Schrödinger picture becomes,

$$|\psi(t)\rangle_s = \exp\left(\frac{-iH_0 t}{\hbar}\right) \exp\left\{\xi^*(t) b_{\mathbf{q}_1} b_{\mathbf{q}_2} - \xi(t) b^\dagger_{\mathbf{q}_1} b^\dagger_{\mathbf{q}_2}\right\} |\psi(0)\rangle. \tag{B.32}$$

The evolution operator is now factorized into a product of the free oscillator evolution operator and a squeezing operator. The free oscillator term only changes the phase of the squeezing effect. If $|\psi(0)\rangle = |0\rangle$, the state vector $|\psi(t)\rangle_s$ becomes

$$|\psi(t)\rangle_s = \exp\left(\frac{-iH_0 t}{\hbar}\right) |0, 0, \xi(t)\rangle\,, \tag{B.33}$$

which is a squeezed vacuum state. If the initial state is coherent, $|\psi(0)\rangle = |\alpha_{\mathbf{q}_1}, \alpha_{\mathbf{q}_2}\rangle$, the state vector $|\psi(t)\rangle_s$ becomes

$$|\psi(t)\rangle_s = \exp\left(\frac{-iH_0 t}{\hbar}\right) S_{\mathbf{q}_1,\mathbf{q}_2}(\xi(t))\, D_{\mathbf{q}_1}(\alpha_{\mathbf{q}_1})\, D_{\mathbf{q}_2}(\alpha_{\mathbf{q}_2})|0\rangle\,, \tag{B.34}$$

which is also a squeezed state, where $S_{\mathbf{q}_1,\mathbf{q}_2}(\xi(t))$ is the two-mode squeezing operator in Eq. (B.21). Since $S_{\mathbf{q}_1,\mathbf{q}_2}(\xi(t))$ does not commute with either $D_{\mathbf{q}_1}(\alpha_{\mathbf{q}_1})$ or $D_{\mathbf{q}_2}(\alpha_{\mathbf{q}_2})$, the state $|\psi(t)\rangle_s$ cannot be written directly as $D_{\mathbf{q}_1}(\alpha_{\mathbf{q}_1})\, D_{\mathbf{q}_2}(\alpha_{\mathbf{q}_2})\, S_{\mathbf{q}_1,\mathbf{q}_2}(\xi(t))|0\rangle$, or $|\alpha_{\mathbf{q}_1}, \alpha_{\mathbf{q}_2}, \xi(t)\rangle$. However, the variance of $X_{\mathbf{q}_1,\mathbf{q}_2}$ is now

$$\langle\psi(t)|(\Delta X_{\mathbf{q}_1,\mathbf{q}_2})^2|\psi(t)\rangle = \frac{1}{4}\left(e^{-2r}\cos^2\frac{\theta}{2} + e^{2r}\sin^2\frac{\theta}{2}\right), \tag{B.35}$$

which is exactly the same as in the two-mode squeezed state $|\alpha_{\mathbf{q}_1}, \alpha_{\mathbf{q}_2}, \xi(t)\rangle$. Therefore, $|\psi(t)\rangle_s$ is also a squeezed state.

Thus, here we have proven that $H_{\mathbf{q}_1,\mathbf{q}_2}$ can generate a two-mode squeezed state $|\psi(t)\rangle_s$ from a vacuum or coherent initial state.

B.4 Factorizing the Squeezing and Displacement Operators

The Baker-Hausdorff formula [6] states that

$$e^{A+B} = e^{A}e^{B}e^{-[A,B]/2}, \tag{B.36}$$

when $[A,[A,B]] = 0$ and $[B,[A,B]] = 0$. When these two conditions are not satisfied, the above relation has to be modified. Here we are interested in the case when

$$A = \alpha a - \alpha^* a^\dagger, \tag{B.37}$$

$$B = \beta a^2 - \beta^* a^{\dagger 2}. \tag{B.38}$$

From the above two expressions, we obtain

$$\begin{aligned} [A,B] &= [\alpha a - \alpha^* a^\dagger, \beta a^2 - \beta^* a^{\dagger 2}] \\ &= 2\beta\alpha^* a - 2\beta^*\alpha a^\dagger \\ &= C, \end{aligned} \tag{B.39}$$

and

$$\begin{aligned} [A,[A,B]] &= [A,C] \\ &= -4i\,\mathrm{Im}(\alpha^2\beta^*). \end{aligned} \tag{B.40}$$

Therefore, C is also a linear operator of a and $a^\dagger$ (like A), and D is a constant instead of being 0. Therefore, e^{A+B} cannot be factorized by using the Baker-Hausdorff formula. Let us now try to find an alternative way to factorize this operator.

First, let us define the function

$$f(\lambda) = e^{\lambda A}e^{\lambda B}. \tag{B.41}$$

We can then calculate the derivative of f:

$$\frac{df(\lambda)}{d\lambda} = e^{\lambda A}(A+B)e^{\lambda B} = Af(\lambda) + e^{\lambda A}Be^{\lambda B}. \tag{B.42}$$

To further simplify the right hand side of the above relation, we need to calculate $[e^{\lambda A}, B]$:

$$[e^{\lambda A}, B] = \sum_0^\infty \frac{\lambda^n}{n!}[A^n, B]. \tag{B.43}$$

Since

$$\begin{aligned}
[A^n, B] &= A^{n-1}[A, B] + [A^{n-1}, B]A \\
&= A^{n-1}C + [A^{n-1}, B]A \\
&= 2A^{n-1}C - DA^{n-2} + [A^{n-2}, B]A^2 \\
&= nA^{n-1}C - \frac{n(n-1)}{2}DA^{n-2}\,,
\end{aligned} \tag{B.44}$$

so

$$\begin{aligned}
[e^{\lambda A}, B] &= \sum_0^\infty \frac{\lambda^n}{(n-1)!}A^{n-1}C - \sum_0^\infty \frac{\lambda^n}{2(n-2)!}DA^{n-2} \\
&= \lambda e^{\lambda A}C - \frac{\lambda^2}{2}De^{\lambda A}\,.
\end{aligned} \tag{B.45}$$

Therefore,

$$\frac{df(\lambda)}{d\lambda} = (A+B)f(\lambda) - \frac{\lambda^2}{2}Df(\lambda) + \lambda e^{\lambda A}Ce^{\lambda B}\,. \tag{B.46}$$

Similar to $[e^{\lambda A}, B]$, we can calculate $[e^{\lambda A}, C]$. The result is even simpler:

$$[e^{\lambda A}, C] = \lambda De^{\lambda A}\,. \tag{B.47}$$

Now we finally arrive at the expression

$$\frac{df(\lambda)}{d\lambda} = (A+B)f(\lambda) + \lambda Cf(\lambda) + \frac{\lambda^2}{2}Df(\lambda)\,. \tag{B.48}$$

Integrating this equation, we can get an explicit expression for $f(\lambda)$:

$$f(\lambda) = f(0)\,e^{\lambda(A+B)+\frac{\lambda^2}{2}C+\frac{\lambda^3}{6}D}\,. \tag{B.49}$$

Since $f(0) = 1$ and $f(1) = e^A e^B$, we get a relation

$$e^A e^B = e^{(A+B)+C/2+D/6}\,. \tag{B.50}$$

Recall that D is a complex number, so

$$e^{(A+C/2)+B} = e^A e^B e^{D/6}\,. \tag{B.51}$$

If $A' = A + C/2 = \gamma a - \gamma^* a^\dagger$, then γ satisfies

$$\gamma = \alpha + \alpha^*\beta\,. \tag{B.52}$$

We can calculate α when β and γ are known. Then we are able to factorize the operator $e^{A'+B}$ into a product of two distinct operators. Here we summarize our results below

$$e^{A'+B} = e^{A}e^{B}e^{D/6}, \tag{B.53}$$

$$A' = \gamma a - \gamma^* a^\dagger, \tag{B.54}$$

$$B = \beta a^2 - \beta^* a^{\dagger 2}, \tag{B.55}$$

$$A = \alpha a - \alpha^* a^\dagger, \tag{B.56}$$

$$D = -4i\mathrm{Im}(\alpha^2\beta^*), \tag{B.57}$$

$$\gamma = \alpha + \alpha^*\beta. \tag{B.58}$$

Appendix C

Derivation of the Phonon Master Equation

In this Appendix we derive the phonon master equation, Eq. (3.109) in Section 3.4.4. In the interaction picture, the density operator for the system and the reservoir as a whole satisfies the Schrödinger equation

$$\frac{\partial P_{PR}}{\partial t} = -\frac{i}{\hbar}\left[V_I(t-t_0),\, P_{PR}\right] . \tag{C.1}$$

Integrating this equation to second order in $V_I(t-t_0)$, we get,

$$\begin{aligned} P_{PR}(t) &= P_{PR}(t_0) - \frac{i}{\hbar}\int_{t_0}^{t} dt' \left[V_I(t'-t_0),\, P_{PR}(t_0)\right] \\ &\quad -\frac{1}{\hbar^2}\int_{t_0}^{t} dt' \int_{t_0}^{t'} dt'' \left[V_I(t'-t_0),\, \left[V_I(t''-t_0)\, P_{PR}(t_0)\right]\right] . \end{aligned} \tag{C.2}$$

Taking the trace over the reservoir, we then have an equation for the reduced density operator for the system $\rho(t) = tr_r\{P_{PR}(t)\}$, where tr_r means "trace over the reservoir",

$$\begin{aligned} \rho(t) &= \rho(t_0) - \frac{i}{\hbar}\int_{t_0}^{t} dt'\; tr_r\left\{\left[V_I(t'-t_0),\, P_{PR}(t_0)\right]\right\} \\ &\quad -\frac{1}{\hbar^2}\int_{t_0}^{t} dt' \int_{t_0}^{t'} dt''\; tr_r\left\{\left[V_I(t'-t_0),\, \left[V_I(t''-t_0)\, P_{PR}(t_0)\right]\right]\right\} . \end{aligned} \tag{C.3}$$

Now we take a coarse-grained average. In other words, we assume

$$\dot{\rho}(t) \cong \frac{\rho(t) - \rho(t-\tau)}{\tau} . \tag{C.4}$$

where $\tau = t - t_0$. This approximation works well when $\rho(t)$ changes slowly with time, so $\rho(t+\tau) \cong \rho(t)$, and $P_{PR}(t-\tau) \cong P_{PR}(t)$. After the coarse-graining, we get Eq. (3.104) in Section 3.4.4:

$$\dot{\rho}(t) \cong -\frac{i}{\hbar\tau}\int_{0}^{\tau} d\tau'\; tr_r\left\{V_I(\tau')P_{PR}(t)\right\}$$

$$-\frac{1}{\hbar^2\tau}\int_0^\tau d\tau' \int_0^{\tau'} d\tau''\; tr_r\left\{V_I(\tau')V_I(\tau'')P_{PR}(t) - V_I(\tau')P_{PR}(t)V_I(\tau'')\right\}$$
$$+h.c. \tag{C.5}$$

where

$$V_I(\tau) = \hbar b_p^\dagger F(\tau) + \hbar b_p F^\dagger(\tau)\,, \tag{C.6}$$
$$F(\tau) = -i\sum_{k,l}\lambda_{kl}\, b_k b_l\, e^{i(\omega_p-\omega_k-\omega_l)\tau}\,, \tag{C.7}$$

where the sum in $F(\tau)$ is over the reservoir modes. To get a master equation for $\rho(t)$, we substitute the particular $V_I(\tau)$ of Eq. (C.6) into Eq. (C.5). In doing this we get terms like $tr_r\left\{b_p^\dagger F(\tau)P_{PR}(t)\right\}$. Such a term can be factorized into a product of the system and reservoir operators,

$$tr_r\left\{b_p^\dagger F(\tau)P_{PR}(t)\right\} = b_p^\dagger\,\rho(t)\,tr_r\left\{F(\tau)\,\rho_r(H_R)\right\}\,. \tag{C.8}$$

This factorization is legitimate around t_0, when

$$P_{PR}(t_0) = \rho_{PR}(t_0) = \rho_P(t_0)\;\rho_r(H_R)\,, \tag{C.9}$$

where $\rho_{PR}(t_0)$ is the Schrödinger picture density operator for the system and the reservoir as a whole at t_0, $\rho_P(t_0)$ is the Schrödinger picture density operator for the system, while $\rho_r(H_R)$ is the Schrödinger picture density operator for the reservoir. Since the reservoir is in thermal equilibrium, the operator $\rho_r(H_R)$ is time-independent. However, at an arbitrary t, the above separation of the system and the reservoir is generally not exact because of the interaction between them. Nevertheless, the factorization is a good approximation as long as the interaction is weak.

After separating of the system and reservoir operators, Eq. (C.5) now becomes,

$$\begin{aligned}\dot\rho(t) = &-\frac{1}{\hbar^2\tau}\int_0^\tau d\tau' \int_0^{\tau'} d\tau''\Big\{b_p^\dagger b_p\,\rho(t)\,\langle F(\tau')F^\dagger(\tau'')\rangle_R \\ &-b_p\,\rho(t)\,b_p^\dagger\,\langle F(\tau'')F^\dagger(\tau')\rangle_R + b_p b_p^\dagger\,\rho(t)\,\langle F^\dagger(\tau')F(\tau'')\rangle_R \\ &-b_p^\dagger\,\rho(t)\,b_p\,\langle F^\dagger(\tau'')F(\tau')\rangle_R\Big\} + h.c.\end{aligned} \tag{C.10}$$

Since we have assumed that the reservoir is in thermal equilibrium, terms like $\langle F(\tau')\rangle_R$ and $\langle F(\tau'')F(\tau')\rangle_R$ have all vanished.

Now let us consider the reservoir averages. Keeping in mind that the reservoir is in thermal equilibrium, we have

$$\langle F(\tau')F^\dagger(\tau'')\rangle_R = \sum_{klmn}\lambda_{kl}\lambda^*_{mn}\,\langle b_k b_l b_m^\dagger b_n^\dagger\rangle_R\, e^{i\omega_p(\tau'-\tau'')-i(\omega_k\tau'+\omega_l\tau'-\omega_m\tau''-\omega_n\tau'')}$$

$$= \sum_{k\neq l} |\lambda_{kl}|^2 (n_k+1)(n_l+1) e^{i(\omega_p-\omega_k-\omega_l)(\tau'-\tau'')} + \sum_k |\lambda_{kk}|^2 (n_k^2+3n_k+2) e^{i(\omega_p-2\omega_k)(\tau'-\tau'')}, \quad \text{(C.11)}$$

and similarly

$$\langle F^\dagger(\tau')F(\tau'')\rangle_R = \sum_{k\neq l} |\lambda_{kl}|^2 n_k n_l e^{-i(\omega_p-\omega_k-\omega_l)(\tau'-\tau'')} + \sum_k |\lambda_{kk}|^2 (n_k^2-n_k) e^{-i(\omega_p-2\omega_k)(\tau'-\tau'')}. \quad \text{(C.12)}$$

The next step is to integrate over τ' and τ''. Let us first make a variable change for τ'': $T = \tau' - \tau''$. Then, the integral over τ'' becomes

$$\int_0^{\tau'} d\tau'' e^{-i(\omega_p-\omega_k-\omega_l)(\tau'-\tau'')} = \int_0^{\tau'} dT\, e^{-i(\omega_p-\omega_k-\omega_l)T}. \quad \text{(C.13)}$$

Since the reservoir is in thermal equilibrium, its correlation time is much shorter than any typical system time. Thus

$$\int_0^{\tau'} dT e^{-i(\omega_p-\omega_k-\omega_l)T} = \pi\delta(\omega_p-\omega_k-\omega_l). \quad \text{(C.14)}$$

The integral over τ' and τ'' now becomes, for instance,

$$\frac{1}{\hbar^2\tau}\int_0^{\tau} d\tau' \int_0^{\tau'} d\tau'' \langle F^\dagger(\tau')F(\tau'')\rangle_R = \frac{\pi}{\hbar^2}\sum_{k\neq l} |\lambda_{kl}|^2 n_k n_l \delta(\omega_p-\omega_k-\omega_l) + \frac{\pi}{\hbar^2}\sum_k |\lambda_{kk}|^2 (n_k^2-n_k)\delta(\omega_p-2\omega_k). \quad \text{(C.15)}$$

Now let us replace $\sum_k$ by $\int d\omega D(\omega)$, then

$$\frac{1}{\hbar^2\tau}\int_0^{\tau} d\tau' \int_0^{\tau'} d\tau'' \langle F^\dagger(\tau')F(\tau'')\rangle_R \quad \text{(C.16)}$$

$$\frac{\pi}{\hbar^2}\int_{0,\omega\neq\omega_p/2}^{\omega_p} d\omega\, D(\omega)\,|\lambda(\omega,\omega_p-\omega)|^2\, n_\omega n_{\omega_p-\omega} + \frac{\pi}{\hbar^2} D(\omega_p/2)\,\delta\omega\,|\lambda(\omega_p/2,\omega_p/2)|^2\,(n^2_{\omega_p/2}-n_{\omega_p/2}). \quad \text{(C.17)}$$

Here $\delta\omega$ is the line-width of the $\omega_p/2$ energy level in the reservoir. Substituting this result back into Eq. (C.10), we finally get the master equation for the system phonons:

$$\dot\rho(t) = -(\Gamma+\gamma)\left(b_p^\dagger b_p\rho - b_p\rho b_p^\dagger\right) - \Gamma\left(\rho b_p^\dagger b_p - b_p^\dagger\rho b_p\right) + h.\,c. \quad \text{(C.18)}$$

$$\Gamma = \frac{\pi}{\hbar^2}\int_{0,\omega\neq\omega_p/2}^{\omega_p} d\omega\, D(\omega)\,|\lambda(\omega,\omega_p-\omega)|^2\, n_\omega n_{\omega_p-\omega} + \frac{\pi}{\hbar^2} D(\omega_p/2)\,\delta\omega\,|\lambda(\omega_p/2,\omega_p/2)|^2\,(n^2_{\omega_p/2}-n_{\omega_p/2}) \quad \text{(C.19)}$$

$$\gamma = \frac{\pi}{\hbar^2}\int_{0,\omega\neq\omega_p/2}^{\omega_p} d\omega\, D(\omega)\,|\lambda(\omega,\omega_p-\omega)|^2\,(n_\omega+n_{\omega_p-\omega}+1) + \frac{\pi}{\hbar^2} D(\omega_p/2)\,\delta\omega\,|\lambda(\omega_p/2,\omega_p/2)|^2\,(2n_{\omega_p/2}+1), \quad \text{(C.20)}$$

which is Eq. (3.109) in Section 3.4.4.

In deriving this master equation, we have assumed that the interaction between the system and the reservoir is weak, and that the correlation or relaxation time for the reservoir is much shorter compared to that of the system. Therefore, this master equation is not exact. Nevertheless, as a first order approximation, this equation gives a reasonably good qualitative description of the system phonons.

Appendix D

Derivations for the Polariton Approach to Optical Phonon Squeezing

D.1 Transformation Matrix and Energies of Polaritons

The polariton operators $\alpha_{\mathbf{k}}$ are related to the photon and transverse optical phonon operators $a_{\mathbf{k}}$ and $b_{\mathbf{k}}$ through Eq. (3.116),

$$\alpha_{\mathbf{k}} = w a_{\mathbf{k}} + x b_{\mathbf{k}} + y a^{\dagger}_{-\mathbf{k}} + z b^{\dagger}_{-\mathbf{k}} \,. \tag{D.1}$$

Notice that we have dropped the polariton branch subscripts because they will automatically appear when we solve the secular equation for the polariton energy, as will be shown below. The coefficients w, x, y, and z can be determined using Eq. (3.119)

$$[\alpha_{\mathbf{k}} \,,\, H] = E_{\mathbf{k}}\, \alpha_{\mathbf{k}} \,, \tag{D.2}$$

where $E_{\mathbf{k}}$ is the polariton energy. Recall that the polariton Hamiltonian in the photon-phonon representation takes the form shown in Eq. (3.112). The Hamiltonian $H_{\text{polariton}}$ only mixes photons and phonons with the same or opposite wave vectors. Thus let us choose a particular $\mathbf{k}$ and $-\mathbf{k}$ and adopt a simplified notation. The Hamiltonian now takes the form

$$\begin{aligned} H'_{\text{polariton}} &= \varepsilon_1(a^{\dagger}_{\mathbf{k}}\, a_{\mathbf{k}} + a^{\dagger}_{-\mathbf{k}}\, a_{-\mathbf{k}}) + \varepsilon_2(b^{\dagger}_{\mathbf{k}}\, b_{\mathbf{k}} + b^{\dagger}_{-\mathbf{k}}\, b_{-\mathbf{k}}) \\ &\quad + \varepsilon_3 \left(a^{\dagger}_{\mathbf{k}} b_{\mathbf{k}} - a_{\mathbf{k}} b^{\dagger}_{\mathbf{k}} - a_{\mathbf{k}} b_{-\mathbf{k}} + a^{\dagger}_{-\mathbf{k}} b^{\dagger}_{\mathbf{k}}\right) \\ &\quad + \varepsilon_3 \left(a^{\dagger}_{-\mathbf{k}} b_{-\mathbf{k}} - a_{-\mathbf{k}} b^{\dagger}_{-\mathbf{k}} - a_{-\mathbf{k}} b_{\mathbf{k}} + a^{\dagger}_{\mathbf{k}} b^{\dagger}_{-\mathbf{k}}\right) \qquad \text{(D.3)} \\ \varepsilon_1 &= \hbar c k \qquad \text{(D.4)} \\ \varepsilon_2 &= \hbar\omega_0 \sqrt{1+\chi} \qquad \text{(D.5)} \end{aligned}$$

$$\varepsilon_3 = i\left(\frac{\hbar^2 ck\omega_0\chi}{4\sqrt{1+\chi}}\right)^{1/2} . \tag{D.6}$$

The commutator $[\alpha_{\mathbf{k}}\ ,\ H]$ can now be calculated

$$\begin{aligned}
[\alpha_{\mathbf{k}}\ ,\ H] &= w[a_{\mathbf{k}},\, H] + x[b_{\mathbf{k}},\, H] + y[a^\dagger_{-\mathbf{k}},\, H] + z[b^\dagger_{-\mathbf{k}},\, H] \\
&= w\left(\varepsilon_1 a_{\mathbf{k}} + \varepsilon_3 b^\dagger_{-\mathbf{k}} + \varepsilon_3 b_{\mathbf{k}}\right) + x\left(\varepsilon_2 b_{\mathbf{k}} + \varepsilon_3 a^\dagger_{-\mathbf{k}} - \varepsilon_3 a_{\mathbf{k}}\right) \\
&\quad + y\left(-\varepsilon_1 a^\dagger_{-\mathbf{k}} + \varepsilon_3 b_{\mathbf{k}} + \varepsilon_3 b^\dagger_{-\mathbf{k}}\right) + z\left(-\varepsilon_2 b^\dagger_{-\mathbf{k}} + \varepsilon_3 a_{\mathbf{k}} - \varepsilon_3 a^\dagger_{-\mathbf{k}}\right) \\
&= (w\varepsilon_1 - x\varepsilon_3 + z\varepsilon_3)\, a_{\mathbf{k}} + (w\varepsilon_3 + x\varepsilon_2 + y\varepsilon_3)\, b_{\mathbf{k}} \\
&\quad + (x\varepsilon_3 - y\varepsilon_1 - z\varepsilon_3)\, a^\dagger_{-\mathbf{k}} + (w\varepsilon_3 + y\varepsilon_3 - z\varepsilon_2)\, b^\dagger_{-\mathbf{k}} \\
&= E_{\mathbf{k}}\left(w a_{\mathbf{k}} + x b_{\mathbf{k}} + y a^\dagger_{-\mathbf{k}} + z b^\dagger_{-\mathbf{k}}\right) .
\end{aligned} \tag{D.7}$$

Comparing the coefficients of the operators in the last equality, we get a set of linear equations:

$$\begin{cases}
(\varepsilon_1 - E_{\mathbf{k}})w - \varepsilon_3 x + \varepsilon_3 z &= 0 \\
\varepsilon_3 w + (\varepsilon_2 - E_{\mathbf{k}})x + \varepsilon_3 y &= 0 \\
\varepsilon_3 x - (\varepsilon_1 + E_{\mathbf{k}})y - \varepsilon_3 z &= 0 \\
\varepsilon_3 w + \varepsilon_3 y - (\varepsilon_2 + E_{\mathbf{k}})z &= 0
\end{cases} \tag{D.8}$$

For this set of equations to have non-trivial solutions, its determinant must be zero:

$$\begin{vmatrix}
\varepsilon_1 - E_{\mathbf{k}} & -\varepsilon_3 & 0 & \varepsilon_3 \\
\varepsilon_3 & (\varepsilon_2 - E_{\mathbf{k}}) & \varepsilon_3 & 0 \\
0 & \varepsilon_3 & -(\varepsilon_1 + E_{\mathbf{k}}) & -\varepsilon_3 \\
\varepsilon_3 & 0 & \varepsilon_3 & -(\varepsilon_2 + E_{\mathbf{k}})
\end{vmatrix} = 0 \tag{D.9}$$

The characteristic polynomial can be simplified into a quadratic form

$$(E^2_{\mathbf{k}})^2 - (\varepsilon_1^2 + \varepsilon_2^2)E^2_{\mathbf{k}} + \varepsilon_1^2\varepsilon_2^2 + 4\varepsilon_1\varepsilon_2\varepsilon_3^2 = 0 . \tag{D.10}$$

The solutions to this equation are

$$E^2_{\mathbf{k}} = \frac{1}{2}\left\{\varepsilon_1^2 + \varepsilon_2^2 \pm \sqrt{(\varepsilon_1^2 - \varepsilon_2^2)^2 - 16\varepsilon_1\varepsilon_2\varepsilon_3^2}\right\} . \tag{D.11}$$

These two solutions correspond to the two branches of the polaritons (since both photons and phonons have positive energy, we ignore the negative energy terms here). Since ε_1, ε_2 and ε_3 are all symmetric for $\pm\mathbf{k}$, the energy for the $\pm\mathbf{k}$ modes polaritons are also the same. Substituting the energy $E_{\mathbf{k}}$ back into Eqs. (D.8), we obtain the following relations between w, x, y, and z

$$x = \frac{(\varepsilon_1 - E_{\mathbf{k}})(\varepsilon_2 + E_{\mathbf{k}})}{2\varepsilon_2\varepsilon_3} w , \tag{D.12}$$

$$y = \frac{\varepsilon_1 - E_{\mathbf{k}}}{\varepsilon_1 + E_{\mathbf{k}}} w , \tag{D.13}$$

$$z = -\frac{(\varepsilon_1 - E_{\mathbf{k}})(\varepsilon_2 - E_{\mathbf{k}})}{2\varepsilon_2\varepsilon_3} w . \tag{D.14}$$

In addition, α satisfies the Boson commutation relation so that

$$[wa_{\mathbf{k}} + xb_{\mathbf{k}} + ya^{\dagger}_{-\mathbf{k}} + zb^{\dagger}_{-\mathbf{k}}\,,\; w^*a^{\dagger}_{\mathbf{k}} + x^*b^{\dagger}_{\mathbf{k}} + y^*a_{-\mathbf{k}} + z^*b_{-\mathbf{k}}] = 1\,, \tag{D.15}$$

which can be simplified to

$$|w|^2 + |x|^2 - |y|^2 - |z|^2 = 1\,. \tag{D.16}$$

Combining this equation with Eqs. (D.14), we are able to express w in terms of $E_{\mathbf{k}}$, ε_1, ε_2, and ε_3, with

$$w = \left(\frac{4\varepsilon_1 E_{\mathbf{k}}}{(\varepsilon_1 + E_{\mathbf{k}})^2} - \frac{\varepsilon_2 E_{\mathbf{k}}(\varepsilon_1 - E_{\mathbf{k}})^2}{\varepsilon_2^2\varepsilon_3^2}\right)^{-\frac{1}{2}}\,. \tag{D.17}$$

We have chosen w to be real since such a constraint simply removes the phase arbitrariness of the polaritons. Together with Eqs. (D.14), x, y, and z can all be determined straightforwardly.

For the particular choice of parameters

$$\begin{cases} \varepsilon_1 &= 1 \\ \varepsilon_2 &= \epsilon \\ \varepsilon_3 &= \frac{i}{2}\sqrt{\chi\epsilon/(1+\chi)} \end{cases} \tag{D.18}$$

where χ is the dimensionless dielectric susceptibility (in MKS unit) of the crystal, and the energy is measured in units of ck, the energies of the polaritons become

$$E^2_{\mathbf{k}} = \frac{1}{2}\left\{\epsilon^2 + 1 \pm \sqrt{(\epsilon^2-1)^2 + \frac{4\chi}{1+\chi}\epsilon^2}\right\}\,, \tag{D.19}$$

which has two branches. If we further assume that ϵ is a number that is not very close to one, or more accurately, assume that $4\epsilon^2\chi/(\epsilon^2-1)^2 \ll 1$, the energies of the two branches can be written approximately as (taking the case $\epsilon > 1$)

$$E^2_{1,\mathbf{k}} = \epsilon^2 + \frac{\epsilon^2}{\epsilon^2-1}\chi \tag{D.20}$$

$$E^2_{2,\mathbf{k}} = 1 - \frac{\epsilon^2}{\epsilon^2-1}\chi\,. \tag{D.21}$$

When ϵ approaches 1, so that $4\epsilon^2\chi/(\epsilon^2-1)^2 \gg 1$, while χ is still much smaller than 1, the energies become

$$E^2_{\mathbf{k}} = (1 + \epsilon^2 \pm 2\epsilon\sqrt{\chi})/2\,, \tag{D.22}$$

which have a very different dependence on χ from the previous case with $4\epsilon^2\chi/(\epsilon^2-1)^2 \ll 1$. Such a change originates from the energy degeneracy between photons and phonons at $\epsilon = 1$. In our calculations, we have fixed ϵ at 1.2 while change the susceptibility χ.

In summary, we have shown in this section how to obtain the transformation matrix $\mathbf{A}$ in Eq. (3.125) and the energies of the polaritons from a given set of parameters ε_1, ε_2, and ε_3.

D.2 Correlations between the Two Polariton Branches

In writing down the equation $[\alpha_{i\mathbf{k}}\,,\ H] = E_{\mathbf{k}}\,\alpha_{i\mathbf{k}}$, we have implicitly assumed that the two branches of the polaritons are independent. However, this constraint is not automatically embodied in the polariton transformation Eq. (3.116). Here we demonstrate that the two branches are not totally independent, and that there are weak interactions between them. Recall that for $j = 1, 2$

$$\alpha_{j\mathbf{k}} = w_j a_{\mathbf{k}} + x_j b_{\mathbf{k}} + y_j a^{\dagger}_{-\mathbf{k}} + z_j b^{\dagger}_{-\mathbf{k}}\,. \tag{D.23}$$

The commutator can be calculated,

$$\begin{aligned}
&[\alpha_{1\mathbf{k}},\ \alpha_{2,-\mathbf{k}}] \\
&= w_1 y_2 + x_1 z_2 - w_2 y_1 + x_2 z_1 \\
&= \frac{w_1 w_2 \left(E^{(2)}_{\mathbf{k}} - E^{(1)}_{\mathbf{k}}\right)}{2\left(\varepsilon_1 + E^{(1)}_{\mathbf{k}}\right)\left(\varepsilon_1 + E^{(2)}_{\mathbf{k}}\right)\varepsilon_2\varepsilon_3^2} \\
&\quad \times \left\{ \left(E^{(1)}_{\mathbf{k}}\right)^2 \left(E^{(2)}_{\mathbf{k}}\right)^2 - \left[\varepsilon_1^2 \left(E^{(2)}_{\mathbf{k}}\right)^2 + \varepsilon_2^2 \left(E^{(1)}_{\mathbf{k}}\right)^2\right] + \varepsilon_1^2\varepsilon_2^2 + 4\varepsilon_1\varepsilon_2\varepsilon_3^2 \right\}\,,
\end{aligned} \tag{D.24}$$

and is generally nonzero. When we take the particular choice of units so that $\varepsilon_1 = 1, \varepsilon_2 = \epsilon$, $\varepsilon_3 = i\sqrt{\chi\epsilon/(4+4\chi)}$, and assume that χ is small, the commutator can then be simplified to

$$[\alpha_{1\mathbf{k}},\ \alpha_{2,-\mathbf{k}}] = \frac{\epsilon - 1}{\epsilon + 1} w_1 w_2\,, \tag{D.25}$$

which is proportional to $\epsilon - 1$. Therefore, when ϵ is somewhat close to one, our assumption of independent branches for polaritons is justified. In other words, if the phonon and photon frequencies are close to each other ($\epsilon \sim O(1)$), the two polariton branches are approximately independent.

Appendix E

Detection of Optical Squeezed States

There are several distinct ways to detect optical squeezed states. It is important to study which of these methods might be more suitable for a potential squeezed phonon detection scheme. For this purpose, we need to understand their most salient features. Here we briefly summarize several detection methods and their respective advantages. These are not described in the standard phonon literature. For more details see Ref. [58].

E.1 Direct Detection

The signature of a single-mode squeezed state is its lower-than-vacuum noise in one of the quadratures. We can detect this variation of noise by counting the photon numbers. Consider a photon detector of efficiency η. Such a device can be thought of as an ideal detector with 100% efficiency plus a mixture of some vacuum noise at the input. The final photocurrent $\langle \hat{m} \rangle$ is related to the input photon number $\langle \hat{n} \rangle$ as

$$\langle \hat{m} \rangle = \eta \langle \hat{n} \rangle , \tag{E.1}$$

$$\begin{aligned} \langle (\Delta \hat{m})^2 \rangle &= \eta^2 \langle (\Delta \hat{n})^2 \rangle + \eta(1-\eta)\langle \hat{n} \rangle \\ &= \eta |\alpha|^2 \left\{ 1 + \eta \left[e^{-2r} \cos^2 \left(\phi - \frac{\theta}{2} \right) + e^{2r} \sin^2 \left(\phi - \frac{\theta}{2} \right) - 1 \right] \right\} , \end{aligned} \tag{E.2}$$

$$\frac{\langle (\Delta \hat{m})^2 \rangle}{\langle \hat{m} \rangle} = 1 + \eta \left(\frac{\langle (\Delta \hat{n})^2 \rangle}{\langle \hat{n} \rangle} - 1 \right) . \tag{E.3}$$

Here $\hat{n}$ is the photon number operator for the input squeezed light, ϕ is the phase of its coherent component, $re^{i\theta}$ is the complex squeezing factor, and $\langle \hat{m} \rangle$ is the measured strength of the photocurrent, which is equal to the number of input photons $\langle \hat{n} \rangle$ times the detector efficiency η.

Equation (E.3), which relates the output noise $\langle(\Delta\hat{m})^2\rangle$ and the input noise $\langle(\Delta\hat{n})^2\rangle$, clearly tells us that if the input light has a sub-Poissonian distribution in the photon number, i.e., $\langle(\Delta\hat{n})^2\rangle < \langle\hat{n}\rangle$, the output photocurrent also has a sub-Poissonian distribution, $\langle(\Delta\hat{m})^2\rangle < \langle\hat{m}\rangle$. Therefore, by measuring the average photocurrent $\langle\hat{m}\rangle$ and its fluctuation $\langle(\Delta\hat{m})^2\rangle$, we can obtain information on the average input photon number and its fluctuation.

This detection scheme is not very sensitive because it depends heavily on the phases ϕ and $\theta/2$, which are properties of the input squeezed state. In this situation, the desired phase lock between ϕ and $\theta/2$ is not guaranteed. Furthermore, this scheme can only detect the statistics of the photon number, but not the quadratures and their noises.

Let us now focus on the effect of the photon detector efficiency η. From the above relation between the output noise $\langle(\Delta\hat{m})^2\rangle$ and the input noise $\langle(\Delta\hat{n})^2\rangle$, it is clear that a relatively small η can prevent squeezing effects from being detected. One term in the output noise is directly proportional to $1-\eta$. Therefore, when the detector efficiency η is small, the information loss is large. The contribution from this term in the output noise can completely dominate the contribution from the input signal noise, so that the squeezing effect in this case is not detectable.

E.2 Ordinary Homodyne Detection

To overcome the problems present in the direct detection method, phase-sensitive approaches must be used. The homodyne detector is such an example (see Fig. E.1). In this scheme, the input squeezed light of single-mode a will be superimposed onto a local oscillator of mode a_L—with the same frequency as the input light—by a symmetric beamsplitter. Here L denotes "Local oscillator". The output annihilation operators d_1 and d_2 satisfy

$$\begin{pmatrix} d_1 \\ d_2 \end{pmatrix} = \begin{pmatrix} r & t \\ t & r \end{pmatrix} \begin{pmatrix} a_L \\ a \end{pmatrix}, \tag{E.4}$$

where r and t are the reflection and transmission coefficients. The coupling matrix should be unitary, so that

$$|r|^2 + |t|^2 = 1 \tag{E.5}$$

$$r^*t + rt^* = 0\,. \tag{E.6}$$

The second condition above implies that

$$\arg\{r\} - \arg\{t\} = \frac{\pi}{2}\,. \tag{E.7}$$

For an Ordinary Homodyne Detector, only the first output is used. The following restrictions on the transmission and reflection coefficients and the local oscillator strength must be imposed

$$|r| \ll |t|, \quad |r||\alpha_L| \gg |t||\alpha|\,, \tag{E.8}$$

where α_L is the amplitude of the local oscillator, and α is the coherent amplitude of the input squeezed light. We also need to introduce a quadrature operator

$$W(\varphi) = \frac{1}{2}\left(e^{i\varphi}a^\dagger + e^{-i\varphi}a\right)\,, \tag{E.9}$$

$$\varphi = \arg\{r\} - \arg\{t\} + \phi_L = \frac{\pi}{2} + \phi_L\,, \tag{E.10}$$

where ϕ_L is the phase of the local oscillator and is generally time-dependent.

The detected photocurrent $\langle \hat{m}_1 \rangle$ and its fluctuation $\langle (\Delta \hat{m}_1)^2 \rangle$ are

$$\langle \hat{m}_1 \rangle = 2\eta|r||t||\alpha_L||\alpha|\cos(\varphi - \phi) \tag{E.11}$$

$$\langle (\Delta \hat{m}_1)^2 \rangle = \eta|r|^2|\alpha_L|^2\left(1 + \eta|t|^2\left[4\langle(\Delta W(\varphi))^2\rangle - 1\right]\right) \tag{E.12}$$

$$\langle (\Delta W(\varphi))^2 \rangle = \frac{1}{4}\left(e^{-2s}\cos^2(\varphi - \frac{\theta}{2}) + e^{2s}\sin^2(\varphi - \frac{\theta}{2})\right)\,. \tag{E.13}$$

Here $\hat{m}_1$ is the detected current operator, and $se^{i\theta}$ is the complex squeezing factor. It can be seen from Eq. (E.12) that there are two contributions to the output noise: one, $\eta|r|^2|\alpha_L|^2$, is from regular shot noise, while the other, $\eta^2|r|^2|t|^2|\alpha_L|^2(4\langle(\Delta W(\varphi))^2\rangle - 1)$, contains the noise of the quadrature $W(\varphi)$. If the input is a beam of squeezed light, the second contribution will be negative, so that the total noise will be less than the shot noise. Therefore, squeezing can be detected by finding sub-Poissonian statistics in the output photocurrent.

In the Ordinary Homodyne Detection scheme, the phase ϕ_L of the local oscillator can be manipulated in such a way as to maximize the squeezing effect in the noise of $W(\varphi)$. We can thus vastly improve the efficiency of detecting any squeezing effect over the direct detection method, whose output is fixed by the input squeezed light.

E.3 Balanced Homodyne Detection

In a Balanced Homodyne Detector, the reflection and transmission coefficients of the beamsplitter satisfy the following conditions

$$|r| = |t|, \quad |\alpha_L| \gg |\alpha|\,. \tag{E.14}$$

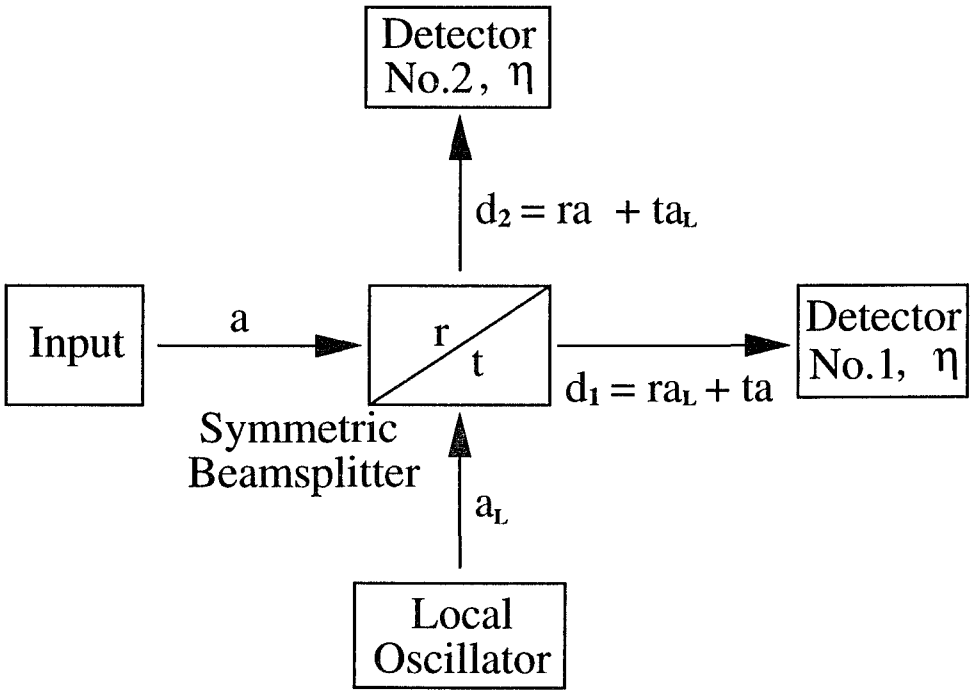

Figure E.1: A schematic diagram of a typical homodyne or heterodyne photon detector, where the ideal symmetric beamsplitter mixes the input and the local oscillator light, and the detectors are photon counters with efficiency η. The local oscillator has the same frequency as the input signal. Notice that the ordinary homodyne detector only uses one of the two photon counters, while the balanced homodyne and heterodyne detectors use both of the photon counters by measuring the photocurrent difference from the two counters.

Both outputs are used and the measured quantity is the current difference $\langle \hat{m}_{12} \rangle$. The result is

$$\hat{m}_{12} = d_1^\dagger d_1 - d_2^\dagger d_2 \,, \tag{E.15}$$

$$\langle \hat{m}_{12} \rangle = 2\eta |\alpha_L| \langle W(\varphi) \rangle \,, \tag{E.16}$$

$$\langle (\Delta \hat{m}_{12})^2 \rangle = \eta |\alpha_L|^2 \left(1 + \eta \left[4 \langle (\Delta W(\varphi))^2 \rangle - 1 \right] \right) \,, \tag{E.17}$$

$$\langle (\Delta W(\varphi))^2 \rangle = \frac{1}{4} \left(e^{-2s} \cos^2(\varphi - \frac{\theta}{2}) + e^{2s} \sin^2(\varphi - \frac{\theta}{2}) \right) \,. \tag{E.18}$$

Here $\langle (\Delta W(\varphi))^2 \rangle$ is the same as in the previous section on Ordinary Homodyne Detection. It can be seen that the balancing scheme has completely eliminated the noise contribution from the local oscillator, thus improving the ability to observe the squeezing effect. Similar to the Ordinary Homodyne Detector, squeezing in the input single photon mode leads to sub-Poissonian statistics in the output photocurrent.

E.4 Heterodyne Detection

Heterodyne Detection is used to detect two-mode squeezed light. The experimental setup is the same as the Balanced Homodyne Detector (see Fig. E.1). The input is a two-mode (of frequencies ω_1 and ω_2) photon squeezed state, while the local oscillator has a frequency

$$\omega_L = (\omega_1 + \omega_2)/2 \,. \tag{E.19}$$

The new quadrature operator for the two modes is

$$W^{(2)}(\varphi) = \frac{1}{2} \mathcal{E}_{c1} \left(e^{i\varphi} a_1^\dagger + e^{-i\varphi} a_1 \right) + \frac{1}{2} \mathcal{E}_{c2} \left(e^{i\varphi} a_2^\dagger + e^{-i\varphi} a_2 \right) \,. \tag{E.20}$$

Here $\mathcal{E}_{ci} = \sqrt{\hbar \omega_i / 2\varepsilon_0 V}$ is a measure of the vacuum noise at the frequency ω_i ($i = 1, 2$), and ε_0 is the vacuum dielectric constant. When the two frequencies ω_1 and ω_2 are close enough, they can be substituted by a common factor $\mathcal{E}_c$. The result will then be essentially the same as that of the Balanced Homodyne Detection.

Appendix F

Quantization of an LC Circuit

In an LC circuit, we can define a phase ϕ [86],

$$\phi = \frac{e^*}{\hbar}\int_{-\infty}^{t} V d\tau\,, \tag{F.1}$$

which can be related to the flux Φ through the inductor by using Faraday's law

$$\Phi = \Phi_0 \frac{\phi}{2\pi}. \tag{F.2}$$

Here $\Phi_0 = 2\pi\hbar/e^*$ is the flux quantum and e^* is the charge of the carriers in the circuit. The Lagrangian of the whole circuit is

$$L = \frac{1}{2}C\left(\frac{\hbar}{e^*}\right)^2\dot{\phi}^2 - \frac{1}{2L}(\Phi - \Phi_x)^2\,, \tag{F.3}$$

with Φ_x the externally applied flux. The canonical momentum is

$$P = \frac{\hbar}{e^*}CV = \frac{\hbar}{e^*}Q\,, \tag{F.4}$$

where Q is the charge on the capacitor, so that the following commutation relation holds:

$$[\phi, P] = i\hbar\,, \tag{F.5}$$

or

$$[\Phi, Q] = i\hbar\,. \tag{F.6}$$

Thus the Hamiltonian of the circuit is

$$H_{LC} = \frac{Q^2}{2C} + \frac{(\Phi - \Phi_x)^2}{2L}\,, \tag{F.7}$$

and the Schrödinger equation of the system is

$$i\hbar\frac{\partial}{\partial t}\Psi = H_{LC}\Psi\,. \tag{F.8}$$

An analogy exists between the dynamics of an LC circuit and a harmonic oscillator, as shown in Table F. Because of these similarities, an LC circuit can be treated as an harmonic oscillator and can be quantized accordingly.

harmonic oscillator	**LC circuit**
Coordinate x	Flux Φ or phase ϕ
Velocity v	Voltage $V = \dot{\Phi} = Q/C$
Momentum p	Charge Q
Mass m	Capacitance C
Spring constant k	1/Inductance, $1/L$
Frequency $\omega = \sqrt{k/m}$	Frequency $\omega = 1/\sqrt{LC}$

Table F.1: Comparison of the physical quantities of a harmonic oscillator and the analog variables in an LC circuit with a superconducting junction.

Appendix G

Rotating Wave Approximation

G.1 Rotating Wave Approximation for Josephson Junctions

Our approach is based on the assumption that, under some physical circumstances described in the paper, we can use the small-phase approximation. Furthermore, in Sec. 5.7 we have also used the rotating wave approximation (RWA) to eliminate the non-number-conserving terms produced by the ϕ^4 expansion. In fact, the RWA corresponds to perturbatively calculating the energy to first-order while keeping the eigenfunctions unchanged. To justify these statements, here we calculate the second order correction on the energy levels, and also the first order correction to the wave functions.

Let us first analyze the complete expansion of ϕ^4

$$\phi^4 = \frac{E_C}{4E_J}(a + a^\dagger)^4 . \tag{G.1}$$

Ignoring the constant part and concentrating on the operator part for now, we can simplify the expansion by writing it as

$$(a + a^\dagger)^4 = 6(a^\dagger a)^2 + 6a^\dagger a + 3 + a^{\dagger 4} + a^4 + 4a^{\dagger 2}(a^\dagger a) + 4(a^\dagger a)a^2 + 6a^{\dagger 2} + 6a^2 . \tag{G.2}$$

Our unperturbed states are number states of a harmonic oscillator $|n\rangle$. There is no degeneracy. The first three terms above contribute to the first-order perturbation in energy and do not affect the eigenstates, because they commute with H_0. The remaining terms contribute to second-order perturbation in energy and do affect the eigenstates, since they mix the number states. Thus the first-order perturbation on the energy is

$$\begin{aligned} \varepsilon_n^{(1)} &= \langle n|\frac{1}{24}\phi^4|n\rangle \\ &= \frac{\hbar\omega}{96\lambda}(6n^2 + 6n + 3), \end{aligned} \tag{G.3}$$

which is only related to those number-conserving terms. On the other hand, the second-order energy perturbation is

$$\begin{aligned}\varepsilon_n^{(2)} &= \sum_{m\neq n}\frac{|\Delta H_n m|^2}{\varepsilon_n^{(0)}-\varepsilon_m^{(0)}} \\ &= \frac{\hbar\omega}{(96\lambda)^2}\left\{-\frac{1}{2}(6+4n)^2(n+2)(n+1)+\frac{1}{2}(4n-2)^2 n(n-1)\right. \\ &\quad \left.-\frac{1}{4}(n+1)(n+2)(n+3)(n+4)+\frac{1}{4}n(n-1)(n-2)(n-3)\right\}. \qquad \text{(G.4)}\end{aligned}$$

As long as λ is not too small, the $(96\lambda)^2$ in the denominator will dominate when n is not large. For example,

$$\varepsilon_0^{(2)} = -\frac{42}{(96\lambda)^2}\hbar\omega\,, \qquad \text{(G.5)}$$

$$\varepsilon_1^{(2)} = -\frac{630}{(96\lambda)^2}\hbar\omega\,, \qquad \text{(G.6)}$$

$$\varepsilon_2^{(2)} = -\frac{2040}{(96\lambda)^2}\hbar\omega\,, \qquad \text{(G.7)}$$

$$\varepsilon_3^{(2)} = -\frac{3150}{(96\lambda)^2}\hbar\omega\,, \qquad \text{(G.8)}$$

$$\cdots\ .$$

When $\lambda = 1$, we have $\varepsilon_0^{(2)} \simeq 0.004\hbar\omega$ while $\varepsilon_2^{(2)} \simeq 0.2\hbar\omega$. In the meantime, $\varepsilon_0^{(1)} \simeq 0.13\hbar\omega$ and $\varepsilon_2^{(1)} \simeq 1.6\hbar\omega$. Therefore, for the RWA to be valid, we need to work in the $n \leq 2$ range so that the second order corrections to the energy is much smaller than the first-order corrections.

We also need to calculate the first-order correction to the eigenstates, to check if we need any further constraints on n. The perturbed states are

$$\begin{aligned}|n\rangle' &= |n\rangle + \sum_{m\neq n}\frac{\Delta H_{mn}}{\varepsilon_n^{(0)}-\varepsilon_m^{(0)}}|m\rangle \\ &= |n\rangle + \frac{1}{96\lambda}\sum_{m\neq n}\frac{(a+a^\dagger)^4}{n-m}|m\rangle \\ &= |n\rangle + \frac{1}{96\lambda}\{-(2n+3)\sqrt{(n+1)(n+2)}|n+2\rangle + (2n-1)\sqrt{n(n-1)}|n-2\rangle \\ &\quad -\frac{1}{4}\sqrt{(n+1)(n+2)(n+3)(n+4)}|n+4\rangle \\ &\quad +\frac{1}{4}\sqrt{n(n-1)(n-2)(n-3)}|n-4\rangle\}\,. \qquad \text{(G.9)}\end{aligned}$$

For example,

$$|0\rangle' = |0\rangle - \frac{1}{96\lambda}\left(6\sqrt{2}|2\rangle + \sqrt{24}|4\rangle\right), \qquad \text{(G.10)}$$

$$|1\rangle' = |1\rangle - \frac{1}{96\lambda}\left(10\sqrt{6}|3\rangle + \sqrt{120}|5\rangle\right), \quad \text{(G.11)}$$

$$|2\rangle' = |2\rangle - \frac{1}{96\lambda}\left(28\sqrt{3}|4\rangle + \sqrt{360}|6\rangle - 6\sqrt{2}|0\rangle\right), \quad \text{(G.12)}$$

$$|3\rangle' = |3\rangle - \frac{1}{96\lambda}\left(36\sqrt{5}|5\rangle + \sqrt{840}|7\rangle - 10\sqrt{6}|1\rangle\right), \quad \text{(G.13)}$$

$$|4\rangle' = |4\rangle - \frac{1}{96\lambda}\left(22\sqrt{30}|6\rangle + \sqrt{1680}|8\rangle - 28\sqrt{3}|2\rangle - \sqrt{24}|0\rangle\right). \quad \text{(G.14)}$$

In the particular case of $\lambda = 1$ ($E_C = E_J$), we have

$$|0\rangle' \cong |0\rangle - 0.09|2\rangle - 0.05|4\rangle, \quad \text{(G.15)}$$

$$|1\rangle' \cong |1\rangle - 0.26|3\rangle - 0.11|5\rangle, \quad \text{(G.16)}$$

$$|2\rangle' \cong |2\rangle - 0.51|4\rangle - 0.20|6\rangle + 0.09|0\rangle, \quad \text{(G.17)}$$

$$|3\rangle' \cong |3\rangle - 0.84|5\rangle + 0.30|7\rangle - 0.26|1\rangle, \quad \text{(G.18)}$$

$$|4\rangle' \cong |4\rangle - 1.26|6\rangle + 0.43|8\rangle - 0.51|2\rangle - 0.05|0\rangle \quad \text{(G.19)}$$

We can clearly see that the correction to the ground state is very small, while the correction on the first excited state is non-negligible. Therefore, it is cautious not to extend our approach to the regime with $n > 1$. The physical reason for this restriction is clear. For large n (large energy), the x^4 term in the potential is larger than the x^2 term, so that the perturbative results are no longer reliable.

G.2 The Time-Evolution Operator of a Linearly-Driven Josephson Junction

In the case of linearly-driven Josephson junction, corresponding to H_2 (current-biased junction) and H_3 (external-field-driven superconducting ring with a Josephson junction) in Section 5.7, the Hamiltonian can be written as

$$H_2 = H_0 + V, \quad \text{(G.20)}$$

$$H_0 = \hbar\mu a^\dagger a - \hbar\nu(a^\dagger a)^2, \quad \text{(G.21)}$$

$$V = \gamma(a + a^\dagger). \quad \text{(G.22)}$$

Here we use case (2) as an example, while case (3) is qualitatively (but not quantitatively because of different parameters) the same. Our goal is to obtain a factorized evolution operator. To achieve this goal, we first employ the interaction picture

$$O_I = e^{iH_0 t/\hbar} O_S e^{-iH_0 t/\hbar}, \quad \text{(G.23)}$$

$$|\Psi_2\rangle_I = e^{iH_0t/\hbar}|\Psi_2\rangle_S\,, \tag{G.24}$$

$$i\hbar\frac{\partial}{\partial t}|\Psi_2\rangle_I = H_I|\Psi_2\rangle_I\,, \tag{G.25}$$

where

$$H_I = \exp(iH_0t/\hbar)\,V\,\exp(-iH_0t/\hbar)\,. \tag{G.26}$$

Since $[a^\dagger a,\,(a^\dagger a)^2] = 0$, we can factor $\exp(-iH_0t/\hbar)$ into $\exp(-i\mu t a^\dagger a)\,\exp[-i\nu t(a^\dagger a)^2]$. So now we have

$$\begin{aligned} H_I &= \exp\left(\frac{i}{\hbar}H_0t\right)\,V\,\exp\left(-\frac{i}{\hbar}H_0t\right) \\ &= e^{i\nu t(a^\dagger a)^2}e^{i\mu t a^\dagger a}\,V\,e^{-i\mu t a^\dagger a}e^{-i\nu t(a^\dagger a)^2} \\ &= e^{i\nu t(a^\dagger a)^2}\,\gamma(e^{-i\mu t}a + e^{i\mu t}a^\dagger)\,e^{-i\nu t(a^\dagger a)^2} \\ &= \gamma\left(e^{2i\nu t a^\dagger a}e^{-i(\nu-\mu)t}a^\dagger + ae^{-2i\nu t a^\dagger a}e^{i(\nu-\mu)t}\right). \end{aligned} \tag{G.27}$$

In the derivation we have used the results from Appendix G.3. If we let

$$|\Psi_2(t)\rangle_I = U(t)\,|\Psi_2(0)\rangle_I\,, \tag{G.28}$$

the Schrödinger equation becomes

$$i\hbar\frac{\partial}{\partial t}U_2^I(t) = H_IU_2^I(t)\,, \tag{G.29}$$

so that we can obtain a formal time-evolution operator

$$U_2^I(t) = T\exp\left(-\frac{i}{\hbar}\int_0^t H_I d\tau\right), \tag{G.30}$$

where T is the time-ordering operator. This expression cannot be easily simplified. However, using the Magnus approximation [66], and accurate to first-order in H_I, we can drop the time-ordering operator. Thus,

$$U_2^I(t) \cong \exp\left(-\frac{i}{\hbar}\int_0^t H_I d\tau\right). \tag{G.31}$$

Recall that a and $a^\dagger$ are operators in the Schrödinger picture. Namely, they are time-independent. Therefore,

$$\begin{aligned} U_2^I(t) &= \exp\left(-\frac{i\gamma}{\hbar}\int_0^t(e^{2i\nu\tau a^\dagger a}e^{-i(\nu-\mu)\tau}a^\dagger + ae^{-2i\nu\tau a^\dagger a}e^{i(\nu-\mu)\tau})d\tau\right) \\ &= \exp\left\{-\frac{i\gamma}{\hbar}\left[\left(\int_0^t e^{2i\nu\tau a^\dagger a}e^{-i(\nu-\mu)\tau}d\tau\right)a^\dagger + a\int_0^t e^{-2i\nu\tau a^\dagger a}e^{i(\nu-\mu)\tau}d\tau\right]\right\} \\ &= e^{\eta a^\dagger - a\eta^\dagger}\,. \end{aligned} \tag{G.32}$$

where

$$\eta = \frac{\gamma}{\hbar\omega}\frac{1-\omega t\, e^{i(1-a^\dagger a/8\lambda)}}{1-a^\dagger a/8\lambda}\,. \tag{G.33}$$

Now the state vector in the interaction picture is

$$|\Psi_2(t)\rangle_I = e^{\eta a^\dagger - a\eta^*}|\Psi_2(0)\rangle_I\,, \tag{G.34}$$

so the state vector in the Schrödinger picture is

$$\begin{aligned}|\Psi_2(t)\rangle_S &= e^{-\frac{iH_0 t}{\hbar}}|\Psi_2(t)\rangle_I \\ &= e^{-i\mu t a^\dagger a}e^{-i\nu t(a^\dagger a)^2}e^{\eta a^\dagger-\eta^* a}|\Psi_2(0)\rangle_I \\ &= e^{-i\mu t a^\dagger a}e^{-i\nu t(a^\dagger a)^2}e^{\eta a^\dagger-\eta^* a}|\Psi_2(0)\rangle_S\,. \end{aligned}\tag{G.35}$$

Now that we have the state vector, we can readily calculate the fluctuations.

G.3 Derivation of Two Useful Relations

Throughout this paper we deal with operators which satisfy the Boson commutation relation $[a, a^\dagger] = 1$. To calculate various commutation relations and fluctuations, we need to compute quantities such as $e^{-\alpha a^\dagger a}ae^{\alpha a^\dagger a}$ and $e^{-\eta_1(a^\dagger a)^2}ae^{\eta_1(a^\dagger a)^2}$. Here we present the computation, in which we have used the Taylor expansion of an exponential operator $e^A = \sum_{n=0}^{\infty} A^n/n!$. Now let us look at $ae^{\alpha a^\dagger a}$ first,

$$\begin{aligned}ae^{\alpha a^\dagger a} &= a\sum_{n=0}^{\infty}\frac{(\alpha a^\dagger a)^n}{n!} = \sum_{n=0}^{\infty}\frac{\alpha^n a(a^\dagger a)^n}{n!} \\ &= \sum_{n=0}^{\infty}\frac{\alpha^n(aa^\dagger)^n a}{n!} = \sum_{n=0}^{\infty}\frac{\alpha^n(a^\dagger a+1)^n}{n!}a \\ &= e^{\alpha(a^\dagger a+1)}a = e^{\alpha a^\dagger a}e^{\alpha}a\,. \end{aligned}\tag{G.36}$$

Therefore,

$$e^{-\alpha a^\dagger a}ae^{\alpha a^\dagger a} = e^{-\alpha a^\dagger a}e^{\alpha a^\dagger a}e^{\alpha}a = e^{\alpha}a\,, \tag{G.37}$$

where α is a complex number.

We can use the same technique to calculate $e^{-\beta(a^\dagger a)^2}ae^{\beta(a^\dagger a)^2}$. Again we will first look at $ae^{\beta(a^\dagger a)^2}$,

$$\begin{aligned}ae^{\beta(a^\dagger a)^2} &= a\sum_{n=0}^{\infty}\frac{(\beta a^\dagger a)^{2n}}{n!} = \sum_{n=0}^{\infty}\frac{a(\beta a^\dagger a)^{2n}}{n!} \\ &= \sum_{n=0}^{\infty}\frac{\beta^{2n}(aa^\dagger)^{2n}a}{n!} = \sum_{n=0}^{\infty}\frac{\beta^{2n}(a^\dagger a+1)^{2n}}{n!}a = e^{\beta(a^\dagger a+1)^2}a\,. \end{aligned}\tag{G.38}$$

Therefore,

$$e^{-\beta(a^\dagger a)^2} a e^{\beta(a^\dagger a)^2} \;=\; e^{-\beta(a^\dagger a)^2} e^{\beta(a^\dagger a+1)^2} a \;=\; e^{\beta(2a^\dagger a+1)} a \;, \qquad \text{(G.39)}$$

where β is a complex number. Both of the above quantities come from the Heisenberg operator $\exp\left(\frac{i}{\hbar}\int_0^t H\,d\tau\right) a \exp\left(-\frac{i}{\hbar}\int_0^t H\,d\tau\right)$. Since the Hamiltonian is Hermitian, α and β should both be purely imaginary numbers. We also have implicitly used the Baker-Hausdorff formula: $e^{A+B} = e^A\, e^B$, if $[A,\, B] = 0$.

Bibliography

[1] K. M. Baird, in *Quantum Metrology and Fundamental Physical Constants*, ed. by P. H. Cutler and A. A. Lucas (Plenum Press, New York, 1983).

[2] Y. Guo and H. Shen, *History of Physics* (Qinghua University Press, Beijing, 1993) (in Chinese).

[3] A. B. Arons, *Development of Concepts of Physics* (Addison-Wesley, Reading, 1965).

[4] B. W. Petley, *The Fundamental Physical Constants and the Frontier of Measurement* (Adam Hilger, Bristol, 1985).

[5] W. Heisenberg, Z. Physik **43**, 172 (1927); or, for example, L. D. Landau and E. M. Lifshitz, *Quantum Mechanics* (Pergamon, Oxford, 1977).

[6] P. Meystre and M. Sargent III, *Elements of Quantum Optics* (Springer-Verlag, Berlin, 1991).

[7] R.J. Glauber, Phys. Rev. **131**, 2766 (1963).

[8] D. Stoler, Phys. Rev. D **1**, 3217 (1970).

[9] H.P. Yuen, Phys. Rev. A **13**, 2226 (1976).

[10] R.E. Slusher, L.W. Hollberg, B. Yurke, J.C. Mertz and J.F. Valley, Phys. Rev. Lett. **55**, 2409 (1985).

[11] See, e.g., special issues on squeezed states: J. Opt. Soc. Am. B **4**, No.10 (1987), and Appl. Phys. B **55**, No.3 (1992).

[12] Y. Yamamoto, in *Coherence, Amplification, and Quantum Effects in Semiconductor Lasers*, ed. by Y. Yamamoto (Wiley, New York, 1991).

[13] M.H. Anderson, J.R. Ensher, M.R. Matthews, C.E. Wieman and E.A. Cornell, Science **269**, 198 (1995).

[14] G.D. Mahan, *Many-Particle Physics* (Plenum, New York, 1981).

[15] F. Nori, R. Merlin, S. Haas, A.W. Sandvik and E. Dagotto, Phys. Rev. Lett. **75**, 553 (1995).

[16] D. Rugar and P. Grütter, Phys. Rev. Lett. **67**, 699 (1991); J. Sidles and D. Rugar, *ibid.* **70**, 3506 (1993).

[17] F. DiFilippo, V. Natarajan, K. Boyce, and D. Pritchard, Phys. Rev. Lett. **68**, 2859 (1992); V. Natarajan, F. DiFilippo, and D. Pritchard, *ibid.* **74**, 2855 (1995).

[18] X. Hu and F. Nori, Phys. Rev. Lett. **76**, 2294 (1996).

[19] X. Hu and F. Nori, Phys. Rev. B **53**, 2419 (1996).

[20] X. Hu and F. Nori, Quantum Phonon Optics: Modulating Quantum Fluctuations of Atomic Displacements Using Squeezed Phonon States, submitted to Rev. Mod. Phys.

[21] X. Hu and F. Nori, Squeezed Quantum States in Josephson Junctions, preprint.

[22] X. Hu and F. Nori, Quantum Fluctuations and Squeezed States in Josephson Junctions, preprint.

[23] D. McDonald, Science **247**, 177 (1990).

[24] V. Narayanamurti, H.L. Störmer, M.A. Chin, A.C. Gossard, and W. Wiegmann, Phys. Rev. Lett. **43**, 2012 (1979); R.G. Ulbrich, V. Narayanamurti, and M.A. Chin, Phys. Rev. Lett. **45**, 1432 (1980); V. Narayanamurti, Science **213**, 717 (1981); in *Nonequilibrium Superconductivity, Phonons, and Kapitza Boundaries*, ed. by K.E. Gray (Plenum, New York, 1981); M. Lax, P. Hu, and V. Narayanamurti, Phys. Rev. B **23**, 3095 (1981).

[25] J.P. Wolfe, Phys. Today **33**(12), 44 (1980); G.A. Northrop and J.P. Wolfe, in *Proceedings on a NATO Advanced Study Institute of Nonequilibrium Phonon Dynamics, Les Arcs, France 1984*, edited. by W.E. Bron (Plenum, New York, 1985); G.A. Northrop, S.E. Hebboul, and J.P. Wolfe, Phys. Rev. Lett. **55**, 95 (1985); S.E. Hebboul and J.P. Wolfe, Z. Phys. B **73**, 437 (1989); S.E. Hebboul, Ph. D. Thesis, University of Illinois, 1987.

[26] S. Tamura, Phys. Rev. B **30**, 849 (1984); S. Tamura and F. Nori, Phys. Rev. B **38**, 5610 (1988); S. Tamura, in *PHONON 89*, edited by S. Hunkulinger, W. Ludwig, and G. Weiss (World Scientific, Singapore, 1989), p. 703. S. Tamura and F. Nori, Phys. Rev. B **41**, 7941 (1990); N. Nishiguchi, S. Tamura, and F. Nori, Phys. Rev. B **48**, 2515 (1993); N. Nishiguchi, S. Tamura and F. Nori, Phys. Rev. B **48**, 14426 (1993).

[27] See, e.g., C.F. Quate, Sci. Am. **241**, 62 (1979).

[28] J.W. Tucker and V.W. Rampton, *Microwave Ultrasonics in Solid-State Physics* (North-Holland, Amsterdam, 1972).

[29] E. Garmire, F. Pandarese, and C.H. Townes, Phys. Rev. Lett. **11**, 160 (1963).

[30] R.Y. Chiao, C.H. Townes, and B.P. Stoicheff, Phys. Rev. Lett. **12**, 592 (1964).

[31] J.A. Giordmaine and W. Kaiser, Phys. Rev. **144**, 676 (1966).

[32] A. Laubereau and W. Kaiser, Rev. Mod. Phys. **50**, 607 (1978).

[33] W.E. Bron, J. Kuhl, and B.K. Rhee, Phys. Rev. B **34**, 6961 (1986).

[34] B.K. Rhee and W.E. Bron, Phys. Rev. B **34**, 7107 (1986).

[35] For recent reviews, see, e.g., S. Ruhman, A.G. Joly and K. Nelson, IEEE J. Quantum Electron. **24**, 460 (1988); W.A. Kütt, W. Albrecht and H. Kurz, *ibid.* **28**, 2434 (1992).

[36] See, e.g., *Ultrafast Phenomena VIII: Proceedings of the 8th International Conference, Antibes Juan-les-Pins, France, June 8-12, 1992*, edited by J.L. Martin (Springer-Verlag, Berlin, 1993).

[37] L. Min and R.J.D. Miller, Appl. Phys. Lett. **56**, 524 (1990).

[38] W. Kütt, G.C. Cho, M. Strahnen, and H. Kurz, Appl. Surf. Sci. **50**, 325 (1990).

[39] O.B. Wright and K. Kawashima, Phys. Rev. Lett. **69**, 1668 (1992).

[40] Y. Yan, E.B. Gamble, and K. Nelson, J. Chem. Phys. **83**, 5391 (1987).

[41] Y. Yan and K. Nelson, J. Chem. Phys. **87**, 6240, 6259 (1987).

[42] J. Chesnoy and A. Mokhtari, Phys. Rev. A 38, 3566 (1988).

[43] T.K. Cheng, S.D. Brorson, A.S. Kazeroonian, J.S. Moodera, G. Dresselhaus, M.S. Dresselhaus, and E.P. Ippen, Appl. Phys. Lett. **57**, 1004 (1990).

[44] G.C. Cho, W. Kütt, and H. Kurz, Phys. Rev. Lett. **65**, 764 (1990).

[45] J.M. Chwalek, C. Uher, J.F. Whitaker, G.A. Mourou, J. Agostinelli, and M. Lelental, Appl. Phys. Lett. **59**, 1923 (1991).

[46] W. Albrecht, Th. Kruse, and H. Kurz, Phys. Rev. Lett. **69**, 1451 (1992).

[47] A. Yamamoto, T. Mishina, Y. Masumoto, and M. Nakayama, Phys. Rev. Lett. **73**, 740 (1994).

[48] D.A. Williams, Phys. Rev. Lett. **69**, 2551 (1992).

[49] H.J. Zeiger, J. Vidal, T.K. Cheng, E.P. Ippen, G. Dresselhaus, and M.S. Dresselhaus, Phys. Rev. B **45**, 768 (1992).

[50] W. Kütt, G.C. Cho, T. Pfeifer, M. Strahnen, and H. Kurz, Digest of CLEO (Optical Society of America, Washington D.C., 1991).

[51] A.V. Kuznetsov and C.J. Stanton, Phys. Rev. Lett. **73**, 3243 (1994).

[52] Yongqian Liu, Ph.D. Thesis, University of Michigan, 1995.

[53] Y. Yang and K. Nelson, Phys. Rev. Lett. **74**, 4883 (1995).

[54] S. De Silvestri, J.G. Fujimoto, E.P. Ippen, E.B. Gamble, L.R. Williams, and K.A. Nelson, Chem. Phys. Lett. **116**, 146 (1985).

[55] S. Fahy and R. Merlin, Phys. Rev. Lett. **73** 1122 (1994).

[56] R. Scholz and A. Stahl, Phys. Stat. Sol. (b) **168**, 123 (1991).

[57] C.W. Gardiner, *Quantum Noise* (Springer, Berlin, 1991).

[58] R. Loudon and P.L. Knight, J. Mod. Opt. **34**, 709 (1987).

[59] C.W. Gardiner and C.M. Savage, Optics Communications **50**, 173 (1984).

[60] A. Yariv, *Quantum Electronics* (Wiley, New York, 1989).

[61] M. Schubert and B. Wilhelmi, *Nonlinear Optics and Quantum Electronics* (Wiley, New York, 1986).

[62] W. Kohn and D. Sherrington, Rev. Mod. Phys. **42**, 1 (1970).

[63] L. Susskind and J. Glogower, Physics **1**, 49 (1964).

[64] P.A.M. Dirac, in *Quantum Theory of Emission and Absorption in Quantum Electrodynamics*, ed. by J. Schwinger (Dover, New York, 1958).

[65] W. Zhang, D.H. Feng, and R. Gilmore, Rev. Mod. Phys. **62**, 867 (1990).

[66] Bruce W. Shore, *The Theory of Coherent Atomic Excitation* (Wiley, New York, 1990), Vol. II.

[67] D.F. Walls and P. Zoller, Phys. Rev. Lett. **47**, 709 (1981).

[68] D.F. Walls, Nature **306**, 141 (1983).

[69] M. Teich and B.E.A. Saleh, Physics Today **43**, 26 (1990).

[70] R. Tanás, in *Coherence and Quantum Optics V*, ed. by E. Wolf and L. Mandel (Plenum, New York, 1986), p. 645.

[71] L. Mandel, Phys. Rev. Lett. **49**, 136 (1982).

[72] J.M. Ziman, *Electrons and Phonons* (Cambridge University Press, Cambridge, 1963).

[73] A.A. Maradudin and A.E. Fein, Phys. Rev. **128**, 2589 (1962).

[74] S. Tamura, private communications.

[75] S. Tamura, Phys. Rev. B **31**, 2574 (1985).

[76] S. Tamura, Phys. Rev. B **31**, 2595 (1985).

[77] K.F. Renk, Detection of High-Frequency Phonons by Phonon-induced Fluorescence, in *Nonequilibrium Phonons in Nonmetallic Crystals*, ed. by W. Eisenmenger and A.A. Kaplyanskii (Elsevier, London, 1986).

[78] O. Madelung, *Introduction to Solid-State Theory* (Springer-Verlag, Berlin, 1978).

[79] A.M. Fox, J.J. Baumberg, M. Dabbicco, B. Huttner, and J.F. Ryan, Phys. Rev. Lett. **74**, 1728 (1995).

[80] Superconducting Electronics, edited by H. Weinstock and M. Nisenoff, (Springer-Verlag, Heidelberg, 1989); H. Weinstock, Physica C **209**, 269 (1993); IEEE Trans. Mag. **27**, 3231 (1991).

[81] Q. Niu, Phys. Rev. Lett. **64**, 1812 (1990).

[82] C. Liu and Q. Niu, Phys. Rev. B **47**, 13031 (1993).

[83] A. Barone and G. Paterno, *Physics and Applications of the Josephson Effect* (Wiley, New York, 1982).

[84] B.D. Josephson, Phys. Lett. **1**, 251 (1962); Adv. Phys. **14**, 419 (1965).

[85] G. Schön and A.D. Zaikin, Phys. Rep. **198**, 237 (1990).

[86] G-L. Ingold and Yu.V. Nazarov, in Ref. [88]. Chapter 2, p.21-107.

[87] M. Tinkham, in Ref. [88]. Chapter 4, p.139-166.

[88] *Single Charge Tunneling*, edited by H. Grabert and M. Devoret (Plenum, New York, 1992).

[89] D.V. Averin and K.K. Likharev, in *Mesoscopic Phenomena in Solids*, ed. by B.L. Altshuler, P.A. Lee and R.A. Webb (Elsevier, 1991), Chapter 6, p. 173-271.

[90] Michael Plischke and Birger Bergersen, *Equilibrium Statistical Physics* (Prentice Hall, New Jersey, 1989).

[91] M. Kardar, Phys. Rev. B **33**, 3125 (1986).

[92] B.L. Schumaker, Phys. Rep. **135**, 317 (1986).

[93] A.J. Leggett, in *Les Houches, Session XLVI, 1986 – Le hasard et la matiere/Chance and Matter* (Elsevier, 1987).

[94] A.O. Caldeira and A. J. Leggett, Phys. Rev. Lett. **46**, 211 (1981).

[95] A. Vourdas, Phys. Rev. A **49**, 12040 (1994).

[96] M. Abramowitz and I.A. Stegun, *Handbook of Mathematical Functions* (Dover, New York, 1973).